THE UNIVERSITY OF QUEENSLAND

DIVISION OF CIVIL ENGINEERING

REPORT CH58/06

TWO SERIES OF DETAILED TURBULENCE MEASUREMENTS IN A SMALL SUBTROPICAL ESTUARINE SYSTEM

AUTHORS: Mark TREVETHAN, Hubert CHANSON
& Richard BROWN

HYDRAULIC MODEL REPORTS

This report is published by the Division of Civil Engineering at the University of Queensland. Lists of recently-published titles of this series and of other publications are provided at the end of this report. Requests for copies of any of these documents should be addressed to the Civil Engineering Secretary.

Division of Civil Engineering
The University of Queensland
Brisbane QLD 4072
AUSTRALIA

Telephone: (61 7) 3365 3619
Fax: (61 7) 3365 4599

URL: http://www.eng.uq.edu.au/civil/

First published in 2006 by
Division of Civil Engineering
The University of Queensland, Brisbane QLD 4072, Australia

ISBN No. 1864998520

The University of Queensland, St Lucia QLD

TWO SERIES OF DETAILED TURBULENCE MEASUREMENTS IN A SMALL SUBTROPICAL ESTUARINE SYSTEM

by

Mark TREVETHAN
Ph.D. candidate, Division of Civil Engineering, School of Engineering,
The University of Queensland, Brisbane QLD 4072, Australia

Hubert CHANSON
Reader, Division of Civil Engineering, School of Engineering,
The University of Queensland, Brisbane QLD 4072, Australia
Ph.: (61 7) 3365 3619, Fax: (61 7) 3365 4599, Email: h.chanson@uq.edu.au
Url: http://www.uq.edu.au/~e2hchans/

and

Richard J. BROWN
Senior lecturer, School of Engineering Systems, Queensland University of Technology.
GPO Box 2434, Brisbane QLD 4001, Australia

REPORT No. CH 58/06
ISBN 1864998520
Division of Civil Engineering, The University of Queensland
March 2006

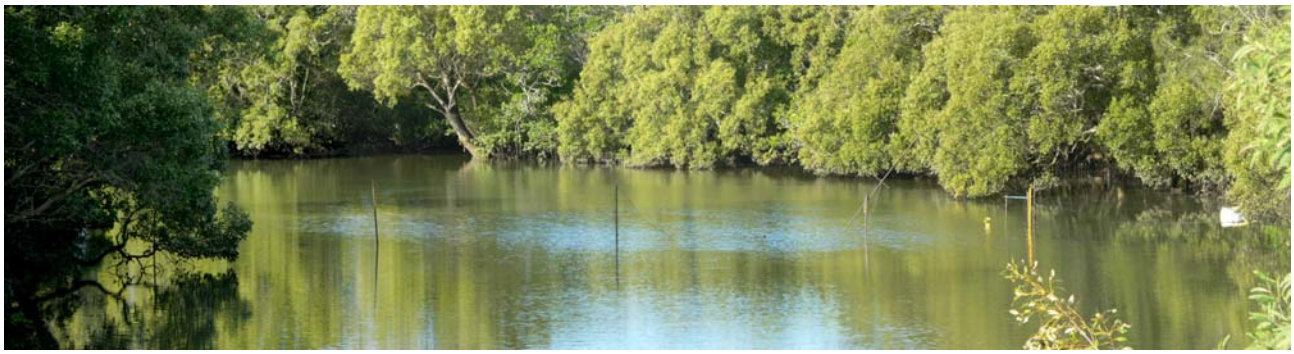

Looking upstream at the sampling site on 16 May 2005 at end of flood tide (Photograph H. CHANSON) - The poles supporting the instrumentation across the creek are visible

Photograph of field work participants during equipment retrieval on 18 May 2006 (field study E6) (Photograph M. TREVETHAN and M. TAKAHASHI)

Photograph of the data acquisition equipment on the left bank during the field study E6 on 18 May 2006 (Photograph C. BOOTH)

ABSTRACT

In natural waterways and estuaries, the momentum mixing is a turbulent process directly relevant to the understanding of sediment transport, release of wastewater into ecosystems and storm-water runoff during flood events. The predictions of contaminant dispersion in estuaries are highly sensitive to specific features of the natural system. They cannot be predicted analytically and must rely upon exhaustive field data for accurate calibration and validation. Herein detailed turbulence and physio-chemistry field measurements were conducted in a small subtropical estuary of Eastern Australia with a semi-diurnal tidal regime. The turbulent velocity measurements were performed continuously at high frequency for 25 hours during spring tide conditions and for 50 hours during neap tide conditions. The velocities were measured with acoustic Doppler velocimetry and a thorough post-processing technique was applied to the velocity signals. The measurement technique used in this study was well suited to the investigation of momentum transport in small estuarine systems with shallow water depths (e.g. less than 0.5 m at low tides).

During the field studies, some tidal asymmetry was observed systematically. The time-averaged streamwise velocity during the ebb tides was smaller than that during the flood tide. The turbulent fluctuations next to the bed were highly intermittent. The third (skewness) and fourth (kurtosis) moments of velocity fluctuations were within the range ±0.6 and -1 to +2 respectively. The horizontal and vertical turbulence intensities were typically within the range of $v_y'/v_x' \sim 1$ and $v_z'/v_x' \sim 0.3$ to 0.8 implying some turbulence anisotropy. The magnitudes were similar to earlier field work results in estuaries and experimental measurements in turbulent open channel flows. The time-averaged Reynolds stresses $\rho*\overline{v_x*v_z}$ were proportional to minus the time-averaged streamwise velocity, and the dimensionless Reynolds stresses $R_{vxvz} = \overline{v_x*v_z}/(v_x'*v_z')$ were similar for both spring and neap tide conditions. The probability distribution functions of tangential Reynolds stresses differed substantially from Gaussian distributions. Based upon auto-correlation analyses, the integral and dissipation time scales were systematically analysed. The dimensionless integral time scales were found to be about : $T_{Ey}/T_{Ex} \sim 1$ and $T_{Ez}/T_{Ex} \sim 2$ to 3 through all the field studies. The findings were consistent with the anisotropy reported above and with an earlier study in a tidal channel. The dissipation time scales were typically between 1 and 10 ms. They were basically independent of the tidal phase, tidal range and sampling elevation. Some observations of momentum mixing coefficients showed a large data scatter spreading over more than three orders of magnitudes, associated with relatively rapid variations with time. The results demonstrated that the assumption of "constant" mixing coefficient was simply untrue.

In addition, some unusual events are reported including some multiple flow reversal events at slack tides, probably induced by some form of resonance. A front was also observed once. The data suggested that the front passage was associated with some temperature anomaly next to the free-surface, and some secondary transverse circulation next to the bed.

A striking feature of the analysed data sets is the large fluctuations in all turbulence characteristics, including the momentum exchange coefficients, during the tidal cycles. This feature was rarely documented, but an important difference between the ADV data sets used in this study from earlier reported measurements is that the present data were collected continuously at high frequency for relatively long periods. It is believed that the present results provided a picture general enough to be used, as a first approximation, to characterise the flow field in similar small subtropical estuaries. A new set of field deployments is planned to clarify the upper estuary dynamics in more details.

Keywords : Turbulence, Subtropical estuary (sub-tropical estuarine system), Momentum mixing, Turbulent Reynolds stresses, Turbulent intensity, Integral time scales, Dissipation time scales, Acoustic Doppler velocimetry, Field measurements, Flow reversal events, Front, Turbulent mixing coefficients.

TABLE OF CONTENTS

	Page
Abstract	iii
Keywords	iii
Table of contents	iv
Notation	v
Preface	viii
1. Introduction	1
2. Investigation site : Eprapah Creek	5
3. Field studies, instrumentation and data processing	14
4. Field observations	30
5. Discussion	52
6. Summary and concluding remarks	72
7. Acknowledgments	76
APPENDICES	
Appendix A - Field data from Eprapah Creek (QLD) on 8-9 March 2005 (Field work E5)	A1
Appendix B - Field data from Eprapah Creek (QLD) on 16-18 May 2005 (Field work E6)	A19
Appendix C - List of field work participants	A57
Appendix D - Summary of turbulence characteristics at Eprapah Creek during the field works E5 (8-9 March 2005) and E6 (16-18 May 2005)	A59
REFERENCES	R1
Internet references	R4
Bibliographic reference of the Report CH58/06	R5

NOTATION

The following symbols are used in this report :

a	coefficient;
b	coefficient (1/s);
d	water depth (m);
CE	dimensionless event search threshold for ADV data post-processing;
F	low-pass/high-pass filter threshold frequency (Hz) for ADV data post-processing;
F_{cut}	cutoff frequency (Hz);
F_{scan}	scanning frequency (Hz) or scan rate;
g	gravity constant: g = 9.80 m/s^2 in Brisbane QLD, Australia;
i	1- integer; 2- directional tensor;
Ku	kurtosis (i.e. dimensionless statistical moment of order 4) defined as: $Ku = \frac{1}{n} * \frac{\sum_{i=1}^{n}(u - \overline{u})^4}{\left(\frac{1}{n} * \sum_{i=1}^{n}(u - \overline{u})^2\right)^2} - 3$ for an infinite number of samples, the (excess) kurtosis of a Gaussian distribution is zero (Ku = 0);
$Ku(V_x)$	kurtosis of streamwise velocity;
$Ku(V_y)$	kurtosis of transverse velocity;
$Ku(V_z)$	kurtosis of vertical velocity;
$Ku(\rho v_x v_y)$	kurtosis of tangential Reynolds stress $\rho * v_x * v_y$;
$Ku(\rho v_x v_z)$	kurtosis of tangential Reynolds stress $\rho * v_x * v_z$;
$Ku(\rho v_y v_z)$	kurtosis of tangential Reynolds stress $\rho * v_y * v_z$;
L	longitudinal, streamwise distance (m) between two landmarks;
l_m	mixing length (m);
N	number of data points;
n	integer;
R	covariance function;
R_{ii}	auto-correlation function;
R_{xx}	normalised auto-correlation function;
R_{vxvy}	dimensionless tangential Reynolds stress in the xy-plane : $R_{vxvy} = \overline{v_x * v_y}/(v_x' * v_y')$;
R_{vxvz}	dimensionless tangential Reynolds stress in the xz-plane;
R_{vyvz}	dimensionless tangential Reynolds stress in the yz-plane;
r	radial co-ordinate;
Sk	skewness (i.e. dimensionless statistical moment of order 3) defined as: $Sk = \frac{1}{n} * \frac{\sum_{i=1}^{n}(u - \overline{u})^3}{\left(\frac{1}{n} * \sum_{i=1}^{n}(u - \overline{u})^2\right)^{3/2}}$ for an infinite number of samples, the skewness of a Gaussian distribution is zero (Sk = 0);

$Sk(V_x)$	skewness of streamwise velocity;
$Sk(V_y)$	skewness of transverse velocity;
$Sk(V_z)$	skewness of vertical velocity;
$Sk(\rho v_x v_y)$	skewness of tangential Reynolds stress $\rho * v_x * v_y$;
$Sk(\rho v_x v_z)$	skewness of tangential Reynolds stress $\rho * v_x * v_z$;
$Sk(\rho v_y v_z)$	skewness of tangential Reynolds stress $\rho * v_y * v_z$;
T	1- averaging period (s); 2- period (s) of tidal cycle from low water to the next low water;
T_E	Eulerian integral time scale (s), also called macro time scale;
T_{Ex}	integral time scale (s) of the x-velocity component;
T_{Ey}	integral time scale (s) of the y-velocity component;
T_{Ez}	integral time scale (s) of the z-velocity component;
t	time (s);
V	instantaneous velocity (m/s);
V_X	instantaneous x-velocity component (m/s);
V_y	instantaneous y-velocity component (m/s);
V_Z	instantaneous z-velocity component (m/s);
V_∞	free-stream velocity (m/s);
$\overline{V}$	time-averaged velocity (m/s)
v	instantaneous velocity fluctuation (m/s) : $v = V - \overline{V}$;
v_x	instantaneous fluctuation (m/s) of V_X : $v_x = V_X - \overline{V_X}$;
v_y	instantaneous fluctuation (m/s) of V_y : $v_y = V_y - \overline{V_y}$;
v_z	instantaneous fluctuation (m/s) of V_Z : $v_z = V_Z - \overline{V_Z}$;
v'	standard deviation of the turbulent velocity fluctuation (m/s);
v_x'	standard deviation of V_X (m/s);
v_y'	standard deviation of V_y (m/s);
v_z'	standard deviation of V_Z (m/s);
WS	number of data points in the post-processing search window;
x	1- distance along the channel bottom (m), positive downstream; 2- Cartesian co-ordinate;
y	1- transverse distance (m) positive towards the left bank; 2- Cartesian co-ordinate;
z	vertical distance (m) positive upwards, with z = 0 at the bed;
δt	time increment (s);
δt_{scan}	sampling scan interval (s) : $\delta t_{scan} = 1/F_{scan}$;
δ_{99}	boundary layer thickness (m) defined in term of 99% of the maximum velocity: $\delta = z(V=0.99*V_\infty)$;
Λ_f	integral time scale (m);
λ_a	acceleration threshold constant;
μ	dynamic viscosity (Pa.s);
ν_T	momentum exchange coefficient (m^2/s), also called "eddy viscosity";
θ	radial co-ordinate;
ρ	water density (kg/m^3);
σ	surface tension between air and water (N/m);

τ	time lag (s);
τ_E	Eulerian dissipation time scale (s), also called Taylor micro-scale;
τ_{Ex}	dissipation time scale (s) of the x-velocity component;
τ_{Ey}	dissipation time scale (s) of the y-velocity component;
τ_{Ez}	dissipation time scale (s) of the z-velocity component;
$\tau_E^{(\delta t)}$	Eulerian dissipation time scale (s) corresponding to the time increment δt;

Subscript

ref	reference values;
x	streamwise direction positive towards downstream;
y	transverse direction positive towards the left bank;
z	vertical direction positive upwards;

Expression

$\rho*v_x*v_y$	instantaneous tangential Reynolds stress (Pa) in the x-y plane;
$\rho*(v_x*v_y)'$	standard deviation of the tangential Reynolds stress (Pa) in the x-y plane;
$\rho*\overline{v_x*v_y}$	time-averaged tangential Reynolds stress (Pa) in the x-y plane;
$\partial / \partial t$	partial derivative with respect of time;
$\|V\|$	absolute value of the velocity;

Abbreviations

ADV	acoustic Doppler velocimeter;
AHD	Australian height datum;
AMTD	adopted middle thread distance, measured upstream from the river mouth;
D.O.	dissolved oxygen content;
HW	high water;
h	hour;
Kurt	kurtosis (Fisher kurtosis or excess kurtosis);
LW	low water;
min.	minute;
Nb	number;
QLD	Queensland, Australia;
Skew	skewness;
Std	standard deviation;
VITA	variable-interval time average.

PREFACE

This report describes two series of detailed experimental measurements of turbulence and physio-chemistry in a small estuarine system in Eastern Australia. The studies were conducted in March and May 2005 in the estuarine zone of Eprapah Creek in South-East Queensland.

The field works took place as part of an on-going interdisciplinary, cross-institutional research collaboration between the University of Queensland (Civil Engineering), the Queensland Environmental Protection Agency (Waterways Services) and the Queensland University of Technology (Engineering Systems). The writers acknowledge the strong support and significant assistance of Dr Ian RAMSAY and John FERRIS (QLD E.P.A.). These field works could not have been performed without the help of numerous people who contributed personally to the preparation, the installation and retrieval of the equipment, and who participated at the continuous, high frequency data collection during days and nights ([1]). The writers are indebted for their help. The new field investigations benefited from the earlier field studies conducted in 2003 and 2004 at Eprapah Creek. The writers are grateful to all the people who assisted with these earlier works, especially the Eprapah Creek Catchment Landcare Association (ECCLA), Mrs Lynn ROBERTS, Mrs Anne STONE and Dr Bernard STONE.

The present report is dedicated to the memory of the late Dr Bernard STONE who was instrumental in facilitating a close collaboration between academics, students and local groups, and who assisted the earlier field works at Eprapah Creek.

The report was edited by Hubert CHANSON and published by the Division of Civil Engineering at the University of Queensland as part of the Hydraulic Model Series under the reference Report CH58/06 with the ISBN 1864998520. Mark TREVETHAN was the lead author of Chapters 4 and 5, and Appendices A, B and D. Hubert CHANSON prepared Chapters 1, 2, 3 and 6. All the writers were involved first hand in the field works and perused each section of the document.

[1]The names of all participants are listed in Appendix C.

1. INTRODUCTION

It is understood that the mixing in natural waterways is a turbulent process. While there is some awareness of mixing of matter in rivers, the understanding of mixing and dispersion processes in estuarine zones remains limited despite relevant applications that include sediment transport, smothering of seagrass and coral, release of organic and nutrient-rich wastewater into ecosystems (including from treated sewage effluent), toxicant release and fate within the environment, and storm-water runoff during flood events. The predictions of contaminant dispersion in estuaries are highly sensitive to specific features of the natural system and they must rely upon exhaustive field data for accurate calibration and validation.

One reason for the minimal attention to this problem in the literature is the very complex variations of hydrodynamic and physio-chemical properties with the tidal phase in an estuary. Very little systematic research on turbulence characteristics in natural estuarine systems was conducted, in particular in small systems. In addition long-duration studies of turbulent properties at high frequency are extremely limited. Most field measurements were conducted for short-periods, or in bursts, often at low frequency : e.g. BOWDEN and FERGUSON (1980), KAWANISI and YOKOSI (1997), STACEY et al. (1999), NIKORA et al. (2002), VOULGARIS and MEYERS (2004), KAWANISI, (2004), RALSTON and STACEY (2005) (Table 1-1). The data lacked spatial and temporal resolution to gain insights into the characteristics of fine-scale turbulence. It is believed that the situation derived partly from limited instrumentation suitable for small estuaries.

The present study is focused on high frequency continuous turbulence data collection in a small subtropical estuary over at least a full diurnal tidal cycle. Field works were conducted in two separate investigations. Measurements were performed with acoustic Doppler velocimetry (ADV). While the instrumentation is well-suited to study turbulent velocities in shallow-waters, it is sometimes assumed wrongly that the velocity signal outputs are "true" turbulent velocity data. This was found grossly incorrect. A new ADV data post-processing technique was developed for turbulence analysis and it was applied herein systematically to the new field work data. The results provide new details of the turbulence field in a small estuary and its variations through a full tidal cycle.

1.1 DEFINITION

Herein the estuarine zone is defined as the river section where mixing of freshwater and seawater occurs. Each estuary is distinctly unique, since topography, river inflow and tidal forcing influence the shape and mixing that occur locally. Estuaries are classified by two main schemes based on topography and salinity structure. These classification schemes were reviewed in PRITCHARD (1952), DYER (1973) and LEWIS (1997). Topographically, the vast majority of the estuaries of South-East Queensland were found to be a drowned river valley (coastal plain) type (DYER 1973, DIGBY et al. 1999). The main topographical features of these coastal plain estuaries are: (a) shallow waters with large width to depth ratio, (b) cross-sections which deepen and widen towards the mouth, (c) a small freshwater inflow to tidal prism volume ratio, (d) large variations of sediment type and size found, (e) a surrounding of extensive mud flats, and (f) a sinuous central channel.

The estuaries of South-East Queensland are classified as wet and dry tropical/subtropical estuaries (DIGBY et al. 1999). The "wet and dry tropical/subtropical estuary" type accounts for 68% of all estuaries in Australia. These estuaries are characterised by short-lived, episodic, high freshwater inflows during the wet season, and very little or no flow during the dry season (Fig. 1-1). Figure 1-1 illustrates the effects of an intense, short storm on the upper estuary of Eprapah Creek (Queensland). During high inflow situations, an estuary is flushed to the mouth with freshwater. After flushing, the estuary quickly recovers because of the significant tidal range. The estuary may change from fully flushed to partially mixed (well stratified) back to vertically homogeneous within a few days after the end of the high flow event.

Table 1-1 - Summary of turbulence field studies in estuarine and tidal channels

Reference (1)	Flow conditions (2)	Instrumentation (3)	Remarks (4)
BOWDEN and FERGUSON (1980)	Eastern Irish Sea, off North Wales Coast (UK)	Electromagnetic current meters (2D) Scan rate: 5.5 Hz, Scan duration: 12 min. 17 s	
OSONPHASOP (1983)	Tidal channel West of French Island, Western Port Bay, off Bass Strait (Australia), semi-diurnal tides Avg depth: 10 m, Width: 900 m, Mid-tide max. velocity: 0.7 m/s	Drag sphere turbulent probe (3D) Scan rate: 9 Hz, Scan duration: 8192 samples	
WEST and SHIONO (1988)	Teign estuary (UK) Water depth range: 1-5 m, Width: 600 m, Mean velocity: 0.25 to 0.8 m/s	Braystroke velocity meters Scan rate: 10 Hz, Scan duration: 205 or 410 s, Averaging period: 100 s	
WEST and ODUYEMI (1989)	Conwy estuary (UK) Water depth range: 1-5 m Tamar estuary (UK) Water depth range: 1-5 m	Electromagnetic current meters Colebrook Intr. Scan rate: 10 Hz, Scan duration: 51 & 102 s	
KAWANISI and YOKOSI (1994)	Ota river estuary (Japan), mixed semi-diurnal tides Avg depth: 3 m, Width: 320 m, Mid-tide velocity: 0.35 m/s, Tidal range: 4 m	Electromagnetic current meters Alec Electronics ACM-200P (2D) Scan rate: 1.6 Hz, Scan duration: 4096 samples, Study duration: 26 h	Spring tide conditions.
KAWANISI and YOKOSI (1997)	Ota river estuary (Japan), mixed semi-diurnal tides Avg depth: 3 m, Width: 320 m, Mid-tide max. velocity: 0.45 m/s, Tidal range: 4 m	ADV Scan duration: 300 s, Study duration: 12 h	Spring tide conditions.
NIKORA et al. (2002)	Beatrix Bay (New Zealand) Avg depth: 38.2 m, Width: 4 km, Mid-tide velocity: 0.02 m/s	Sontek ADVs Scan rate: 10 & 25 Hz, Scan duration: 300 s, Study duration: 7 days	
KAWANISI (2004)	Ota river estuary (Japan), mixed semi-diurnal tides Avg depth: 3 m, Width: 320 m, Mid-tide velocity: 0.3 m/s, Tidal range: 4 m	Nortek High Resolution Current Profiler HRCP (1.5 MHz) Scan rate: 0.33 Hz, Study duration: 24 h	Spring tide conditions
VOULGARIS and MEYERS (2004)	Bly Creek, North Inlet, Georgetown NC (USA), semi-diurnal tides Avg depth: 1 m, Width: 30 m, Mid-tide velocity: 0.2 to 0.5 m/s, Avg tidal range: 1.4 m	Sontek 3D ADV (10 MHz) Scan rate: 10 Hz, Scan duration: 12 min., Study duration: up to 7 days	
RALSTON and STACEY (2005)	Subtidal channels, Central San Francisco Bay (USA), mixed semi-diurnal tides Avg depth: 1 m, Mid-tide velocity: 0.1 to 0.3 m/s	ADVs Scan rate: 8 Hz, Scan duration: 19.5 min., Study duration: 25 h	
Present study	Eprapah Creek Qld (Australia), mid-estuary, semi-diurnal tides Avg depth: 2 m, Width: 30 m, Mid-tide velocity: 0.1 & 0.3 m/s, Tidal range: 1.2 & 2.45 m	Sontek 3D ADV (10 MHz) & 2D microADV (16 MHz) Scan rate: 25 Hz, Scan duration: continuous, Study duration: 25 & 50 h	Field studies E5 (spring tides) and E6 (neap tides).

Fig 1-1 - Photographs of a typical wet and dry subtropical estuary : Eprapah Creek, Queensland (Photographs H. CHANSON)
(Left) Photograph of the upper estuary during dry conditions - View from the right bank at Site 3B on 2 Aug. 2004 at 14:10 looking upstream - Note the very low water level at the start of flood tide, and the wooden debris
(Right) Photograph of the same section on 1 December 2005 around 14:30 after 130 mm of rain around midnight the night before, looking upstream - Note the strong freshwater flushing (flow from background to foreground), the high water level and the "brownish" colour of the flow highlighting sediment suspension

1.2 STRUCTURE OF THE REPORT

To date, very limited quantitative information is available on the turbulence properties in subtropical estuarine systems, partly because of a lack of field deployment of fine instrumentation logged continuously at high frequency for a full tidal cycle. It is the purpose of this research report to document the turbulence characteristics in a small subtropical estuary during two distinct field studies. The new turbulent velocity measurements were performed about mid-estuary at Eprapah Creek associated with some detailed physio-chemistry data collection. The results provide an unique characterisation of the turbulence field under unsteady estuarine conditions and of the associated mixing processes. The findings yield a new understanding of the momentum mixing mechanisms in such a small estuarine system.

After the introduction section (Section 1), Section 2 reviews some earlier studies of the estuarine zone of Eprapah Creek. Section 3 details the new field study conditions, the instrumentation and the signal post-processing techniques. Turbulent flow properties are presented in Section 4. Section 5 include some discussions on unusual flow features such as flow reversal events and some front passage observations, and it details the effect of tidal phase and tidal range on the turbulent time scales and momentum exchange coefficient.

The full data sets are presented in Appendices A and B. All the field work participants are listed in Appendix C. Appendix D summarises the range of turbulence characteristics at Eprapah Creek during the two field works. Bibliographic references are listed at the end of the report.

2. INVESTIGATION SITE : EPRAPAH CREEK

2.1 PRESENTATION

New field investigations were conducted in the estuarine zone of Eprapah Creek (Australia) in 2005. Eprapah Creek (Longitude 153.30º East, Latitude -27.567º South) is a subtropical stream located in the Eastern part of Australia, in the Redlands Shire close to Brisbane City. The creek flows directly into Moreton Bay at Victoria Point off the Pacific Ocean (Fig. 2-1). The stream is basically 12.6 km long with about 3.8 km of estuarine zone. In the estuary, the water depth is typically about 1 to 2 m mid-stream, and the width is about 20-30 m. This is a relatively small estuary with a narrow, elongated and meandering channel (Fig. 2-1, 2-2 and 2-3). The channel is bordered with forests and trees, and it is relatively well-protected from wind effects. Figure 2-3 shows several surveyed cross-sections in the upper estuary. The locations of the surveyed measurement sites are shown in Figure 2-1A. The tides are mixed semi-diurnal and the range is about 1.2 to 2.5 m. The most upstream extent of estuary corresponds to Sites 3B to 4 shown in Figure 2-1A depending upon the tidal conditions.

The catchment area is about 39 km^2. It is mostly urban in the lower reaches and semi rural/rural residential in the upper reaches. It includes several conservation areas hosting endangered species: e.g., koalas, swamp wallabies, sea eagles. Average hydrological conditions are listed in Table 2-1 for a 50-year period.

Table 2-1 - Average hydrological conditions at Redlands meteorological station for the period 1953-2003 (Reference: Australian Bureau of Meteorology)

Meteorological Parameter (1)	Average value (2)	Units (3)
Air temperature at 09:00	20.5	ºC
Average humidity at 09:00	67	%
Average wind speed at 09:00	8.6	km/h
Average yearly rainfall	1284.3	mm
Maximum monthly rainfall	909.7	mm
Maximum daily rainfall	241.0	mm
Average number of rainy days	116	days/year
Average sunny days	81	days/year
Average number of overcast days	60	days/year

Notes : Redlands meteorological station : Long.: 153.250º E, Lat.: -27.528º S; Eprapah Creek catchment is located less than 10 km from the meteorological station

Fig. 2-1 - Eprapah Creek estuarine zone
(A) Map and definition sketch
Blue circle : water quality and fish sampling station in 2003 and 2004. Red square : instantaneous velocity and water quality measurement site in 2003. Black square : instantaneous velocity and water quality sampling site in 2003, 2004 and 2005

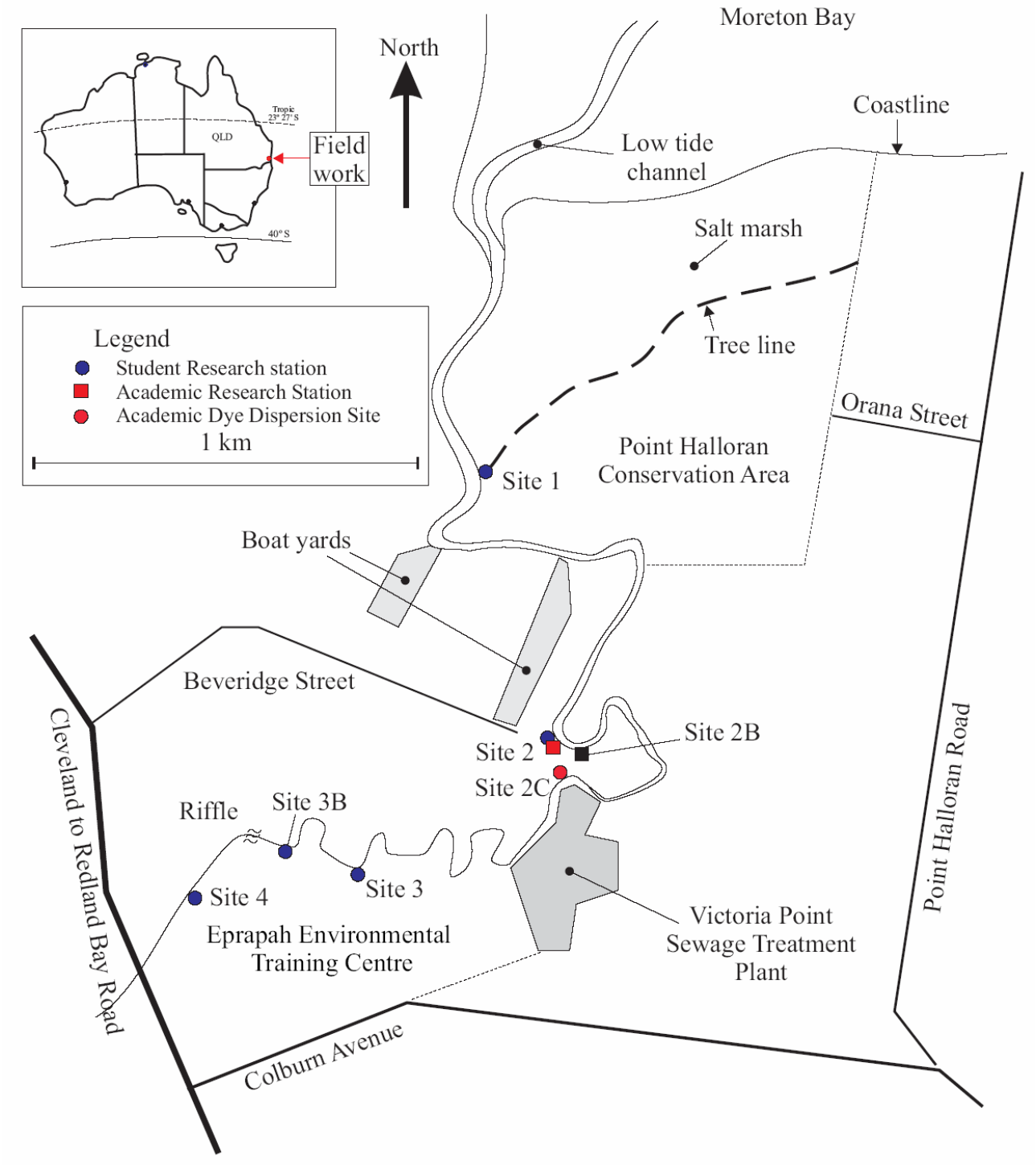

(B) Aerial map of Eprapah Creek (Qld Department of Natural Resources and Mines, 2001)

Fig. 2-2 - Photographs of Eprapah Creek estuarine zone
(A) Site 1 (AMTD 0.6 km) on 2 Sept. 2004 at sunrise and low tide, looking upstream with marinas in background (Photograph S. AOKI)

(B) Site 2 (AMTD 2.0 km) on 4 Apr. 2003 looking downstream, early mid morning (Courtesy of CIVL4140 Group 2, 2003/1)

(C) Site 3 (AMTD 3.1 km) on 2 Sept. 2004 around 9:30 am during end of flood tide (Photograph H. CHANSON) - Students interacting with EPA scientific officers conducting a vertical profile of physio-chemistry measurements

(D) Site 4 (AMTD 3.8 km) on 4 April 2003 looking downstream (Photograph H. CHANSON)

Fig. 2-3 - Surveyed cross-sections of Eprapah Creek estuarine zone at Sites 2, 2B, 2C and 3, looking downstream - Dates of the surveys are shown in the legend

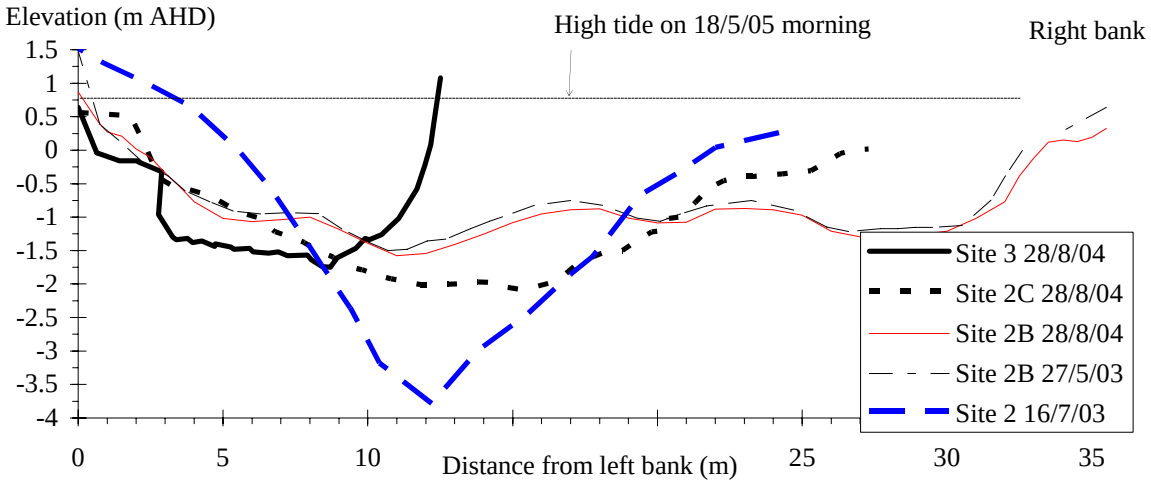

2.2 PREVIOUS STUDIES AND INVESTIGATIONS

Water quality and ecology have been closely monitored at Eprapah Creek (Victoria Point QLD) for over 30 years by Redland Shire Council, Queensland Environmental Protection Agency (EPA), the University of Queensland and local community groups (e.g. O'BRIEN and FEARON 2001). The creek was heavily polluted in 1998 by illegal discharges of tributyl-tin (TBT) and chemical residues. Although the estuarine zone includes two environmental parks, there are some marinas and boat yards, and a major sewage treatment plant discharge that affect the natural system (JONES et al. 1999) (Fig. 2-1). The upstream catchment has been adversely affected by large-scale poultry farms, wineries, land clearance and semi-urban development. Recent works included the constructions of new shopping centres and residential lots less than 500 m from the upper estuary in 2003-05.

A series of detailed field measurements were undertaken in the estuarine zone of Eprapah Creek in 2003 and 2004 (CHANSON 2003, BROWN et al. 2004, FERRIS et al. 2004, CHANSON et al. 2004, 2005a). Field works took place on four different days (Table 2-2). Tidal conditions and sampling locations are listed in Table 2-2, and the sites are shown in Figure 2-1. Sites 1, 2, 2B, 3, 3B and 4 were located at AMTD 0.6, 2, 2.1, 3.1, 3.4 and 3.8 km respectively where AMTD is the upstream distance from river mouth ([1]) (Table 2-3).

The results and outcomes of these field studies in Eprapah Creek estuary were six-fold. First the investigations provided some unique snapshots of a small estuarine system. Such short-term monitorings were valuable because they were conducted systematically at high frequency with simultaneous measurements at several sampling sites, and they encompassed comprehensive, multi-disciplinary surveys (Table 2-2). The field works provided a broad range of simultaneous data covering hydrodynamics, water quality and ecology. The single-day studies complemented traditional long-term monitoring.

Second field experience highlighted some recurrent problem with the acoustic Doppler velocimetry including ADVs, ADCPs and ADPs (CHANSON et al. 2005b). Basic data analysis showed conclusively that turbulence properties could not be derived from unprocessed acoustic Doppler signals. Even "classical" despiking methods were not directly applicable to unsteady estuary flows. While the acoustic Doppler velocimetry is a relatively simple technique, unprocessed

[1]AMTD = Adopted Middle Thread Distance measured upstream from the mouth.

ADV/ADCP/ADP data should not be used, even for a study of time-averaged velocity components. Instead a detailed post-processing technique was developed and applied (CHANSON et al. 2005b).
Third the Eprapah Creek estuary is a turbulent flow system with complex patterns. It is a tidal dominated system with some strong flushing at mid-tide especially during spring tide periods. But some low frequency velocity fluctuations were recorded suggesting the influence of large-scale vortical structures and possibly some resonance. Physio-chemistry was dominated by flood tides, the daily cycle (day/night), and sewage effluent releases from the treatment plant and catchment runoff.
Fourth the measurements highlighted contrasting outcomes. Some results were positive, showing diverse bird and fish activities, together with strong turbulence levels and flushing at mid-tide. But others demonstrated on-going pollution including low dissolved oxygen and pH levels in the upper ([2]) estuarine zone, surface slicks, high proportion of exotic fish. In turn we must query : how can we define accurately "key water quality indicators" to describe the diversity of such a subtropical estuary (CHANSON et al. 2005a) ?
Fifth two field studies (E1 and E4) were conducted during extreme, but opposite meteorological conditions. One study took place immediately after an intense storm. Field measurements highlighted strong freshwater flushing during and shortly after storm periods. Another study was conducted after a long drought period during which the catchment received less than 40 mm of rain in four months (May-Aug 2004) compared to a 50-year average rainfall of 322 mm for the same period. The estuary hydrodynamics was totally tide-dominated during the drought, and the measurements suggested a drastic impact of the drought on the fish population (CHANSON et al. 2005a).
Sixth the field works provided unique personal experiences and fostered interactions between academics, professionals, local community groups and students. Field studies complemented traditional lectures, and such personal experiences were at least as important as the academic and professional experiences (CHANSON 2004a).

[2]The upper estuary is the upstream estuarine section. Conversely the lower estuary is the downstream end of the estuary next to the river mouth.

Table 2-2 - Summary of past field investigations at Eprapah Creek in 2003 and 2004

Field study reference	E1	E2	E3	E4
Date	4 April 2003	17 July 2003	24 Nov. 2003	2 Sept. 2004
Tides (Victoria Point)	05:16 (0.67 m) 11:03 (2.22 m) 17:24 (0.57 m) 23:31 (2.41 m)	00:00 (2:63 m) 06:44 (0.60 m) 12:19 (1.92 m) 18:01 (0.59 m)	03:27 (0.21 m) 09:50 (2.74 m) 16:29 (0.46 m) 21:53 (2.11 m)	06:02 (0.40 m) 11:52 (2.21 m) 18:02 (0.56 m) 11:59 (2.29 m)
Study period	06:00-18:00	06:00-14:00	08:00-16:00	06:00-18:00
Study focus	One tidal cycle	Flood tide	Ebb tide	One tidal cycle
Weather	Sunny	Overcast	Overcast with few showers	Sunny to overcast with brief shower
Remarks	Short intense rainstorm on 4 Apr. 2003 evening			Long drought period
Reference(s)	CHANSON (2003)	FERRIS et al. (2004), CHANSON et al. (2004)	FERRIS et al. (2004), CHANSON et al. (2004)	CHANSON et al. (2005a,b)

Field study reference	E1	E2	E3	E4
Acoustic Doppler velocimetry				
ADV sampling period(s)	10:08-10:42 10:43-10:44 11:45-12:18 11:19-11:57 11:58-12:29 12:29-12:52 12:53-13:11 13:12-13:53 13:53-14:09	6:26-14:10	8:25-15:35	7:55-13:40 14:26-17:57
ADV velocity range (m/s)	0.3 / 1.0 / 0.3 / 0.3 / 0.3 / 1.0 / 1.0 / 1.0 / 1.0	0.3	1.0	0.3
Continuous sampling frequency (Hz)	25	25	25	25
Sampling volume location	Site 2B, 0.50 m below surface, 14.2 m from left bank	Site 2, 0.50 m below surface, 8.0 m from left bank	Site 2B, 0.50 m below surface, 10.7 m from left bank	Site 2B, 0.0525 m above bed, 10.7 m from left bank

Field study reference	E1	E2	E3	E4
Physio-chemistry sampling				
Continuous sampling site ([1])	Site 2B, 0.50 m below surface, 13.9 m from left bank	Site 2, 0.50 m below surface, 7.7 m from left bank	Site 2B, 0.50 m below surface, 10.4 m from left bank	Site 2B, 0.0525 m above bed, 10.4 m from left bank
Continuous sampling frequency (Hz) ([1])	0.2	0.2	0.5	0.33
Vertical profile locations from a boat mid-stream ([2])	Sites 1, 2, 2B and 3	River mouth, Site 2, AMTD 2.7 km	Sites 1, 2 and 3	Sites 1, 2 and 3
Surface sampling from bank	Sites 1, 2, 3 and 4	Site 2	--	Sites 1, 2 and 3
Water temperature (ºC) (mid-estuary, Site 2) ([1]) ([3])	23.7 [20.4-28.4]	16.7 [15.5-18.5]	25.5 [22.7-28.0]	17.14 [15.9-18.1]
Conductivity (mS/cm) (mid-estuary, Site 2) ([1]) ([3])	34.5 [23.9-48.3]	37.2 [29.8-48.4]	50.0 [42.7-55.1]	48.6 [41.0-53.6]
Turbidity (NTU) (mid-estuary, Site 2) ([1]) ([3])	9.4 [5.8-13.9]	11.0 [7.2-*24.6*]	19.9 [7.1-43]	22.9 [7.2-??]

Field study reference	E1	E2	E3	E4
Ecological sampling				
Bird activity observations	Sites 1, 2, 3 and 4	Site 2	Site 2	Sites 1, 2, 3
Fish and macro-invertebrate sampling ([4])	Sites 1, 2, 3 and 4	Site 2	--	Sites 1, 2, 3
Fish activity in recirculation zones next to outer bank	--	--	Site 2	--

Notes: ([1]) measured with YSI6600 probe; ([2]) measured with YSI6920 probe; ([3]) mean values [extreme values in square brackets] for the study period; ([4]) using fish trap and dip net; *Italic data*: possibly incorrect data.

Table 2-3 - Location of the sampling sites along Eprapah Creek estuary

Site (1)	AMTD km (2)	Sampling (3)	Remarks (4)
River mouth	0		
1	0.6	Surface sampling from right bank.	
2	2.0	Surface sampling from left bank.	Platform.
2B	2.1	Surface sampling from left bank.	
2C		Surface sampling from left bank.	
STP	2.7	Treatment plant effluent release point	
3	3.1	Surface sampling from right bank.	Platform.
3B	3.4	Surface sampling from right bank.	Platform.
4	3.8	Surface sampling from right bank.	Platform. Platypus pool.

Notes : AMTD : adopted middle thread distance; Sampling sites are shown in Figure 2-1A.

3. FIELD STUDIES, INSTRUMENTATION AND DATA PROCESSING

3.1 FIELD STUDIES

New field experiments were conducted at Eprapah Creek in March and May 2005. In each case, the focus was a study of the turbulence during a full diurnal tidal cycle (i.e. 24 h 50 min.). Each field study took place at the same location about mid-estuary (Site 2B). Turbulence measurements were performed continuously at high frequency (25 Hz) for 25 and 50 hours for the studies E5 and E6 respectively (Table 3-1). Table 3-1 lists details of the tidal conditions, weather, and instrumentation setup for each investigation using the same presentation as shown in Table 2-2. Some photographs of the field investigations are shown in Figure 3-1.

The first investigation was performed during spring tide conditions. The tidal range was up to 2.45 m (Table 3-1). Strong mid-tide currents were observed at the investigation site, and the water depth at low tide was less than 0.6 m at the ADV sampling position. During the second investigation in May 2005, the tidal range was about 1.2 m (i.e. neap tide). A large number of instruments were deployed across the creek and data-logged simultaneously (Section 3.2). In particular, two acoustic Doppler velocimetry systems were deployed at the same location but at two different vertical elevations. It is worth commenting that a number of boat passages occurred about 27 h. 30 min. after the start of the experiment and lasted for about 3 h. 30 min..

For both field studies, the freshwater surface runoff was recorded as zero at the Redland Bay to Cleveland road bridge (Fig. 2-1A). While there might have been some groundwater runoff, its influence was small and not detectable. Further the wind conditions were calm to moderate. There was no wind wave at the sampling site. This was also noted during the previous field studies.

Details of the instrumentation are reported in the next paragraph. Then the data processing is explained. Lastly additional comments are reported. Note that the full data sets are reported in Appendices A and B, and the lists of the field work personnel are detailed in Appendix C.

Fig. 3-1 - Photographs of the field investigations
(A) Site 2B on 8 March 2005 at 15:00 (low tide) (Photograph H. CHANSON) - View from the left bank - Note the low water level and the rocks in the middle of the creek

(B) Site 2B on 9 March 2005 mid-morning (high tide) (Photograph H. CHANSON) - View from mid-stream looking at the ADV towards the left bank - Note the high water level

(C) Site 2B on 16 May 2005 at 15:15 (end of flood tide) (Photograph H. CHANSON) - Looking upstream from Site 2 - The poles supporting the instrumentation are clearly visible

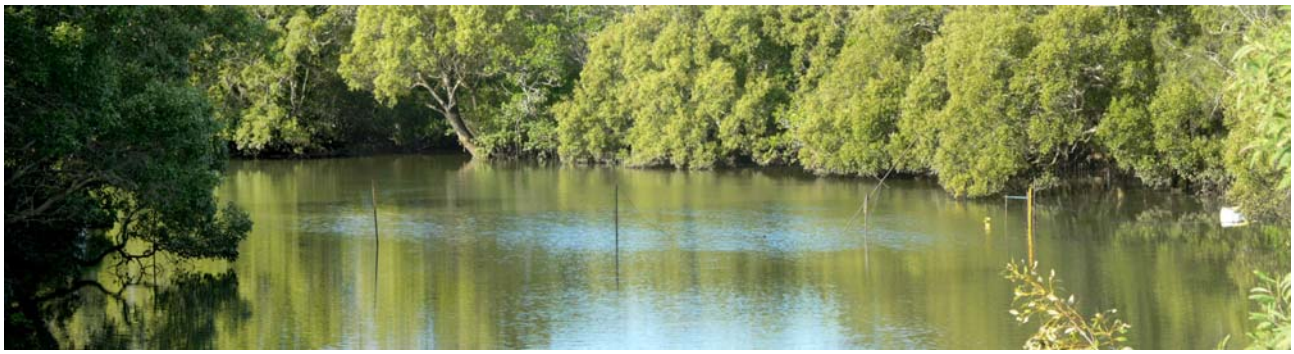

(D) Boat passage beside the ADV/YSI6600 support system on 17 May 2005 afternoon (Photograph H. CHANSON) - View from the left bank, boat direction from left to right (backward motion)

(E) Probe supports seen from the right navigation channel on 17 May 2005 morning (Photograph M. TAKAHASHI) - The pole in the foreground supports two In-Situ™ Troll LTS9000 probes

Table 3-1 - Summary of field investigation conditions at Eprapah Creek in 2005

Field study reference	E5	E6
Date	8-9 March 2005	16-18 May 2005
Tides (Victoria Point)	8 March 2005: 01:33 (0.54 m) 08:22 (2.72 m) 15:12 (0.55 m) 20:42 (2.12 m) 9 March 2005: 02:50 (0.42 m) 09:10 (2.79 m) 15:55 (0.46 m) 21:29 (2.25 m)	16 May 2005: 02:54 (2.19 m) 10:03 (0.97 m) 15:46 (1.67 m) 21:21 (1.06 m) 17 May 2005: 03:58 (2.17 m) 11:01 (0.90 m) 16:59 (1.77 m) 22:41 (1.04 m) 18 May 2005: 04:59 (2.17 m) 11:52 (0.81 m) 17:59 (1.93 m) 23:51 (0.96 m)
Study period	14:55 on 8 March 2005 to 16:00 on 9 March 2005	09:50 on 16 May 2005 to 10:36 on 18 May 2005
Study focus	Diurnal tidal cycle	Two diurnal tidal cycles
Weather	Sunny to overcast	Sunny to overcast
Remarks		Heavy Navigation passages on 17 May 2005 between 13:29 and 17:00
Acoustic Doppler velocimetry		
ADV sampling period(s)	14:55 on 8 March 2005 to 16:00 on 9 March 2005	09:50 on 16 May 2005 to 10:36 on 18 May 2005
ADV velocity range (m/s)	1.0	1.0
Continuous sampling frequency (Hz)	25	25
Sampling volume location	Site 2B, 0.095 m above bed, 10.7 m from left bank	Site 2B, 10.7 m from left bank microADV-UQ : 0.2 m above bed ADV-QUT : 0.4 m above bed
Physio-chemistry sampling		
Continuous sampling site ([1])	Site 2B, 0.095 m above bed, 10.4 m from left bank	Site 2B, 0.4 m above bed, 10.4 m from left bank
Continuous sampling frequency (Hz) ([1])	0.167 (every 6 s)	0.0833 (every 12 s)
Vertical profile locations from a boat mid-stream ([2])	River mouth, Sites 2 and 2C, AMTD 2.7 km (on 10 March 2005)	River mouth, Sites 1, 2 and 2C, AMTD 2.7 km, Site 3 (on 17 May 2005)
Water temperature (ºC) (Site 2B) ([1]) ([3])	25.8 [24.1-26.9]	21.1 [20.2-21.8]
Conductivity (mS/cm) (Site 2B) ([1]) ([3])	50.7 [44.3-56.0]	47.2 [43.9-50.2]
Turbidity (NTU) (Site 2B) ([1]) ([3])	*626* *[6.5-1849]*	12.6 [3.4-*747*]

Notes: ([1]) measured with YSI6600 probe; ([2]) measured with YSI6920 probe; ([3]) : mean values [extreme values in square brackets] for the study period; *Italic data* : possibly incorrect data.

3.2 INSTRUMENTATION

Turbulent velocity measurements were conducted with two acoustic Doppler velocimeters : (1) a Sontek™ UW ADV (10 MHz, serial 0510) equipped with a 5 cm down-looking three-dimensional sensor mounted on a rigid stem, and (2) a Sontek™ micro-ADV (16 MHz, serial number A641F) with a two-dimensional side-looking head with a distance to sampling volume of 5 cm. The probes were located at Site 2B, about the middle of the channel in a moderate bend to the right when looking downstream at 10.7 m from the left bank (Fig. 2-1A). All ADVs were logged continuously at 25 Hz during each investigation (Table 3-1).

The first velocimeter (3D ADV 10 MHz ([3])) was used for both field works ([4]). It was installed at the same position for both field studies but with different vertical elevations (Table 3-1). The second system ([5]) was used for the field study E6 only. Figure 3-2 illustrates the mounting of the ADVs. During the field study E6, the ADV systems were positioned vertically, and their sampling volumes were aligned vertically and located at 0.2 and 0.4 m above the bed (Table 3-1). The 2D microADV heads were facing towards the right bank and the microADV signal outputs provided the two horizontal velocity components.
Next to the 3D ADV system (10 MHz), a physio-chemical probe YSI™6600 was deployed and data-logged continuously at respectively 0.167 Hz and 0.083 Hz for the field studies E5 and E6 respectively (Table 3-1) ([6]). The physio-chemistry probe sensors were positioned 0.3 m apart horizontally from the 3D ADV control volume. Both the YSI™6600 probe and the ADV(s) were held by a metallic frame, and the probes were installed outside of the support system to limit the support wake effects.
During the study E6 on 16-18 May 2005, six In-Situ™ Troll LTS9000 probes were deployed additionally across the creek at Site 2B (Fig. 3-3). Figure 3-4 presents the respective positions of each LTS9000 probe. Each probe recorded continuously pressure, temperature and conductivity at 0.167 Hz (every 6 s).

Fig. 3-2 - Mounting of both ADV systems used during the 16-18 May 2005 investigation (Field study E6) (Photograph H. CHANSON) - Photograph taken during the field work preparation

[3]The Sontek™ UW ADV (10 MHz, serial 0510) was equipped with a three-heads sensor collecting simultaneously the three velocity components. Herein the system is called the 3D ADV (10 MHz).
[4]It was the same ADV system that was used during the four earlier field studies (CHANSON 2003, CHANSON et al. 2005a,b).
[5]The Sontek™ microADV (16 MHz, serial number A641F) was equipped with a 2D side-looking head recording simultaneously the two horizontal velocity components. It is called herein the 2D microADV (16 MHz).
[6]The data were logged continuously and there was no time constant.

Fig. 3-3 - Photograph of two Troll LTS9000 probes on 16 May 2005 before installation (Photograph M. TAKAHASHI) - The probe sensors at just below the photograph bottom

Fig. 3-4 - Sketch of the channel cross-section at Site 2B, looking downstream, with the details of the instrumentation deployed on 16-18 May 2005 (Field study E6)

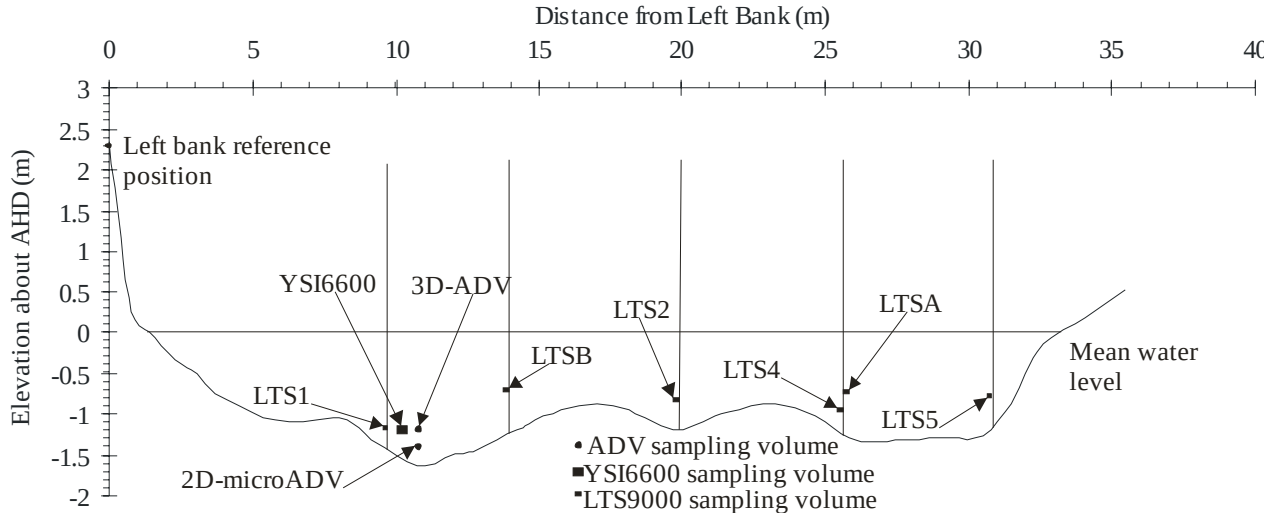

Fig. 3-5 - Water sampling mid-stream on 17 May 2005 at 09:24 (mid ebb-tide) (Photograph H. CHANSON) - The YSI6920 probe is lowered in water (foreground right)

In addition, vertical profiles of physio-chemical parameters were conducted in the middle of the creek at several sites. They were performed at high tide and during ebb flow using a physio-chemistry probe YSI™6920 lowered from a boat drifting with the flow (Fig. 3-5). Measurements included water temperature, conductivity pH, dissolved oxygen content and turbidity taken every 20 to 50 cm.
Additional observations were obtained with several 35-mm and digital cameras, including a Sony™ DSC-T33, a Panasonic™ Limux DMC-FZ20GN (shutter: 8 to 1/2,000 s) and a Canon™ A85 (shutter: 15 to 1/2,000 s).

3.3 DATA PROCESSING : ACOUSTIC DOPPLER VELOCITY DATA

3.3.1 Past and present experiences

The acoustic Doppler velocimetry (ADV) is designed to record instantaneous velocity components at a single-point with relatively high frequency. Measurements are performed by measuring the velocity of particles in a remote sampling volume based upon the Doppler shift effect (e.g. VOULGARIS and TROWBRIDGE 1998, McLELLAND and NICHOLAS 2000). The probe head includes one transmitter and two or three receivers ([7]). The sampling volume is located typically 5 cm from the transmitter, but some studies showed that the distance might change slightly (e.g. CHANSON et al. 2000). Its size is determined by the sampling conditions. In a standard configuration with a standard ADV (10 MHz) unit, the sampling volume is about the shape of a cylinder of water with a diameter of 6 mm and a height of 9 mm. With the microADV (16 MHz), the sampling volume is believed to be three times smaller in terms of volume (SONTEK 2001) : that is, about a cylinder of water with a diameter of 4.2 mm and a height of 6.2 mm.

[7]The Sontek™ UW ADV (10 MHz) unit had 3 receivers, while the Sontek™ microADV (16 MHz) system had two receivers.

An ADV system records simultaneously 12 values with each sample: three velocity components, three signal strength values, three correlation values and three signal-to-noise ratios ([8]). Signal strengths and correlations are used primarily to determine the quality and accuracy of the velocity data, although the signal strength (i.e. acoustic backscatter intensity) may be related to the instantaneous suspended sediment concentration with proper calibration (e.g. FUGATE and FRIEDRICHS 2002, NIKORA and GORING 2002, VOULGARIS and MEYERS 2004). Herein the study was focused on the velocity signals, and the correlation and signal-to-noise ratio values were only used during the post-processing to validate the samples.

Past and present experiences demonstrated recurrent problems with "raw" ADV velocity data that were evidenced by high levels of noise and spikes in all velocity components (NIKORA and GORING 1998, McLELLAND and NICHOLAS 2000, WAHL 2003, CHANSON et al. 2005b). In turbulent flows, the ADV velocity fluctuations characterise the combined effects of the Doppler noise, signal aliasing, velocity fluctuations, installation vibrations and other disturbances. The signal may be further affected adversely by velocity shear across the sampling volume and boundary proximity. LEMMIN and LHERMITTE (1999) and CHANSON et al. (2000,2002) discussed the inherent noise of an ADV system. Spikes may be caused by aliasing of the Doppler signal. McLELLAND and NICHOLAS (2000) explained the physical processes while NIKORA and GORING (1998) and GORING and NIKORA (2002) developed techniques to eliminate these "spikes" in steady flow situations. VOULGARIS and TROWBRIDGE (1998), MARTIN et al. (2002) and KOCH and CHANSON (2005) discussed the averaging effect of sharp mean velocity gradients near a boundary and low correlations in high-turbulent shear regions. In summary : "raw" ADV velocity data should never be used without adequate post-processing.

For all field studies, present experience demonstrated recurrent problems with the velocity data (CHANSON 2003, CHANSON et al. 2005a,b). The ADV systems were oriented with the xy-plane being horizontal, the x-direction aligned with the flow direction and positive downstream, the y-direction towards the left bank and the z-direction positive upwards. Typical results are shown in Figure 3-6. Figure 3-6 presents the three velocity components recorded during the field study E6 for about 3 hours near the end of the investigation, starting at mid ebb tide (t = 200,000 s) and ending at about low tide. In Figure 3-6A, the measured water depth is also shown (right vertical axis). The velocity data shown in Figure 3-6 are un-processed. Some major disturbance induced by individuals walking in the water next to the ADV is marked with a thick line in Figure 3-6A at the end of the record. For all field works, the velocity data exhibited disturbances, including large numbers of "spikes", that were not true, genuine turbulent velocities. For example, a lot of "noise" is seen in Figure 3-6 between t = 203,000 and 209,000 s probably caused by a combination of Doppler noise and aliasing errors. Some problem was also experienced with the vertical velocity component, possibly because of some wake effects caused by the stem. Since the probe was mounted vertically down-looking, vertical velocities were small and these effects were deemed negligible. Other disturbances were caused by navigation next to the probe sensors as illustrated in Figure 3-1D. CHANSON et al. (2005b) discussed further problems experienced during the earlier field studies.

In summary, past and present experiences suggested that turbulence properties could not be extrapolated from the unprocessed ADV data sets during the field works. Classical ADV "despiking" techniques were tested in-depth, especially the acceleration thresholding and phase-space thresholding methods. The results demonstrated systematically that "conventional" ADV despiking techniques were not suitable in a natural estuarine system (CHANSON et al. 2005b).

3.3.2 ADV data post-processing technique

In the present study, the post-processing technique of CHANSON, TREVETHAN and AOKI (2005b) was used systematically. A summary follows.

[8]In addition, the Sontek™ ADV and microADV systems provided a communication error flag for each sample.

The ADV signal post-processing includes three stages. That is (1) an initial velocity signal check, (2) the detection, elimination and replacement of large disturbances and (3) the treatment of small disturbances. Each stage comprises two steps: velocity error detection and data replacement.

(1) Velocity signal check

The ADV velocity data are "cleaned" by removing communication errors, low signal-to-noise ratio data (< 5 dB) and low correlation samples (< 60%). This stage may be performed by an industrial software (e.g. WinADV).

(2) Large event detection and replacement ("Pre-filtering")

The effects of major disturbances are eliminated and replaced. Such disturbances may include navigation, probe movement, aquatic life activities. For each velocity component, the signal is filtered with a low-pass/high-pass filter threshold F (F_{ref} = 0.1 Hz). The occurrence of navigation, probe motion and other events is tested on the high-pass filtered component by comparing the ratio of local standard deviation to the event search region standard deviation with a threshold value CE (CE_{ref} = 1.5). Exceedance implies disturbance. Note that local standard deviations are calculated for WS data points (WS_{ref} = 1000).

(3) Small disturbance detection and substitution ("Despiking")

The phase-space thresholding technique is used. For each velocity component, the signal is filtered with a low-pass/high-pass filter threshold F (F_{ref} = 0.1 Hz). The same frequency threshold F is used for "pre-filtering" and "despiking". The high-pass filtered signal is tested with an "universal" criterion (GORING and NIKORA 2002).

In Stages 1, 2 and 3, all erroneous data are replaced by the mean of the end points. This technique was selected for its simplicity, reliability and suitability to very-large data sets similar to present data records. Further it does not infer any trend. Replacement is performed on the velocity signal in Stage 2 and on the high-pass filtered signal in Stage 3. Stage 3 is iterated until the number of new errors in an iteration converges to zero. At the end of Stage 3, the low-passed filtered signals are added back in before further turbulence analysis. Further, all velocity components are considered erroneous if any one velocity component is replaced in Stages 1, 2 or 3. The justification is based upon the ADV transformation of radial velocities into Cartesian co-ordinates implying that a corrupted Cartesian velocity component must derive from corrupted radial components (e.g. McLELLAND and NICHOLAS 2000). In Stage 3, present experience and data analyses showed that the initial pre-filtering stage has a significant effect on the data sets. Further the acceleration thresholding technique was thoroughly tested with acceleration threshold criterion λ_a between 0.012 and 1.5. The technique was unsuited to the estuarine flow conditions, while the phase-space thresholding method appeared more robust.

Comments

Comparative analyses of un-processed, "despiked-only" and post-processed velocity data highlighted the necessity of such an advanced post-processing method. It was found that "conventional despiking" would accept a large amount of erroneous data points that would be otherwise removed and that could represent up to 12% of the entire data set (CHANSON et al. 2005b). The effect of the complete post-processing is illustrated in Figures and 3-6 and 3-7 where Figure 3-7 shows the post-processed velocity signal for the data shown in Figure 3-6.

While the acoustic Doppler velocimetry is a relatively simple technique, present results demonstrated that unprocessed ADV data could not be used to study the turbulence field, including time-averaged velocity components. It is acknowledged that further field data are necessary to validate in-depth the post-processing technique, by comparing post-processed data with independent data acquired simultaneously at the same location in the natural system. At present, the selection of more appropriate techniques is intricate since no independent data set (i.e. "true data set") is available. Comparisons between post-processing techniques are basically limited to an assessment of the number of removed spikes, and some subjective evaluation of differences in turbulent velocity properties.

Fig 3-6 - Acoustic Doppler velocimetry signal in Eprapah Creek - Study E6, 18 May 2005 between 07:33 and 10:37, 3D ADV (10 MHz) - Probe sensor location: 0.4 m above the bed - Raw unprocessed signals

(A) Unprocessed instantaneous streamwise velocity component V_X, positive downstream - Comparison with measured water depth

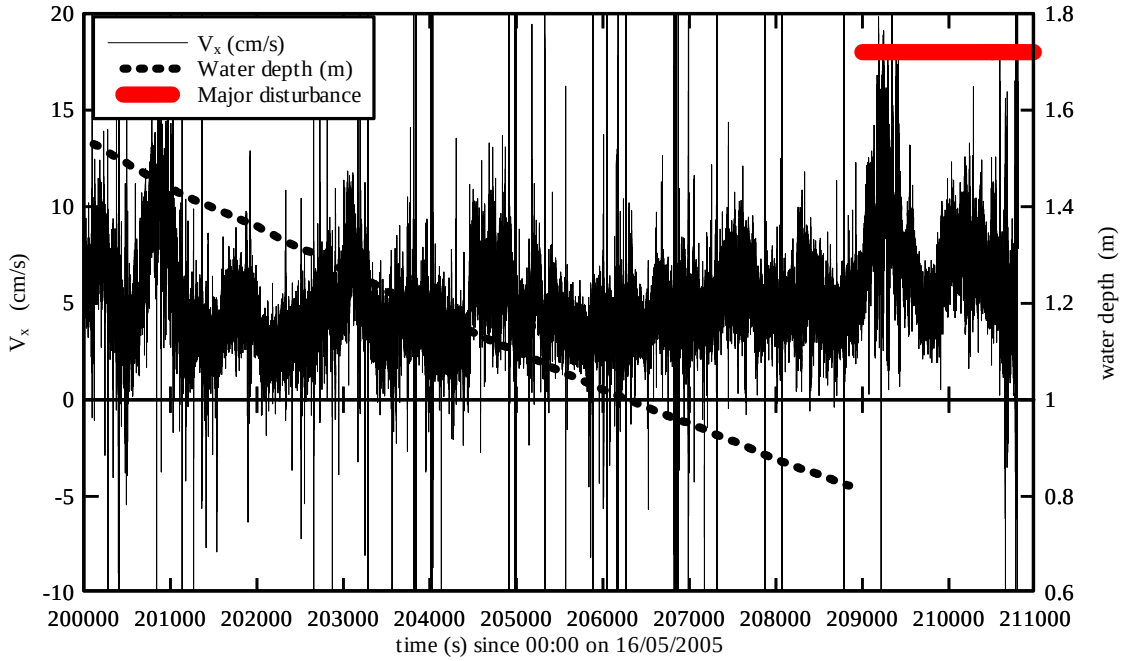

(B) Unprocessed instantaneous transverse velocity component V_y, positive towards the left bank

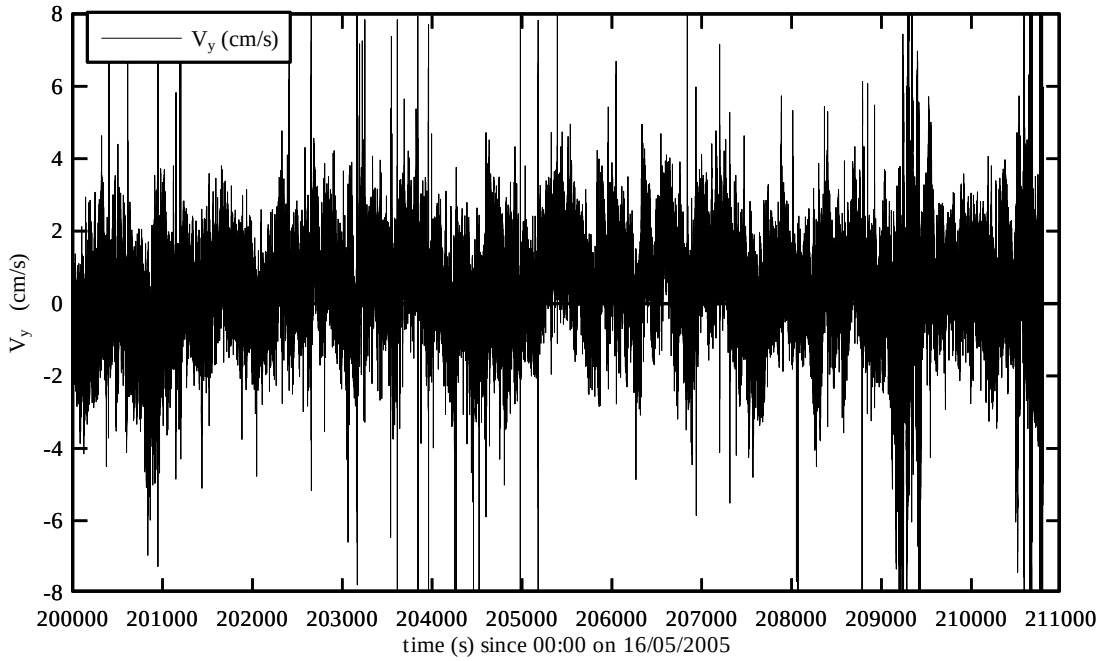

(C) Unprocessed instantaneous vertical velocity component V_Z, positive upwards

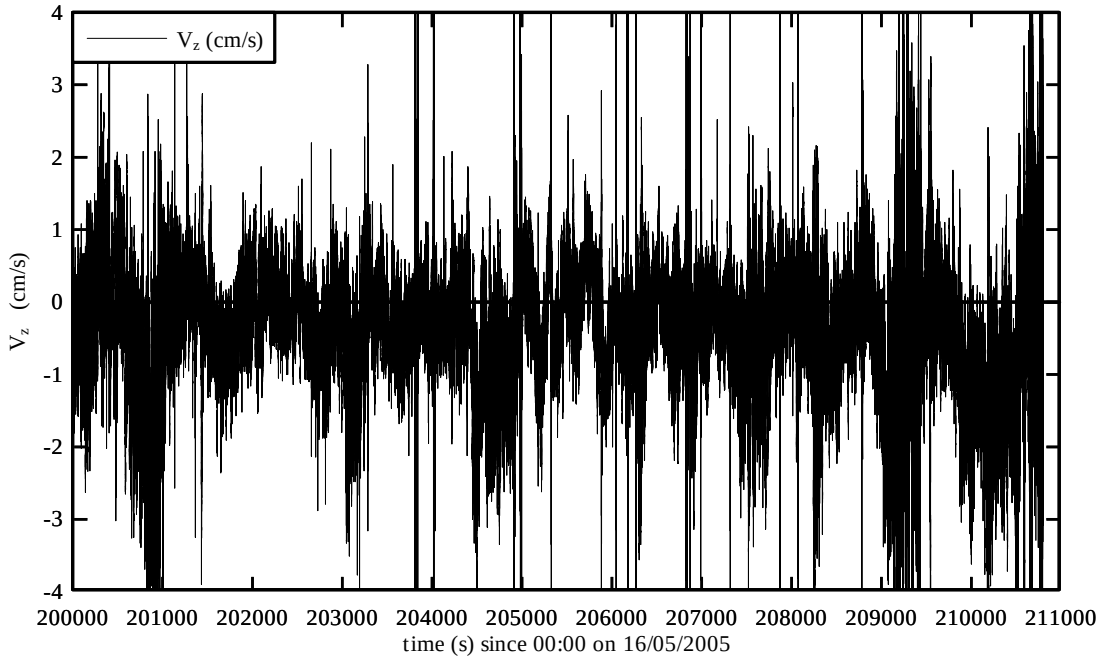

Fig 3-7 - Acoustic Doppler velocimetry signal in Eprapah Creek - Study E6, 18 May 2005 between 07:33 and 10:37, 3D ADV (10 MHz) - Probe sensor location: 0.4 m above the bed - Post-processed signals

(A) Post-processed instantaneous streamwise velocity component V_X - Comparison with measured water depth

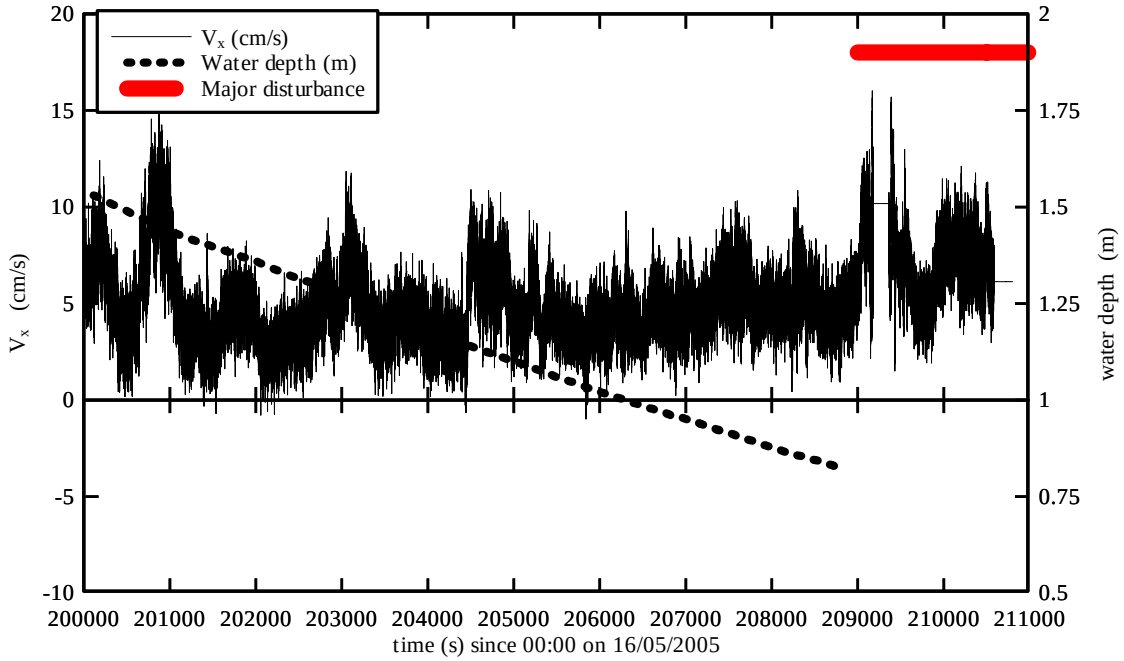

(B) Post-processed instantaneous transverse velocity component V_y

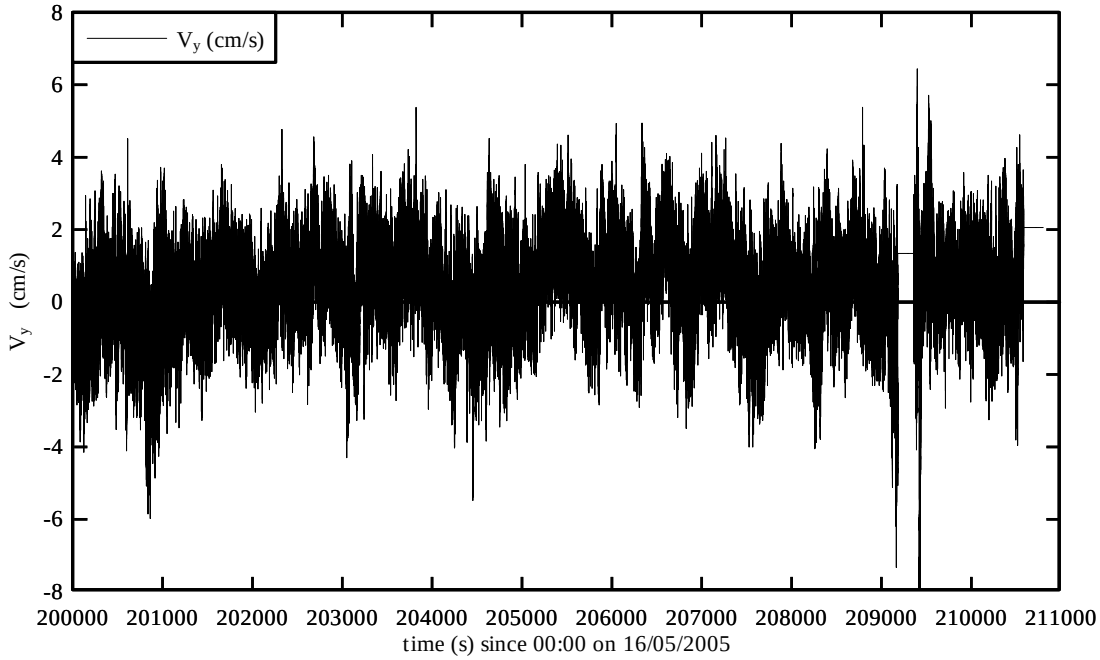

(C) Post-processed instantaneous vertical velocity component V_z

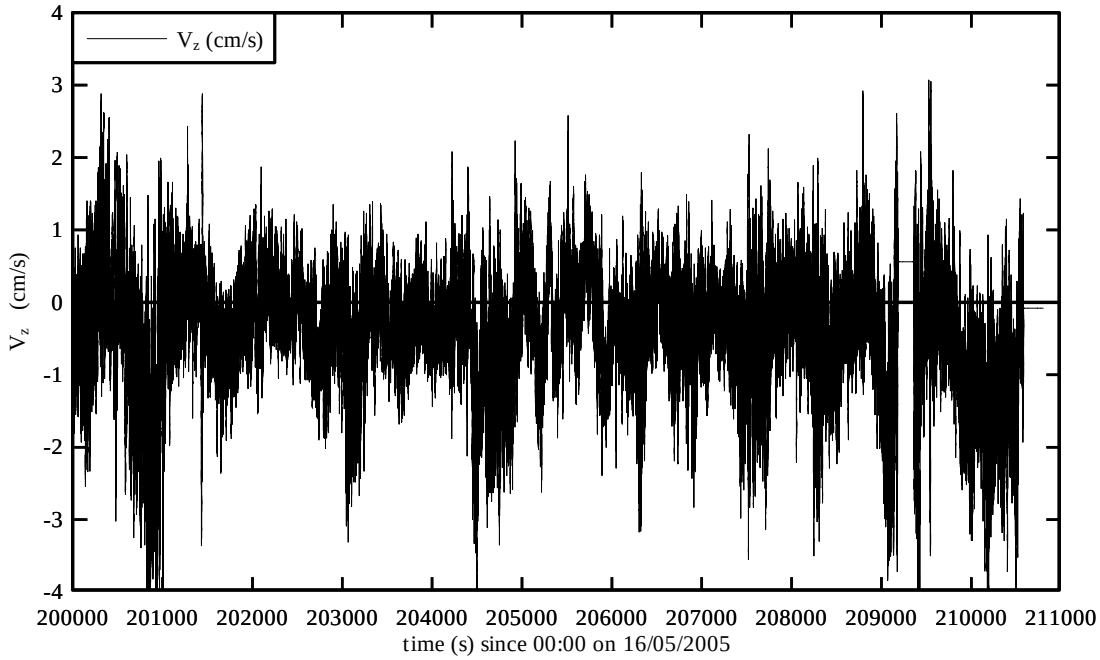

3.4 CALCULATIONS OF THE TURBULENCE PROPERTIES

The post-processed data sets included the three instantaneous velocity components V_X, V_Y and V_Z. A basic turbulence analysis yielded the four statistical moments of each velocity component, their respective dissipative and integral time scales, the tensor of instantaneous Reynolds stresses, and the statistical moments of the tangential Reynolds stresses.

The standard deviation characterises the magnitude of the fluctuations about a time-averaged mean. The skewness Sk and kurtosis Ku give some information regarding the temporal distribution of the

fluctuations around its mean value and its deviations from a Gaussian distribution. A non-zero skewness indicate some degree of temporal asymmetry of the turbulent fluctuations : e.g., acceleration versus deceleration, sweep versus ejection. The skewness retains some sign information and it can be used to extract basic information without ambiguity. A kurtosis ([9]) larger than zero is associated with a peaky signal : e.g., produced by intermittent turbulent events. Although turbulence is a random process, hence Gaussian, "the small departures from a Gaussian probability distribution are the most interesting features of the turbulence: for instance, the triple products like $\overline{v_x * v_x * v_y}$, which would be zero in a Gaussian process, are connected with energy transfer by the turbulence" (BRADSHAW 1971, p. 22).

3.4.1 Characteristic time scales

The normalised auto-correlation function R_{XX} of the x-velocity component is defined as :

$$R_{XX}(\tau) = \frac{R(v_X(t), v_X(t-\tau))}{v_X'^2} \qquad (3\text{-}1)$$

for a single-point measurement, where v is the instantaneous velocity fluctuation : $v = V - \overline{V}$, $\overline{V}$ is the time average velocity component, V is the instantaneous velocity, R is the covariance function, the subscript x refers to the x-velocity component, t is the time, v_X' is the standard deviation of the velocity component and τ is the time lag. Figure 3-8 presents a typical auto-correlation function.

The dissipation time scale may be estimated from the curvature of the auto-correlation function at $\tau = 0$. It is also called the Taylor micro scale. In the neighbourhood of $\tau = 0$, the shape of the auto-correlation function is about a parabola :

$$R_{XX}(\tau) \approx 1 - \left(\frac{\tau}{\tau_{Ex}}\right)^2 \qquad \tau \approx 0 \quad (3\text{-}2)$$

where τ_{EX} is the Eulerian dissipation time scale. τ_{EX} is a measure of the most rapid changes that occur in the fluctuations of $v_X(t)$ (Fig. 3-8). Indeed it is reasonable to expect a relationship between τ_{EX} and the highest frequencies occurring in the fluctuations. τ_{EX} is viewed as the smallest energetic time scale.

Using a Taylor series expansion of the auto-correlation function, the dissipation time scale may also be expressed as :

$$\tau_{Ex} = \sqrt{2 * \frac{v_X'^2}{\left(\frac{\partial v_X}{\partial t}\right)^2}} \qquad (3\text{-}3)$$

HALLBACK et al. (1989) and FRANSSON et al. (2005) used the above result to obtain a measured time scale $\tau_{EX}(\delta t)$ based upon the time increment δt :

$$\tau_{Ex}(\delta t) = \sqrt{2 * \frac{v_X'^2}{\left(\frac{\delta v_X}{\delta t}\right)^2}} \qquad (3\text{-}4)$$

[9]A common kurtosis definition is the Fisher kurtosis or excess kurtosis. For example, the kurtosis of the x-velocity component is defined as :

$$Ku(V_X) = \overline{v_X^4}/(v_X')^2 - 3$$

The calculation of $\tau_{Ex}^{(\delta t)}$ is repeated for several time increments δt. Following KOCH and CHANSON (2005), the results are fitted by a quadratic expression :

$$\tau_{Ex}^{(\delta t)} = \tau_{Ex} + a * \delta t + b * \delta t^2 \quad (3\text{-}5)$$

The above method is deemed a more accurate way to estimate τ_{Ex} than using Equation (3-2) especially when the smallest time increment δt ([10]) is larger than the dissipation time scale τ_{Ex} (HALLBACK et al. 1989, FRANSSON et al. 2005, KOCH and CHANSON 2005). The calculation is repeated for each velocity component V_x, V_y and V_z.
For the x-velocity component, the corresponding Eulerian integral time scale is defined as :

$$T_{Ex} = \int_{\tau=0}^{+\infty} R_{xx}(\tau) * d\tau \quad (3\text{-}6a)$$

T_{Ex} is a rough measure of the longest connection in the turbulent behaviour of $v_x(t)$. It is also called a macro time scale.
The integral time scale is related to the space integral scale Λ_f by :

$$\Lambda_f = \overline{V} * T_E \quad (3\text{-}7)$$

where $\overline{V}$ is the time averaged convective velocity. The integral scale Λ_f is a measure of the longest connection between the velocities at two points of the flow field (HINZE 1975, p. 43).
In the present study, the integral time scale integration was calculated between τ = and the first crossing of $R_{xx} = 0$:

$$T_{Ex} = \int_{\tau=0}^{\tau(R_{xx}(\tau)=0)} R_{xx}(\tau) * d\tau \quad (3\text{-}6b)$$

following PIQUET (1999).

Fig. 3-8 - Definition sketch of a velocity auto-correlation function

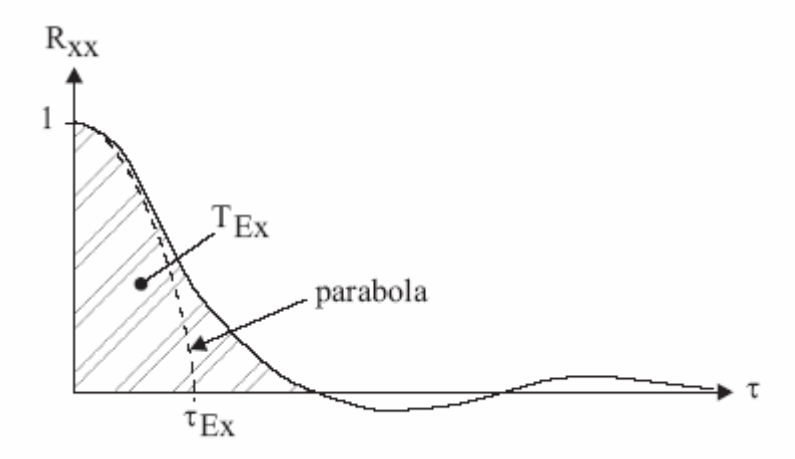

3.4.2 Reynolds stresses

The Reynolds stress tensor includes the normal stresses and the tangential stresses. The latter are usually negative. The Reynolds stresses are also called the turbulent stresses. The Reynolds stress describes a transport effect resulting from turbulent motion induced by velocity fluctuations with its

[10]The smallest time increment is a function of the scan rate F_{scan} : $\delta t_{scan} = 1/F_{scan}$.

subsequent increase of momentum exchange and of mixing (PIQUET 1999). Turbulent transport is a property of the flow.
Each instantaneous Reynolds stress may be defined as : $\rho * v_x * v_y$ and it is characterised by its four statistical moments including the time-averaged tangential stress $\rho * \overline{v_x * v_y}$ and its standard deviation $\rho * (v_x * v_y)'$ where ρ is the fluid density. In open channel flows, the skewness and kurtosis of the Reynolds stress fluctuations are large (NEZU and NAKAGAWA 1993, p.182).

3.4.3 Calculations of the velocity fluctuations

The turbulent velocity fluctuation v is defined as : $v = V - \overline{V}$ where $\overline{V}$ is a time average velocity component. When the flow is gradually time-variable, $\overline{V}$ is the low-pass filtered velocity component. $\overline{V}$ is sometimes called the variable-interval time average or VITA (PIQUET 1999). A cutoff frequency 1/T must be selected such that the averaging time T is greater than the characteristic period of fluctuations, and small with respect to the characteristic period for the time-evolution of the mean properties. The deviation of the instantaneous velocity from the ensemble average is the turbulent velocity fluctuation. Note that the upper limit of the filtered signal is the Nyquist frequency or Nyquist limit. It is the highest frequency that can be coded at a given sampling rate in order to recover all Fourier components of a periodic waveform. If the signal is sampled at 25 Hz, the highest frequency which can be expected to be present in the sampled signal is 12.5 Hz.
In natural systems such as an estuary, the selection of the cutoff frequency is a critical process. In the present study, all turbulence data were processed using samples that contain 5,000 data points (T = 200 s) every 10 s along the entire data sets of both field works E5 and E6. The sample size of 5,000 samples or 200 s was chosen to be much larger than the instantaneous velocity fluctuation time scales, to contain enough data points to yield statistically meaningful results, and to be considerably smaller than the period of tidal fluctuations.
In a study of boundary layer flows, FRANSSON et al. (2005) proposed to use a cutoff frequency F_{cut} for the high-pass filtering as :

$$F_{cut} = \frac{V_\infty}{5 * \delta_{99}} \qquad (3\text{-}8)$$

where V_∞ is the boundary layer free-stream velocity and δ_{99} is the (Blasius-based) boundary layer thickness. The above expression is naturally based upon the convective velocity V_∞ and the streamwise scale ($\propto \delta_{99}$) of the streaky structures (FRANSSON et al. 2005). In Eprapah Creek around mid-tide, Equation (3-8) would yield an averaging time $T \approx 1/F_{cut}$ that is close to the selected value of T = 200 s.
Lastly note that the statistical calculations were not conducted when more 20% of the 5,000 data points were found to be corrupted/repaired during the data post-processing (Section 3.3).

3. 5 DATA ACCURACY

The accuracy on the velocity measurements was 1%.
With the physio-chemistry probes YSI6920 and YSI6600, the data accuracy was : ±2% of saturation concentration for dissolved oxygen., ±0.5% for conductivity, ±0.15ºC for temperature, ±0.2 unit for pH, ±0.02 m for depth, ±1% of reading for salinity. The accuracy was ±5% for turbidity. Note that the turbidity spike fileter was on. No information was available on the data accuracy on chlorophyll levels.
The data accuracy of the Troll LTS9000 probes was ±0.1ºC for temperature, ±0.5% for conductivity and ±0.01 m for depth.

3.5.1 Clock synchronisation

At the start of each field work, the clocks of the physio-chemistry probes (YSI6600, Troll LTS9000) and of the ADV data acquisition computers were synchronised within one second with a GPS clock.

For the 16-18 May 2005 study, the clocks of the two ADV computers were synchronised at the start within 0.04 seconds. However it was observed that the synchronisation was erroneous by about 60 s within 24 hours.

3.5.2 Probe calibration

Both YSI6600 and YSI6920 probes were calibrated before and after each field trip. They gave identical results in water solutions of known properties.

The Troll LTS9000 probes were calibrated prior to and after the field work. They were also checked in-situ with the YSI6600 probe and a mercury thermometer in a large bucket field with creek water at the end of the field study.

3.6 PRACTICAL EXPERIENCE AND PROBLEMS

It must be emphasised again and again that a careful preparation of field works is essential and crucial. In particular, all the instrumentation must be thoroughly calibrated and tested beforehand. Redundant instrumentations must be used to double- and triple-check all the data. Manual readings are an essential part of field works. In the present studies, the air temperature and free-surface elevation were recorded manually every 15 minutes. In addition, a manual logbook must be continuously kept, with recordings of any flow features, atmospheric events, disturbances. Such a manual logbook is a necessary tool to complement the data post-processing. Herein manual entries included unusual front patterns during the flood tide, atmospheric conditions including rain and winds, navigation events, fish and bird activities around the probes, ADV signal problems ('spikes', 'noise' …).

With the ADV system, some problems were experienced with the vertical velocity component (Section 4). It is believed that the ADV emitter, stem and body created some wake which affected adversely the vertical velocity. Similar problems with the V_Z component were observed in earlier studies (e.g. CHANSON 2003, AOKI 2006, *Pers. Comm.*). Since the probe was mounted vertically with a down-looking head and the vertical velocities were small, the effects on the horizontal velocity components were deemed negligible.

Although the YSI6600 water quality probe was set to record data every 6 to 12 s, the data files indicated that a few points were not recorded (once every five minutes roughly), while some records were written twice. The problem was not critical because the data acquisition timing was accurate within 1/100th of a second. It increased the complexity of data processing and analysis, but it did not affect the accuracy of the data.

4. FIELD OBSERVATIONS

4.1 PRESENTATION

Two field investigations were conducted on 8-9 March 2005 (field work E5) and 16-18 May 2005 (field work E6) at Site 2B about mid-estuary of Eprapah Creek (Table 3-1). Figure 4-1 illustrates the channel cross-section at Site 2B with the respective high and low water levels. The transverse location of the acoustic Doppler velocimetry (ADV) system(s) is shown also. Table 4-1 summarises the tidal conditions.

Turbulence and physio-chemistry data are presented herein. For the velocity data, the streamwise component V_x is positive downstream, the transverse component V_y is positive towards the left bank and the vertical velocity component V_z is positive upwards. Section 4.2 presents the statistical moments of the velocity components and tangential Reynolds stresses, as well as turbulence intensities, correlation coefficients of Reynolds stresses, and turbulence time scales (integral and dissipation). The full data sets are reported in Appendices A and B for the field studies E5 (8-9 March 2005) and E6 (16-18 May 2005) respectively. A summary of the turbulence properties is presented in Appendix D. The ADV signal post-processing was discussed in Section 3.3. The techniques to calculate turbulent velocity fluctuations, Reynolds stresses and characteristic time scales were presented in Section 3.4.

The physio-chemistry data are presented in Section 4.3. Note that physio-chemistry data analysis was limited because the discharge data from the sewage treatment plant were not readily available.

Fig. 4-1 - Surveyed cross-section at Site 2B with high-tide and low-tide water levels on 9 March and 18 May 2005, looking downstream

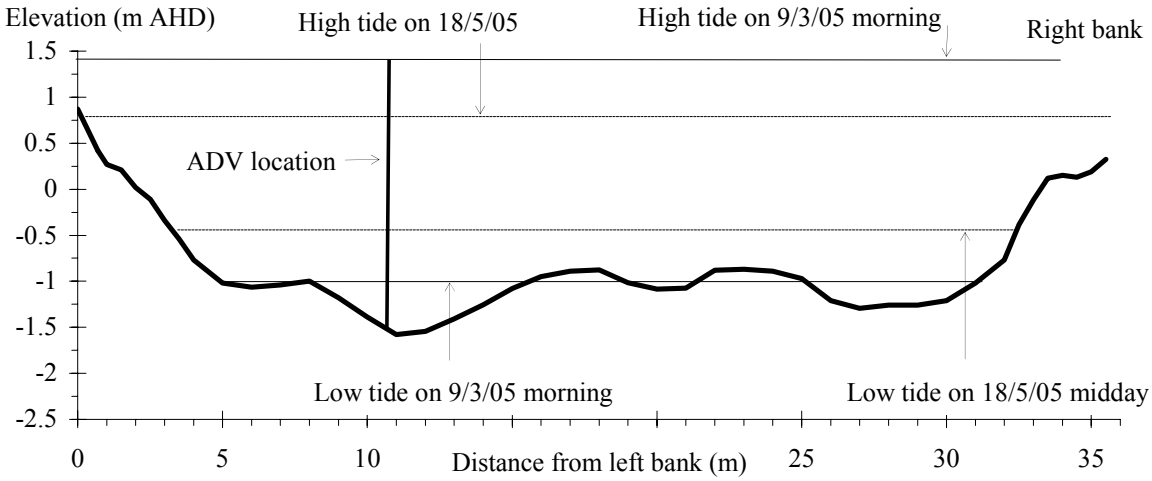

Table 4-1 - Summary of tidal conditions at Eprapah Creek in March and May 2005

Field study reference	E5	E6
Date	8-9 March 2005	16-17-18 May 2005
Tides (Victoria Point)	8 March 2005: 01:33 (0.54 m) 08:22 (2.72 m) 15:12 (0.55 m) 20:42 (2.12 m) 9 March 2005: 02:50 (0.42 m) 09:10 (2.79 m) 15:55 (0.46 m) 21:29 (2.25 m)	16 May 2005: 02:54 (2.19 m) 10:03 (0.97 m) 15:46 (1.67 m) 21:21 (1.06 m) 17 May 2005: 03:58 (2.17 m) 11:01 (0.90 m) 16:59 (1.77 m) 22:41 (1.04 m) 18 May 2005: 04:59 (2.17 m) 11:52 (0.81 m) 17:59 (1.93 m) 23:51 (0.96 m)
Study period	14:55 on 8 March 2005 to 16:00 on 9 March 2005	09:50 on 16 May 2005 to 10:36 on 18 May 2005

4.2 TURBULENCE DATA

4.2.1 Statistical moments of velocity data

Time-averaged streamwise velocity data indicated that the largest ebb and flood velocities occurred around the low tide during the field works E5 and E6. Note that the ADV sampling volumes were located at 0.1 m above the bed (E5) and at 0.2 m and 0.4 m above the bed (E6). Figure 4-2 shows the time-averaged streamwise velocity and water depth as functions of time at Site 2B during a tidal cycle for both field studies. The streamwise velocity maxima are obvious in Figure 4-2A (field study E5) around t = 95,000 to 97,000 s. The tidal range was large (2.37 m maximum tidal range, Table 3-1) and the spring tidal forcing generated large flow velocities. KAWANISI and YOKOSI (1994) observed similar maximum flood and ebb velocities around low tide during some field works in an estuarine channel in Japan (Table 1-1). Figure 4-2 shows further that the magnitude of the flood tide velocity was on average larger than the ebb tide velocity for both field works E5 and E6. Note that maximum time-averaged transverse velocities occurred also about low tide during both field works E5 and E6.

The velocity data showed multiple flow reversals around high tides. Figure 4-2B shows an example around high tide during the field work E6 between t = 50,000 and 65,000 s, where the time t is counted since 00:00 on 16/05/2005. During the field work E6, several flow reversals were also observed about low tides (Fig. 4-2B, between 75,000 and 80,000 s) although fewer than at high tides. Multiple flow reversals are discussed in more details in Section 5.2.

During the second tidal cycle of the field work E5, long episodes of velocity oscillations were observed, with periods of approximately 3 hours during the flood tide. Such large oscillation periods are seen in Figure 4-2A between t = 100,000 and 130,000 s. These had a noticeable effect on most turbulence parameters.

Figure 4-2 illustrates some low-frequency fluctuations of the streamwise velocity with periods between 20 minutes and 2 hours. These velocity oscillations were observed during both field studies and they included multiple flow reversals around slack periods and longer velocity oscillations around mid-tide. These long-period waves were possibly generated by some resonance caused by the tidal forcing interacting with the estuarine system geometry. Similar oscillations were reported in earlier field studies at Eprapah Creek (e.g. CHANSON 2003, pp. 19-23). These features were likely to affect the turbulence field in the estuary. For example, during the field study E6, the amplitude of the low-frequency velocity oscillations was about that of the tidal current (Fig. 4-2B).

That means that the rate of energy dissipation in bottom friction by the mean flow motion was about four times that of the tide alone ([1]).

Fig. 4-2 - Time-averaged streamwise velocity $\overline{V_X}$ (positive downstream) and water depth as functions of time during a tidal cycle - Data collected at Site 2B, Eprapah Creek during field work E5 (8-9 March 2005) and field work E6 (16-18 May 2005) - Time-averaged velocity data calculated for 5,000 data points every 10 s along the entire data set of both field works
Legend: [—] time-averaged streamwise velocity (cm/s); [—] water depth at site 2B; [ ] flood tide.

(A) Time-averaged streamwise velocity data collected 0.1 m above the bed during field work E5.

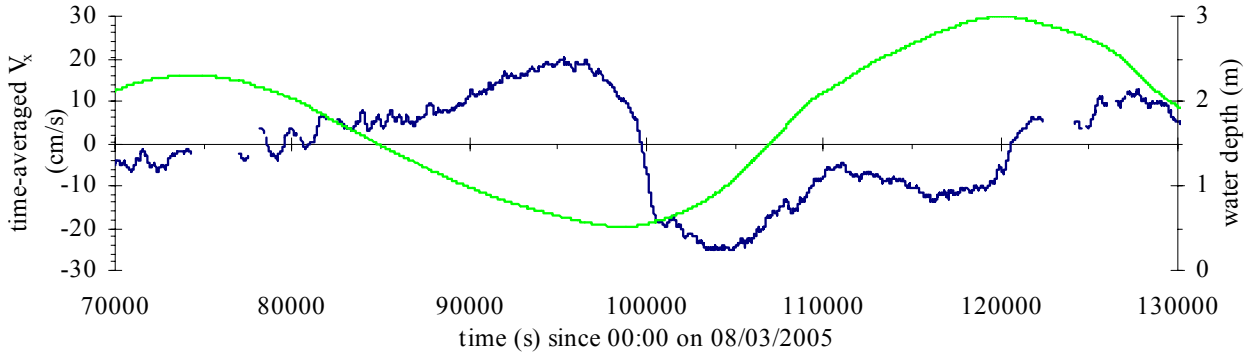

(B) Time-averaged streamwise velocity data collected 0.4 m above the bed during field work E6

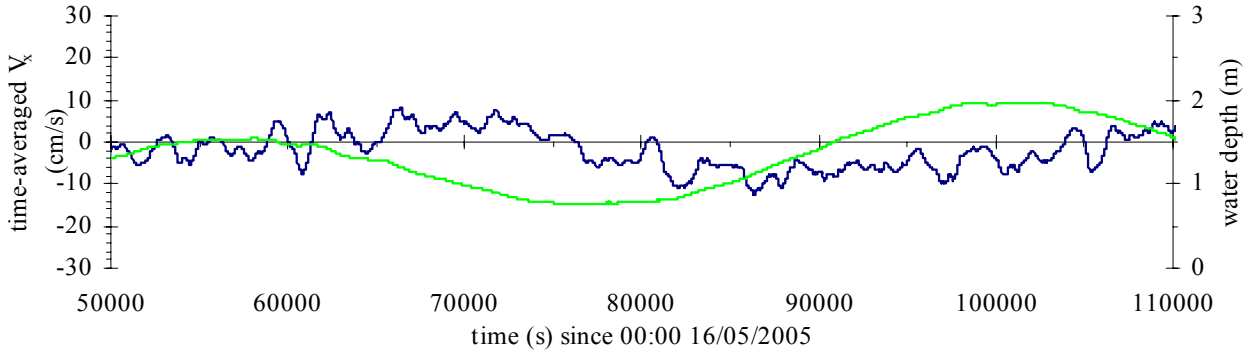

The direction of time-averaged transverse velocity $\overline{V_y}$ varied with the tide. Figure 4-3 shows the time-averaged transverse velocity $\overline{V_y}$ as a function of the time-averaged streamwise velocity $\overline{V_X}$ for the field works E5 and E6. In Figure 4-3, the transverse velocity was predominantly towards the outer river bend (i.e. positive towards left bank) during the ebb tide, while it was towards the river inner end (i.e. towards right bank) during the flood tide. The time-averaged transverse velocity was about zero around slack tides (i.e. $\overline{V_X} \approx 0$) during both field works E5 and E6 (Fig. 4-3).

Time-averaged vertical velocity $\overline{V_Z}$ data were negative (towards bed) at the beginning of the flood tide in both field works E5 and E6. This is illustrated in Figure 4-4. Figure 4-4 presents the time-averaged vertical velocity as a function of the time-averaged streamwise velocity for both field studies. Negative time-averaged vertical velocities were observed for the first half of the flood tide, and they were approximately zero for the remainder of the tidal cycle in both field works E5 and E6. These negative downward velocities are an anomaly that requires further investigation. As

[1]HINWOOD (2006, Pers. Comm.).

mentioned in Section 3.3, the observations of vertical velocity measured with the down-looking 3D ADV must be considered with caution (CHANSON 2003).

Fig. 4-3 - Time-averaged transverse velocity $\overline{V_Y}$ (positive towards left bank) as a function of the time-averaged streamwise velocity $\overline{V_X}$ (positive downstream) - Data collected at Site 2B, Eprapah Creek - Velocimeter : 3D ADV (10 MHz), Probe sensor position : 0.1 m above bed during field work E5 (8-9 March 2005) and 0.4 m above bed during field work E6 (16-18 May 2005) - Time-averaged velocities calculated for 5,000 data points every 10 s along the entire data set for each field study - Legend: [•] data collected during field work E5; [•] data collected during field work E6

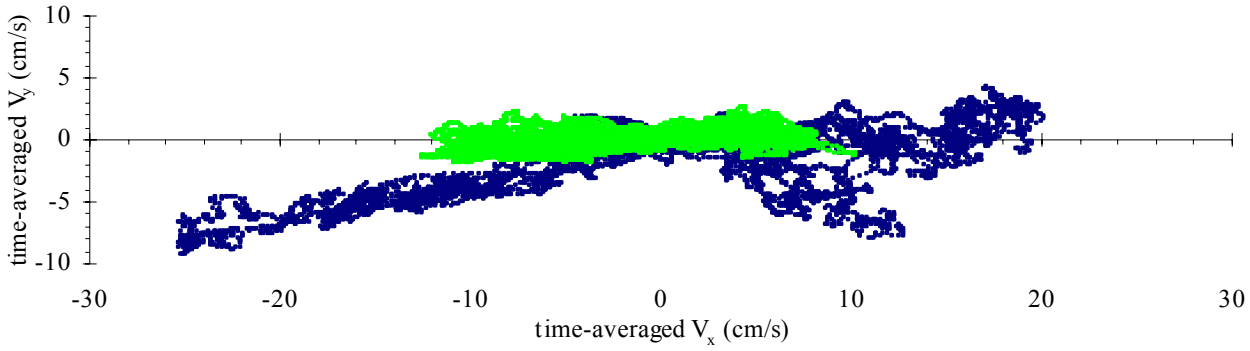

Fig. 4-4 - Time-averaged vertical velocity $\overline{V_Z}$ (positive upwards) as a function of the time-averaged streamwise velocity $\overline{V_X}$ (positive downwards) - Data collected at Site 2B, Eprapah Creek - Probe sensor position: 0.1 m above the bed for field work E5 (8-9 March 2005) and 0.4 m above the bed for field work E6 (16-18 May 2005) - Velocimeter : 3D ADV (10 MHz), Time-averaged velocity calculated for 5,000 data points every 10 s along the entire data sets of both field works
Legend: [•] data collected during field work E5; [•] data collected during field work E6

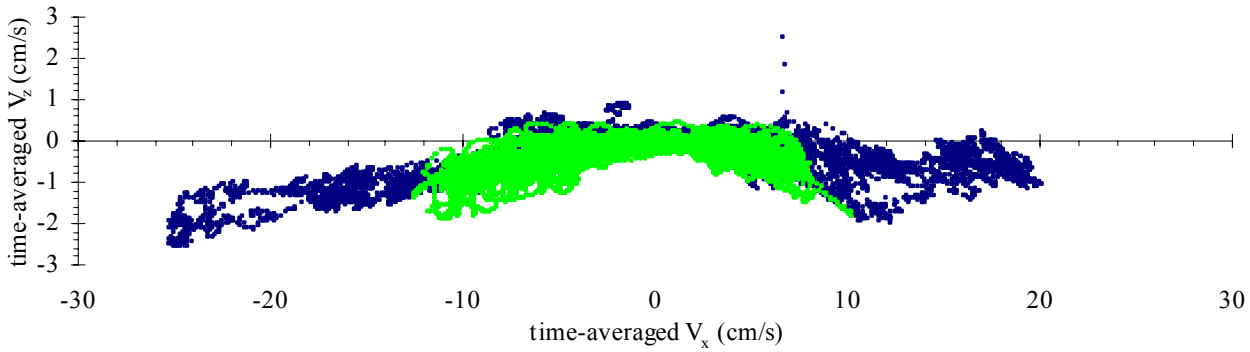

The standard deviation of the velocity represents the average magnitude of velocity fluctuations about a time-averaged mean. It is similar to a magnitude of turbulent velocity fluctuations. During the field works E5 and E6, the standard deviations of all velocity components were the largest during the flood tide, with standard deviations maxima occurring typically at the beginning of the flood tide. KAWANISI and YOKOSI (1994) reported similarly large turbulence fluctuations at the beginning of the flood tide next to the bed in an estuary of Japan. OSONPHASOP (1983) observed also larger turbulence fluctuations during the flood tide in a tidal channel in Australia (Table 1-1). Figure 4-5 shows the standard deviations of streamwise velocity v_X' as a function of time-averaged

streamwise velocity $\overline{V_X}$. Note the large standard deviations of streamwise velocity during the flood tide ($\overline{V_X} < 0$) for both field works (Fig. 4-5). The largest velocity standard deviations were typically observed at the beginning of the flood tide in shallow water depths (Fig. 4-5, grey/light symbols). The standard deviations of the horizontal velocity components v_X' and v_Y' were of a similar magnitude and they were approximately twice as large as the standard deviations of vertical velocity v_Z' for both field works. In Eprapah Creek, some strong correlation between streamwise velocity magnitude and velocity standard deviations was particularly obvious during spring tides (Fig. 4-5A, left handside).

During spring tides (field study E5), the standard deviations of all velocity components were typically three to four times larger than those for neap tides (field work E6). The larger velocity standard deviations were likely caused by the increased tidal forcing of the spring tide on 8-9 March 2005 and possibly by the lower ADV sampling position and the proximity of the bed. During the field work E6, the velocity standard deviations collected at 0.2 m above the bed (2D microADV 16 MHz) were slightly smaller than those recorded at 0.4 m above the bed (3D ADV 10 MHz). The difference may be the result of a combination of different instrumentation and sampling locations.

Fig. 4-5 - Standard deviations of streamwise velocity v_X' as a function of time-averaged streamwise velocity $\overline{V_X}$ (positive downstream) - Data recorded at 2B, Eprapah Creek - Velocimeter : 3D ADV (10 MHz), Probe sensor location: 0.1 m above the bed during field work E5 (8-9 March 2005) and 0.4 m above the bed during field work E6 (16-18 May 2005) - Standard deviations calculated for 5,000 data points every 10 s along the entire data set of both field works
Legend: [•] data collected throughout data set; [•] data during first half of flood tide.

(A) Standard deviations of streamwise velocity at 0.1 m above the bed during field work E5

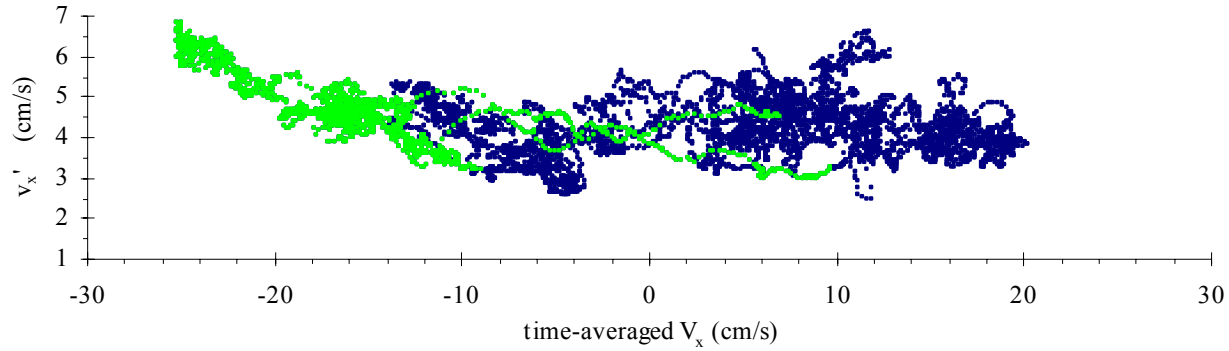

(B) Standard deviations of streamwise velocity at 0.4 m above the bed during field work E6

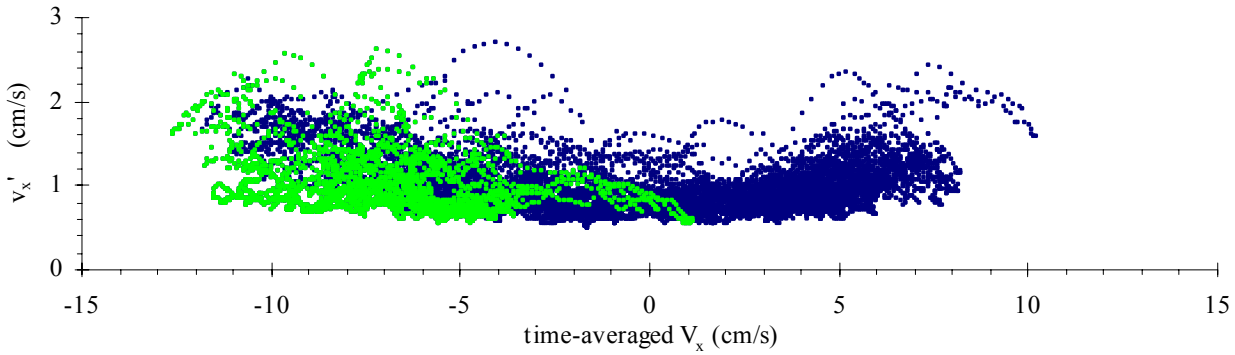

During both field works E5 and E6, the skewness and kurtosis of all velocity components fluctuated significantly. They exhibited characteristics that differed from expected skewness and kurtosis for a Gaussian distribution. For an infinite number of samples, the skewness and (excess) kurtosis of a Gaussian distribution are both zero. For a finite-size data set, the expected deviations for a Gaussian distribution are : $|Sk| < 4*\sqrt{15/N}$ and $|Ku| < 4*\sqrt{96/N}$, where N is the number of data points (PRESS et al. 1992). Skewness and kurtosis values within the above limits correspond to data sets with skewness and kurtosis close to those of a Gaussian distribution, while values outside the limits do not. An example is shown in Figure 4-6 where the kurtosis of the streamwise velocity is compared with the expected deviations (dashed lines) for a segment of the field study E5.
During the field work E6, the skewness and kurtosis magnitudes of all velocity components were systematically larger than those recorded during the field study E5. Some velocity data for the field work E6 exhibited negative kurtosis values that exceeded the Gaussian limits. The field work E5 data did not show these negative kurtosis periods (e.g. Fig 4-6). Overall most events during which the velocity component kurtosis exceeded the Gaussian limits were characterised by positive kurtosis values (field studies E5 and E6). Skewness values that exceeded Gaussian limits were evenly distributed between positive and negative skewness events. Samples which exhibited both skewness and kurtosis values outside of the expected Gaussian limits constituted 4% of all samples for V_x and V_y, and 12% of all V_z samples for the field work E5. For the study E6, between 12% to 26% of all samples presented both skewness and kurtosis values outside of the expected Gaussian distribution deviations, depending upon the instrumentation and velocity component.
For the field work E5 (spring tide), approximately 60 % of all samples showed skewness and kurtosis within the expected Gaussian range for all velocity components. During the field work E6 (neap tide), some differences in terms of skewness and kurtosis were observed between the data collected at 0.2 m above the bed and at 0.4 m above the bed. At 0.4 m above te bed, about 60 % of streamwise and transverse velocity samples had skewness and kurtosis within the expected Gaussian limits. At 0.2 m above the bed, only about 40 % of the velocity samples were within Gaussian limits in terms of skewness and kurtosis. The difference could be related to the different instruments.
For the field works E5 and E6, extended periods when values of skewness, kurtosis or both exceeded Gaussian limits appeared randomly dispersed. These extended periods did not seem to be related to the tidal cycle nor velocity amplitude. They may be considered as anomalies that may require further investigation.

Fig. 4-6 - Kurtosis values of streamwise velocity as a function of time (since 00:00 on 08/03/2005) - Data collected at Site 2B, Eprapah Creek - Velocimeter : 3D ADV (10 MHz), Probe sensor location: 0.1 m above the bed during field work E5 (8-9 March 2005) - Kurtosis values calculated for 5,000 data points every 10 s along entire data set
Legend: [——] kurtosis values of streamwise velocity; [– – –] kurtosis of Gaussian limits ($|Ku| < 4*\sqrt{96/N}$) for N = 5,000 data points

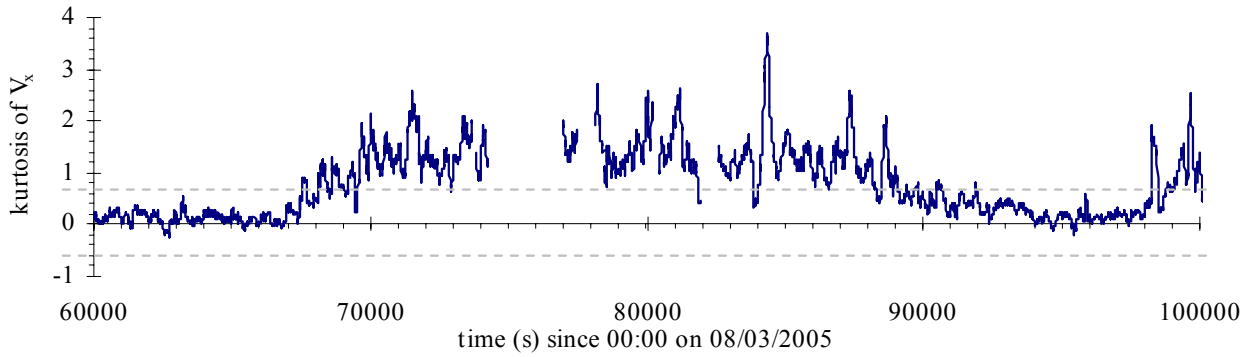

OSONPHASOP (1983) reported experimental measurements of turbulent velocity components in a tidal channel in Southern Australia. While he observed that the probability distribution functions of velocity fluctuations differed consistently from a Gaussian distribution, the skewness and kurtosis data were about one order of magnitude lower than present findings ([2]).
Figure 4-6 shows some kurtosis values of streamwise velocity data for a long period during which the kurtosis value exceeded the expected Gaussian distribution deviations. This anomaly commenced at approximately 18:00 (66,200 s) on 8 March 2005 until about 01:00 (90,000 s) on 9 March 2005. In Figure 4-6, the expected deviation from the Gaussian distribution ($|Ku| < 4*\sqrt{96/N}$) are shown in dashed lines, and it was exceeded for approximately seven hours. Note an absence of kurtosis data around 750,000 s. Statistical calculations were not performed when more than 20% of the data samples were corrupted/repaired during the data post-processing (Section 3.3).

Fig. 4-7 - Vertical turbulence intensity v_Z'/v_X' as a function of time-averaged streamwise velocity $\overline{V_X}$ (positive downstream) - Data collected at Site 2B, Eprapah Creek - Velocimeter : 3D ADV (10 MHz), Probe sensor location: at 0.1 m above the bed during field work E5 (8-9 March 2005) and at 0.4 m above the bed during field work E6 (16-18 May 2005) - Turbulence intensities calculated for 5,000 data points every 10 s along entire data set for both field works
Legend: [•] data collected during field work E5; [•] data collected during field work E6.

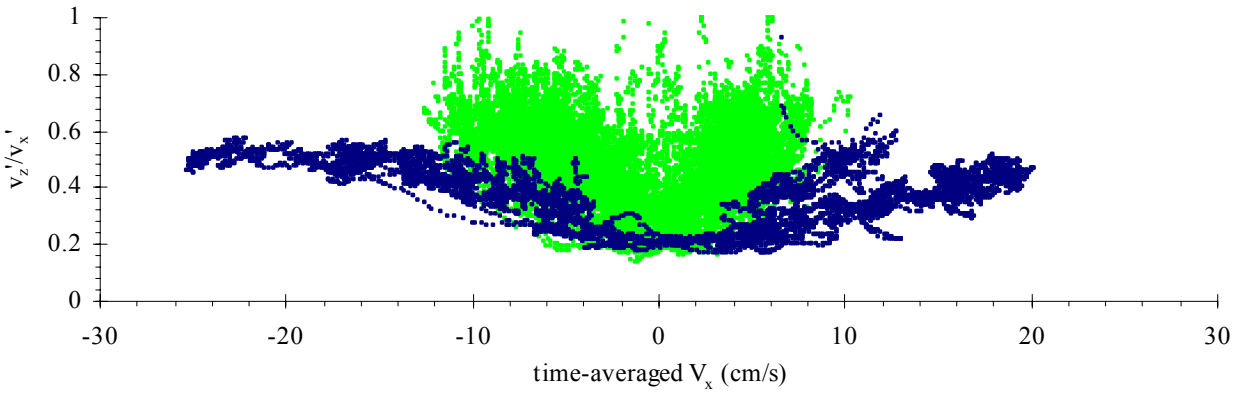

4.2.2 Turbulence intensity

The turbulence intensity is a dimensionless parameter characterising the turbulence structure as opposed to absolute values. The horizontal turbulence intensity v_y'/v_x' showed no discernable tidal trend, but the vertical turbulence intensity v_z'/v_x' presented some variations with tidal phase. The vertical turbulence intensity v_z'/v_x' increased with increasing streamwise velocity magnitude for both field works E5 and E6. Figure 4-7 shows the vertical turbulence intensity v_z'/v_x' as a function of time-averaged streamwise velocity for both field works. v_z'/v_x' tended to increase with increasing magnitude of the streamwise velocity $|\overline{V_X}|$, although the scatter of vertical turbulence intensity was larger during the field work E6 than during the field work E5. In both field works, the vertical turbulence intensities were of similar magnitude to some field work results by KAWANISI and YOKOSI (1994), and WEST and SHIONO (1988). Interestingly, the magnitude of vertical turbulence intensities were comparable with experimental measurements in turbulent open channel flows where $v_z'/v_x' = 0.5$ to 0.6 (NEZU and NAKAGAWA 1993**,** XIE 1988).
The horizontal turbulence intensities v_y'/v_x' for both field works were approximately twice as large as the vertical turbulence intensities implying some form of anisotropy. The horizontal turbulence

[2]Note that the present definition of kurtosis is in fact the excess kurtosis. OSONPHASOP (1983) listed raw kurtosis data.

intensity v_y'/v_x' was approximately equal to 1, indicating that turbulence fluctuations in the streamwise and transverse directions were of similar magnitude. They were higher than laboratory observations in straight prismatic rectangular channels which yielded : $v_y'/v_x' = 0.5$ to 0.7 (NEZU and NAKAGAWA 1993, KOCH and CHANSON 2005).

4.2.3 Statistical moments of tangential Reynolds stresses

The time-averaged tangential Reynolds stress $\rho*\overline{v_x*v_z}$ varied with the tide in both field works E5 and E6. Figure 4-8 illustrates the trend by showing the time-averaged Reynolds stress $\rho*\overline{v_x*v_z}$ as a function of time-averaged streamwise velocity. The magnitude of the time-averaged Reynolds stress $\rho*\overline{v_x*v_z}$ data was similar to the field data of OSONPHASOP (1983). Figure 4-8 shows also that the time-averaged Reynolds stress $\rho*\overline{v_x*v_z}$ was predominantly positive during the flood tide and predominantly negative during the ebb tide. The finding is consistent with the earlier results of OSONPHASOP (1983) and KAWANISI and YOKOSI (1994) in tidal channels. However, tidal trends in terms of time-averaged Reynolds stresses $\rho*\overline{v_x*v_y}$ and $\rho*\overline{v_y*v_z}$ were not discernable for field works E5 and E6.
The magnitudes of all time-averaged tangential Reynolds stresses were at least an order of magnitude larger during the field work E5 (spring tide) than those for the field work E6 (neap tide). The larger magnitude of Reynolds stresses during the field work E5 resulted from increased tidal forcing during the spring tide conditions. Note that, during the latter field work E6, the time-averaged Reynolds stress $\rho*\overline{v_x*v_y}$ were of similar magnitude at 0.2 m and 0.4 m above the bed.

Fig. 4-8 - Time-averaged Reynolds stress $\rho*\overline{v_x*v_z}$ as a function of time-averaged streamwise velocity - Data collected at Site 2B, Eprapah Creek - Velocimeter : 3D ADV (10 MHz), Probe sensor location : at 0.1 m above the bed during field works E5 (8-9 March 2005) and at 0.4 m above the bed during E6 (16-18 May 2005) - Time-averaged Reynolds stress calculated for 5,000 data points every 10 s along the entire data set of both field works
Legend: [•] data collected during field work E5; [•] data collected during field work E6

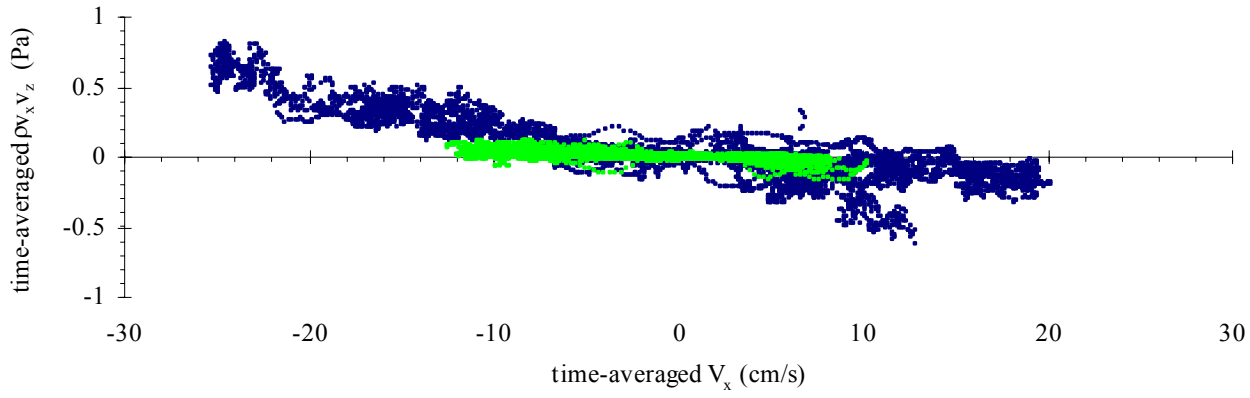

Fig. 4-9 - Standard deviations of tangential Reynolds stress $(\rho*v_X*v_Z)'$ as functions of time-averaged streamwise velocity (positive downstream) - Data collected at Site 2B, Eprapah Creek - Velocimeter : 3D ADV (10 MHz), Probe sensor location: at 0.1 m above the bed during field work E5 (8-9 March 2005) and at 0.4 m above the bed during field work E6 (16-18 May 2005) - Standard deviations calculated for 5,000 data points every 10 s along entire data set for both field works
Legend: [•] data collected during field work E5; [•] data collected during field work E6

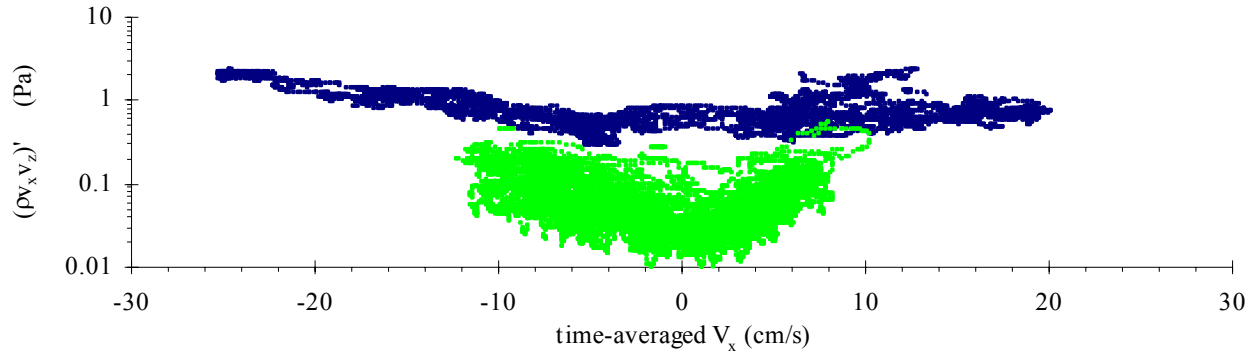

The standard deviations of tangential Reynolds stresses increased with increasing streamwise velocity. Figure 4-9 shows the standard deviations of $\rho*v_X*v_Z$ as functions of the time-averaged streamwise velocity for the field works E5 and E6. Note the logarithmic scale of the vertical axis (Fig. 4-9). The standard deviations of all tangential Reynolds stresses were the largest at the beginning of flood tide. The scatter of the standard deviations of Reynolds stress $\rho*v_X*v_Y$ was comparatively greater than the scatter of standard deviations of Reynolds stresses $\rho*v_X*v_Z$ and $\rho*v_Y*v_Z$. The magnitude of the standard deviations of all tangential Reynolds stresses during field work E5 were one order of magnitude greater than those observed during the field work E6 (Fig. 4-9). Again, it was likely that this was caused by the spring tidal forcing in the study E5 as opposed to the neap tidal forcing for the field work E6.

At the beginning of the flood tide during the field work E5, all skewness values of Reynolds stress $\rho*v_X*v_Z$ greatly exceeded the expected Gaussian distribution limits ($|Sk| < 4*\sqrt{15/N}$). This anomaly was not observed in terms of the skewness of the other tangential Reynolds stresses $\rho*v_X*v_Y$ and $\rho*v_Y*v_Z$ during the field work. During the field work E6, the skewness values of tangential Reynolds stresses were typically within the expected Gaussian distribution limits. The skewness values of Reynolds stress $\rho*v_X*v_Z$ showed trends related to the tidal cycle for both field works E5 and E6. The skewness of $\rho*v_X*v_Z$ was predominantly positive during the flood tide and predominantly negative during the ebb tide. During both field works E5 and E6, the skewness of the Reynolds stresses $\rho*v_X*v_Y$ and $\rho*v_Y*v_Z$ showed little discernable trends over the tidal cycle.

The kurtosis values of all tangential Reynolds stresses exceeded the expected Gaussian distribution limits ($|Ku| < 4*\sqrt{96/N}$) for both field works E5 and E6. Figure 4-10 shows some example with a logarithmic scale for the vertical axis. For the field work E5, the kurtosis values of all tangential Reynolds stresses increased about the slack tide: i.e., around zero streamwise velocity. A different trend for all tangential Reynolds stress kurtosis values occurred during the field work E6. The kurtosis values of Reynolds stress $\rho*v_X*v_Y$ collected with the 2D microADV (16 MHz) system at 0.2 m above the bed were the lowest at slack tide and increased with increasing streamwise velocity magnitude. Although less obvious, a similar trend for kurtosis values of all tangential Reynolds stresses recorded with the 3D ADV (10 MHz) unit at 0.4 m above the bed were observed during the field work E6. Figure 4-10 shows an example of the differences in tangential Reynolds stress kurtosis values between the field works E5 and E6. The different trends of kurtosis values of

tangential Reynolds stresses might be related to the different tidal forcing conditions
OSONPHASOP (1983) reported some experimental data in terms of skewness and kurtosis of tangential Reynolds stress $\rho*v_X*v_Z$. The present data were of similar order magnitude as OSONPHASOP's (1983) findings for both the skewness and kurtosis. Both data sets (OSONPHASOP's and present studies) demonstrated that the probability distribution functions of the tangential Reynolds stress $\rho*v_X*v_Z$ were not Gaussian.
A summary of all tangential Reynolds stress statistics is reported in Appendix D.

Fig. 4-10 - Kurtosis values of Reynolds stress $\rho*v_X*v_Z$ as functions of time-averaged streamwise velocity (positive downstream) - Data collected at Site 2B, Eprapah Creek - Velocimeter : 3D ADV (10 MHz), Probe sensor location: at 0.1 m above the bed during field work E5 (8-9 March 2005) and at 0.4 m above the bed during field work E6 (16-18 May 2005) - Kurtosis values calculated for 5,000 data points every 10 s along entire data set of both field works.
Legend: [•] data collected during field work E5; [•] data collected during field work E6; [– – –] expected deviations from Gaussian distribution limits ($|Ku| < 4*\sqrt{96/N}$)

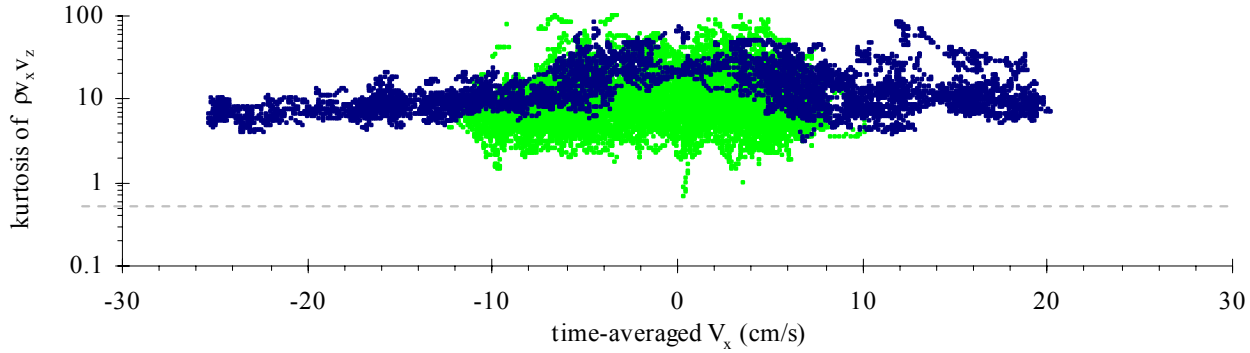

4.2.4 Correlation coefficient of tangential Reynolds stresses
The correlation coefficient of a tangential Reynolds stress is a dimensionless Reynolds stress. It is defined as : $R_{VXVZ} = \overline{v_X*v_Z}/(v_X'*v_Z')$. During field works E5 and E6, the coefficient of correlation R_{VXVZ} varied with the tidal cycle. Figure 4-11 presents the correlation coefficient R_{VXVZ} as a function of the time-averaged streamwise velocity for the field works E5 and E6. The data showed that the dimensionless tangential stress R_{VXVZ} was predominantly positive during the flood tide and predominantly negative during the ebb tide for both field works E5 and E6. A similar trend in terms of R_{VXVZ} was reported by KAWANISI and YOKOSI (1994) in an estuary in Japan.
In both field works E5 and E6, the values of the dimensionless Reynolds stress R_{VXVZ} were within the range of observed values reported in other estuarine studies by KAWANISI and YOKOSI (1994), WEST and ODUYEMI (1989) and WEST and SHIONO (1988). They were also similar to those obtained in flume experiments by NEZU and NAKAGAWA (1993).
Figure 4-11 shows that the magnitude of the Reynolds stress correlation coefficient R_{VXVZ} for field works E5 and E6 was greater during the flood tide than during the ebb tide. This asymmetry between flood and ebb tide, with larger magnitudes of dimensionless Reynolds stress during the flood tide, were also reported by KAWANISI and YOKOSI (1994).
The correlation coefficients of Reynolds stresses R_{VXVY} and R_{VYVZ} showed no simple tidal trend during the field works E5 or E6. Note however that the scatter of all Reynolds stress correlation coefficients were greater during the field work E6 than those for the field work E5.

Fig. 4-11 - Correlation coefficient of tangential Reynolds stress R_{VXVZ} as a function of time-averaged streamwise velocity (positive downstream) - Data collected at Site 2B, Eprapah Creek - Velocimeter : 3D ADV (10 MHz), Probe sensor location: at 0.1 m above the bed during field work E5 (8-9 March 2005) and at 0.4 m above the bed during field work E6 (16-18 May 2005) - Correlation coefficients of Reynolds stress calculated for 5,000 data points every 10 s along the entire data set from both field works - Legend: [•] data collected during field work E5; [•] data collected during field work E6

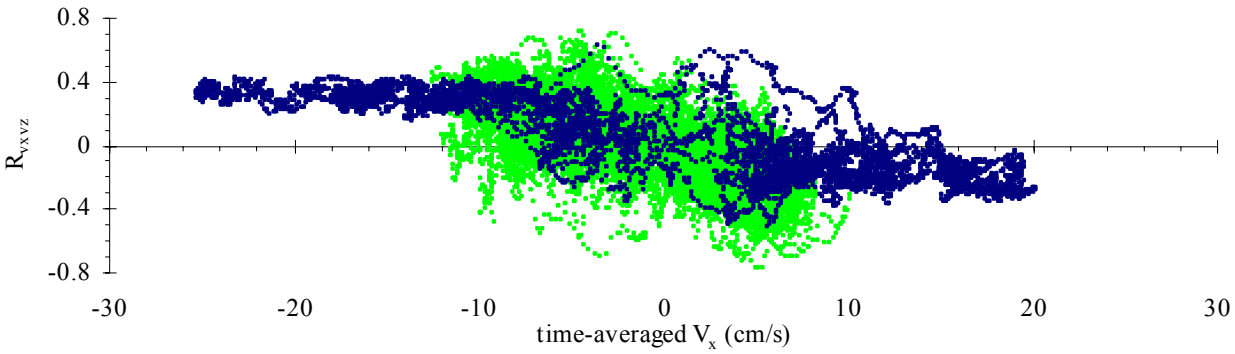

4.2.5 Turbulence time scales

4.2.5.1 Integral time scales

The integral time scale of a velocity component is a measure of the longest connection in the turbulent behaviour of that velocity component. For the field works E5 and E6, the integral time scales of all velocity components varied over the tidal cycle. Figure 4-12 presents the integral time scale of the streamwise velocity as a function of time-averaged streamwise velocity $\overline{V_X}$ for field works E5 and E6. Note the logarithmic scale of the vertical axis.

The integral time scales of streamwise velocity T_{EX} were larger during the flood tide than during the ebb tide for both field works. Figure 4-12 shows that the streamwise integral time scales increased with increased streamwise velocity during both field works. However, during the field work E5, the integral time scale seemed to reach a maximum as the streamwise velocity exceeded a certain magnitude of approximately 15 cm/s. Figure 4-12 illustrates further that the streamwise integral time scales could be up to two orders of magnitude smaller during the slack tide periods around zero streamwise velocity.

The maxima of streamwise integral time scales for the field work E5 (spring tide) were smaller than those during the field work E6 (neap tide). For the field work E6, the integral time scale maxima recorded at 0.2 m above the bed were greater than those recorded 0.4 m above the bed.

Streamwise integral time scales were largest at the beginning of the flood tide and smallest at the beginning of the ebb tide for both field works E5 and E6. The integral time scales of streamwise velocity decreased during the end of the flood tide and increased during the last section of the ebb tide.

Transverse integral time scale maxima appeared to be affected by the magnitude of tidal velocity. The largest transverse integral time scales were recorded in the sampling volume located at 0.2 m above the bed during the field work E6 and the smallest transverse time scales were observed for the largest velocity magnitudes during the field work E5.

Fig. 4-12 - Integral time scales of streamwise velocity as functions of time-averaged streamwise velocity $\overline{V_X}$ (positive downstream) - Data collected at Site 2B, Eprapah Creek - Velocimeter : 3D ADV (10 MHz), Probe sensor location : at 0.1 m above the bed during field work E5 (8-9 March 2005) and at 0.4 m above the bed during field work E6 (16-18 May 2005) - Integral time scales calculated over 5,000 data points every 10 s along entire data set for both field works.
Legend: [•] data collected during field work E5; [•] data collected during field work E6

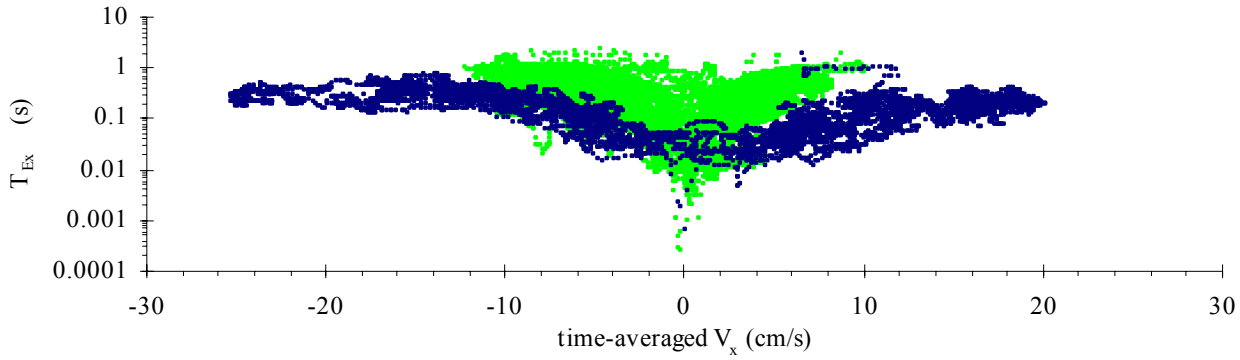

Some differences in transverse integral time scales calculated from data recorded on the 2D microADV (16 MHz) and the 3D ADV (10 MHz) were observed. Figure 4-13 shows the integral time scales of transverse velocity as functions of time-averaged streamwise velocity at 0.2 m and 0.4 m above the bed for the field work E6. Data recorded with the 2D microADV system (0.2 m above the bed in field work E6) indicated transverse integral time scale maxima about slack tide with time scales decreasing with increasing streamwise velocity. The data recorded by the 3D ADV unit (0.4 m above the bed field work E6) yielded transverse integral time scale minima about slack tide and increasing integral time scales with increasing streamwise velocity. Note that the transverse integral time scales at 0.1 m above the bed during field work E5 with the 3D ADV (10 MHz) exhibited similar tidal trends to data measured on the same 3D ADV at 0.4 m above the bed during field work E6. At present it is not known whether this problem was related to the instrumentation or to some flow condition differences.

Fig. 4-13 - Integral time scales of transverse velocity as functions of time-averaged streamwise velocity (positive downstream) - Data collected at Site 2B, Eprapah Creek - Probe sensor location: at 0.2 m above the bed and 0.4 m above the bed during field work E6 (16-18 May 2005) - Integral time scales calculated over 5,000 data points every 10 s along entire data set for both field works - Legend: [•] data collected at 0.2 m above the bed during field work E6; [•] data collected at 0.4 m above the bed during field work E6.

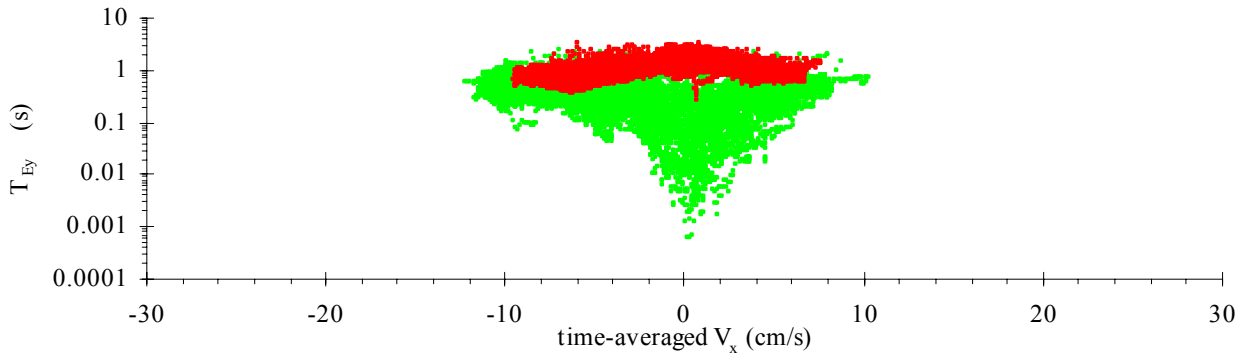

Vertical velocities were recorded at 0.1 m above the bed during the field work E5 and at 0.4 m above the bed in the field work E6. Figure 4-14 presents the resulting integral time scales T_{EZ} as functions of time-averaged streamwise velocity for both field works. In Figure 4-14, the smallest vertical integral time scales were observed around slack tide. The vertical integral time scales maxima were smaller for field work E5 than those of field work E6. Figure 4-14 shows also that the slack tide vertical integral time scales were at least an order of magnitude smaller during field work E5 than those of field work E6.
Present integral time scale data were about one order of magnitude greater than the integral time scale data of OSONPHASOP (1983) observed in a tidal channel in Southern Australia. The differences may be a combination of different bathymetry and instrumentation (Table 1-1, columns 2 and 3). The present study was conducted in a narrower channel with a more sophisticated velocimetry system and a faster data acquisition.

Fig. 4-14 - Integral time scales of vertical velocity as functions of time-averaged streamwise velocity (positive downstream) - Data collected at Site 2B, Eprapah Creek - Velocimeter : 3D ADV (10 MHz), Probe sensor location: at 0.1 m above the bed during field work E5 (8-9 March 2005) and at 0.4 m above the bed during field work E6 (16-18 May 2005) - Integral time scales calculated over 5,000 data points every 10 s along entire data set for both field works.
Legend: [•] data collected during field work E5; [•] data collected during field work E6.

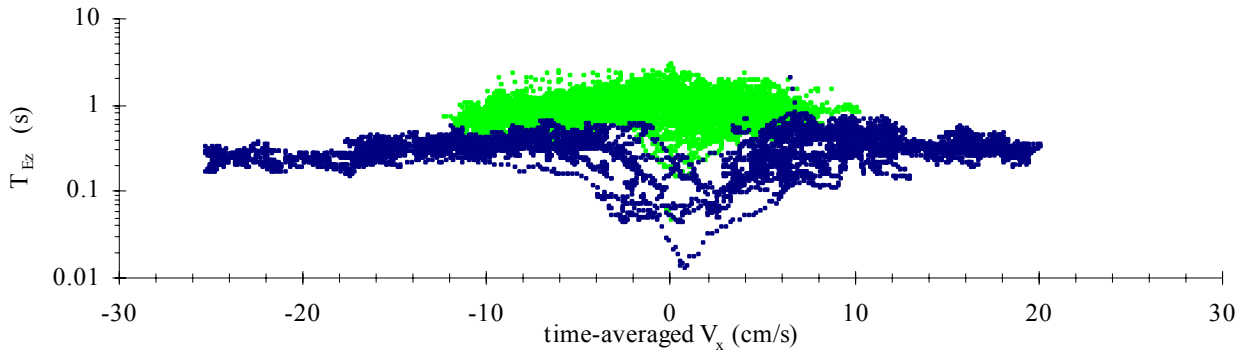

4.2.5.2 Dissipation time scales
The dissipation time scale, also called Taylor micro scale, is a measure of the most rapid changes that occur in the fluctuations of a velocity component. Physically the Taylor micro scale τ_E is a characteristic timescale of the smaller eddies which are primary responsible for the dissipation of energy. Dissipation time scales of the streamwise and transverse velocities did not vary much with the tide during both field works E5 or E6. They were typically about 0.002 to 0.02 s for both field works.
The dissipation time scales of the vertical velocity τ_{EZ} tended to vary over the tidal cycle. Figure 4-15 shows the vertical dissipation time scale as a function of the time-averaged streamwise velocity for the field works E5 and E6. Note the logarithmic scale of the vertical axis. In Figure 4-15, the vertical dissipation time scales increased by approximately an order of magnitude as the streamwise velocity increased for both field works. The scatter of dissipation time scales was the greatest for the field work E6.
The dissipation time scales were consistently smaller than the time between two consecutive samples (i.e. $1/F_{scan}$ = 0.04 s). The findings indicate that high-frequency sampling must be required with sampling rates of at least 25 to 50 Hz or more. Slower sampling rates would yield turbulence properties that ignore a range of eddy time scales relevant to the dissipation processes. Lastly, since the sampling frequency was not fast enough, calculated dissipation time scale values were only estimates of the "true" dissipation time scales (Section 3.4). It was difficult therefore to assess accurately the cause of differences in time scales between vertical and horizontal time scales.

4.2.5.3 Discussion

For both field studies, the dimensionless transverse and vertical integral time scales were respectively: T_{Ey}/T_{Ex} ~ 1 and T_{Ez}/T_{Ex} ~ 2 to 3. In a tidal channel in Southern Australia, OSONPHASOP (1983) observed T_{Ey}/T_{Ex} ~ 1.7 and T_{Ez}/T_{Ex} ~ 2.2 for z/d = 0.1 to 0.6 (i.e. between 1 and 6 m above the bed).

For the field studies E5 and E6, the dimensionless transverse and vertical dissipation time scales were respectively: τ_{Ey}/τ_{Ex} ~ 1 and 4 for the 3D ADV (10 MHz) and 2D microADV (16 MHz) systems respectively, and τ_{Ez}/τ_{Ex} ~ 4 to 7 (3D ADV (10 MHz)). The discrepancy between the ADV and microADV results might be a combination of different instrumentation, probe sensor location and local bed topography (e.g. rock or boulder).

During the field work E6, some cross-correlation between the two velocimeters was not conducted because of difficulties in synchronisation (Section 3.5.1). Some estimates of the space integral scales were derived from Equation (3-7) :

$$\Lambda_{fx} = \overline{V_x} * T_{Ex} \quad (4\text{-}1a)$$

$$\Lambda_{fy} = \overline{V_x} * T_{Ey} \quad (4\text{-}1b)$$

$$\Lambda_{fx} = \overline{V_x} * T_{Ex} \quad (4\text{-}1c)$$

where $\overline{V_x}$ is the time averaged convective velocity. The integral scales are some measures of the longest connection between the velocities at two points of the flow field (HINZE 1975).

Applications of Equation (4-1) to both field studies give some horizontal integral length scales between 0.5 and 10 cm while the vertical integral length scales were about 2 to 10 cm. The results may be used as a guide for suitable separation distances between velocimeter control volumes in future field works.

Fig. 4-15 – Dissipation time scales of vertical velocity as functions of time-averaged streamwise velocity (positive downstream) - Data collected at Site 2B, Eprapah Creek - Velocimeter : 3D ADV (10 MHz), Probe sensor location: at 0.1 m above the bed during field work E5 (8-9 March 2005) and at 0.4 m above the bed during field work E6 (16-18 May 2005) - Dissipation time scales averaged over 5,000 data points every 10 s along entire data set for both field works.
Legend: [•] data collected during field work E5; [•] data collected during field work E6.

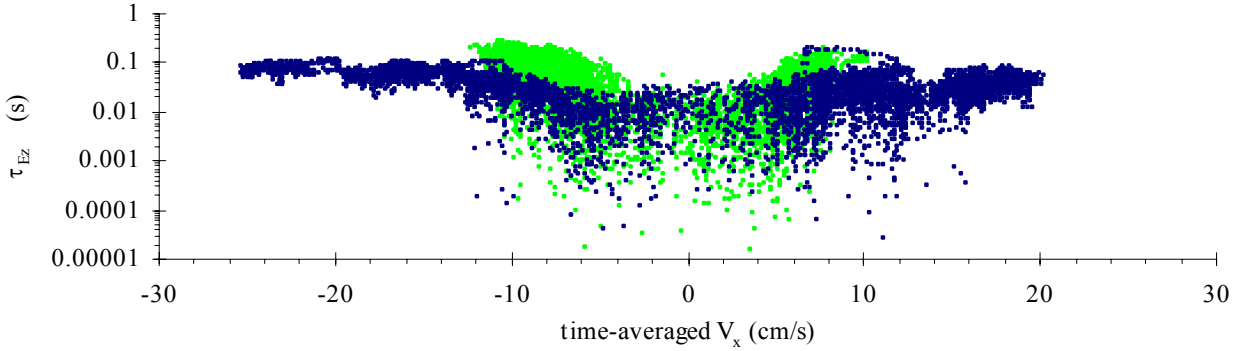

4.3 PHYSIO CHEMISTRY RESULTS

4.3.1 Physio-chemistry point measurements with the YSI6600 probe

Water temperature and conductivity data were collected continuously by the YSI6600 probe during

both field works. The probe sensors were located 0.3 m beside the 3D ADV sampling volume for both field works. That is, the YSI6600 probe sensors were 0.1 m above the bed and 0.4 m above the bed for the field studies E5 and E6 respectively. The results herein describe the variation of physio-chemistry parameters over the investigation period and provide some information on the main driving factors. Air temperature and water depth at Site 2B Eprapah Creek were used to outline some external factors that affected the physio-chemistry data.
Changes in conductivity seemed to be driven primarily by the variation of the tide for both field works E5 and E6. Figure 4-16 shows the conductivity as a function of relative depth z/d where z is the height of probe sensor above the bed and d is the measured water depth at Site 2B. The conductivity range during the field work E5 was larger than that for the field work E6, possibly because of the greater tidal range during the field study E5. Conductivity maxima were larger during the field work E5 because of the increased penetration of the tidal front from spring tidal forcing. Conductivity maxima were approximately 56 mS/cm during the study E5, while, during the field work E6, the conductivity maxima were approximately 50 mS/cm. Minima of water conductivity were approximately 44 mS/cm for both field works. Small oscillations in conductivity were observed throughout the field work E6 and during the first ebb tide of field work E5.
The water temperature was predominantly controlled by the air temperature, the time of day and the ebb/flood phase in both field works E5 and E6, as previously observed during earlier field studies in the estuary. Figure 4-17 presents the water temperature as a function of relative depth z/d for both studies. Small oscillations in water temperature were observed during the ebb tides of field work E5 and throughout most of field work E6. These small fluctuations in water temperature and conductivity exhibited periods of up to 90 minutes. They are difficult to comprehend at present due to unavailability of discharge and temperature data from the sewage treatment plant upstream of Site 2B. Without effluent discharge data, the influence of the discharge on physio-chemistry cannot be determined and further discussion would be speculative.

4.3.2 Simultaneous cross-sectional measurements of physio-chemistry

During the field work E6, additional physio-chemistry data were collected simultaneously across the creek at Site 2B. Water temperature, conductivity and water level data were collected every 6 s by six LTS9000 probes at several transverse distances from the left bank. Table 4-2 lists the elevations above the bed and transverse locations across the cross-section of the six LTS9000 probes and of the YSI6600 probe. Figure 4-18 shows a sketch of the channel cross-section looking downstream with the respective positions of the probes.
The water conductivity and temperature data were consistent with the YSI6600 probe point measurement data discussed in Section 4.3.1. At certain periods, during the field work E6, large differences in water temperature across the cross-section were observed. For other periods, the water temperature measurements were nearly identical for all probes. These cross-sectional differences in water temperature appeared to occur predominantly about low tide, although other "random" events were observed. Several unusually large changes in water temperature occurred across the cross-section during the investigation period.
One such event with unexplained variations in water temperature occurred between 125,000 s (12:00 on 17/05/2005) and 135,000 s (15:00 on 17/05/2005), where the time is counted since midnight (00:00) on 16/05/2005. Figure 4-19 shows water temperature and conductivity as functions of time for the entire data set. For the event between t = 125,000 and 135,000 s, Figure 4-19 illustrates that the water temperature increased and the conductivities decreased throughout the cross-section. The magnitude of changes in water temperature and conductivity depended upon the sampling position in the cross-section. Anomalously low water temperatures were recorded by the probes LTS-1 and LTS-4 which were closest to the bed, while anomalously high temperatures were recorded next to the surface (probes LTS-A and LTS-B). Note also that the air temperature rose to a maximum around 125,000-135,000 s when the tide was as its lowest, facilitating warming of the water. The observed stratification could be caused directly to the upper layers of water being heated

from above or to the warmer water rising and cooler water settling near the bed ([3]). Note, however, that some navigation took place at Site 2B after 135,000 s (13:30 on 17/05/2005), and these had no direct influence on the anomaly.

Fig. 4-16 - Conductivity as a function of relative depth z/d for field works E5 and E6 - Data collected by YSI6600 probe at Site 2B, Eprapah Creek every 6 s at 0.1 m above the bed for field work E5 (8-9 March 2005) and every 12 s at 0.4 m above the bed during field work E6 (16-18 May 2005).
Legend: [•] data collected during field work E5; [•] data collected during field work E6.

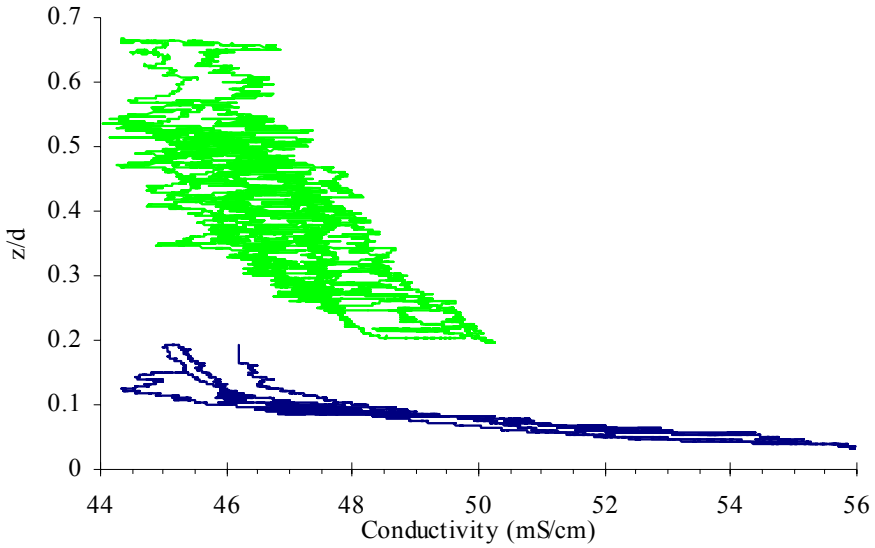

Fig. 4-17 - Water temperature as a function of relative depth z/d for field works E5 and E6 - Data collected by YSI6600 probe at Site 2B, Eprapah Creek every 6 s at 0.1 m above the bed for field work E5 (8-9 March 2005) and every 12 s at 0.4 m above the bed during field work E6 (16-18 May 2005).
Legend: [•] data collected during field work E5; [•] data collected during field work E6.

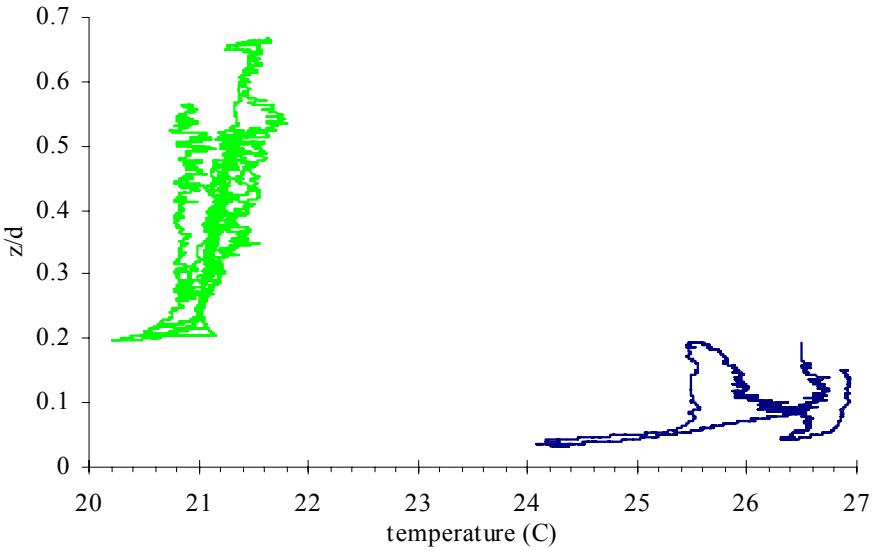

[3]HINWOOD (2006, Pers. Comm.).

Fig. 4-18 - Cross-sectional locations of physio-chemistry sampling volumes at Site 2B during the field study E6 (16-18 March 2005) - Looking downstream

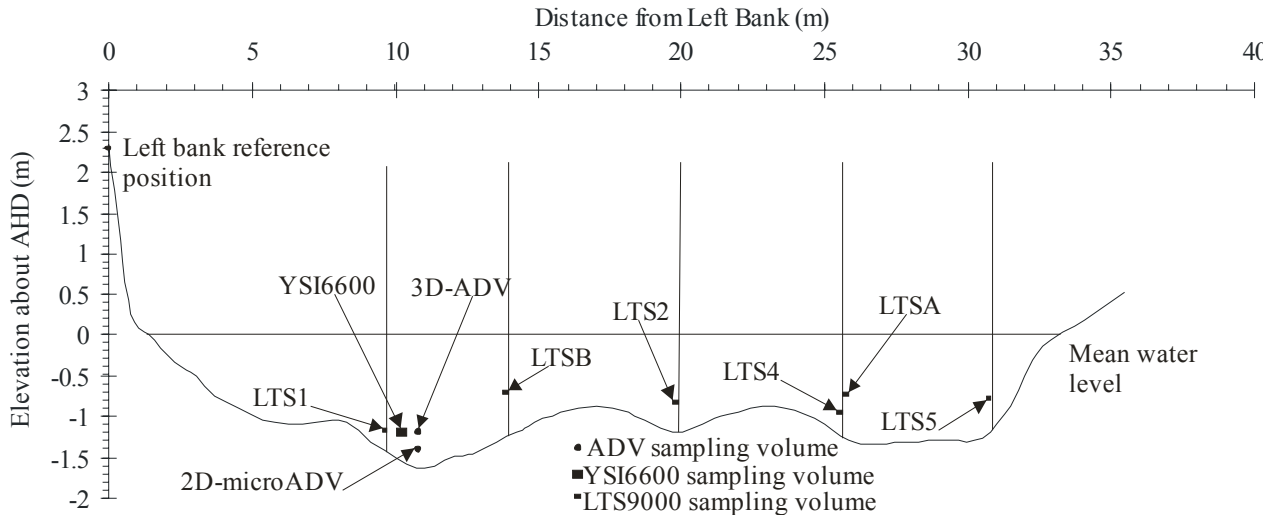

Table 4-2 - Vertical and transverse positions of physio-chemistry probe sensors deployed at Site 2B, Eprapah Creek during the field work E6 (16-18 May 2005)

Probe name (1)	Transverse position (m) (2)	Height above the bed (m) (3)
YSI6600	10.4	0.40
LTS-1	10.1	0.29
LTS-2	20.0	0.41
LTS-4	25.6	0.15
LTS-5	31.0	0.38
LTS-A	25.6	0.59
LTS-B	14.0	0.59

Note : transverse position measured from the left bank.

Trends in conductivity data were similar across the cross-section, but some differences in conductivity over the cross-section seemed unusually large. The causes of these differences in measured conductivity are not known. Without information on the effluent data from the sewage treatment plant, it is inappropriate to speculate. The conductivity in the cross-section seemed to decrease greatly during low tide. The water conductivity at low tide varied depending on the position of each probe in the cross-section.
The differences in water temperature and conductivity between the probes were most noticeable about low tides, possibly because of preferential flow in the two main "low-flow" channels at Site 2B (Fig. 4-1). The large variations could also be related to the increased relative depth of some probe sensors. At low tide, the relative probe sensor depths z/d varied within the range of 0.18 to 0.73, whereas the relative depths of all probes were very similar at high tides (i.e. z/d = 0.07 to 0.28).

Fig. 4-19 – Cross-sectional water temperature and conductivity data as functions of time - Data collected every 6 s for positions indicated in Table 4-2 at Site 2B. Eprapah Creek during field work E6 (16-18 May 2005)
Legend: [——] data from probe LTS-1; [- - - -] data from probe LTS-2; [——] data from probe LTS-4; [——] data from probe LTS-5; [- - - -] data from probe LTS-A; [- - - -] data from LTS-B.

(A) Water temperature data from LTS 9000 probes at Site 2B Eprapah Creek.

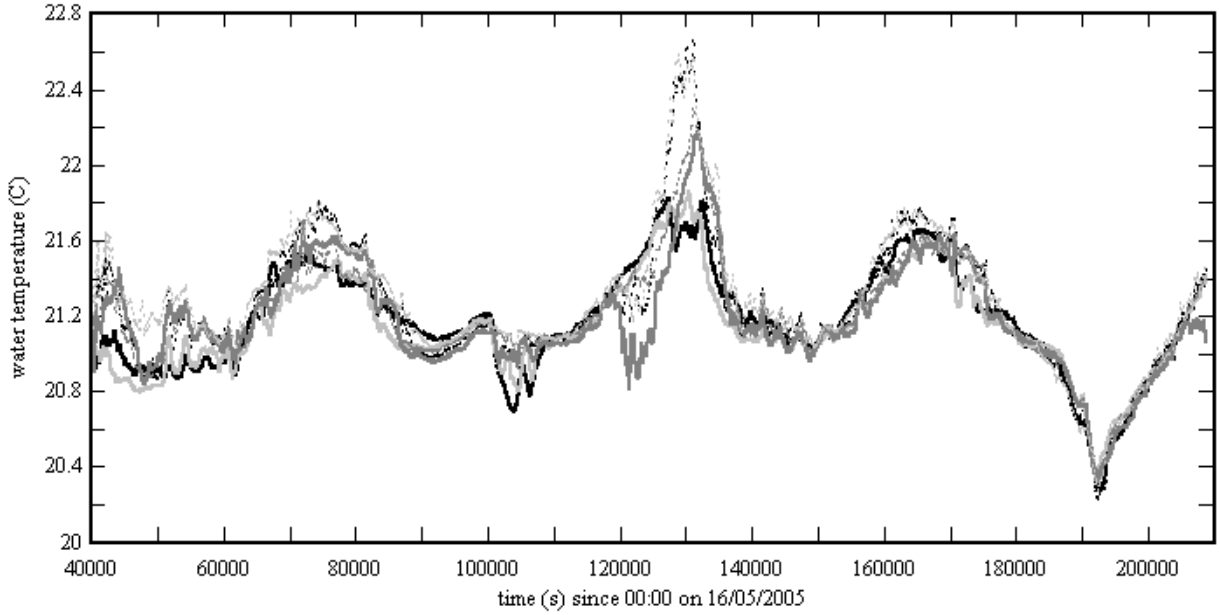

(B) Conductivity data from LTS 9000 probes at Site 2B Eprapah Creek.

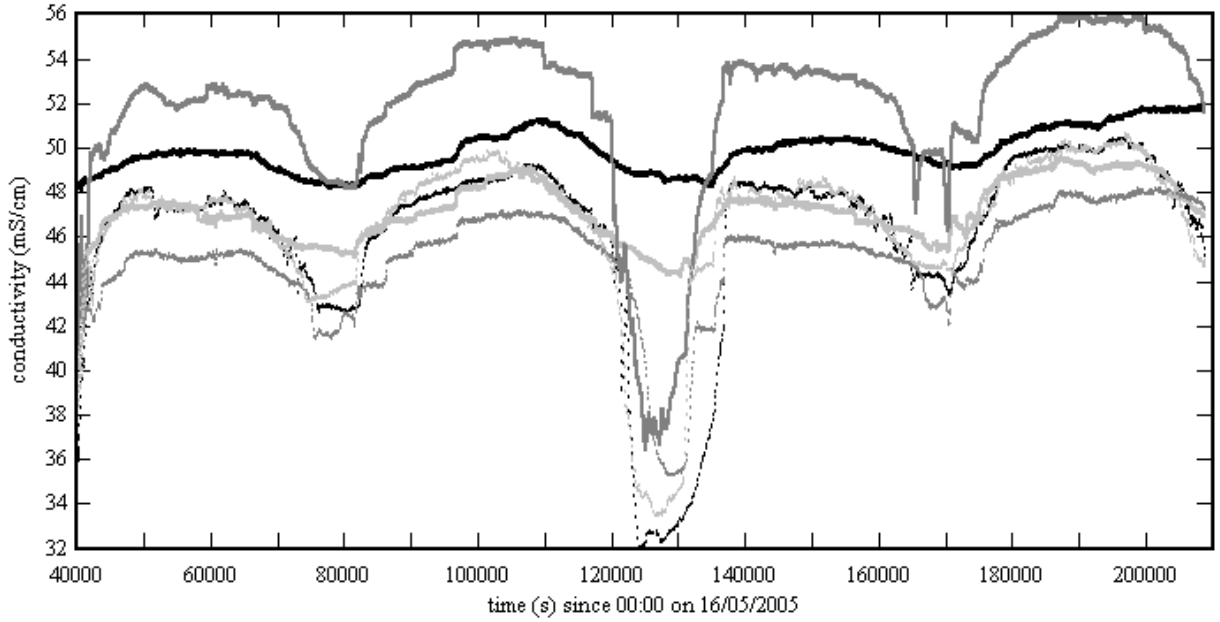

4.3.3 Vertical profiles of physio-chemistry measurements with the YSI6920 probe

For both field works, vertical profiles of physio-chemistry were recorded at several longitudinal locations between the river mouth and the upper estuary. Measurements were conducted in the middle of the creek during the ebb tide and the full data sets are presented in Appendices A and B. Figures 4-20 and 4-21 present typical results in terms of water temperature, conductivity, and dissolved oxygen content.

The vertical profiles of physio-chemical parameters suggested that the estuarine zone was well-mixed during the spring tide conditions (field study E5). The estuary waters were well-mixed both vertically and longitudinally as illustrated in Figure 4-20.

During the neap tide conditions of field work E6, however, the estuarine zone was stratified from the river mouth to the upper estuary (Fig. 4-21). This is seen in Figure 4-21B highlighting a freshwater lens over a saltwater wedge. During earlier field works at Eprapah Creek, some vertical stratification was observed during the field works E1 (4 April 2003) and E2 (17 July 2003) with neap tide conditions, but a stratification was not seen during the field studies E3 (23 Nov. 2003) and E4 (2 Sept. 2004) in spring tide conditions.

In addition, the data during the field study E6 showed large longitudinal gradients in terms of water conductivity, dissolved oxygen and pH levels. In the upper estuary (Site 3), the measured dissolved oxygen and pH were about 25% and 6.9 respectively. These values may be compared with the Australian and New Zealand guidelines for fresh and marine waters (ANZECC 2000) that specified standards for recreational estuarine water quality with pH levels within a 7 to 8.5 range and dissolved oxygen contents between 80% and 110%. Present results seemed to demonstrate some pollution at the time of field study E6, especially in the upper estuary. Similar findings of poor water quality were reported earlier at Eprapah Creek (e.g. CHANSON et al. 2005a).

In summary, the present measurements add to earlier results suggesting that the Eprapah Creek estuarine zone is fairly well-mixed during spring tides and it is partially stratified during neap tides.

Fig. 4-20 - Vertical profiles of water temperature, conductivity and dissolved oxygen collected at Eprapah Creek (QLD) on 10 March 2005 - Data sampled with a YSI6920 probe lowered from a boat drifting mid-stream with the current during the early ebb tide
(A) Water temperatures at the river mouth (AMTD 0 km), Site 2 (AMTD 2 km), Site 2C and AMTD 2.7 km (treatment plant outfall)

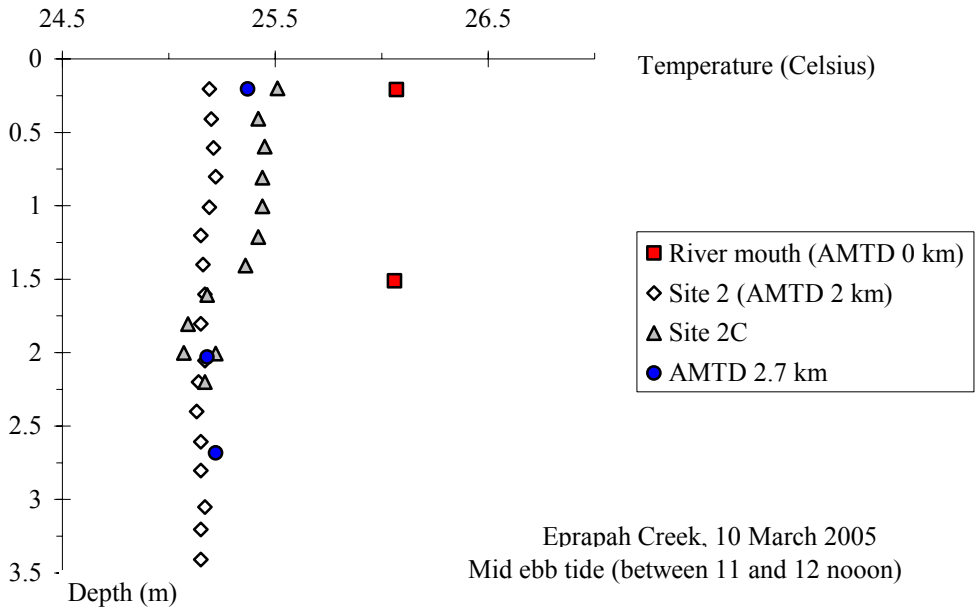

(B) Water conductivities at the river mouth (AMTD 0 km), Site 2 (AMTD 2 km), Site 2C and AMTD 2.7 km (treatment plant outfall)

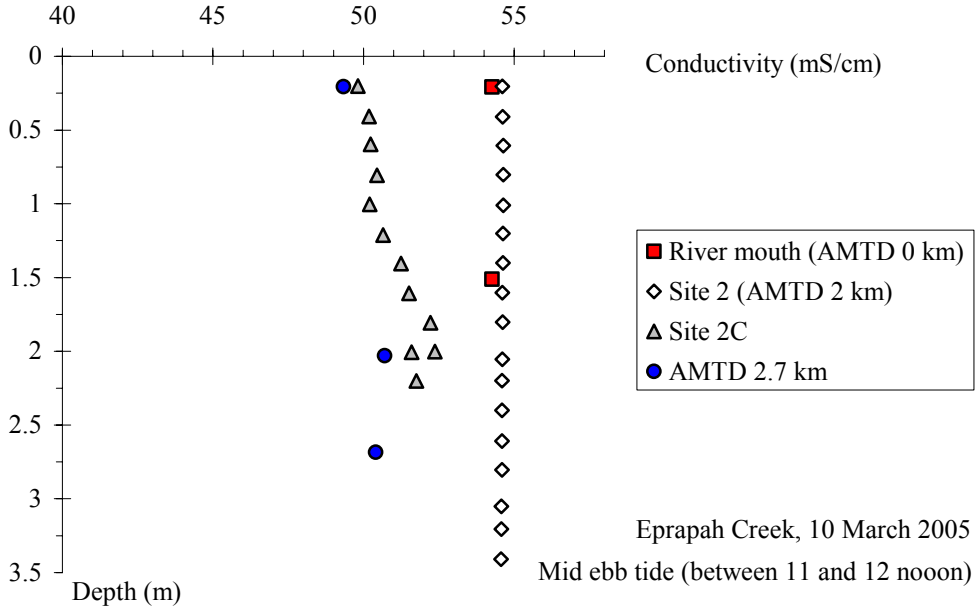

(C) Dissolved oxygen contents at the river mouth (AMTD 0 km), Site 2 (AMTD 2 km), Site 2C and AMTD 2.7 km (treatment plant outfall)

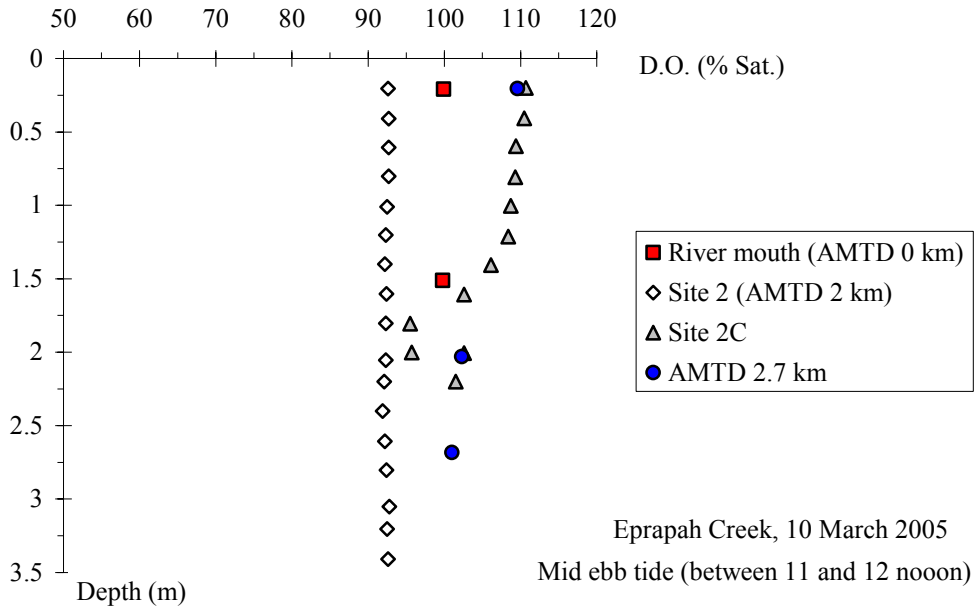

Fig. 4-21 - Vertical profiles of water temperature, conductivity and dissolved oxygen collected at Eprapah Creek (QLD) on 17 May 2005 - Data sampled with a YSI6920 probe lowered from a boat drifting mid-stream with the current during the mid ebb tide
(A) Water temperatures at the river mouth (AMTD 0 km), Site 1 (AMTD 0.6 km), Site 2 (AMTD 2 km), AMTD 2.7 km (treatment plant outfall) and Site 3 (AMTD 3.1 km)

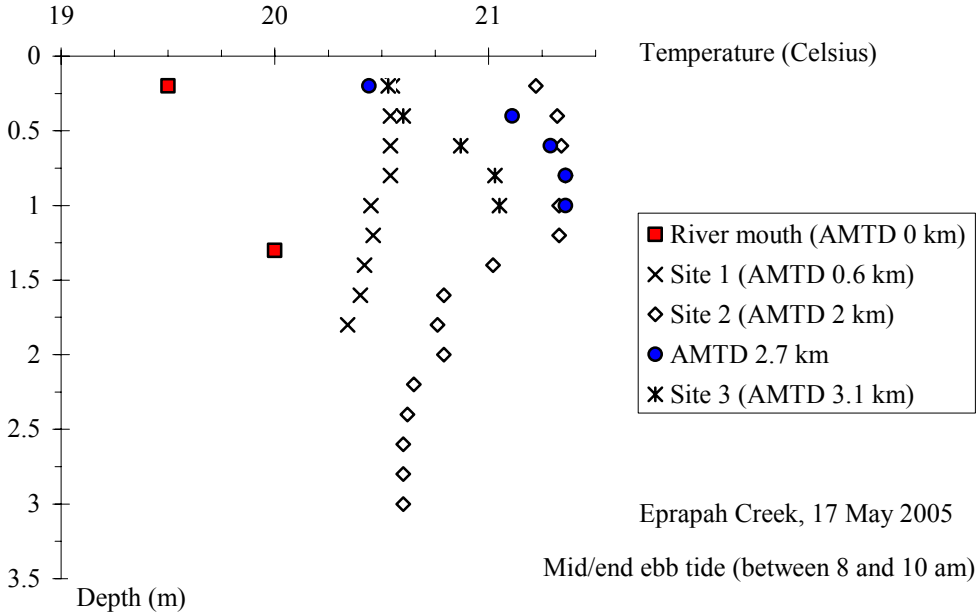

(B) Water conductivities at the river mouth (AMTD 0 km), Site 1 (AMTD 0.6 km), Site 2 (AMTD 2 km), AMTD 2.7 km (treatment plant outfall) and Site 3 (AMTD 3.1 km)

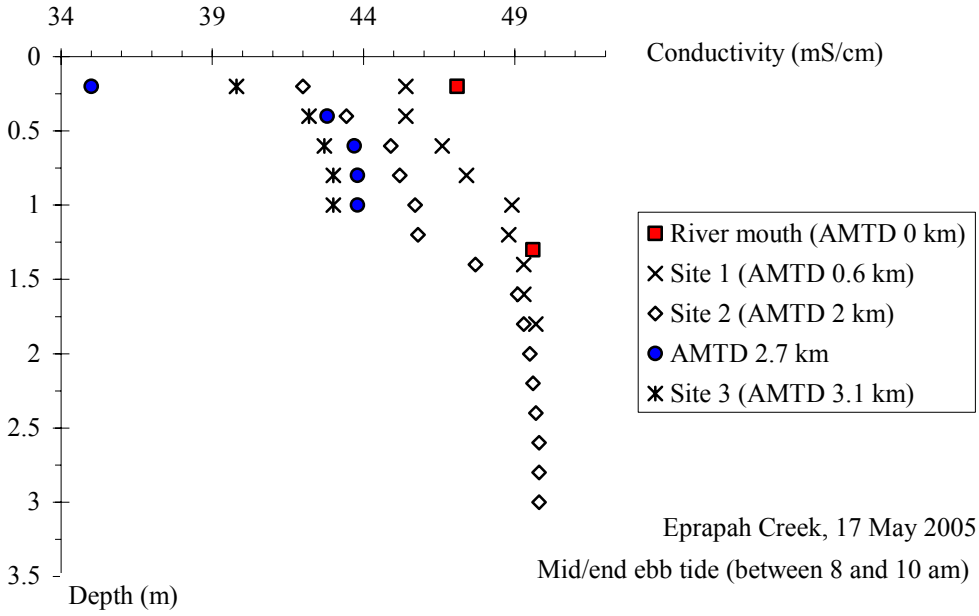

(C) Dissolved oxygen contents at the river mouth (AMTD 0 km), Site 1 (AMTD 0.6 km), Site 2 (AMTD 2 km), AMTD 2.7 km (treatment plant outfall) and Site 3 (AMTD 3.1 km)

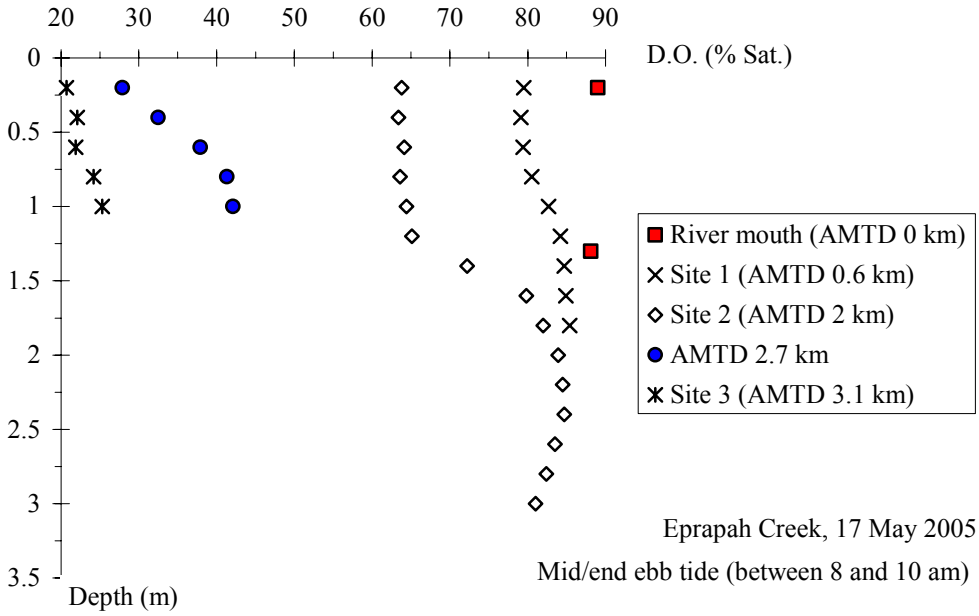

5. DISCUSSION

5.1 PRESENTATION

During the field works E5 (8-9 March 2005) and E6 (16-18 May 2005), a few interesting and unusual phenomena were observed and these are discussed in the Sections 5.2 and 5.3 presenting some multiple flow reversal events observed during both field works, and the effect of a front seen during the field work E6. The Section 5.4 compares some turbulence characteristics in relation to the tidal phase, and the influence of vertical sampling elevation and tidal range differences. The Section 5.5 presents some results in terms of the Prandtl mixing length and of the momentum mixing coefficient for the field works E4 and E5.

Both field works E5 and E6 were conducted at the same sampling site (Site 2B) about mid-estuary of Eprapah Creek. Turbulence data were sampled continuously at 10.7 m from the left bank during both field studies. The same 3D ADV (10 MHz) system collected high frequency velocity data at 0.1 m above the bed (field work E5) and 0.4 m above the bed (field work E6). A 2D microADV (16 MHz) system was used during the field work E6 with the sampling volume located 0.2 m above the bed. Some caution is required for any comparison of data collected during different field works because of some differences in instrumentation, sampling elevation and tidal range.

5.2 MULTIPLE FLOW REVERSALS

For all tidal cycles, multiple flow reversals were observed around the slack tide periods during the field work E6. Multiple flow reversals were also observed around the first high water slack during the field work E5 ([1]). A multiple flow reversal event is defined herein as a rapid succession of changes in streamwise velocity direction ([2]). Figure 5-1 shows an example of multiple flow reversals that occurred at high tide during the field work E6 between t = 52602 and 62492 s since 00:00 on 16/05/2005. In Figure 5-1, the time-averaged streamwise velocities $\overline{V_x}$ are shown for two sampling locations (0.2 and 0.4 m above the bed), and the measured water depth at Site 2B is also shown (dotted line, right vertical axis). Altogether nine changes in flow direction were recorded during the flow reversal event.

The observations of time-averaged streamwise velocity data showed that multiple flow reversals occurred at all sampling elevations : i.e., 0.1 m above the bed during the field work E5 (spring tide), and 0.2 and 0.4 m above the bed during the field work E6 (neap tide). At the free-surface, visual observations of free-surface velocity by the writers suggested primarily singular flow reversals during slack periods for both field works. These observations seemed to suggest that multiple flow reversals occurred possibly predominantly close to the bed for these two field studies.

The duration of each event and the number of changes in velocity directions were not the same throughout the field works. Table 5-1 lists the basic characteristics of each flow reversal event in terms of the tidal phase, event duration and number of flow reversals. Note two unusual flow reversal events : i.e., MFR2 and MFR3 of field work E6. In both events, more flow reversals occurred at 0.2 m above the bed than at 0.4 m above the bed. The duration of each event was also longer at 0.2 m above the bed than at 0.4 m above the bed. These differences in number of flow reversals and event duration between different vertical elevations may suggest the existence of strong vertical gradient and secondary currents. These could potentially have some effect on the turbulent mixing in the estuarine section.

[1] That is, around t = 70000 to 80000 s since 00:00 on 08/03/2005.

[2] As such the present definition of flow reversal is linked to the sampling volume longitudinal, transverse and vertical locations, and to a lesser extent to the sampling frequency.

Fig. 5-1 - Multiple flow reversals at Site 2B, Eprapah Creek during the field work E6 (16-18 May 2005) about high water between t = 52602 and 62492 s since 00:00 on 16/05/2005 - Time-averaged streamwise velocity $\overline{V_x}$ at 0.2 and 0.4 m above the bed, and measured water depth - Time-averaged velocity data calculated for 5,000 data points every 10 s
Legend: —— streamwise velocity at 0.4 m above the bed; —— streamwise velocity at 0.2 m above the bed; - - - - water depth at YSI6600 probe (Site 2B);

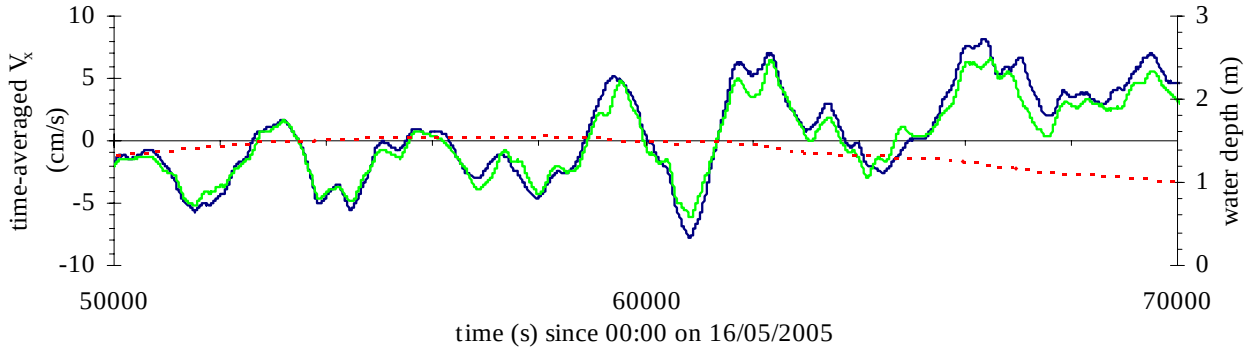

Table 5-1 - Summary of flow reversal events recorded during field work E5 (8-9 March 2005) and field work E6 (16-18 May 2005).

Field study code	Flow reversal type and designation	Tidal phase	Duration of flow reversal event (s)		Number of change of flow direction	
E5	SFR1	LW	N/A		1	
	MFR1	HW	2970		7	
	SFR2	LW	N/A		1	
	SFR3	HW	N/A		1	
			At 0.4 m	At 0.2 m	At 0.4 m	At 0.2 m
E6	MFR1	HW	12540	12000	9	9
	MFR2	LW	4500	6650	3	5
	MFR3	HW	2360	7260	3	9
	MFR4	LW	1670	1980	3	3
	MFR5	HW	5710	6090	5	5
	MFR6	LW	6780	6850	5	5
	MFR7	HW	9310	9440	7	7

Notes: HW = high water; LW = low water; MFR = multiple flow reversal; SFR = single flow reversal.

Figure 5-2 shows each flow reversal event in relation to the tidal phase. It presents the measured water depth as a function of time since midnight on the first day of field works, and the flow reversal events are indicated. In addition, the time-averaged streamwise velocity $\overline{V_x}$ data during each multiple flow reversal event are shown. The longest flow reversal events seemed to occur predominantly around high water periods, with a lesser number of events at low water periods. In fact the only high water slack tide when multiple flow reversals were not observed was the second

tidal cycle of field work E5 ([3]) (Fig. 5-2A). At high waters, the flow reversal events tended to exhibit a larger number of flow direction changes than at low waters.
A comparison between spring tides (field work E5) and neap tides (field work E6) suggests further that longer flow reversal events were observed at neap tides. Figure 5-2 shows also that the velocity magnitudes between two successive flow reversals were larger during neap tide conditions (field work E6) than during spring tides (field work E5). For field work E5, the velocity magnitude between flow reversals was less than 4 cm/s while, during field work E6, the velocity magnitude between multiple flow reversals could reach up to 10 cm/s.

Fig. 5-2 - Position of flow reversal events and corresponding time-averaged streamwise velocity $\overline{V_x}$, Site 2B, Eprapah Creek during field works E5 (8-9 March 2005) and E6 (16-18 May 2005)
(A) Flow reversal at 0.1 m above the bed, 10.7 m from left bank during field work E5 (spring tide)
Legend: —— data 0.1 m above the bed for field work E5; - - - - - water depth at Site 2B

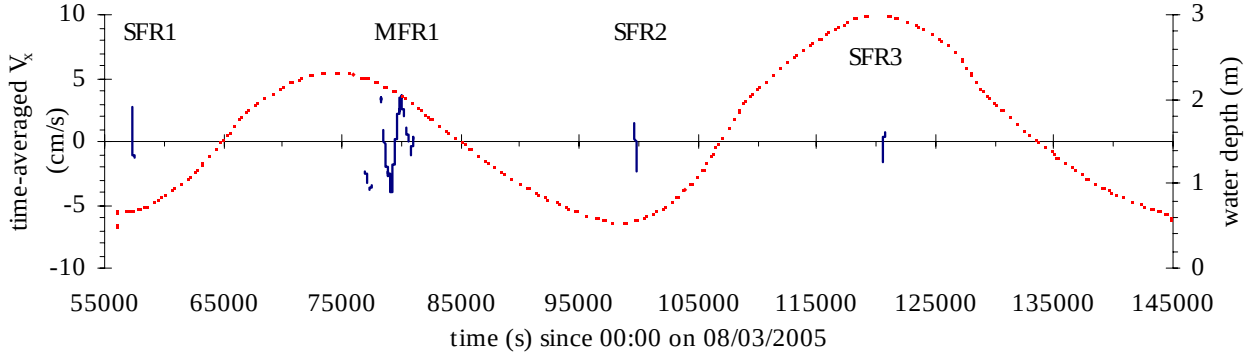

(B) Flow reversals at 0.2 and 0.4 m above the bed, 10.7 m from left bank during field work E6 (neap tide) - Legend: —— data 0.2 m above the bed for field work E6; —— data 0.4 m above the bed for field work E6; - - - - - water depth at Site 2B

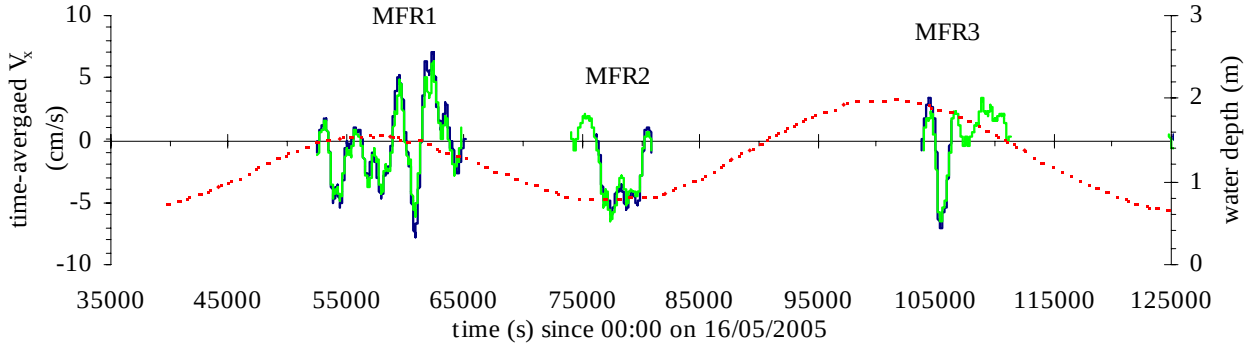

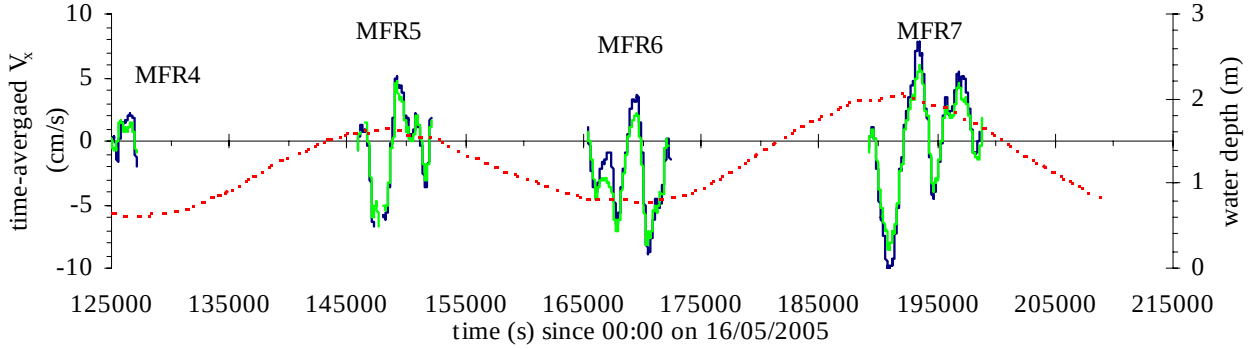

[3]That is, for t = 98880 to 146280 s since 00:00 on 08/03/2005

During the field work E6, three main flow reversal half-periods ([4]) were observed around the slack tides (Table 5-2). These characteristic half-periods were between 610 and 800 s, 1010 and 1200 s, and 2010 and 2200 s. For the field work E5, the half-periods were predominantly between 610 and 800 s, and between 1010 and 1200 s. These characteristic half-periods may be compared with the characteristic resonance times of Eprapah Creek estuarine zone.

Resonance is the fluctuations caused by the reflection of tidal forcing from certain geographical landmarks, such as the banks of the creek and the meanders. The period of resonance is related to the distance and depth of water between two bathymetric landmarks ([5]). Note that bathymetric landmarks may be located within the estuary (internal resonance) or within the surrounding bay or ocean (external resonance). Some characteristic resonance times of Eprapah Creek estuary are summarised in Table 5-3, and these may be compared with most frequently observed flow reversal half-periods in both field works E5 and E6.

Several resonance periods were found to be comparable to twice some half-periods (Tables 5-2 and 5-3). The comparison suggests that some internal resonance was associated with the average distance between meanders, with the half estuary length and with the full length of the estuarine zone. Some external resonance was linked possibly with some East-West resonance in the Moreton Bay.

For the field works E5 and E6, the range of flow reversal half-periods seemed related to either low or high water slack tide. For example, during field works E6, flow reversal events with half-periods of 610 to 1000 s and 2210 to 3200 s occurred only about high water, while half-periods of 3200 to 5000 s were only observed at low tide slack.

Table 5-2 - Predominant flow reversal half-periods observed during the field works E5 and E6 at Eprapah Creek (Site 2B)

Observed flow reversal half-period (s) (1)	Total Nb of observed flow reversals (E5 & E6) (2)	Averaged velocity magnitude between reversals (cm/s) (3)
10 to 30	2	0.01
110 to 500	12	0.44
610 to 900	15	1.15
1010 to 1600	19	2.40
2010 to 2600	13	3.85
3010 to 3400	3	2.72

Notes: Averaged velocity magnitude = average of the time-averaged streamwise velocities between flow reversal for the flow durations listed; Flow reversal half-period = time between two successive, consecutive changes in flow direction.

[4] That is, the time between two successive/consecutive changes in flow direction.

[5] If the streamwise distance between two bathymetric landmarks is L, the resonance period of the first harmonic is $2*L/\sqrt{g*d}$ where d is the average water depth between the landmarks and g is the gravity acceleration (9.80 m/s^2).

Table 5-3 - Characteristic resonance times of Eprapah Creek estuarine zone

Theoretical resonance period (s) (1)	Bathymetric landmarks of theoretical resonance (2)
14	Transverse width of creek.
200 to 350	Average distance between 90° bends (between mouth and Site 2B)
750	Distance between Site 2B and upstream extent of estuary
1400	Longitudinal length of entire estuary
2200	Distance between estuary mouth and Peel Island (Moreton Bay)
3200	Distance between estuary mouth to North Stradbroke Island

A comparison between the field works E5 and E6 seemed to suggest that spring and neap tidal conditions affected the response of Eprapah Creek estuary to the tidal forcing. During the neap tidal conditions (field work E6), multiple flow reversals occurred about all low and high waters. For the spring tidal conditions (field work E5), singular rapid flow reversals occurred for most low and high waters. A comparison between Figures 5-2A and 5-2B shows that the velocity magnitude between flow reversals during spring tidal conditions (field work E5) was smaller than the flow reversal velocity magnitudes during neap tidal conditions (field work E6).
Overall it seemed that the increased flow velocity of spring tidal conditions reduced the impact of the resonance fluctuations (or flow reversal events) about slack tides in Eprapah Creek estuarine zone.

5.3 OBSERVED FRONT

During the field work E6, a front was observed propagating upstream shortly after the field measurements started (Fig. 5-3). The front occurred during the early flood tide. At approximately 12:20 (44400 s since 00:00 on 16/05/2005), the leading edge of the front reached the experimental cross-section (Fig. 5-3C). Traces of the front were seen until approximately 13:22 on 16/05/2005 when the last observation of surface slicks, foam or floating debris was recorded. Figures 5-3A to 5-3C show various stages of the front propagating upstream through the experimental cross-section at Site 2B.
The effects of the front passage on the turbulence and physio-chemistry were tested. The data showed that the front migration affected primarily some water temperature readings at Site 2B but not the conductivity readings. Figure 5-4 shows the water temperature data collected by the six LTS9000 probes and by the YSI6600 probe. In Figure 5-4, the time t is shown in seconds with t = 0 when the front leading edge was first observed reaching the experimental cross-section (i.e. 44400 s since 00:00 on 16/05/2005). Some obvious effect on the water temperature was recorded with the probe LTSB located the closest to the water surface next to the main navigation channel (Fig. 5-4B). These temperature readings remained higher than all other probe readings presented in Figure 5-4A. In the same tidal phase (low water to mid flood tide) for all other three tidal cycles of the field work E6, such larger temperature readings (detected by the probe LTSB) were not observed.

Fig. 5-3 - Photographs of the front observed at Site 2B Eprapah Creek between 12:00 and 13:22 on 16/05/2005 during the field work E6 (Photographs M. TREVETHAN & H. CHANSON)
(A) Experimental cross-section at 12:03 before front arrival

(B) Front approaching the experimental cross-section shortly before 12:20 - Front leading edge is highlighted by surface slicks, foams and floating debris

(C) Front crossing the experimental cross-section at 12:22 on 16/05/2005

Fig. 5-4 - Water temperature data collected at Site 2B, Eprapah Creek during the field work E6 (16-18 May 2005) around the passage of the front - Data collected using 6 LTS-9000 probes sampling every 6 s and a YSI6600 probe sampling every 12 s - t = 0 when leading edge of front reached the cross-section

Legend: —— LTS1 probe; — — LTS2 probe; — - - - YSI6600 probe; - - - - LTS4 probe; —— LTS5 probe; —— LTSA probe; - - - - LTSB probe

(A) Water temperature data collected at Site 2B about passage of front

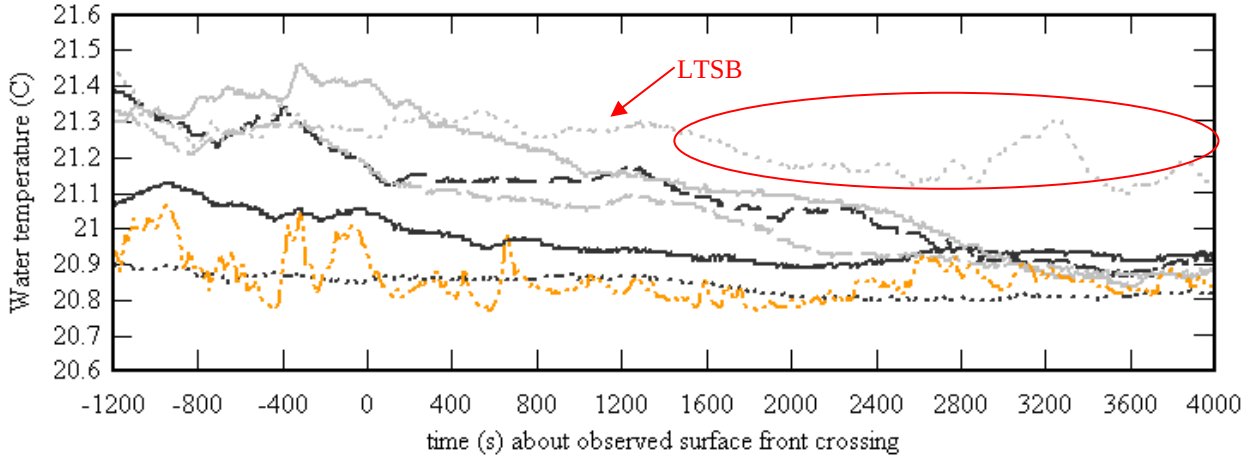

(B) Sketch of probe position and water level at t = 0

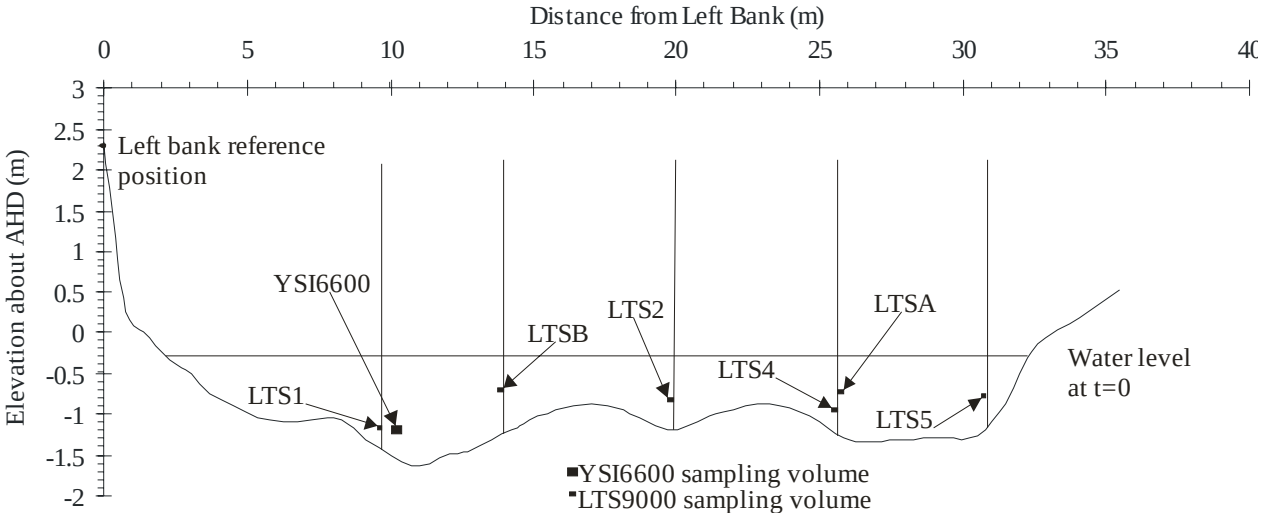

Physio-chemical data collected by the YSI6600 probe ([6]) are presented in Figure 5-5. The YSI6600 data showed no obvious influence of the front on the measured physio-chemistry parameters including temperature, pH, dissolved oxygen, turbidity and conductivity. Such a lack of influence could be related to the probe position relatively close to the bed, since Figure 5-4A suggested possibly that the influence of the front was potentially greater next to the free-surface.

The passage of the front seemed to coincide with some anomaly in terms of time-averaged velocity data. No effect of the front passage was observed in terms of the time-averaged streamwise velocity $\overline{V_x}$ (Fig. 5-6A), but the time-averaged transverse velocity $\overline{V_y}$ data were affected by the passage of the front (Fig. 5-6B). Figure 5-6B shows that, between t = -300 and 1300 s, the time-averaged transverse velocities $\overline{V_y}$ recorded at 0.2 and 0.4 m above the bed flowed in opposite directions: that is, towards the left and right banks respectively. This situation indicates the occurrence of some

[6]The YSI6600 probe was located approximately 0.4 m above the bed, 10.4 m from left bank. The position of the YSI6600 probe sensors is shown in Figure 5-4B.

form of secondary currents at that location, when the front passed through the experimental cross-section.

During the front event, the time-averaged streamwise velocity data $\overline{V_x}$ at both 0.2 and 0.4 m above the bed were negative : i.e., the waters flowed in the upstream (flood tide) direction (Fig. 5-6A). At 0.4 m above the bed, $\overline{V_x}$ was larger than that observed at 0.2 m above the bed. Both data sets showed similar fluctuations of time-averaged velocity.

Fig. 5-5 - Selected physio-chemical characteristics collected by the YSI6600 probe located 0.4 m above the bed at Site 2B, Eprapah Creek during the field work E6 (16-18 May 2005) - Sampling every 12 s - t = 0 when leading edge of front reached the cross-section.
Legend: —— Conductivity; —— water temperature; — — turbidity; —— pH; - - - - depth; - - - - Fluorescence; — — Chlorophyll; —— DO

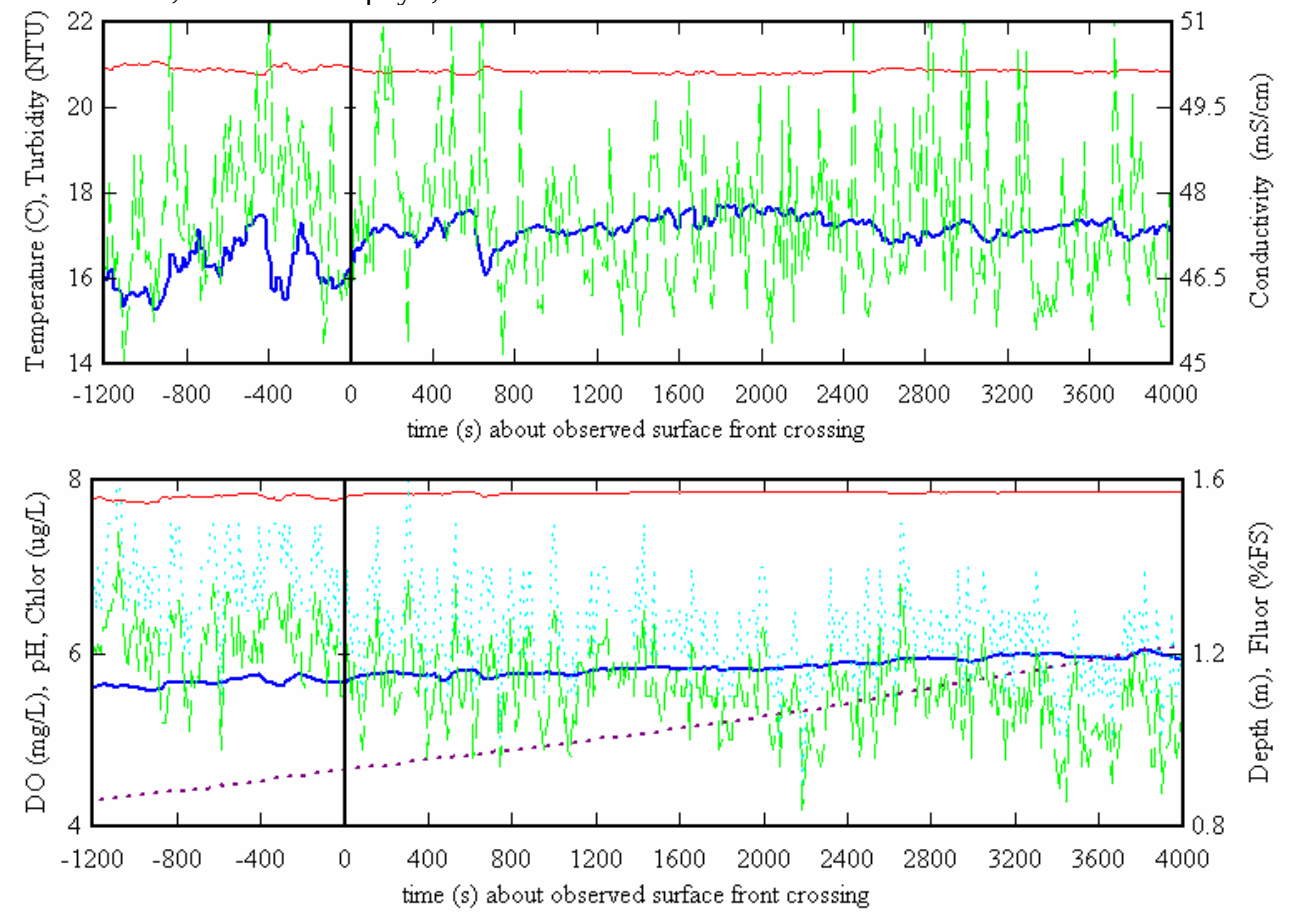

Fig. 5-6 - Time-averaged velocity data collected at Site 2B, Eprapah Creek during the field work E6 (16-18 May 2005) - Data at 0.2 m and 0.4 m above the bed collected by 2D microADV (16 MHz) and 3D ADV (10 MHz) respectively, both located at 10.7 m from left bank
Legend: - - - - velocity data 0.2 m above the bed; —— velocity data 0.4 m above the bed;
(A) Time-averaged streamwise velocity $\overline{V_x}$

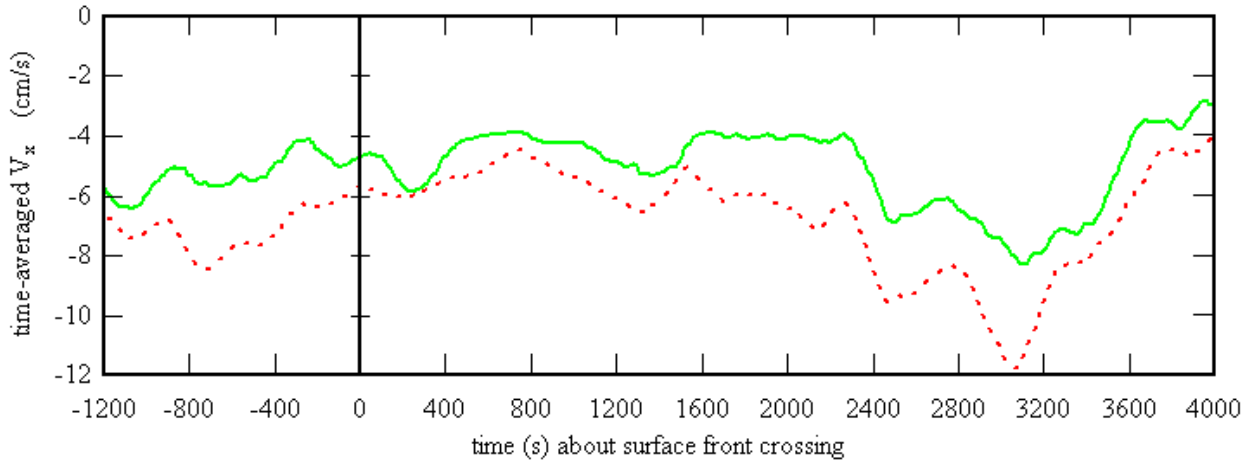

(B) Time-averaged transverse velocity $\overline{V_y}$

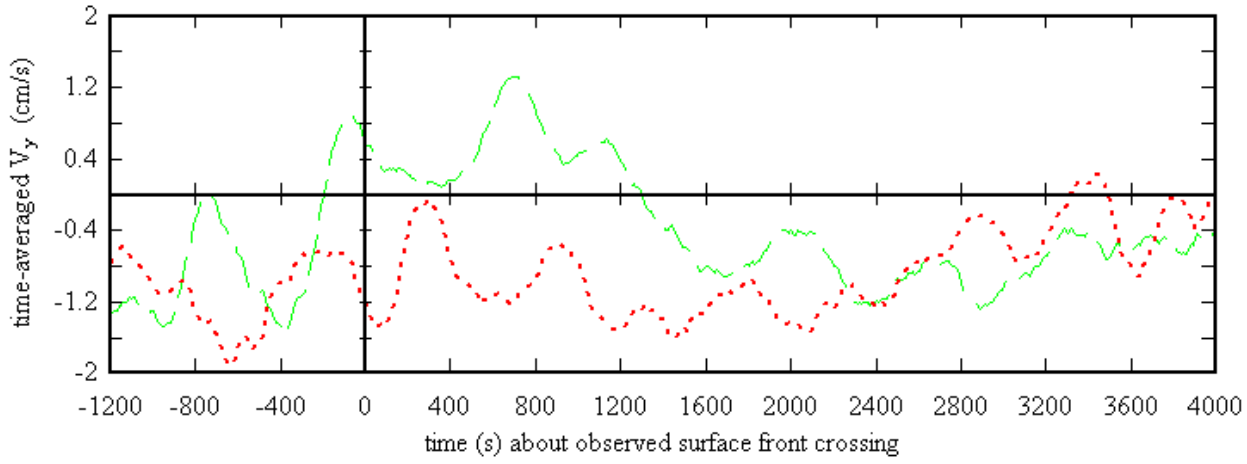

Discussion

Tidal intrusion fronts are relatively common feature at or near some estuary mouths (e.g. KIRBY and PARKER 1982, DYER 1997, THAIN et al. 2004). They are often seen forming a distinctive V-shape of foam and debris at the surface. A front is basically a zone of marked local gradients that indicates some form of singularity in terms of one or more parameters.

Fronts like the one observed in field work E6 are considered to be a natural process in estuaries. However the observed front was the first front observed at Eprapah Creek by the authors despite earlier field investigations (Tables 2-2 and 3-1). The front was observed only during the first flood tide on 16 May 2005 and it was not seen again for the rest of the field study.

The passage of this front seemed to have some effect on the water temperature next to the surface and on the transverse velocity next to the bed. Other effects on physio-chemistry characteristics were not noticeable. Vertical profiles of water conductivity showed that the estuary was stratified during the ebb tide (Section 4.3.3). Water temperature readings suggested some slight temperature stratification with warmer waters next to the free-surface. Turbulent velocity records indicated opposite transverse velocity directions between 0.2 and 0.4 m above the bed implying some strong secondary circulation.

5.4 TURBULENCE COMPARISON BETWEEN TIDAL CYCLES

Turbulence properties were recorded for a total of nearly 75 hours between the field works E5 and E6. Herein, some turbulence characteristics are compared as functions of the tidal phase and the influence of the tidal cycles is discussed. During the field work E5 and E6, two tidal cycles occurred every 25 hours at Eprapah Creek. These two tidal cycles were of slightly different periods and tidal ranges indicating that a diurnal inequality existed in the tides during the field works. Figure 5-7 shows an example of a 25 hour record of water levels with a diurnal inequality. Herein minor tide and major tide refer to the smallest and largest of the two tidal cycles respectively, as shown in Figure 5-7. Each "tide" starts at low water (LW1) and ends at low water (LW2). The tidal ranges and periods of each tidal cycle for the field works E5 and E6 are listed in Table 5-4.

Fig. 5-7 - Sketch of diurnal inequality typically observed during the field works E5 and E6 at Eprapah Creek QLD

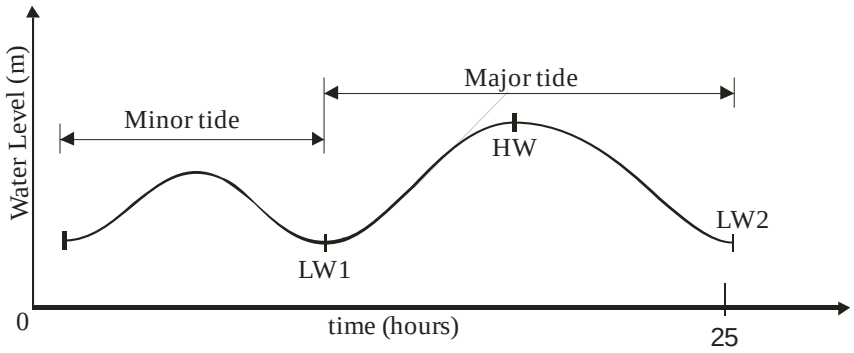

Section 5.4.1 investigates the trends in turbulence characteristics related to the tidal phase that were observed during a majority of tidal cycles of field works E5 and E6. In Section 5.4.2 turbulence characteristics collected simultaneously at 0.2 and 0.4 m above the bed are compared for the same tidal cycles (field work E6). During the field work E6, the data were collected at 0.2 and 0.4 m above the bed with different instrumentation : i.e., 2D microADV (16 MHz) and 3D ADV (10 MHz) respectively. Hence caution is required. In Section 5.4.3 the turbulence characteristics under spring (field work E5) and neap (field work E6) tide conditions are compared. Here the comparison applied to data collected with the same 3D ADV (10 MHz) system, but the sampling volume locations differed : i.e., 0.1 and 0.4 m above the bed for the field works E5 and E6 respectively. Note that all comparisons (Section 5.4) were made between similar tidal cycle types : i.e., minor tide versus minor tide, and major tide versus major tide.

Table 5-4 - Period and average tidal range of the tidal cycles observed during the field works E5 and E6 at Eprapah Creek QLD

Field Study	Designation	Tidal type	Time LW1 to LW2 (s)	Period T (hours)	Average tidal range (m)
(1)	(2)	(3)	(4)	(5)	(6)
E5	TC51	minor	56880 to 98880	11.67	1.71
	TC52	major	98880 to 146280	13.17	2.44
E6	TC61	minor	37560 to 76380	10.78	0.81
	TC62	major	76380 to 127500	14.20	1.28
	TC63	minor	127500 to 170148	11.85	0.97
	TC64	major	170148 to 217320	13.10	1.19

Notes: Average tidal range = average tidal range between LW1 to HW and HW to LW2 for each tidal cycle; LW1 = first low water of tidal cycle; LW2 = second low water of tidal cycle; HW = high water.

5.4.1 Turbulence characteristics during a tidal cycle

Field observations showed systematically the large standard deviations of all velocity components at the beginning of the flood tide for all tidal cycles during the field works E5 and E6. In particular, a rapid increase in velocity standard deviations was noted at the beginning of each flood tide during the field work E5 with spring tide conditions.

Typical field measurements of standard deviations of the streamwise velocity v_X' are shown in Figure 5-8 for two tidal cycles during the field works E5 and E6. Figure 5-8, as other similar plots in Section 5.4, shows the magnitude of a turbulence property (herein v_X') relative to the position in a tidal cycle. The data for a tidal cycle were collected from a low water (LW1) to the next one (LW2), and they are presented in a circular plot. The polar coordinates (r, θ) are: r = turbulence characteristic (herein v_X'), and $\theta = 2*\pi*t/T$ where T is the period of tidal cycle from the first low water (LW1) to the second low water(LW2) (Table 5-4, column 5) and t is the position in tidal cycle with t = 0 at LW1 and t = T at LW2. In Figure 5-8, the Cartesian coordinates are: $x = r*\cos(2*\pi*t/T)$ and $y = r*\sin(2*\pi*t/T)$. The high and low waters are indicated as well as the direction of increasing time. From the first low water (y = 0 on positive x-axis), the time variations of the data progress anticlockwise until the second low water (y = 0 on positive x-axis).

In Figure 5-8, the grey circles represent an approximate mean standard deviation of streamwise velocity. The presentation illustrates that v_X' was systematically larger during the flood tide than during the ebb tide for both field works. It was also found that the standard deviations of all tangential Reynolds stresses were larger than average at the beginning of flood tide ($0 < \theta < \pi/2$) for both field works.

Fig. 5-8 - Standard deviations of streamwise velocity v_X' during a tidal cycle - Data collected at Site 2B, Eprapah Creek using the 3D ADV (10 MHz) system - The units are cm/s

(A) v_X' (cm/s) for major tide (TC52), field work E5, 3D ADV (10 MHz) system at 0.1 m above the bed

(B) v_X' (cm/s) for first major tide (TC62), field work E6, 3D ADV (10 MHz) system at 0.4 m above the bed

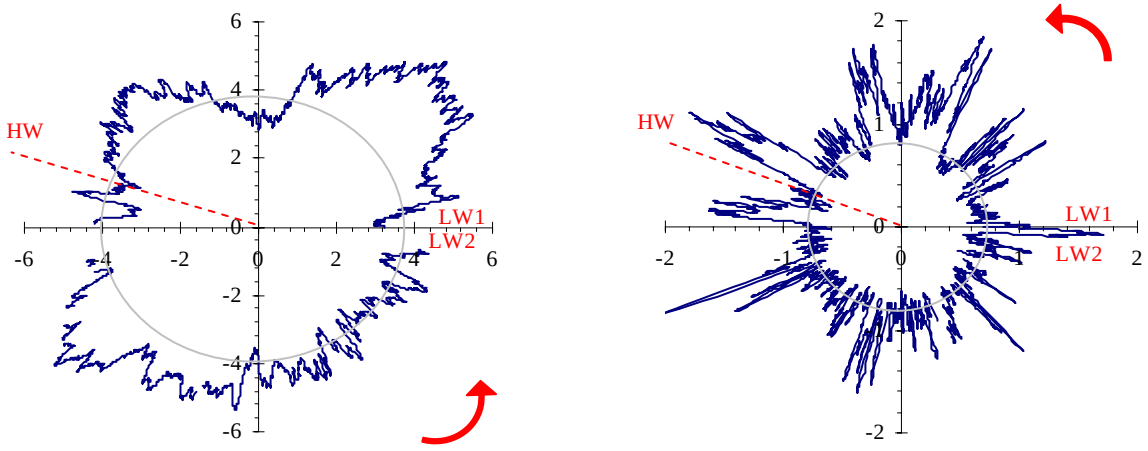

The analysis of integral and dissipation time scales of all velocity components showed no obvious trends with tidal phase for both field works. Dissipation time scales seemed independent of the tidal phase. Trends of integral time scales differed between field works E5 and E6. The integral time scales of all velocity components seemed to decrease about low water in field work E5, but this trend was not observed during the field work E6. During the field work E5, the smaller integral time scales at low waters could be related to the low water depths and relatively larger velocities experienced around low water slacks, possibly because of the spring tidal conditions (see Section 5.4.3).

5.4.2 Effect of vertical elevation on flow turbulence during field work E6

The effects of vertical sampling elevation were tested during the field work E6 with continuous data collection at 0.2 and 0.4 m above the bed. The standard deviations of streamwise and transverse velocities were of similar magnitude at both vertical elevations throughout the field work. Figure 5-9 presents the standard deviations of the streamwise velocity v_X' during the first minor and major tides. It is seen that the fluctuations in v_X' experienced similar trends at both elevations throughout both tidal cycles. In comparison, fluctuations in terms of the standard deviations of transverse velocity v_Y' were not as well correlated at 0.2 and 0.4 m above the bed.

Fig. 5-9 - Effect of vertical sampling elevation on standard deviations of streamwise velocity v_X' - Data collected at Site 2B, Eprapah Creek at 0.4 (3D ADV) and 0.2 m (2D microADV) above the bed, both 10.7 m from left bank for the field work E6 (16-18 May 2005) - The units are cm/s
Legend: —— data at 0.2 m above the bed; —— data at 0.4 m above the bed
(A) v_X' (cm/s) for first minor tide (TC61) (B) v_X' (cm/s) for first major tide (TC62)

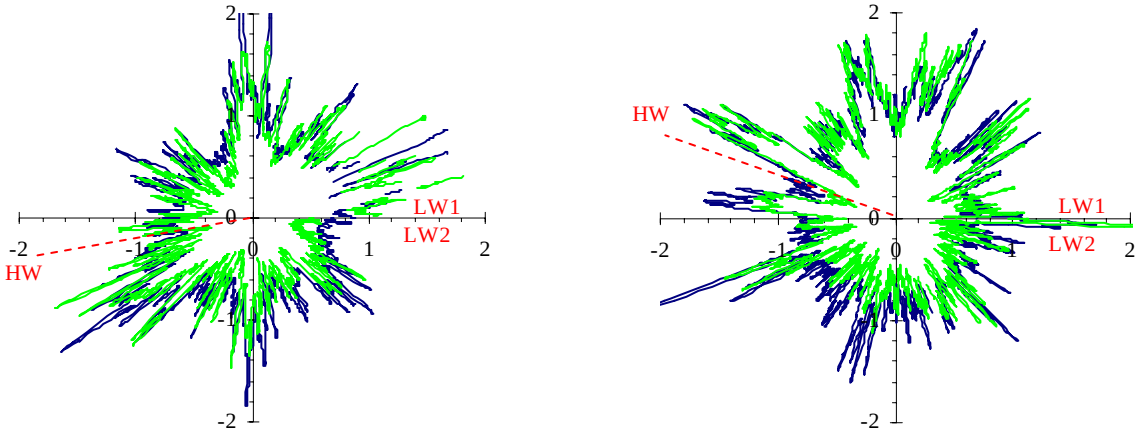

The standard deviations of the tangential Reynolds stress $(\rho*v_X*v_Y)'$ were of similar magnitude at 0.2 and 0.4 m above the bed throughout field work E6. This is illustrated in Figure 5-10 showing the standard deviations of the Reynolds stress $(\rho*v_X*v_Y)'$ during two tidal cycles. In Figure 5-10, it is seen that the fluctuations in $(\rho*v_X*v_Y)'$ experienced similar trends at 0.2 and 0.4 m above the bed although a comparison between Figures 5-10A and 5-10B shows differences between the minor tide data (Fig. 5-10A) and the major tide data (Fig. 5-10B).

The horizontal dissipation time scales seemed independent of the tidal phase and the streamwise dissipation time scales were independent of the vertical sampling elevation. This is illustrated in Figure 5-11 showing the streamwise and transverse integral time scales τ_{Ex} and τ_{Ey} at 0.2 and 0.4 m above the bed during two tidal cycles. (Note that the axes have a logarithmic scale and the units are μs.) In Figure 5-11, the dissipation time scales exhibited a circular shape which indicated an

independence from the tidal phase. The streamwise dissipation time scales τ_{Ex} appeared to have a similar order of magnitude throughout the entire field work E6. However the transverse dissipation time scales τ_{Ey} were larger at 0.2 m above the bed than at 0.4 m above the bed. The transverse dissipation time scales at 0.2 m above the bed were mostly between 0.001 and 0.1 s, while those at 0.4 m above the bed were between 0.0007 and 0.01 s typically. For the field work E6, such differences in dissipation time scales between 0.2 and 0.4 m above the bed might also be related to some difference in instrumentation.

Fig. 5-10 - Effects of vertical sampling elevation on the standard deviations of tangential Reynolds stress $(\rho*v_x*v_y)'$ during a tidal cycle - Data collected at Site 2B, Eprapah Creek at 0.4 (3D ADV) and 0.2 m (2D microADV) above the bed, both 10.7 m from left bank for field work E6 (16-18 May 2005) - The units are Pa

Legend: —— data at 0.2 m above the bed; —— data at 0.4 m above the bed

(A) $(\rho*v_x*v_y)'$ (Pa) for first minor tide (TC61) (B) $(\rho*v_x*v_y)'$ (Pa) for first major tide (TC62)

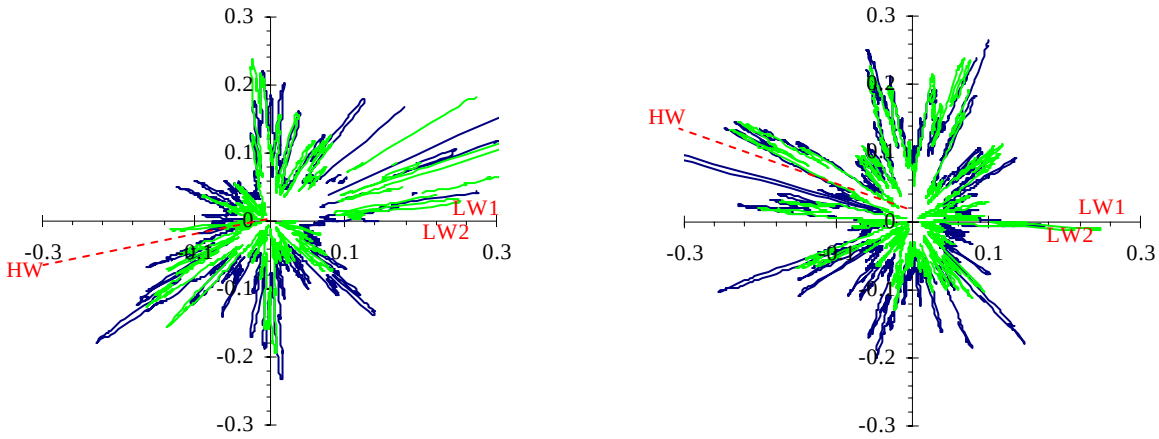

Fig. 5-11 - Effects of vertical sampling elevations on the horizontal dissipation time scales τ_{Ex} and τ_{Ey} - Data collected at Site 2B, Eprapah Creek at 0.2 (2D microADV) and 0.4 m (3D ADV) above the bed, both 10.7 m from left bank during field work E6 (16-18 May 2005) - The axes have a logarithmic scale and the units are microseconds

Legend: —— data at 0.2 m above the bed; —— data at 0.4 m above the bed

(A) τ_{Ex} for first minor tide (TC61) (B) τ_{Ex} for first major tide (TC62)

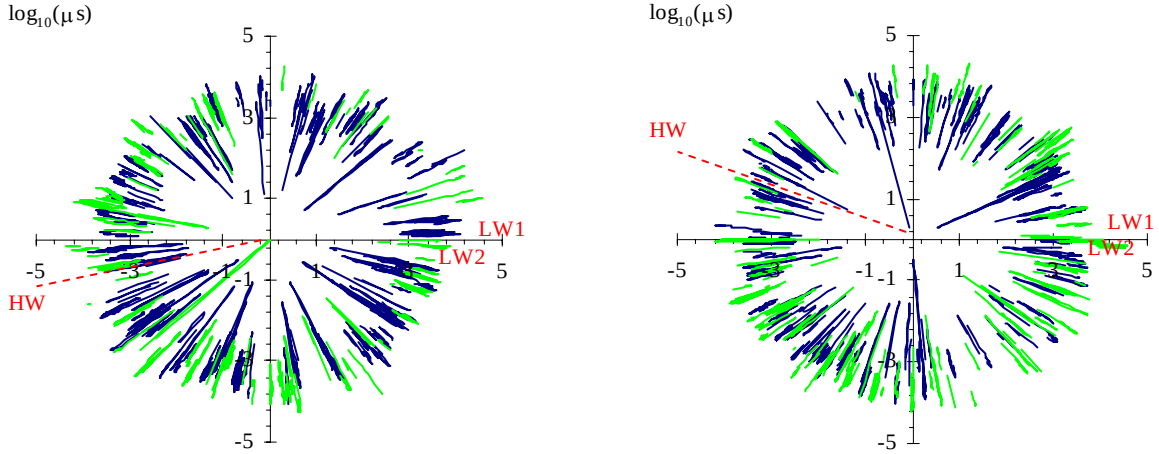

(C) τ_{Ey} for first minor tide (TC61)

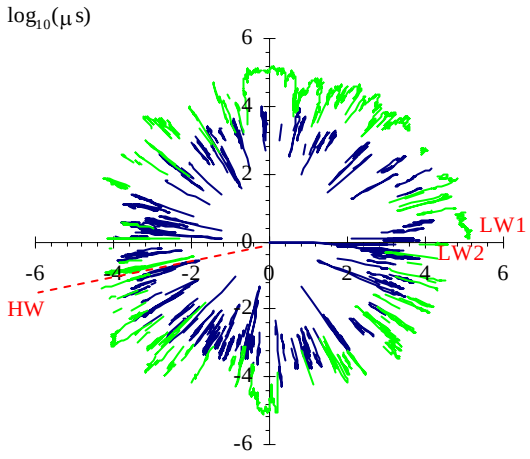

(D) τ_{Ey} for first major tide (TC62)

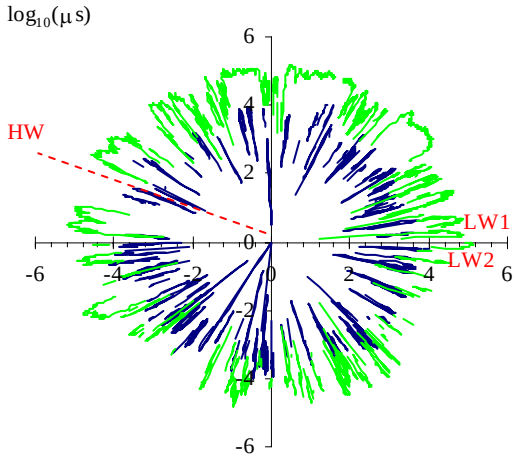

Fig. 5-12 - Effects of vertical sampling elevation in the streamwise integral time scales T_{Ex} - Data collected at Site 2B, Eprapah Creek at 0.2 (2D microADV) and 0.4 m (3D ADV) above the bed, both 10.7 m from left bank during field work E6 (16-18 May 2005) - The axes have a logarithmic scale and the units are milliseconds

Legend: —— data at 0.2 m above the bed; —— data at 0.4 m above the bed

(A) T_{Ex} for first minor tide (TC61)

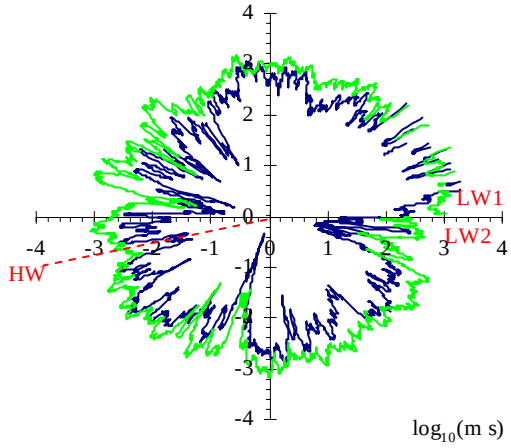

(B) T_{Ex} for first major tide (TC62)

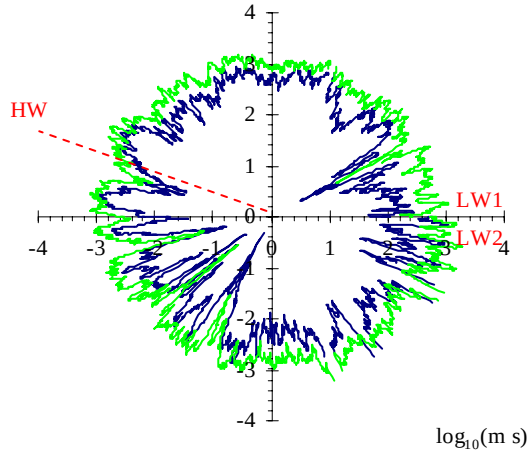

The trends in time-variations of streamwise integral time scales T_{Ex} were similar at 0.2 and 0.4 m above the bed, but no trend was easily discerned in terms of transverse integral time scales T_{Ey}. Figure 5-12 shows the streamwise integral time scales T_{Ex} at 0.2 and 0.4 m above the bed for two tidal cycles during the field work E6. (Note that the axes have a logarithmic scale and the units are ms.) Horizontal integral time scales were slightly larger at 0.2 m above the bed than those at 0.4 m above the bed. The horizontal integral time scales were typically between 0.4 and 2 s at 0.2 m above the bed and between 0.06 and 1 s at 0.4 m above the bed.

5.4.3 Turbulence property comparison between spring and neap tidal conditions

A systematic comparison between E5 and E6 field work data may provide some insights into the properties of the extreme tide conditions. The standard deviations of the horizontal velocity components (v_x' and v_y') were approximately four times larger during the spring tide conditions

(field work E5) than for the neap tide conditions of field study E6. Figure 5-13 illustrates the standard deviations of the streamwise velocity v_X' variation during two tidal cycles. It shows also some differences in the time-variations of v_X' between the minor and major tides, with some increased asymmetry for the major tidal cycles (Fig. 5-13B).

Fig. 5-13 - Effects of spring tide conditions on the standard deviations of streamwise velocity v_X' during a tidal cycle - Data collected at Site 2B, Eprapah Creek using the 3D ADV system at 0.1 m above the bed for field work E5 and 0.4 m above the bed for field work E6 - The units are cm/s
Legend: —— v_X' 0.1 m above the bed (field work E5); —— v_X' 0.4 m above the bed (field work E6)

(A) v_X' (cm/s) for second minor tide (TC63) for field work E6 and minor tide (TC51) for field work E5

(B) v_X' (cm/s) for second major tide (TC64) for field work E6 and major tide (TC52) for field work E5

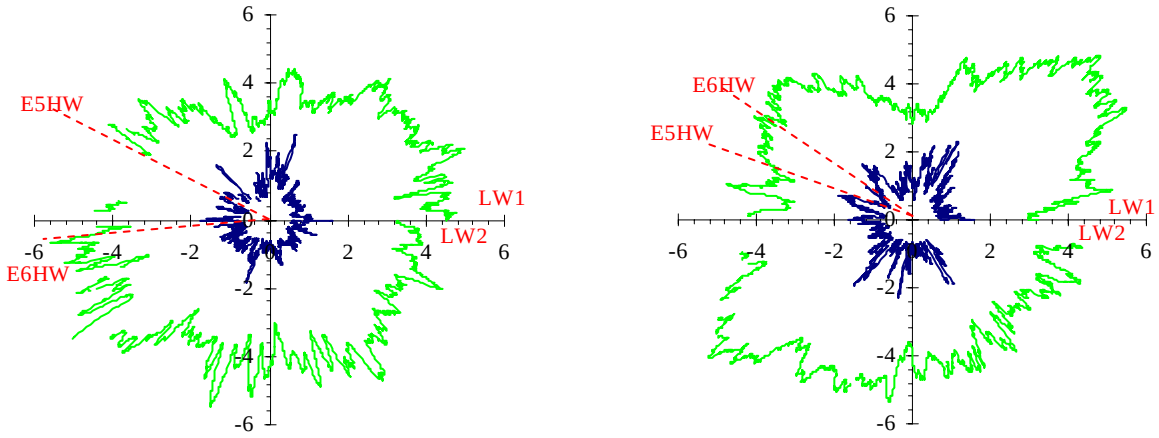

Fig. 5-14 - Effects of spring tide conditions on the standard deviations of tangential Reynolds stress $(\rho*v_X*v_Z)$' during a tidal cycle - Data collected at Site 2B, Eprapah Creek using 3D ADV at 0.1 m above the bed (field work E5) and 0.4 m above the bed (field work E6), 10.7 m from left bank in both field works - The units are Pa - Legend: —— $(\rho*v_X*v_Z)$' 0.1 m above the bed (field work E5); —— $(\rho*v_X*v_Z)$' 0.4 m above the bed (field work E6)

(A) $(\rho*v_X*v_Z)$' (Pa) for second minor tide (TC63) for field work E6 and minor tide (TC51) for field work E5

(B) $(\rho*v_X*v_Z)$' (Pa) for second major tide (TC64) for field work E6 and major tide (TC52) for field work E5

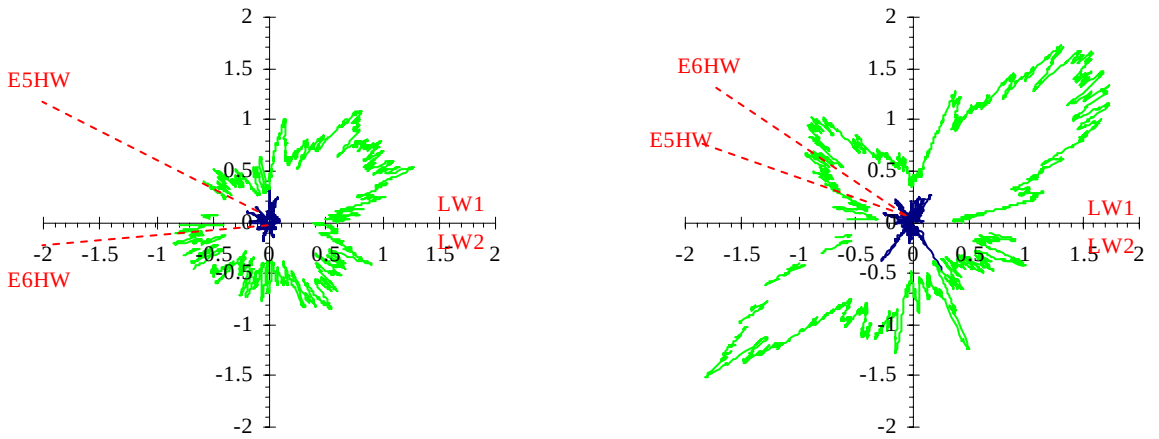

Fig. 5-15 - Effects of spring tide conditions on the dissipation time scales in streamwise τ_{E_X} and vertical τ_{E_Z} during a tidal cycle - Data collected at Site 2B, Eprapah Creek using the 3D ADV system at 0.1 m above the bed (field work E5) and 0.4 m above the bed (field work E6), 10.7 m from left bank in both field works - The axes have a logarithmic scale and the units are microseconds - Legend: —— data at 0.1 m above the bed (field work E5); —— data at 0.4 m above the bed (field work E6)

(A) τ_{E_X} for second minor tide (TC63) for field work E6 and minor tide (TC51) for field work E5

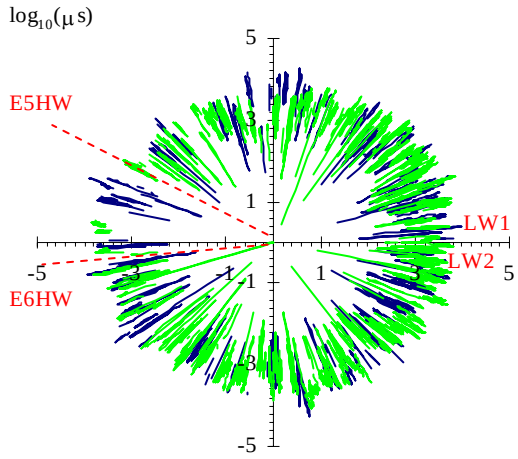

(B) τ_{E_X} for second major tide (TC64) for field work E6 and major tide (TC52) for field work E5

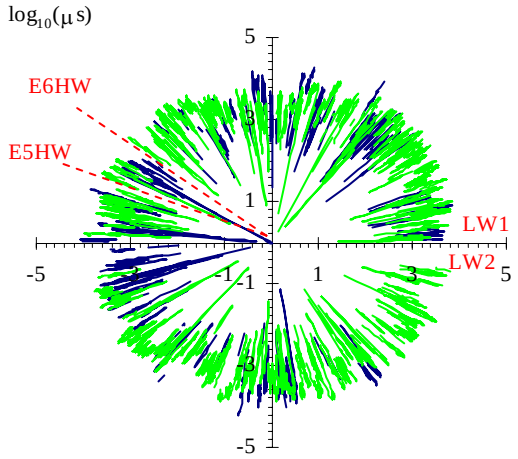

(C) τ_{E_Z} for second minor tide (TC63) for field work E6 and minor tide (TC51) for field work E5

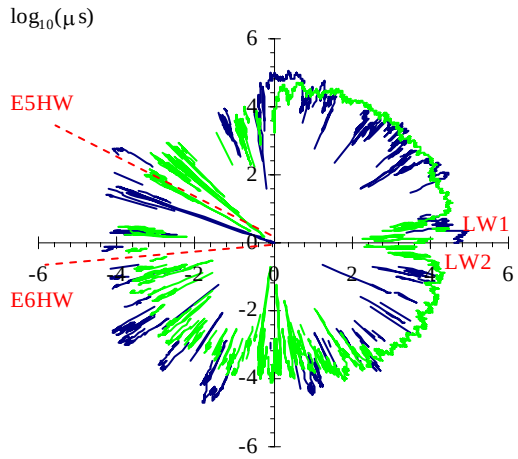

(D) τ_{E_Z} for second major tide (TC64) for field work E6 and major tide (TC52) for field work E5

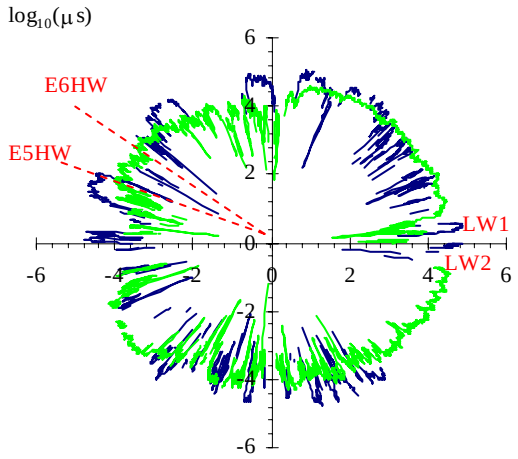

The standard deviations of the vertical velocity v_Z' were at least two times larger during the spring tide conditions than those during the neap tidal conditions.

The standard deviations of the tangential Reynolds stresses $(\rho*v_X*v_Z)'$ and $(\rho*v_X*v_Y)'$ were an order of magnitude larger during the spring tidal conditions (field work E5) than those during the neap tidal conditions (field work E6). Figure 5-14 presents the standard deviations of Reynolds stress $(\rho*v_X*v_Z)'$ for two tidal cycles in each field study. It shows some significant differences in the time-variations of $(\rho*v_X*v_Z)'$ between spring and neap tides. Comparatively larger asymmetries were seen during the major tidal cycle (Fig. 5-14B), but some asymmetry was also noted during the minor tidal cycle (Fig. 5-14A). The finding is valid for both field works E5 and E6.

For the field works E5 and E6, all dissipation time scales seemed independent of the tidal range as well as the tidal phase. Figure 5-15 illustrates the streamwise τ_{Ex} and vertical τ_{Ez} dissipation time scales for field works E5 and E6 during two tidal cycles. Basically, the dissipation time scales for spring (field work E5) and neap (field work E6) tide conditions were about the same. The dissipation time scales were relatively symmetrical throughout each tidal cycle. Both horizontal dissipation time scales τ_{Ex} and τ_{Ey} seemed of similar magnitude under spring and neap tide conditions : i.e., typically between 0.0007 to 0.01 s.

The vertical dissipation time scales τ_{Ez} had also a similar order of magnitude for both spring and neap tide conditions. The magnitude of the vertical dissipation time scales τ_{Ez} was however larger than those of both horizontal time scales: i.e., τ_{Ez} between 0.001 to 0.09 s typically.

The integral time scales of all velocity components were smaller during spring tide conditions (field work E5) than during neap tide conditions (field work E6). The smaller integral time scales during spring tides might be related to the larger flow velocities of the spring tidal forcing. Figure 5-16 shows the streamwise integral time scales T_{Ex} of field works E5 and E6 during two tidal cycles.

The integral time scales of all velocity components were typically between 0.1 and 0.5 s for field work E5 (spring tide) and between 0.1 and 2 s for field work E6 (neap tide). The time variations in horizontal integral time scales showed similar trends between the streamwise and transverse directions, but a less obvious trend between vertical and horizontal integral time scale. Some asymmetry in time variations of integral time scales during a tidal cycle indicates that the tidal phase seemed to affect the integral time scales of all velocity components.

Table 5-5 summarises the range of all dissipation and integral time scales that were observed during the field works E5 and E6. In Table 5-5 the elevation above the bed and the instrumentation are indicated (columns 2 and 3).

Fig. 5-16 - Effects of spring tide conditions on the integral time scales of streamwise velocity T_{Ex} during a tidal cycle - Data collected at Site 2B, Eprapah Creek using the 3D ADV system at 0.1 m above the bed (field work E5) and 0.4 m above the bed (field work E6), 10.7 m from left bank in both field works - The axes have a logarithmic scale and the units are milliseconds

Legend: —— data at 0.1 m above the bed (field work E5); —— data at 0.4 m above the bed (field work E6)

(A) T_{Ex} for second minor tide (TC63) for field work E6 and minor tide (TC51) for field work E5

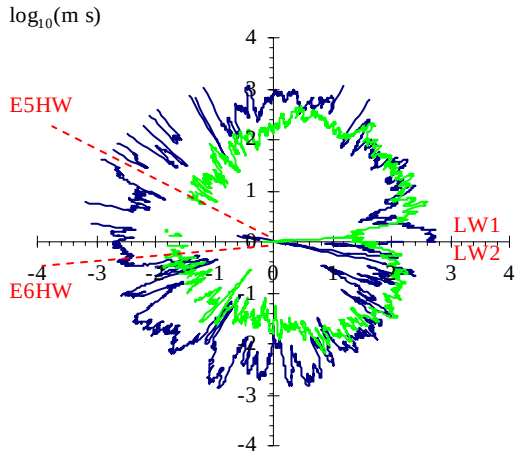

(B) T_{Ex} for second major tide (TC64) for field work E6 and major tide (TC52) for field work E5

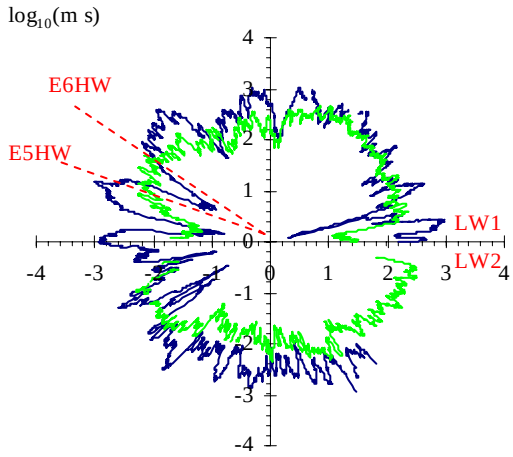

Table 5-5 - Summary of integral and dissipation time scales ranges for the majority of samples collected during the field works E5 and E6 at Eprapah Creek

Field study	Sampling elevation above the bed (m)	Instrumentation	Dissipation time scales			Integral time scales		
			τ_{Ex} (s)	τ_{Ey} (s)	τ_{Ez} (s)	T_{Ex} (s)	T_{Ey} (s)	T_{Ey} (s)
(1)	(2)	(3)	(4)	(5)	(6)	(7)	(8)	(9)
E5 (spring tide)	0.1	3D ADV (10 MHz)	0.0007 to 0.01	0.0007 to 0.01	0.001 to 0.05	0.02 to 0.4	0.03 to 0.4	0.1 to 0.5
E6 (neap tide)	0.4	3D ADV (10 MHz)	0.0007 to 0.01	0.0007 to 0.01	0.003 to 0.09	0.06 to 1	0.07 to 1	0.6 to 2
	0.2	2D microADV (16 MHz)	0.0009 to 0.02	0.001 to 0.1	--	0.4 to 2	0.7 to 2	--

Note: -- : data not available for that velocity component.

5.5 TURBULENT MIXING PARAMETERS

Some estimates of the momentum exchange coefficient, ν_T and mixing length l_m were derived for the field works E4 and E5 (Table 5-6). The results provide some information on the turbulent mixing in the estuarine zone.

In turbulent flows, the Reynolds stress tensor is derived from the vertical velocity gradient:

$$- \rho * \overline{v_x * v_z} = \rho * \nu_T * \frac{\partial \overline{V_x}}{\partial z} \quad (5\text{-}1)$$

where ν_T is the momentum exchange coefficient, also called "eddy viscosity", x is the streamwise direction and z is the direction normal to the solid boundary. During momentum exchanges, a mixing length l_m characterises the dimensions of the lumps of fluid which move in a normal direction (PRANDTL 1925). It is a local property of the flow. Within the assumptions of the mixing length theory, the mixing length may be expressed as :

$$- \rho * \overline{v_x * v_z} = \rho * l_m^2 * \frac{\partial \overline{V_x}}{\partial z} * \left| \frac{\partial \overline{V_x}}{\partial z} \right| \quad (5\text{-}2)$$

where the absolute value function was introduced to account that the sign of the tangential Reynolds stress must change with that of $\partial\overline{V_x}/\partial z$. The above equation is called Prandtl mixing length hypothesis (SCHLICHTING 1979, SCHLICHTING and GERSTEN 2000).

Herein the momentum exchange coefficient ν_T and mixing length l_m were calculated when the sampling elevation z was relatively close to the bed (Table 5-6, column 4), and it was reasonable to assume that $\partial\overline{V_x}/\partial z \approx \overline{V_x}/z$ since $\overline{V_x}(z=0) = 0$. Equations (5-1) and (5-2) become :

$$\nu_T \approx \left| \frac{\overline{v_x * v_z}}{\frac{\overline{V_x}}{z}} \right| \quad (5\text{-}3)$$

$$l_m^2 \approx \frac{\left|\overline{v_x * v_z}\right|}{\left(\frac{\overline{V_x}}{z}\right)^2} \qquad (5\text{-}4)$$

"Eddy viscosity" and mixing length data were calculated using Equations (5-3) and (5-4) for the field studies E4 and E5. The sampling volume elevation z was 0.05 and 0.1 m respectively for these studies (Table 5-6).

Figure 5-17 shows the momentum exchange coefficient during flood and ebb tides for both field studies. Despite some scatter during the ebb tide, the momentum exchange coefficient ν_T appears to be a function of the time-averaged streamwise velocity $\overline{V_x}$ that is positive downstream. The values of momentum mixing coefficient were generally greater during the flood tide than those observed during the ebb tide. KAWANISI (2004) observed similarly that the "eddy viscosity" values were greater during the flood than ebb tide in a Japanese estuary. For the field works E4 and E5, the momentum exchange coefficient values were typically between 1 E-5 and 5 E-4 m^2/s. The results were comparable to momentum exchange coefficient values observed in estuarine tidal channels by KAWANISI (2004) and RALSTON and STACEY (2005). The dimensionless "eddy viscosity" $\nu_T/(z*\sqrt{g*d})$ data were between about 0.00005 and 0.001 for both field studies, where g is the gravity acceleration and d is the water depth at the sampling location.

The mixing length l_m characterises the dimensions of the lumps of fluid which move in the vertical direction z during turbulent mixing. Figure 5-18 presents the dimensionless mixing length l_m/z as a function of the time-averaged streamwise velocity $\overline{V_x}$ for the field works E4 and E5. The mixing length seemed larger during the flood tide than for the ebb tide. The mixing length l_m data were between 0.002 and 0.06 m for both field works.

Overall the observations of momentum mixing coefficients showed a large data scatter spreading over more than three orders of magnitudes, and associated with relatively rapid variations with time (Fig. 5-17). The assumption of "constant" mixing coefficient is simply untrue in the estuarine zone of Eprapah Creek, although commonly used in numerical modelling of contaminant transport in rivers and estuaries.

Figure 5-17 - Momentum exchange coefficient ν_T as a function of time-averaged streamwise velocity $\overline{V_x}$ (positive downstream) - Data collected at Site 2B Eprapah Creek at z = 0.1 m above the bed during field work E5 (08/03/2005) and z = 0.05 m for field work E4 (02/09/2004) - Momentum exchange coefficient calculated for 5,000 data points every 10 s along the entire data set
Legend: [•] data for field work E5; [•] data for field work E4

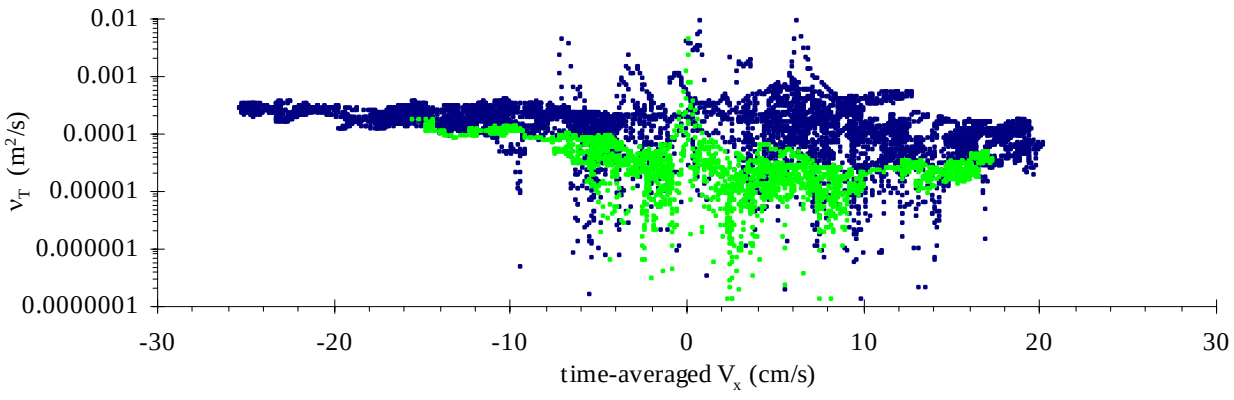

Figure 5-18 - Dimensionless mixing length l_m/z as a function of time-averaged streamwise velocity $\overline{V_X}$ (positive downstream) - Data collected at Site 2B Eprapah Creek at z = 0.1 m above the bed during field work E5 (08/03/2005) and z = 0.05 m for field work E4 (02/09/2004) - Mixing length calculated for 5,000 data points every 10 s along the entire data set
Legend: [•] data for field work E5; [•] data for field work E4

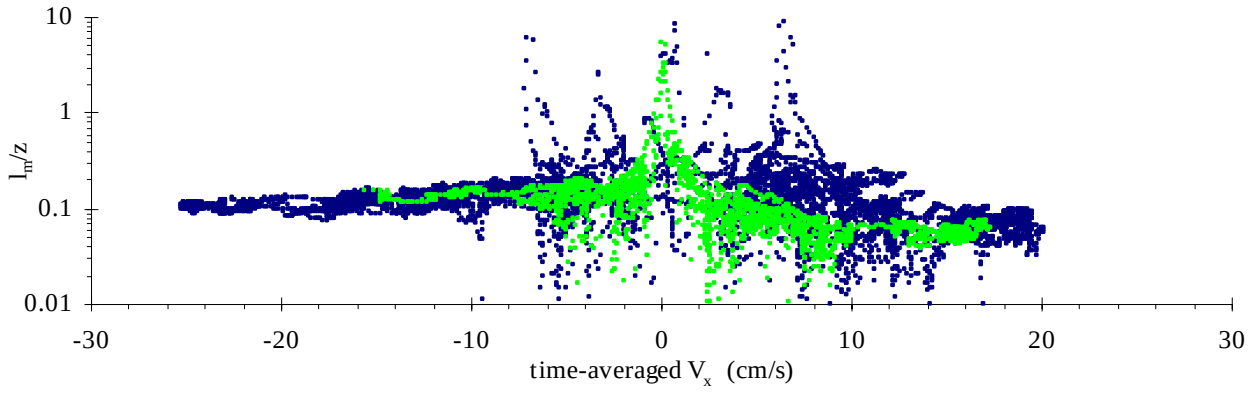

Table 5-6 - Turbulence field measurements at Eprapah Creek QLD during the field works E4 and E5

Ref. (1)	Dates (2)	Tidal range (m) (3)	z (m) (4)	ADV system (5)	Sampling rate (Hz) (6)	Sampling duration (7)	Probe location (8)
E4	2 Sept. 2004	1.81	0.052	10 MHz	25	6 & 3 hours	AMTD 2.1 km, 10.4 m from left bank.
E5	8-9 March 2005	2.37	0.095	10 MHz	25	25 hours	AMTD 2.1 km, 10.4 m from left bank.

6. SUMMARY AND CONCLUDING REMARKS

Detailed turbulence and physio-chemistry field measurements were conducted in a small subtropical estuary of Eastern Australia with a semi-diurnal tidal regime. The estuarine system is a drowned river valley (coastal plain) type that is shallow with large width to depth ratio, with a cross-section which deepens and widens towards the mouth, a small freshwater inflow, extensive mud flat surroundings and a sinuous central channel (Fig. 6-1). The turbulent velocity measurements were performed continuously at high frequency for 25 hours during spring tide conditions and for 50 hours during neap tide conditions. The data were collected as part of a series of large-scale, on-going field experiments also involving physio-chemistry measurements, monitoring of the local meteorological conditions, and some other measurements. Turbulent velocities were measured with acoustic Doppler velocimetry. A thorough post-processing technique was developed and applied to remove electronic noises, physical disturbances and Doppler effects. The post-processed data sets included the instantaneous velocity components, the statistical moments of each velocity component, the instantaneous Reynolds stress tensor, and the statistical moments of the tangential Reynolds stresses. An auto-correlation analysis yielded further the Eulerian dissipation and integral time scales. Mixing length and "eddy viscoisty" results were further deduced.

The two field studies were conducted with a maximum tidal range of 2.45 m (spring tide) and 1.2 m (neap tide) respectively. During the neap tide study, the estuary was stratified and exhibited strong vertical and longitudinal gradients in physio-chemical parameters. In contrast, the estuary was relatively well-mixed during the field study with spring tide conditions.

1. Estuarine flow turbulence

The estuarine flow is a fluctuating process. That is, the bulk parameters (e.g. water depth, time-average streamwise velocity) were time-dependant and they fluctuated with periods comparable to tidal cycles and other large-scale processes. However turbulence properties depended upon the instantaneous local flow properties and were little affected by the flow history. The structure and temporal variability of turbulence characteristics were influenced by a variety of mechanisms. This resulted in behaviour which deviated from that for equilibrium turbulent boundary layer induced by velocity shear only.

Some tidal asymmetry was observed systematically. The time-averaged streamwise velocity during the ebb tides was smaller than that during the flood tide. The finding was consistent with earlier field observations in estuaries. The turbulent fluctuations next to the bed were highly intermittent. They were likely caused by a combination of 'background' fluctuations and high-energy events ([1]). The flow region next to the bed might also be influenced by physio-chemical and biological activities. The normalised third (skewness) and fourth (kurtosis) moments of velocity fluctuations appeared to be within the range ±0.6 and -1 to +2 respectively (App. D). The transverse and vertical turbulence intensities were typically within the range of $v_y'/v_x' \sim 1$ and $v_z'/v_x' \sim 0.3$ to 0.8 implying some turbulence anisotropy. The magnitudes were similar to earlier field work studies and experimental measurements in turbulent open channel flows.

The time-averaged Reynolds stresses $\rho * \overline{v_x * v_z}$ were proportional to minus the time-averaged streamwise velocity $\overline{V_x}$. The order of magnitude of $\rho * \overline{v_x * v_z}$ differed between spring and neap tide conditions, but the dimensionless Reynolds stresses $R_{vxvz} = \overline{v_x * v_z}/(v_x' * v_z')$ were similar for both spring and neap tide conditions. The probability distribution functions of tangential Reynolds stresses differed substantially from Gaussian distributions. The normalised third and fourth

[1]Such high-energy events (HEE) were discussed by NIKORA et al. (2002).

moments of tangential Reynolds stresses appeared to be within the range ±2.3 and +2 to +30 respectively.
The integral time scales ranged typically between 0.01 and 2 s for all the data sets. These are rough measures of the longest connection in the turbulent behaviour of each velocity component. The dimensionless integral time scales were about : T_{Ey}/T_{Ex} ~ 1 and T_{Ez}/T_{Ex} ~ 2 to 3 through all the field studies. The findings were consistent with the anisotropy reported above and with an earlier study in a tidal channel. The dissipation time scales are a measure of the smallest energetic time scales and of the most rapid changes that occur in the turbulent fluctuations of a velocity component. Present results indicated that the dissipation time scales were typically between 1 and 10 ms. Further the dissipation time scales were basically independent of the tidal phase, tidal range and sampling elevation (within z = 0.1 to 0.4 m). They were related with the microscopic turbulence structures and were little affected by the mean flow properties and history.
The momentum mixing coefficients were derived for two field studies. The quantitative values spread over more than three orders of magnitudes, and they were associated with relatively rapid variations with time. These results were comparable to other study results in tidal channels, and demonstrate that any assumption of "constant" mixing coefficient is simply untrue in estuarine systems.
A striking feature of the analysed data sets is the large fluctuations in all turbulence characteristics during the tidal cycles. This feature was rarely documented, but an important difference between the ADV data sets used in this study from earlier reported measurements is that the present data were collected continuously at high frequency during relatively long periods. Present results suggested indeed that turbulence data collected at lower frequencies cannot capture accurately the turbulence dissipative processes.

2. Comparative analyses

During a full diurnal tidal cycle, the two tidal cycles were of slightly different periods and tidal ranges indicating that a diurnal inequality existed in the tides during the field works. Differences in turbulence properties were observed between the minor and major tidal cycles.
In addition a comparative analysis demonstrated basic differences in turbulence properties between neap and spring tide conditions. During spring tides, the tidal forcing was associated with drastically larger turbulence levels and tangential Reynolds stress magnitude.

3. Unusual events

Around high and low tide slacks, some multiple flow reversal events were observed. These were documented. The flow reversal events were observed more frequently during the neap tide field study, and they are believed to be linked with some internal and external resonance.
During the second field trip with neap tides and some stratification, a front was observed once. All the instruments were operating at the time. The data suggested that the front passage was associated with some temperature anomaly next to the free-surface, and some secondary circulation next to the bed.

It is believed that the present results provided a picture general enough to be used, as a first approximation, to characterise the flow field in similar small subtropical estuaries. A new set of field deployment is planned to clarify the upper estuary dynamics in more detail. The measurement techniques used in this study showed that they were suitable for investigating momentum transport mechanisms for small estuarine systems with shallow water depths (less than 0.5 m at low tides).

Fig. 6-1 - Photographs of Eprapah Creek, Redlands QLD (Photographs H. CHANSON)
(A) Site 2B at low tide on 31 Aug. 2004 around 17:00, view from the left bank - Note the two low flow channels in the foreground and in the background behind the rocks

(B) Site 2B during early flood tide on 9 March 2005 around 06:00 at sunrise, view from the left bank

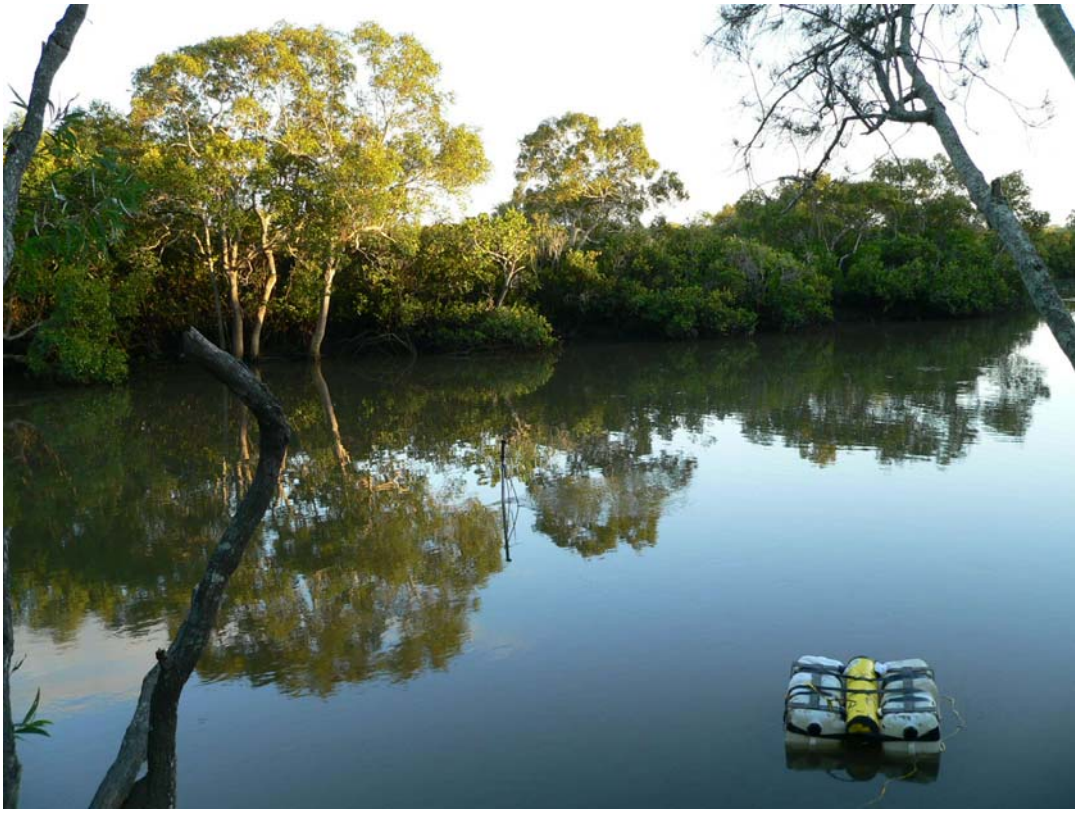

(C) Site 2B at high tide on 9 March 2005, looking at the left bank from a boat

7. ACKNOWLEDGMENTS

The writers thank Professor Shin-ichi AOKI (Toyohashi University of Technology), Dr Jon HINWOOD (Monash University), and Robert SCHWARTZ (Qld E.P.A.) for their detailed review of the report and their valuable comments.

The writers acknowledge the strong support and assistance of Dr Ian RAMSAY and John FERRIS (Qld E.P.A.). They thank all the people who participated to the field works, in particular Dave McINTOSH (Q.U.T.), Carlos GONZALEZ (The University of Queensland), Ben LIM (Q.U.T.), Clive BOOTH (The University of Queensland) and Jon JAMES (Q.U.T.).

The first writer acknowledges the financial support of the Australian Research Council in the form of an APA-I scholarship (grant LP0347242).

APPENDIX A – FIELD DATA FROM EPRAPAH CREEK (QLD) ON 8-9 MARCH 2005 (FIELD WORK E5)

A.1 - PRESENTATION

New data were collected at Eprapah Creek (Australia) during the field work E5 on the 8-9 March 2005. Measurements were performed at Site 2B that is located 2.1 km upstream of the river mouth. Turbulence data were collected with a 3D ADV Sontek 10MHz (down-looking head) logged continuously at 25 Hz throughout the investigation period. The ADV sampling volume was located 0.1 m above the bed and 10.7 m from the left bank. Physio-chemistry data were collected by a YSI6600 probe logged every 6 s during the investigation period. The YSI6600 sampling volume was located approximately 0.1 m above the bed and 10.4 m from the left bank reference position: that is, 0.3 m apart from the ADV sampling volume. Instantaneous water temperature, conductivity, water level, pH, turbidity, and dissolved oxygen samples were recorded.

Vertical profiles of physio-chemistry were performed on 10 March 2005 at the river mouth, at Site 2, at Site 2C and at the treatment plant outfall (AMTD 2.7 km). Measurements were conducted in the middle of the creek at several sites. They were performed during the ebb flow using a physio-chemistry probe YSI™6920 lowered from a boat drifting with the flow.

In addition manual readings of air temperature and water depth were collected at Site 2B every 15 minutes during the investigation. Air temperature readings were collected on a Mercury thermometer, and water levels were measured from measuring staff attached to instrumentation frame. Manual water level readings matched closely those recorded by YSI6600 modelling and are not shown herein.

Turbulent flow properties

The appendix includes instantaneous velocities and tangential Reynolds stresses, the time-averages and standard deviations of each instantaneous parameter, vertical and horizontal turbulence intensities, Reynolds stress correlation coefficients, and integral and dissipation time scales. Herein turbulence intensities are defined as the ratio of standard deviation of the transverse or vertical velocities to standard deviation of the streamwise velocity (horizontal: v_y'/v_x'; vertical: v_z'/v_x'). The correlation coefficient of Reynolds stress is a dimensionless ratio of covariance of two velocity components divided by the product of the standard deviations of those two tangential velocities ($R_{vxvy} = \overline{v_x v_y}/(v_x' v_y')$; $R_{vxvz} = \overline{v_x v_z}/(v_x' v_z')$; $R_{vyvz} = \overline{v_y v_z}/(v_y' v_z')$).

PIQUET (1999) defined the integral time scale T_E as:

$$T_E = \int_{\tau=0}^{\tau(R_{ii}\,(\tau)=0)} R_{ii}(\tau)\,d\tau \qquad \text{(A1)}$$

where τ is the time lag, R_{ii} is the normalised auto-correlation function, i is a direction tensor (i= x, y, z), and $\tau(R_{ii}\,(\tau)=0)$ is the time lag for which $R_{ii}=0$ (Fig. A-1A). Integral time scales are equal to the area under the normalised auto-correlation curve up to $R_{ii}(\tau)=0$. Fig. A-1A illustrates the calculation of the integral time scale. The integral time scale T_E is a measure of the longest connection in the turbulent behaviour of $v(\tau)$.

The dissipation time scale τ_E is a measure of the most rapid changes that occur in the turbulent fluctuations of velocity v(t) (HINZE (1975)). It is related to the curvature of the auto-correlation function at the origin ($\tau = 0$). Using the Taylor series expansion of the auto-correlation function, the dissipation time scale τ_E may be expressed as:

Fig. A-1 - Definition sketch for the dissipation and integral time scales.

(A) Calculation of the integral time scale using the area under the auto-correlation function

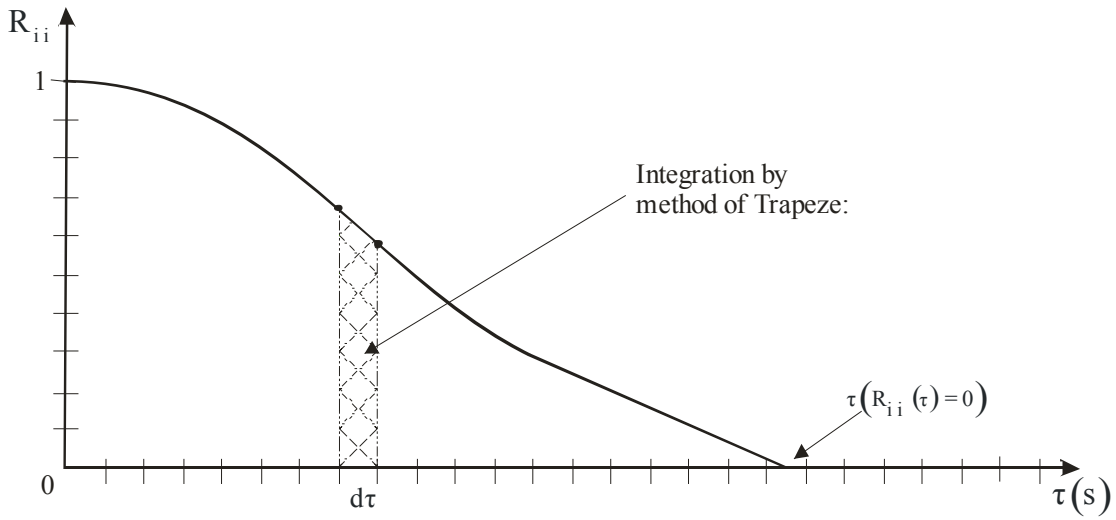

(B) Estimation of the dissipation time scale using a quadratic interpolation

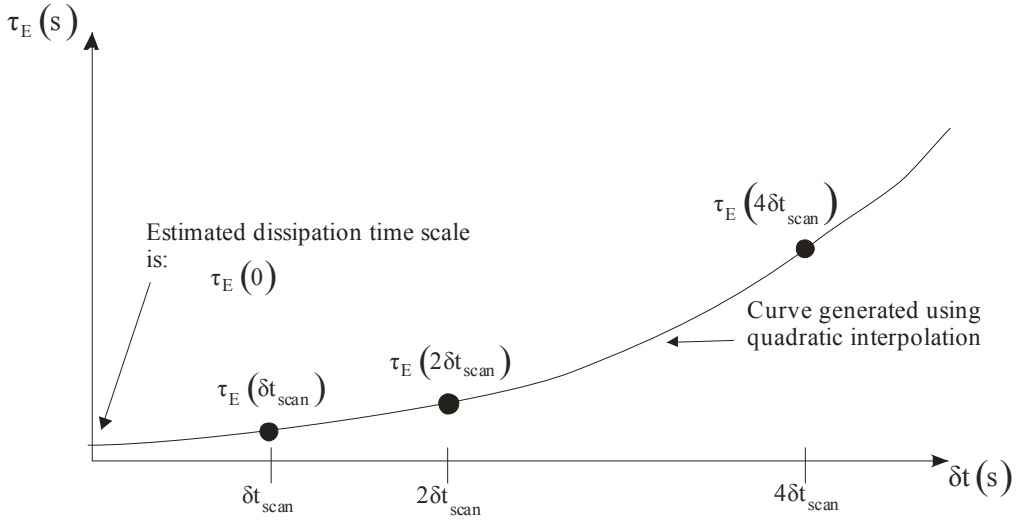

$$\tau_E = \sqrt{\frac{2\,v'^2}{\left(\frac{\delta v}{\delta t}\right)^2}} \qquad \text{(A2)}$$

HALLBACK et al. (1989), FRANSSON et al. (2005), and KOCH and CHANSON (2005) used the above to obtain a measured time scale $\tau_E(\delta t)$ based upon the time increment δt:

$$\tau_E(\delta t) = \sqrt{\frac{2\,v'^2}{\left(\frac{\delta v}{\delta t}\right)^2}} \qquad \text{(A3)}$$

where v' standard deviation of velocity component, δt_{scan} is the experimental scan rate ($1/F_{scan}$, F_{scan}=25 Hz), δt is the incremental time scale calculation sampling rate ($\delta t_{scan} \leq \delta t \leq 4\,\delta t_{scan}$). As the dissipation time scale τ_E is smaller than the sampling time scale δt_{scan}, several values of $\tau_E(\delta t)$

were calculated to estimate the dissipation time scale τ_E. The dissipation time scale τ_E equals $\tau_E(0)$ when δt tends to zero: $\tau_E = \tau_E(0)$. Quadratic interpolation may be used (KOCH and CHANSON 2005) to extrapolate the value of $\tau_E(0)$ from those $\tau_E(\delta t)$ calculated. $\tau_E(\delta t)$ was calculated for $\delta t = \delta t_{scan}$, $2*\delta t_{scan}$, and $4*\delta t_{scan}$, and these values of $\tau_E(\delta t)$ were used to solve for $\tau_E(0)$ through:

$$\tau_E(\delta t) = \tau_E(0) + a\,\delta t^2 + b\,\delta t \qquad \text{(A4)}$$

where a and b are constants calculated from best data fit. Fig. A-1B explains the calculation of the dissipation time scale through quadratic interpolation.

The turbulence properties were calculated for 5000 data points (200 s) every 10 s along the entire data set. The instantaneous velocity fluctuations v were calculated at each data point as $v = V - \overline{V}$ where V is the instantaneous velocity measurement and $\overline{V}$ is the time-average calculated over 5000 data points. Instantaneous tangential Reynolds stresses were calculated using the instantaneous velocity data. During this investigation the positive velocity directions were downstream ($V_x>0$), towards left bank ($V_y>0$), and upwards ($V_z>0$).

Notation

F_{scan}	sampling frequency (Hz);
i	directional tensor;
$R_{i\,i}$	auto-correlation function;
R_{vxvy}	correlation coefficient of tangential Reynolds stress $\rho v_x v_z$: $R_{vxvy} = \overline{v_x v_y} / (v'_x v'_y)$
R_{vxvz}	correlation coefficient of Reynolds stress $\rho v_x v_y$: $R_{vxvz} = \overline{v_x v_z} / (v'_x v'_z)$
R_{vyvz}	correlation coefficient of Reynolds stress $\rho v_y v_z$: $R_{vyvz} = \overline{v_y v_z} / (v'_y v'_z)$
T_E	Eulerian integral time scale (s);
T_{Ex}	Eulerian integral time scale of streamwise velocity (s);
T_{Ey}	Eulerian integral time scales of transverse velocity (s);
T_{Ez}	Eulerian integral time scale of vertical velocity (s);
V	instantaneous velocity (m/s);
V_x	instantaneous streamwise velocity (m/s);
V_y	instantaneous transverse velocity (m/s);
V_z	instantaneous vertical velocity (m/s);
$\overline{V}$	time-averaged velocity (m/s);
$\overline{V_x}$	time-averaged streamwise velocity (m/s);
$\overline{V_y}$	time-averaged transverse velocity (m/s);
$\overline{V_z}$	time-averaged vertical velocity (m/s);
v	turbulent velocity fluctuation (m/s) : $v = V - \overline{V}$
v'_x	standard deviation of streamwise velocity (m/s);

v_y' standard deviation of transverse velocity (m/s);

v_z' standard deviation of vertical velocity (m/s);

v_y'/v_x' horizontal turbulence intensity;

v_z'/v_x' vertical turbulence intensity;

δt time scale sampling rate (s);

δt_{scan} sampling scan rate (s);

$\rho v_x v_y$ instantaneous tangential Reynolds stress (Pa);

$\rho v_x v_z$ instantaneous tangential Reynolds stress (Pa);

$\rho v_y v_z$ instantaneous tangential Reynolds stress (Pa);

$\rho \overline{v_x v_y}$ time-averaged tangential Reynolds stress (Pa);

$\rho \overline{v_x v_z}$ time-averaged tangential Reynolds stress (Pa);

$\rho \overline{v_y v_z}$ time-averaged tangential Reynolds stress (Pa);

$\left(\rho v_x v_y\right)'$ standard deviation of tangential Reynolds stress (Pa);

$\left(\rho v_x v_z\right)'$ standard deviation of tangential Reynolds stress (Pa);

$\left(\rho v_y v_z\right)'$ standard deviation of tangential Reynolds stress (Pa);

τ time lag (s);

τ_E Eulerian dissipation time scale (s);

τ_{Ex} Eulerian dissipation time scale of streamwise velocity (s);

τ_{Ey} Eulerian dissipation time scale of transverse velocity (s);

τ_{Ez} Eulerian dissipation time scale of vertical velocity (s);

A.2 - TURBULENCE DATA

Fig. A-2 - Instantaneous velocity data collected at Site 2B Eprapah Creek (QLD) during field work E5 on 8-9 March 2005 - 3D ADV (10 MHz), scan rate: 25 Hz, Probe sensor: 0.1 m above bed, 10.7 m from left bank, Post-processed data

(A) Instantaneous streamwise velocity V_x

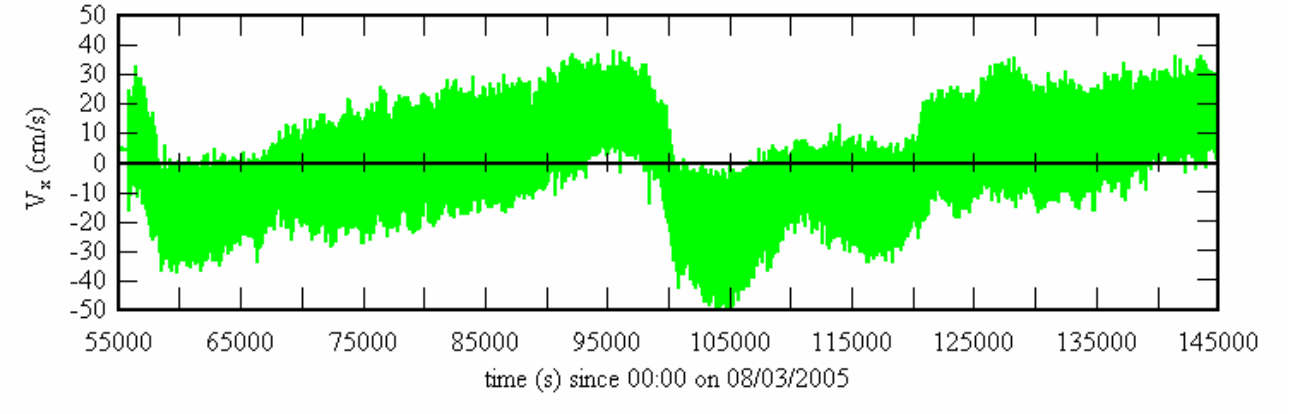

(B) Instantaneous transverse velocity V_y

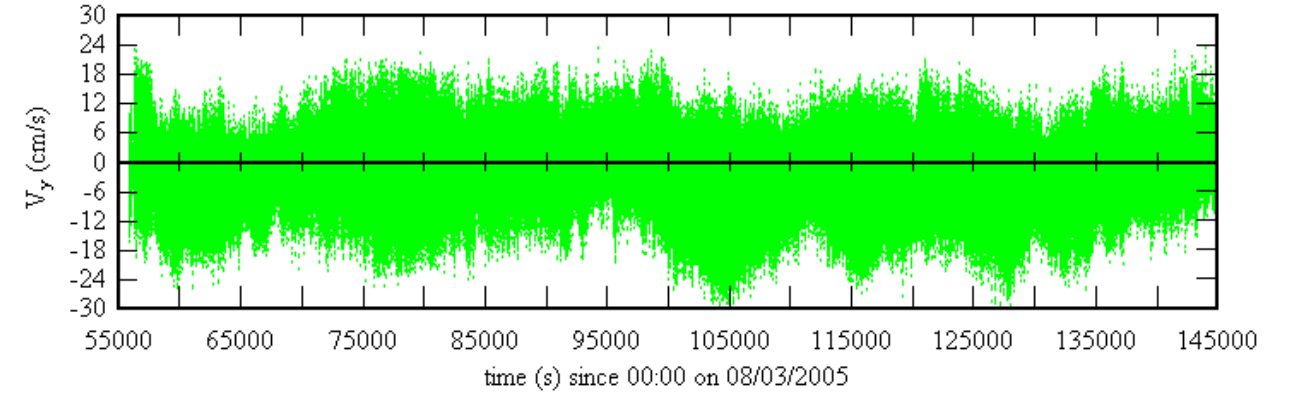

(C) Instantaneous vertical velocity V_z

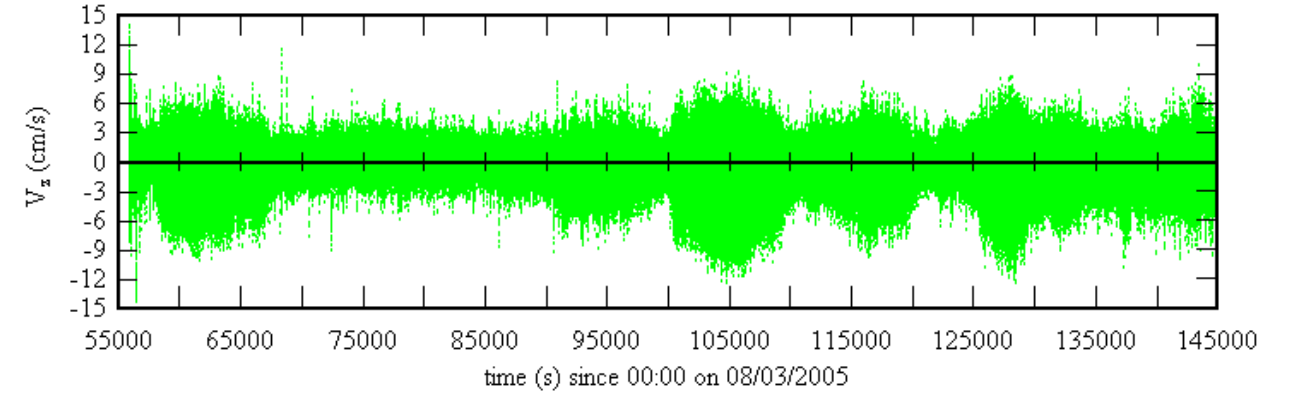

Fig. A-3 - Time-averaged velocity data collected at Site 2B Eprapah Creek (QLD) during field work E5 on 8-9 March 2005 - 3D ADV (10 MHz), scan rate: 25 Hz, Probe sensor: 0.1 m above bed, 10.7 m from left bank - Time-average based upon 5000 data points (3.33 minutes) taken every 10 s along entire data set

(A) Time-averaged streamwise velocity $\overline{V_x}$

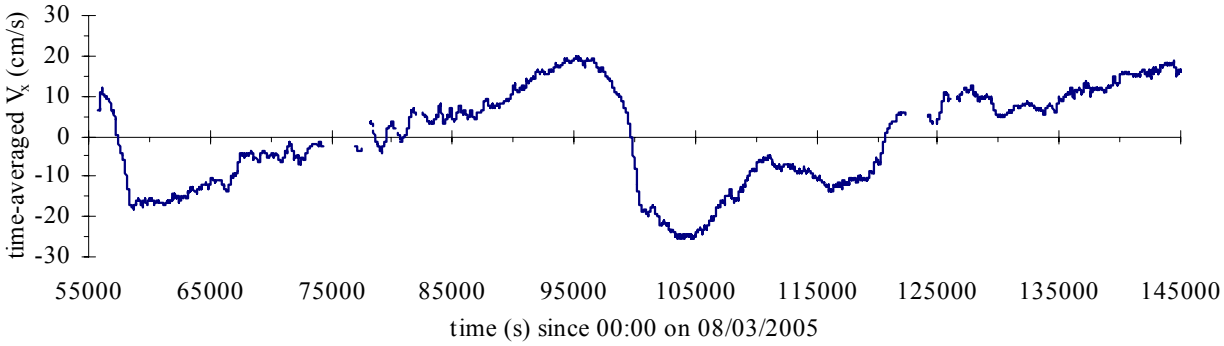

(B) Time-averaged transverse velocity $\overline{V_y}$

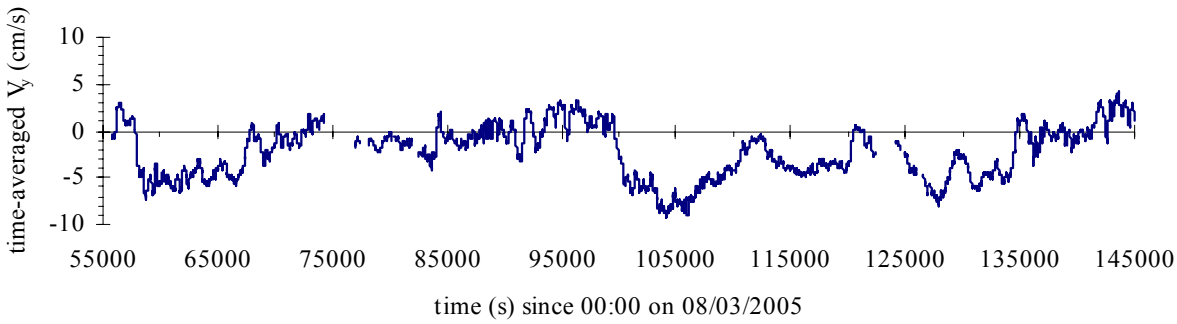

(C) Time-averaged vertical velocity $\overline{V_z}$

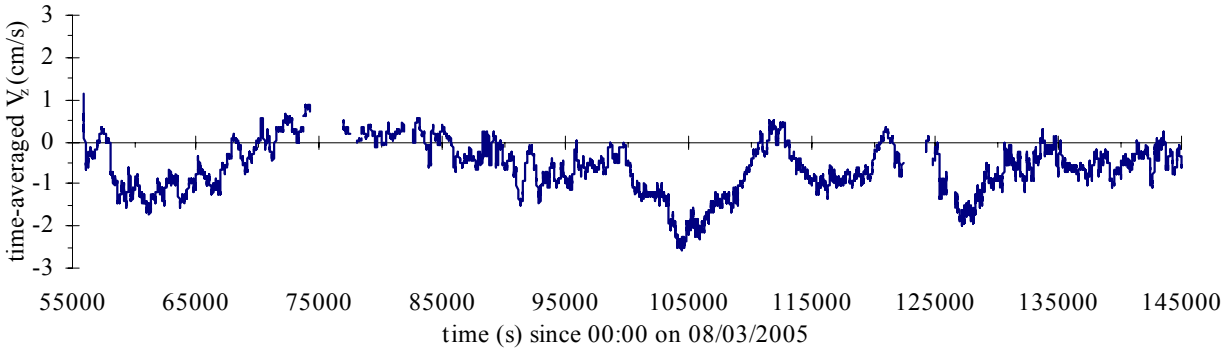

Fig. A-4 - Standard deviations of velocity data collected at Site 2B Eprapah Creek (QLD) during field work E5 on 8-9 March 2005 - 3D ADV (10 MHz), scan rate: 25 Hz, Probe sensor: 0.1 m above bed, 10.7 m from left bank - Standard deviations based upon 5000 data points (200 s) taken every 10 s along entire data set

(A) Standard deviations of streamwise velocity v_x'

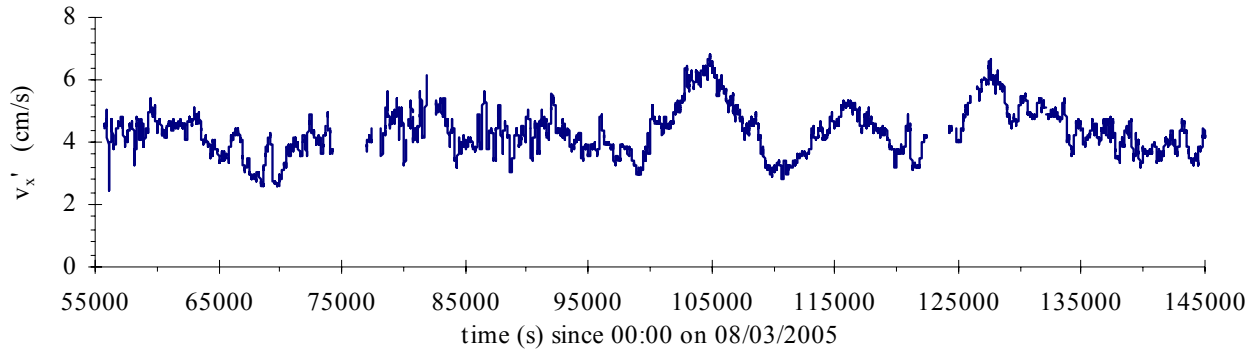

(B) Standard deviations of transverse velocity v_y'

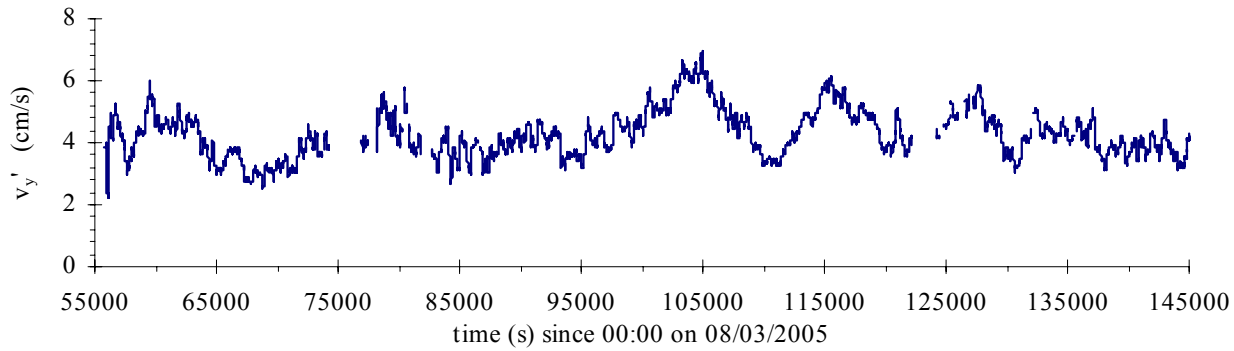

(C) Standard deviations of vertical velocity v_z'

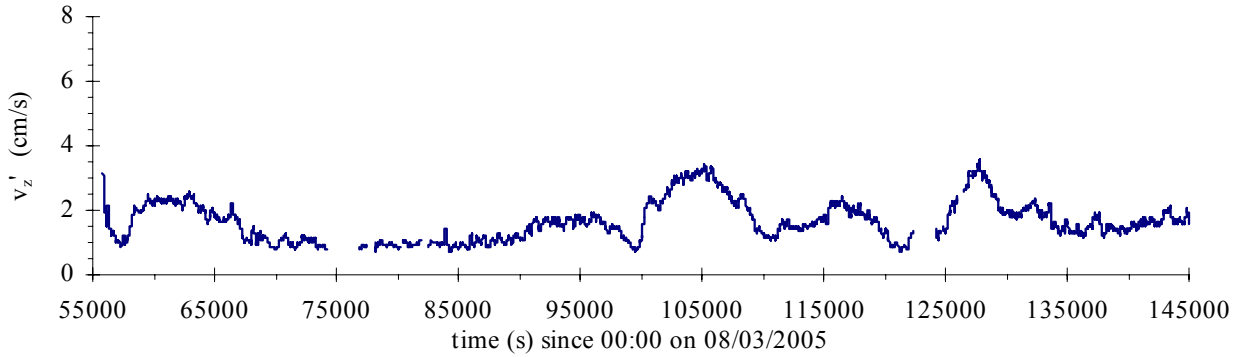

Fig. A-5 - Instantaneous tangential Reynolds stress data collected at Site 2B Eprapah Creek (QLD) during field work E5 on 8-9 March 2005 - 3D ADV (10 MHz), scan rate: 25 Hz, Probe sensor: 0.1 m above bed, 10.7 m from left bank - Instantaneous Reynolds stresses calculated every sample along entire data set (eg. $v_x = V_x - \overline{V_x}$) with $\overline{V_x}$ based upon 5000 data points (3.33 minutes).

(A) Instantaneous tangential Reynolds stress $\rho v_x v_y$

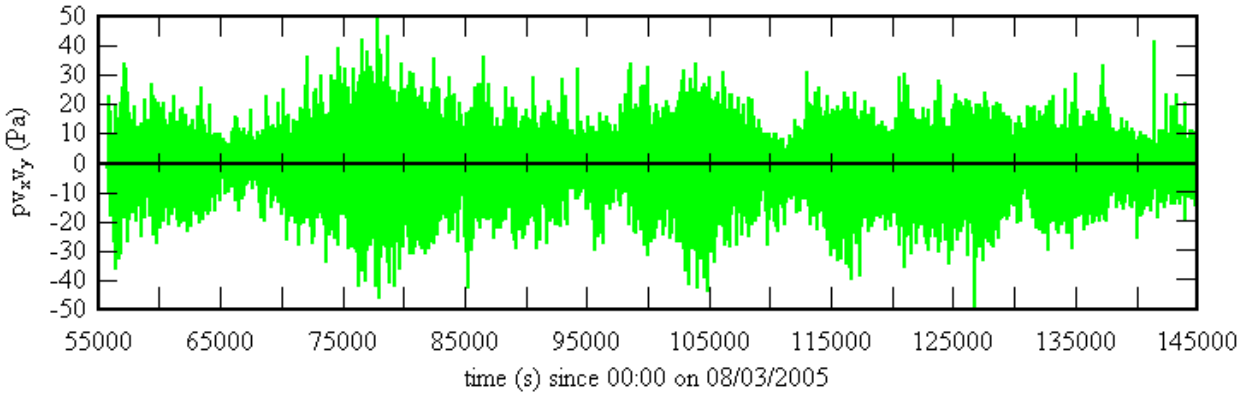

(B) Instantaneous tangential Reynolds stress $\rho v_x v_z$

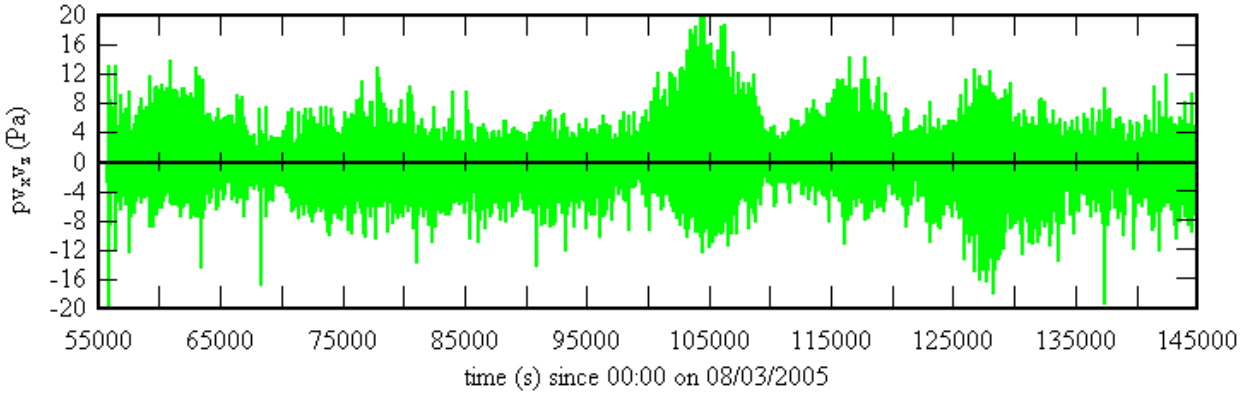

(C) Instantaneous tangential Reynolds stress $\rho v_y v_z$

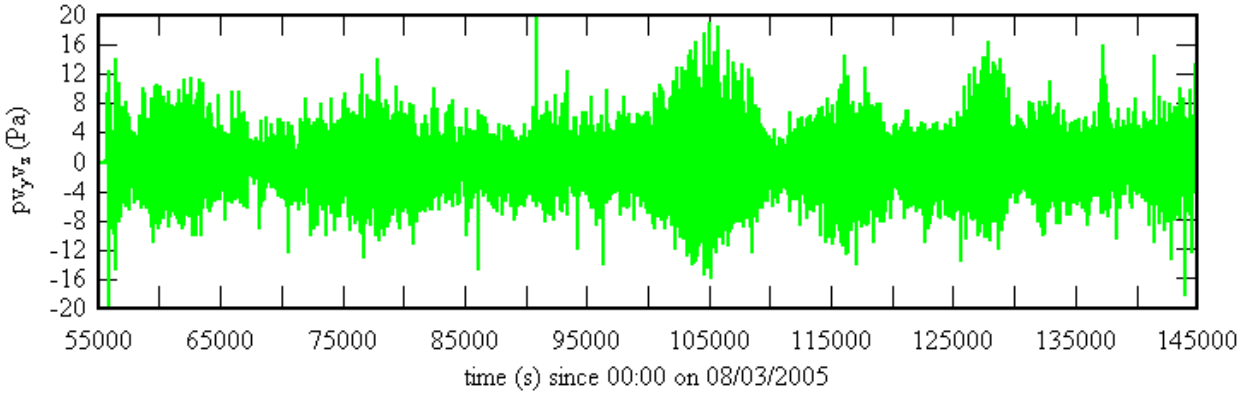

Fig. A-6 - Time-averaged tangential Reynolds stress data collected at Site 2B Eprapah Creek (QLD) during field work E5 on 8-9 March 2005 - 3D ADV (10 MHz), scan rate: 25 Hz, Probe sensor: 0.1 m above bed, 10.7 m from left bank - Time-averaged Reynolds stress based upon 5000 data points (3.33 minutes) taken every 10 s along entire data set

(A) Time-averaged tangential Reynolds stress $\rho\overline{v_x v_y}$

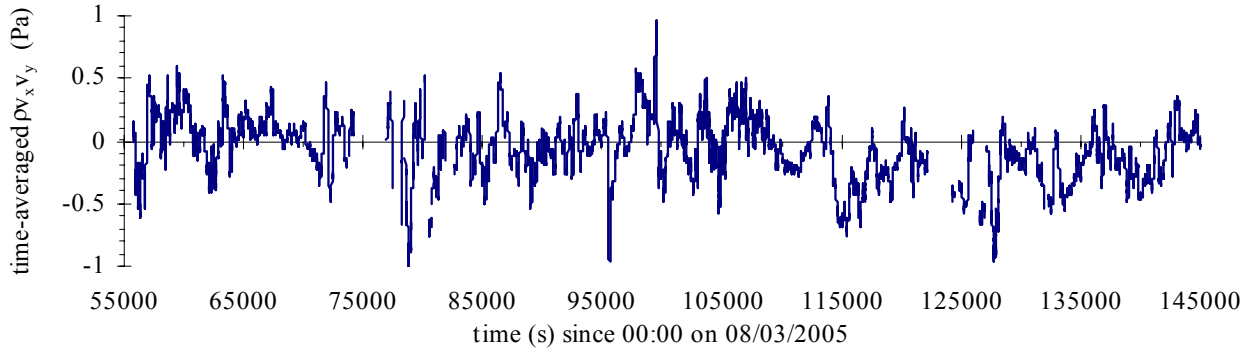

(B) Time-averaged tangential Reynolds stress $\rho\overline{v_x v_z}$

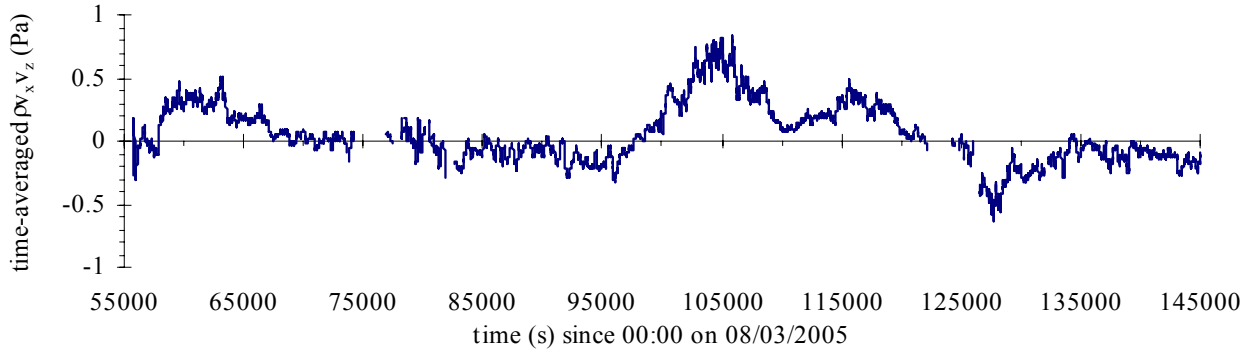

(C) Time-averaged tangential Reynolds stress $\rho\overline{v_y v_z}$

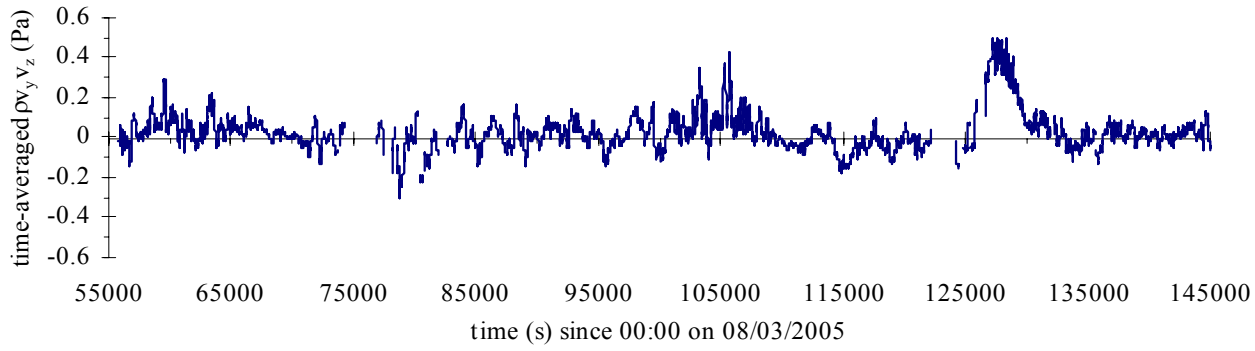

Fig. A-7 - Standard deviations of tangential Reynolds stress data collected at Site 2B Eprapah Creek (QLD) during field work E5 on 8-9 March 2005 - 3D ADV (10 MHz), scan rate: 25 Hz, Probe sensor: 0.1 m above bed, 10.7 m from left bank - Standard deviations of Reynolds stress based upon 5000 data points (3.33 minutes) taken every 10 s along entire data set

(A) Standard deviations of tangential Reynolds stress $\left(\rho v_x v_y\right)'$

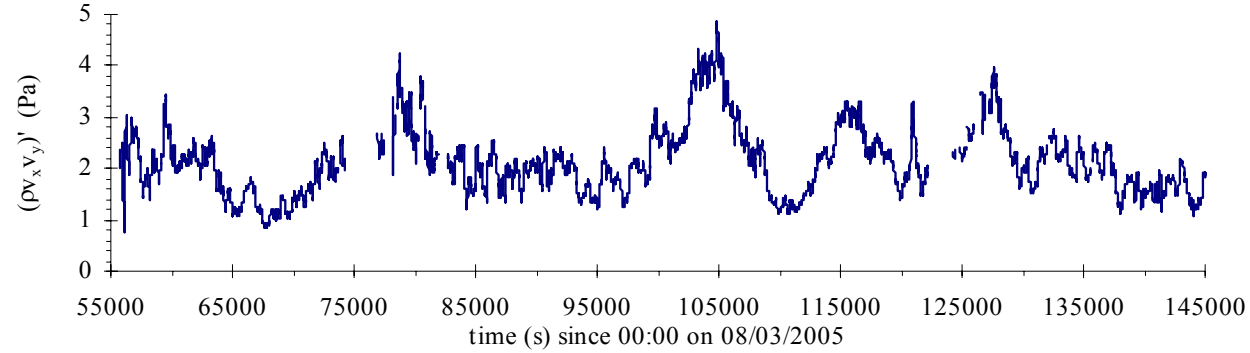

(B) Standard deviations of tangential Reynolds stress $\left(\rho v_x v_z\right)'$

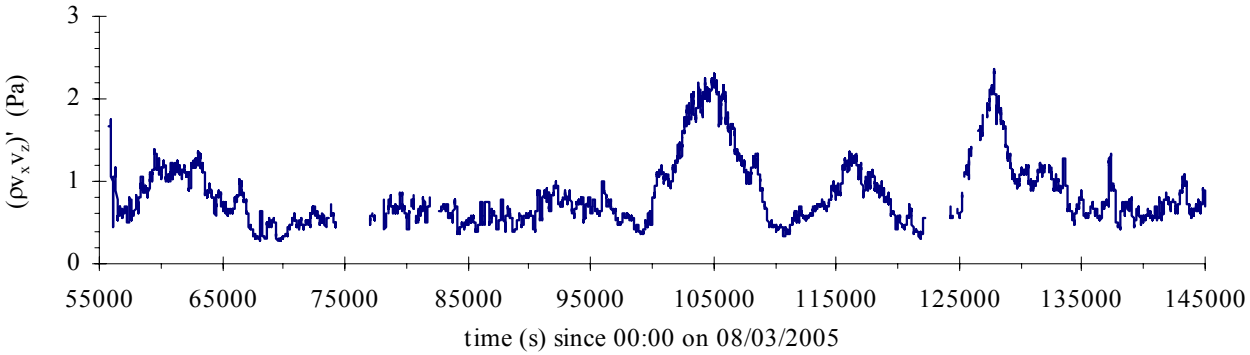

(C) Standard deviations of tangential Reynolds stress $\left(\rho v_y v_z\right)'$

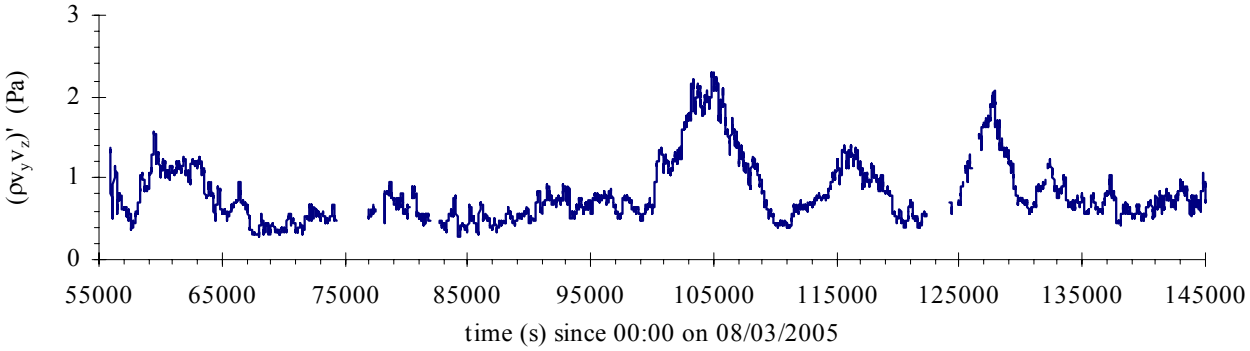

Fig. A-8 - Integral time scales T_E of velocity data collected at Site 2B Eprapah Creek (QLD) during field work E5 on 8-9 March 2005 - 3D ADV (10 MHz), scan rate: 25 Hz, Probe sensor: 0.1 m above bed, 10.7 m from left bank - Integral time scales based upon average of 20 correlation curves (250 data points) collected from 5000 data points (3.33 minutes) taken every 10 s along entire data set

(A) Integral time scales of streamwise velocity T_{Ex}

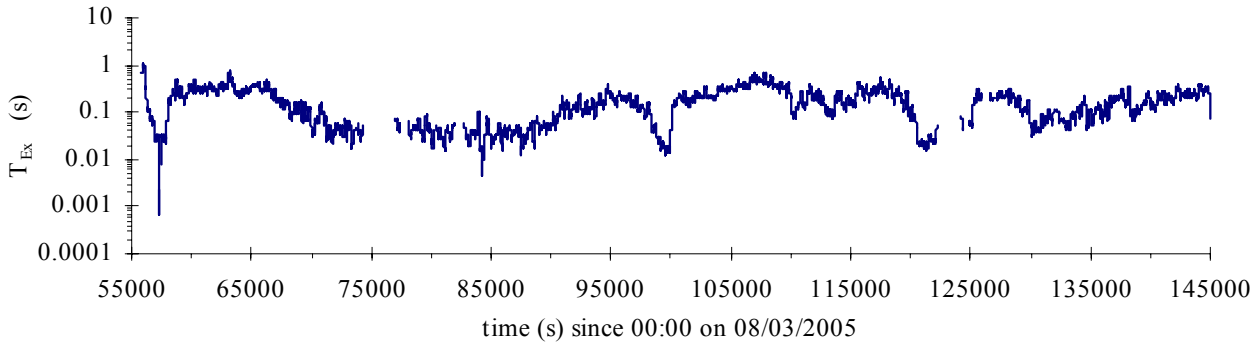

(B) Integral time scales of transverse velocity T_{Ey}

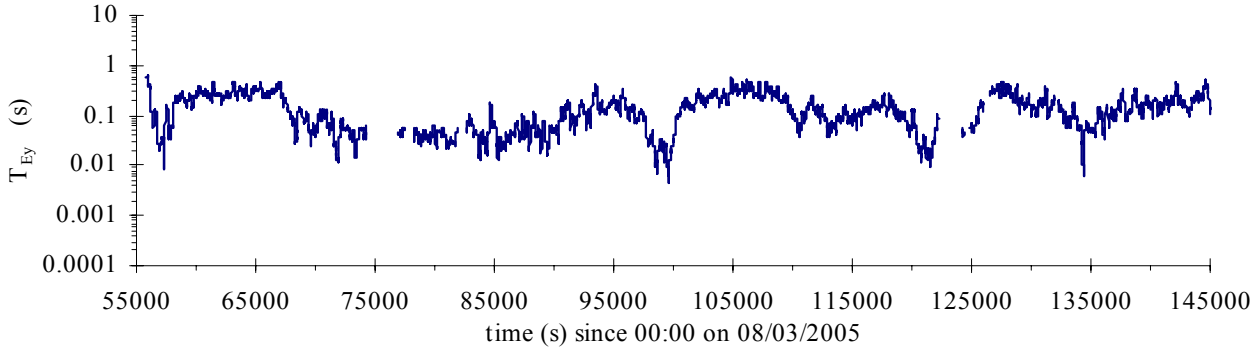

(C) Integral time scales of vertical velocity T_{Ez}

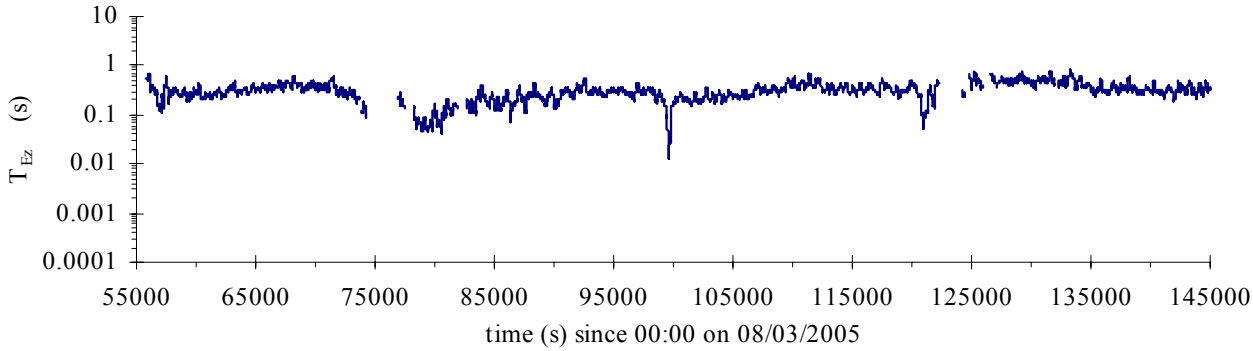

Fig. A-9 - Dissipation time scales τ_E of velocity data collected at Site 2B Eprapah Creek (QLD) during field work E5 on 8-9 March 2005 - 3D ADV (10 MHz), scan rate: 25 Hz, Probe sensor: 0.1 m above bed, 10.7 m from left bank - Dissipation time scales time-averaged over 5000 data points (3.33 minutes) taken every 10 s along entire data set.

(A) Dissipation time scales of streamwise velocity τ_{Ex}

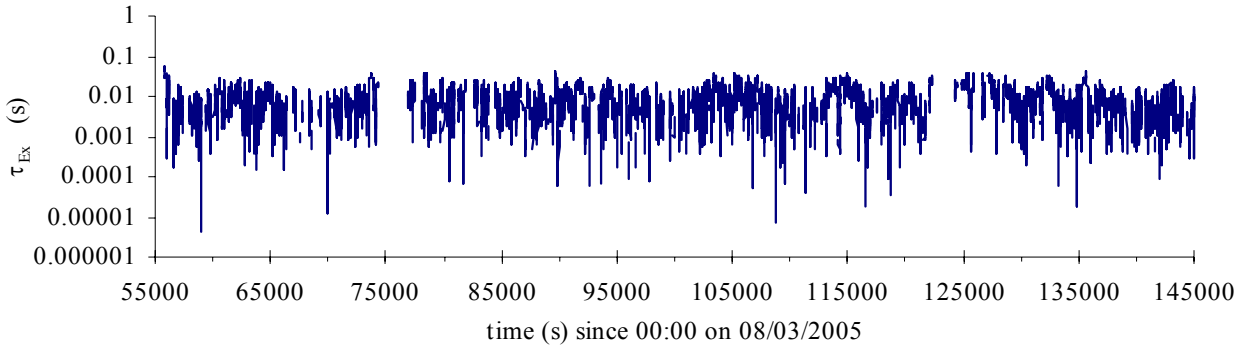

(B) Dissipation time scales of transverse velocity τ_{Ey}

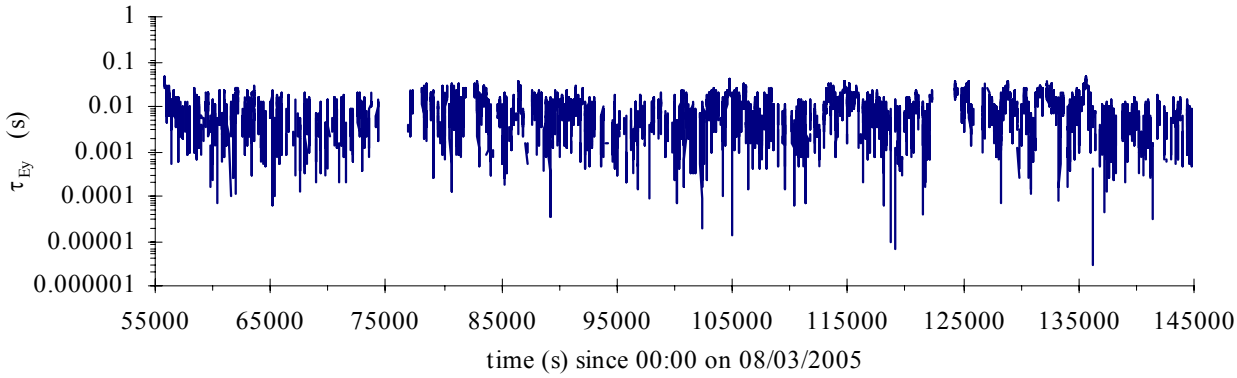

(C) Dissipation time scales of vertical velocity τ_{Ez}

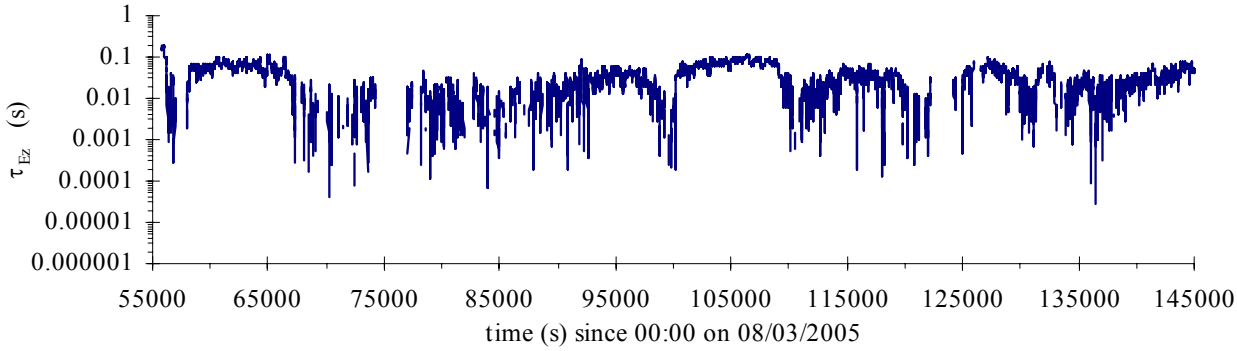

Fig. A-10 - Correlation coefficients of tangential Reynolds stress data collected at Site 2B Eprapah Creek (QLD) during field work E5 on 8-9 March 2005 - 3D ADV (10 MHz), scan rate: 25 Hz, Probe sensor: 0.1 m above bed, 10.7 m from left bank - Correlation coefficients of Reynolds stress based upon 5000 data points (3.33 minutes) taken every 10 s along entire data set.

(A) Correlation coefficient of tangential Reynolds stress R_{vxvy}

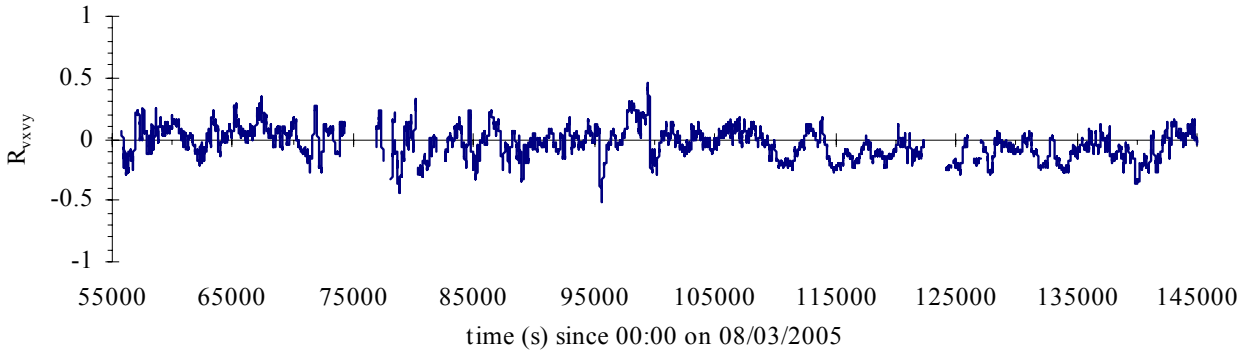

(B) Correlation coefficient of tangential Reynolds stress R_{vxvz}

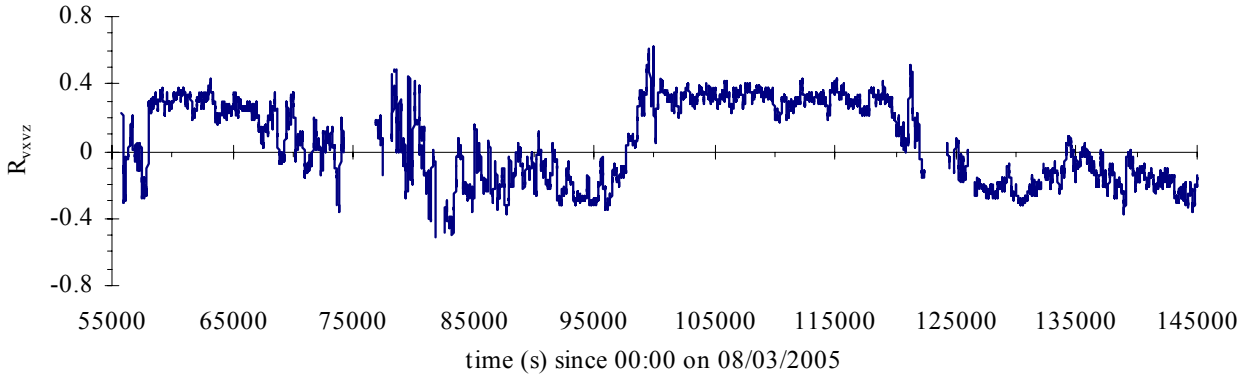

(C) Correlation coefficient of tangential Reynolds stress R_{vyvz}

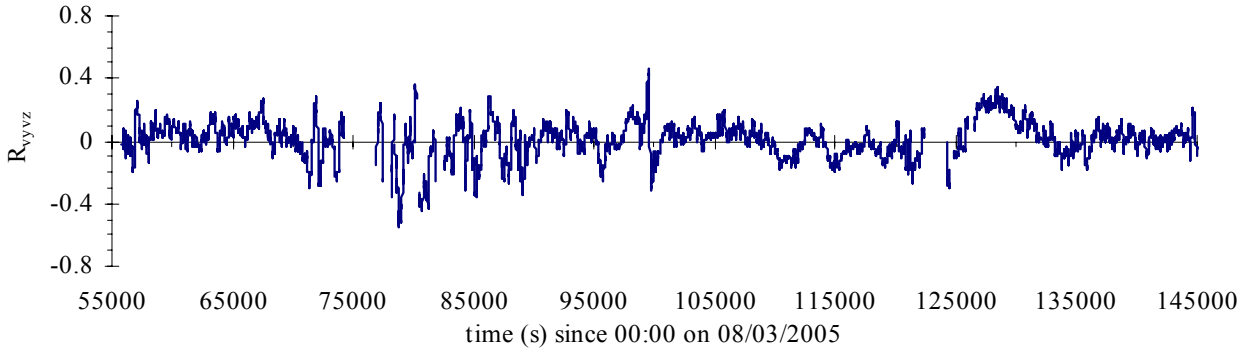

Fig. A-11 - Turbulence intensities data collected at Eprapah Creek (QLD) during field work E5 on 8-9 March 2005 - 3D ADV (10 MHz), scan rate: 25 Hz, Probe sensor: 0.1 m above bed, 10.7 m from left bank - Turbulence intensities based upon 5000 data points (3.33 minutes) taken every 10 s along entire data set.

(A) Horizontal turbulence intensity v_y'/v_x'

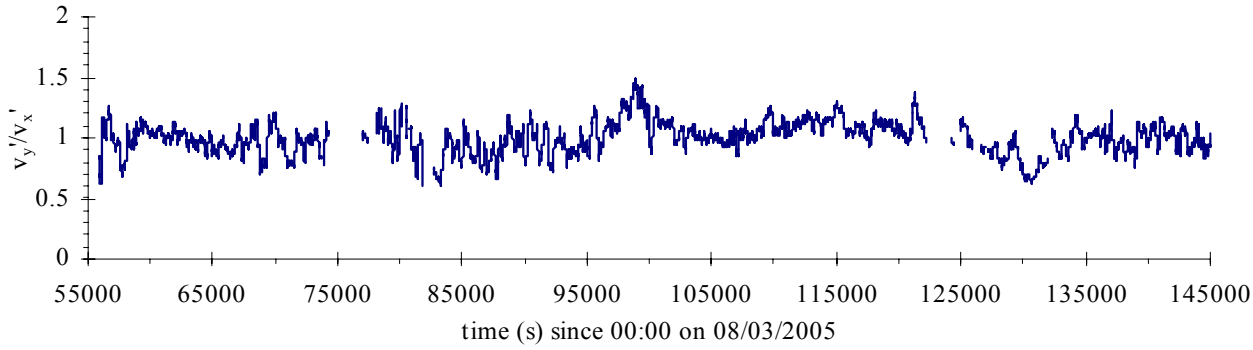

(B) Vertical turbulence intensity v_z'/v_x'

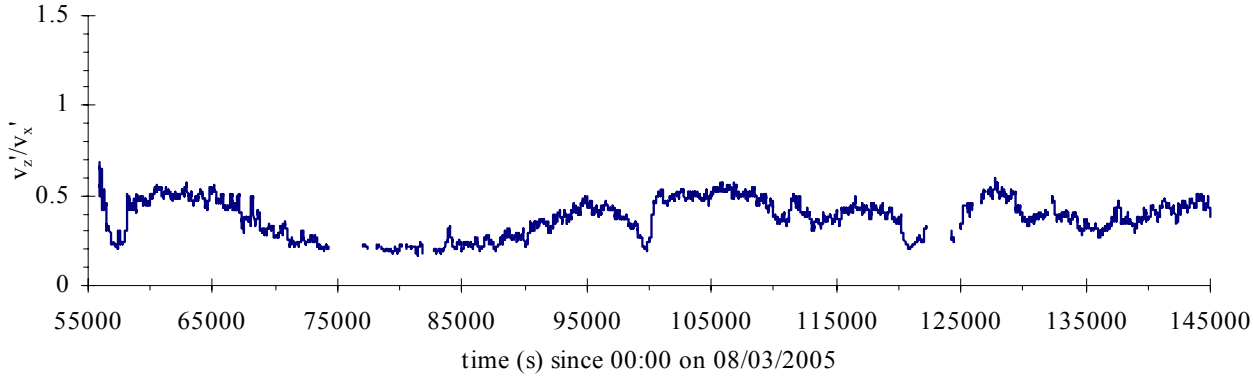

A.3 – PHYSIO-CHEMISTRY DATA

Fig. A-12 - Instantaneous air temperature and water depth data collected at Site 2B, Eprapah Creek (QLD) during field work E5 (8-9 March 2005) - Air temperature data collected every 15 minutes and water depth collected every 6 s using YSI6600 probe throughout field work E5.
Legend: [——] water depth Site 2B; [•] air temperature; [ ] period of darkness

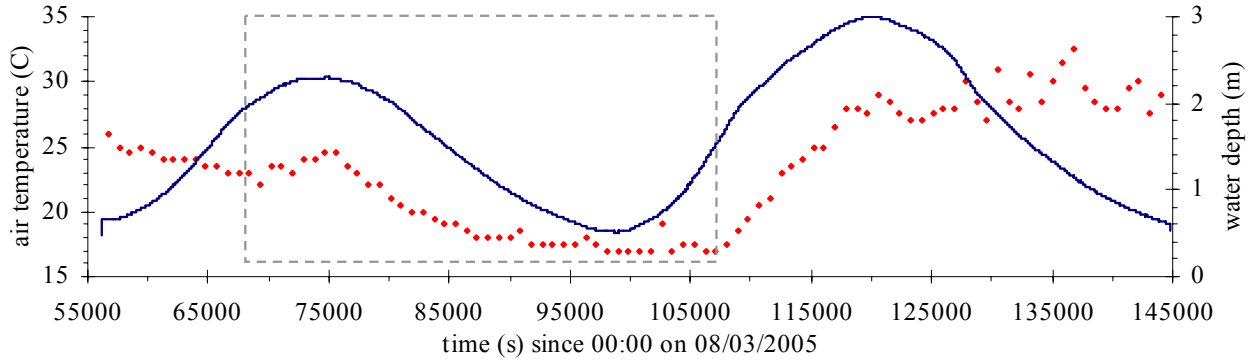

Fig. A-13 - Instantaneous water temperature and conductivity data collected at Site 2B, Eprapah Creek (QLD) during field work E5 on 8-9 March 2005 - Data sampled every 6 s at 0.1 m above bed, 10.4 m from left bank reference position.
Legend: [——] water temperature; [——] conductivity.

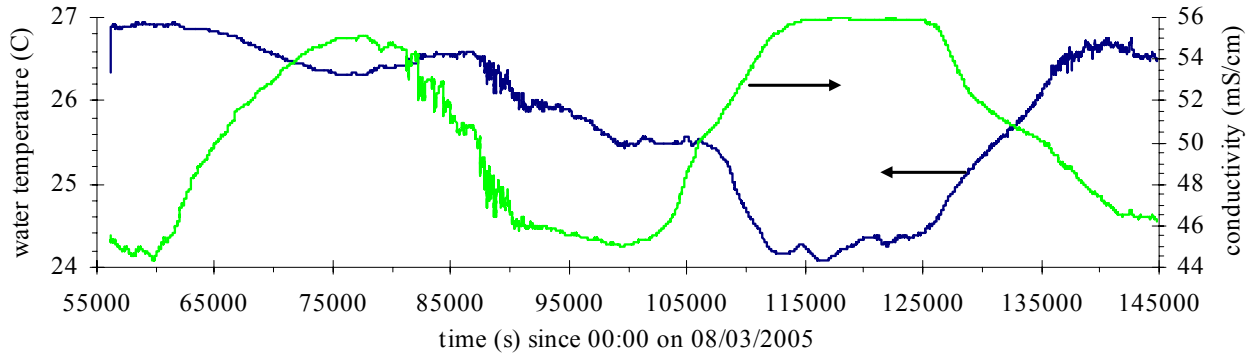

Fig. A-14 - Vertical profiles of water temperature, conductivity, dissolved oxygen, turbidity and pH collected at Eprapah Creek (QLD) on 10 March 2005 - Data sampled with a YSI6920 probe lowered from a boat drifting mid-stream with the current during the early ebb tide
(A) Water temperatures at the river mouth (AMTD 0 km), Site 2 (AMTD 2 km), Site 2C and AMTD 2.7 km (treatment plant outfall)

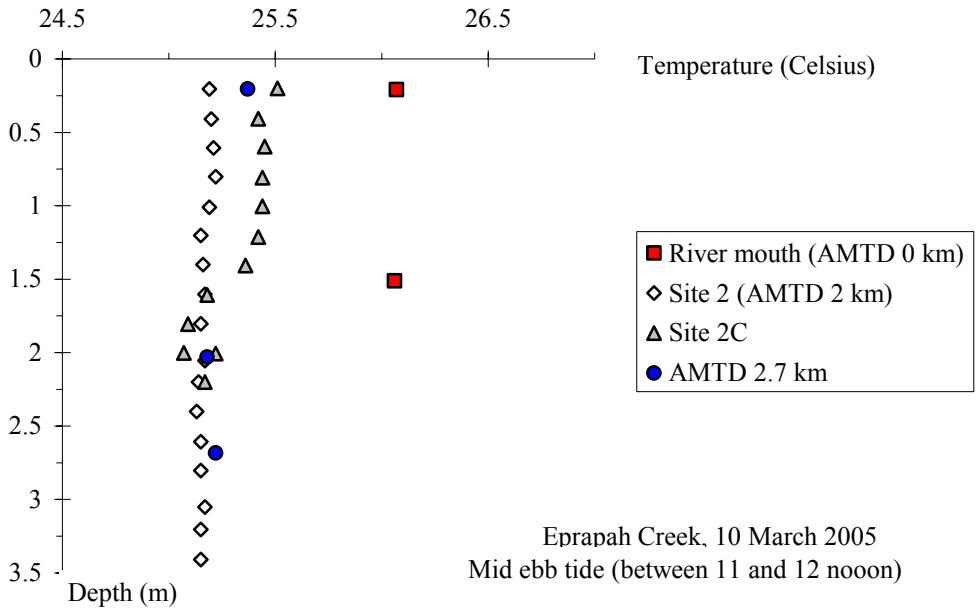

(B) Water conductivities at the river mouth (AMTD 0 km), Site 2 (AMTD 2 km), Site 2C and AMTD 2.7 km (treatment plant outfall)

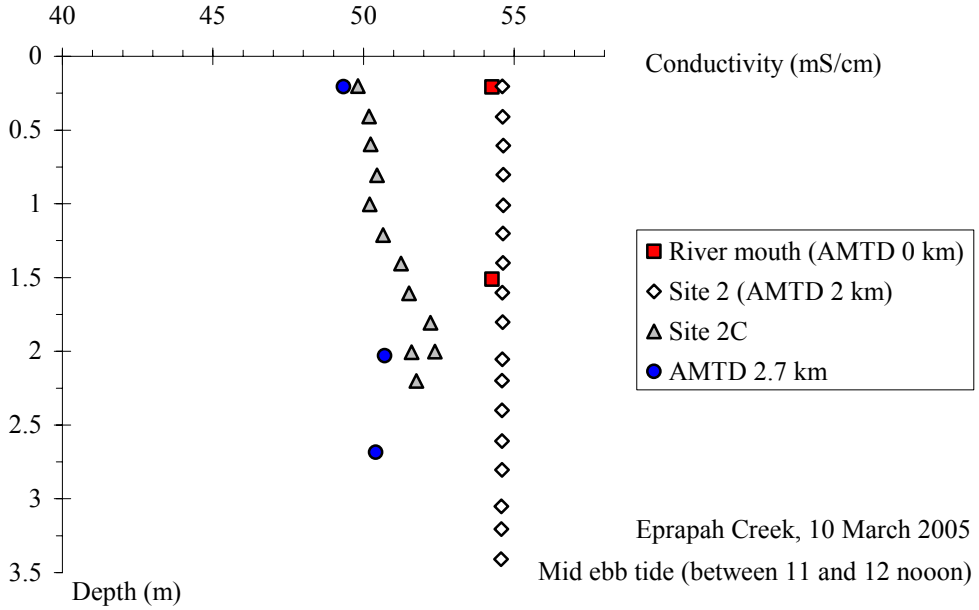

(C) Dissolved oxygen contents at the river mouth (AMTD 0 km), Site 2 (AMTD 2 km), Site 2C and AMTD 2.7 km (treatment plant outfall)

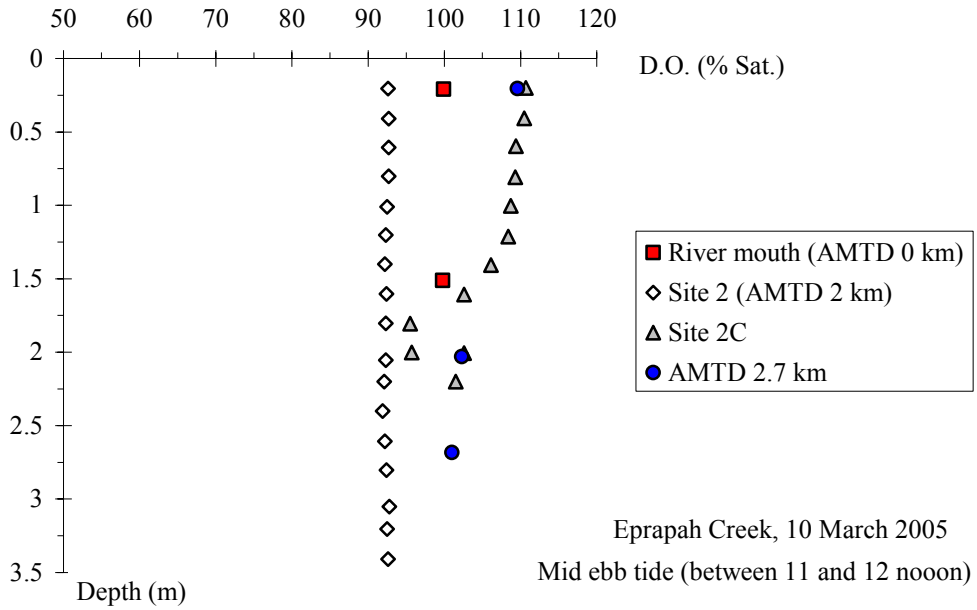

(D) Turbidities at the river mouth (AMTD 0 km), Site 2 (AMTD 2 km), Site 2C and AMTD 2.7 km (treatment plant outfall)

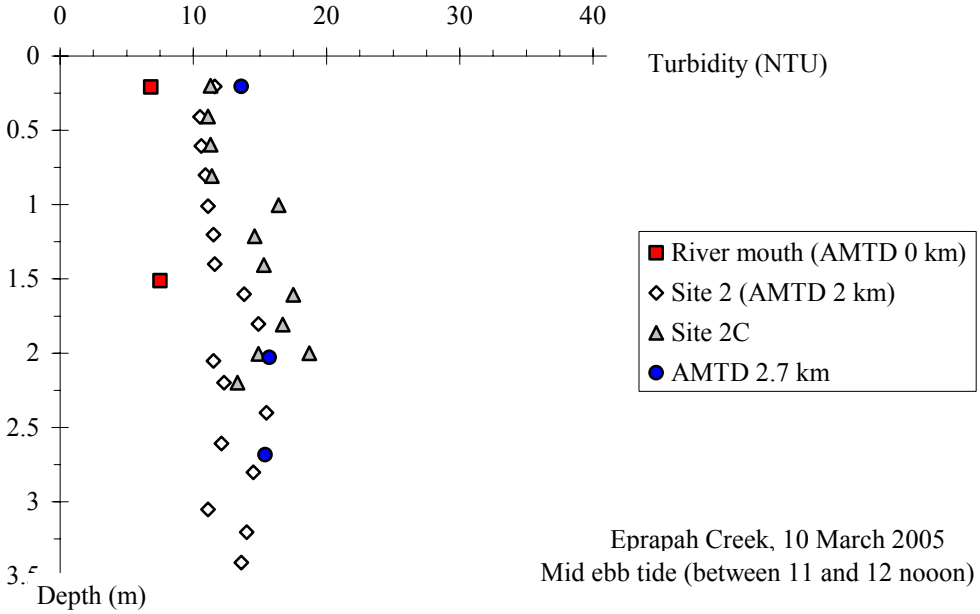

(E) pH levels at the river mouth (AMTD 0 km), Site 2 (AMTD 2 km), Site 2C and AMTD 2.7 km (treatment plant outfall)

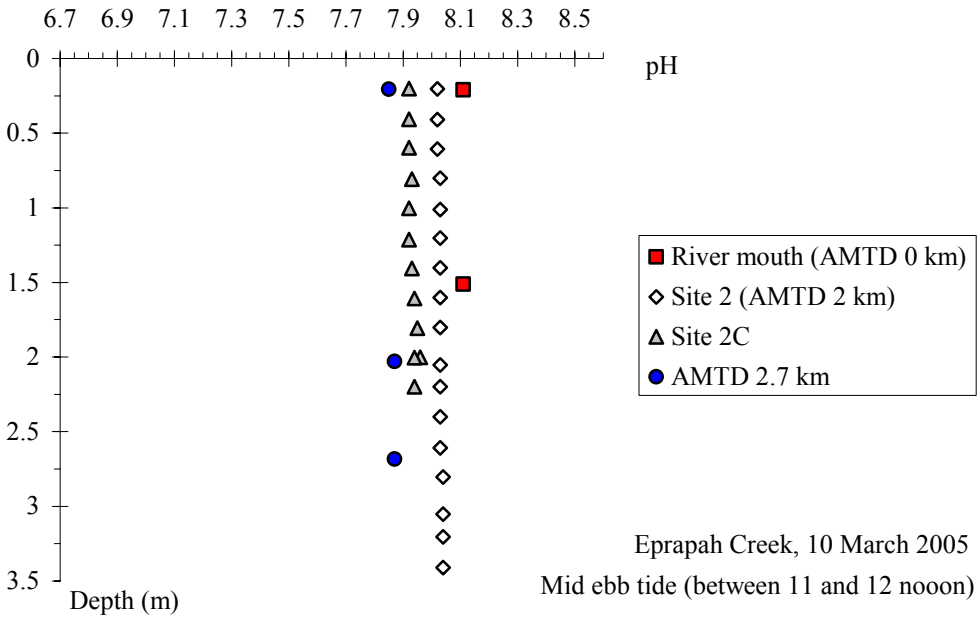

APPENDIX B – FIELD DATA FROM EPRAPAH CREEK (QLD) ON 16-18 MAY 2005 (FIELD WORK E6)

B.1 - PRESENTATION

New data were collected at Eprapah Creek (Australia) during the field work E6 on the 16-18 May 2005. Measurements were performed at Site 2B that is located 2.1 km upstream of the river mouth. Turbulence data were collected with a 3D ADV Sontek 10MHz (down-looking head) and 2D-microADV Sontek 16MHz (side-looking head) logged continuously at 25 Hz throughout the investigation period. The 3D ADV sampling volume was located 0.4 m above the bed and the 2D-microADV sampling volume was located 0.2 m above the bed. Both ADV sampling volumes were vertically aligned 10.7 m from the left bank.

Physio-chemistry data were collected by a YSI6600 probe logged every 12 s during the investigation period and 6 LTS9000 probes. The YSI6600 sampling volume was located approximately 0.4 m above the bed and 10.4 m from the left bank reference position: that is, 0.3 m apart from the 3D ADV sampling volume. Instantaneous water temperature, conductivity, water level, pH, turbidity, and dissolved oxygen samples were recorded. The LTS9000 probes measured water level, water temperature and conductivity every 6 s at various elevations above the bed and transverse positions across the experimental cross-section at Site 2B.

Vertical profiles of physio-chemistry were performed on 17 May 2005 at the river mouth, at Site 1, at Site 2, at the treatment plant outfall (AMTD 2.7 km) and at Site 3 (AMTD 3.1 km). Measurements were conducted in the middle of the creek at several sites. They were performed during the ebb flow using a physio-chemistry probe YSI™6920 lowered from a boat drifting with the flow.

In addition manual readings of air temperature and water depth were collected at Site 2B every 15 minutes during the investigation period. Air temperature readings were collected on a Mercury thermometer, and water levels were measured from measuring staff attached to instrumentation frame. Manual water level readings matched closely those recorded by YSI6600 modelling and are not shown.

Turbulent flow properties

This appendix includes instantaneous velocities and tangential Reynolds stresses, the time-averages and standard deviations of each instantaneous parameter, vertical and horizontal turbulence intensities, Reynolds stress correlation coefficients, and integral and dissipation time scales. Herein turbulence intensities are defined as the ratio of standard deviation of the transverse or vertical velocities to standard deviation of the streamwise velocity (horizontal: v_y'/v_x' ; vertical: v_z'/v_x'). The correlation coefficient of Reynolds stress is a dimensionless ratio of covariance of two velocity components divided by the product of the standard deviations of those two tangential velocities ($R_{vxvy} = \overline{v_x v_y}/(v_x' v_y')$; $R_{vxvz} = \overline{v_x v_z}/(v_x' v_z')$; $R_{vyvz} = \overline{v_y v_z}/(v_y' v_z')$).

PIQUET (1999) defined the integral time scale T_E as:

$$T_E = \int_{\tau=0}^{\tau(R_{ii}(\tau)=0)} R_{ii}(\tau)\,d\tau \qquad \text{(A1)}$$

where τ is the time lag, R_{ii} is the normalised auto-correlation function, i is a direction tensor (i= x, y, z), and $\tau(R_{ii}(\tau)=0)$ is the time lag for which $R_{ii}=0$ (Fig. A-1A). Integral time scales are equal to the area under the normalised auto-correlation curve up to $R_{ii}(\tau)=0$. Fig. A-1A illustrates the calculation of the integral time scale. The integral time scale T_E is a measure of the longest connection in the turbulent behaviour of $v(\tau)$.

Fig. B-1 - Definition sketch for the dissipation and integral time scales.

(A) Calculation of the integral time scale using the area under the auto-correlation function

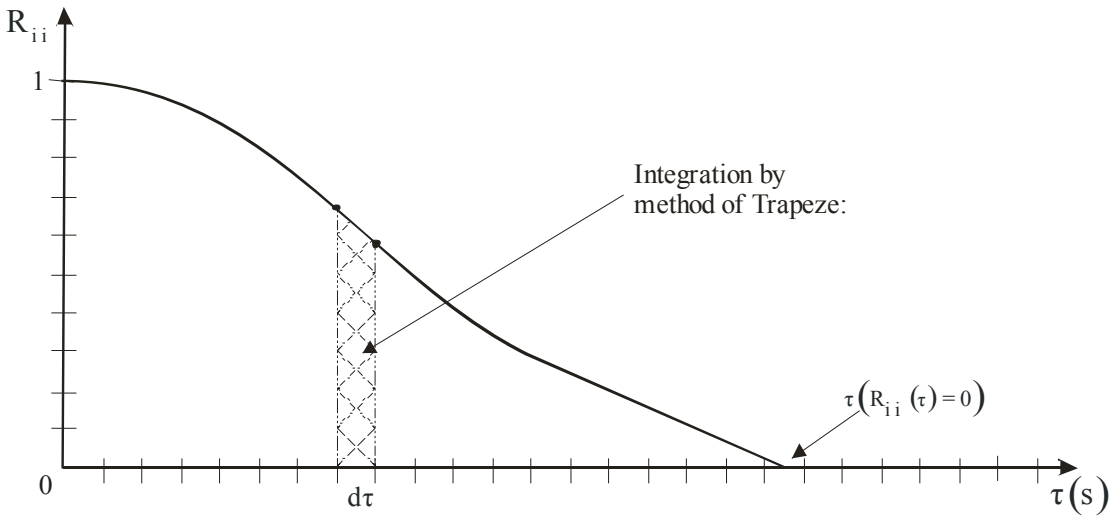

(B) Estimation of the dissipation time scale using a quadratic interpolation

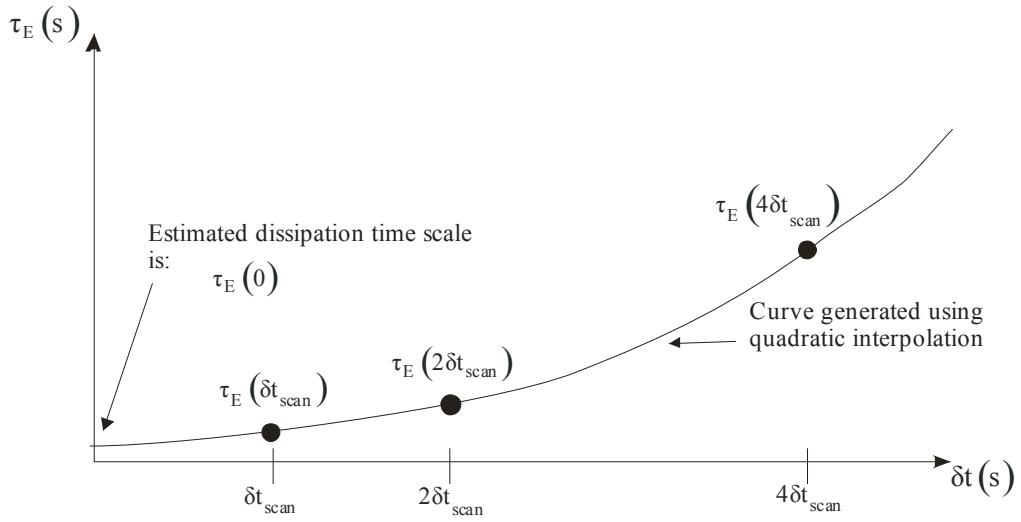

The dissipation time scale τ_E is a measure of the most rapid changes that occur in the turbulent fluctuations of velocity v(t) (HINZE 1975). It is related to the curvature of the auto-correlation function at the origin ($\tau = 0$). Using the Taylor series expansion of the auto-correlation function, the dissipation time scale τ_E may be expressed as:

$$\tau_E = \sqrt{\frac{2\,v'^2}{\left(\frac{\delta v}{\delta t}\right)^2}} \qquad \text{(B2)}$$

HALLBACK et al. (1989), FRANSSON et al. (2005), and KOCH and CHANSON (2005) used the above to obtain a measured time scale $\tau_E\left(\delta t\right)$ based upon the time increment δt:

$$\tau_E\left(\delta t\right) = \sqrt{\frac{2\,v'^2}{\left(\frac{\delta v}{\delta t}\right)^2}} \qquad \text{(B3)}$$

where v' standard deviation of velocity component, δt_{scan} is the experimental scan rate ($1/F_{scan}$, F_{scan}=25 Hz), δt is the incremental time scale calculation sampling rate ($\delta t_{scan} \le \delta t \le 4\,\delta t_{scan}$). As the dissipation time scale τ_E is smaller than the sampling frequency F_{scan}, several values of $\tau_E(\delta t)$ were calculated to estimate the dissipation time scale τ_E. The dissipation time scale τ_E equals $\tau_E(0)$ when δt tends to zero: $\tau_E = \tau_E(0)$. Quadratic interpolation may be used (KOCH and CHANSON 2005) to extrapolate the value of $\tau_E(0)$ from those $\tau_E(\delta t)$ calculated. $\tau_E(\delta t)$ was calculated for $\delta t = \delta t_{scan}$, $2*\delta t_{scan}$, and $4*\delta t_{scan}$, and these values of $\tau_E(\delta t)$ were used to solve for $\tau_E(0)$ through:

$$\tau_E(\delta t) = \tau_E(0) + a\,\delta t^2 + b\,\delta t \qquad \text{(B4)}$$

where a and b are constants calculated from best data fit. Fig. B-1B explains the calculation of the dissipation time scale through quadratic interpolation.

The turbulence properties were calculated for 5000 data points (200 s) every 10 s along the entire data set. The instantaneous velocity fluctuations v were calculated at each data point as $v = V - \overline{V}$ where V is the instantaneous velocity measurement and $\overline{V}$ is the time-average calculated over 5000 data points. Instantaneous tangential Reynolds stresses were calculated using the instantaneous velocity data. During this investigation the positive velocity directions were downstream (V_x>0), towards left bank (V_y>0), and upwards (V_z>0).

Notation

f_s	sampling frequency (Hz);
i	directional tensor;
$R_{i\,i}$	auto-correlation function
R_{vxvy}	correlation coefficient of tangential Reynolds stress $\rho v_x v_z$: $R_{vxvy} = \overline{v_x v_y} / (v'_x v'_y)$
R_{vxvz}	correlation coefficient of Reynolds stress $\rho v_x v_y$: $R_{vxvz} = \overline{v_x v_z} / (v'_x v'_z)$
R_{vyvz}	correlation coefficient of Reynolds stress $\rho v_y v_z$: $R_{vyvz} = \overline{v_y v_z} / (v'_y v'_z)$
T_E	Eulerian integral time scale (s);
T_{Ex}	Eulerian integral time scale of streamwise velocity (s);
T_{Ey}	Eulerian integral time scales of transverse velocity (s);
T_{Ez}	Eulerian integral time scale of vertical velocity (s);
V	instantaneous velocity (m/s);
V_x	instantaneous streamwise velocity (m/s);
V_y	instantaneous transverse velocity (m/s);
V_z	instantaneous vertical velocity (m/s);
$\overline{V}$	time-averaged velocity (m/s);
$\overline{V_x}$	time-averaged streamwise velocity (m/s);
$\overline{V_y}$	time-averaged transverse velocity (m/s);

$\overline{V_z}$ time-averaged vertical velocity (m/s);

v turbulent velocity fluctuation (m/s) :

$v = V - \overline{V}$

v_x' standard deviation of streamwise velocity (m/s);

v_y' standard deviation of transverse velocity (m/s);

v_z' standard deviation of vertical velocity (m/s);

v_y'/v_x' horizontal turbulence intensity;

v_z'/v_x' vertical turbulence intensity;

δt sampling time step (s);

$\rho v_x v_y$ instantaneous tangential Reynolds stress (Pa);

$\rho v_x v_z$ instantaneous tangential Reynolds stress (Pa);

$\rho v_y v_z$ instantaneous tangential Reynolds stress (Pa);

$\rho\overline{v_x v_y}$ time-averaged tangential Reynolds stress (Pa);

$\rho\overline{v_x v_z}$ time-averaged tangential Reynolds stress (Pa);

$\rho\overline{v_y v_z}$ time-averaged tangential Reynolds stress (Pa);

$\left(\rho v_x v_y\right)'$ standard deviation of tangential Reynolds stress (Pa);

$\left(\rho v_x v_z\right)'$ standard deviation of tangential Reynolds stress (Pa);

$\left(\rho v_y v_z\right)'$ standard deviation of tangential Reynolds stress (Pa);

τ time lag (s);

τ_E Eulerian dissipation time scale (s);

τ_{Ex} Eulerian dissipation time scale of streamwise velocity (s);

τ_{Ey} Eulerian dissipation time scale of transverse velocity (s);

τ_{Ez} Eulerian dissipation time scale of vertical velocity (s).

B.2 – TURBULENCE DATA

B.2.1 – Acoustic Doppler velocimetry, 3D ADV (10 MHz) located 0.4 m above the bed

Fig. B-2 - Instantaneous velocity data collected at Site 2B Eprapah Creek (QLD) during field work E6 on 16-18 May 2005 - 3D ADV (10 MHz), scan rate: 25 Hz, Probe sensor: 0.4 m above bed, 10.7 m from left bank, Post-processed data

(A) Instantaneous streamwise velocity V_x

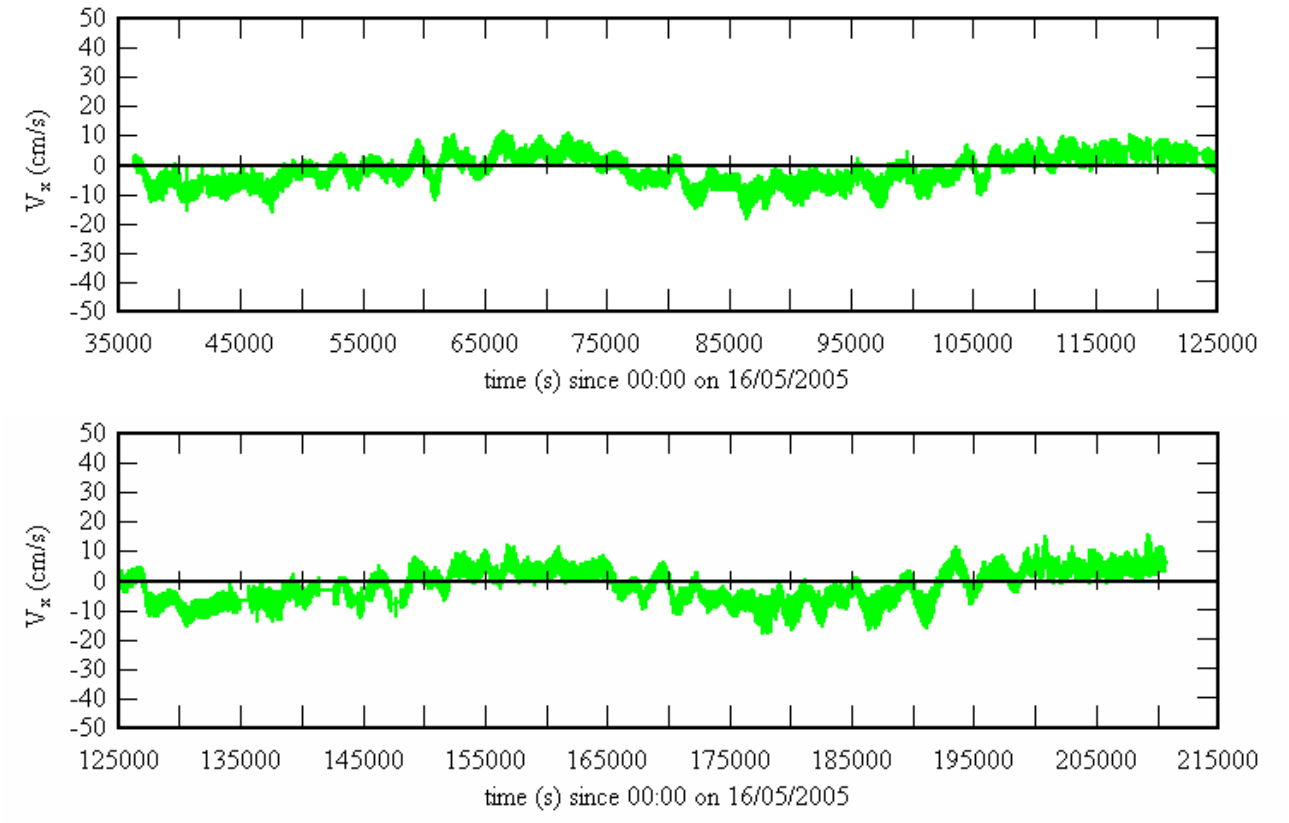

(B) Instantaneous transverse velocity V_y

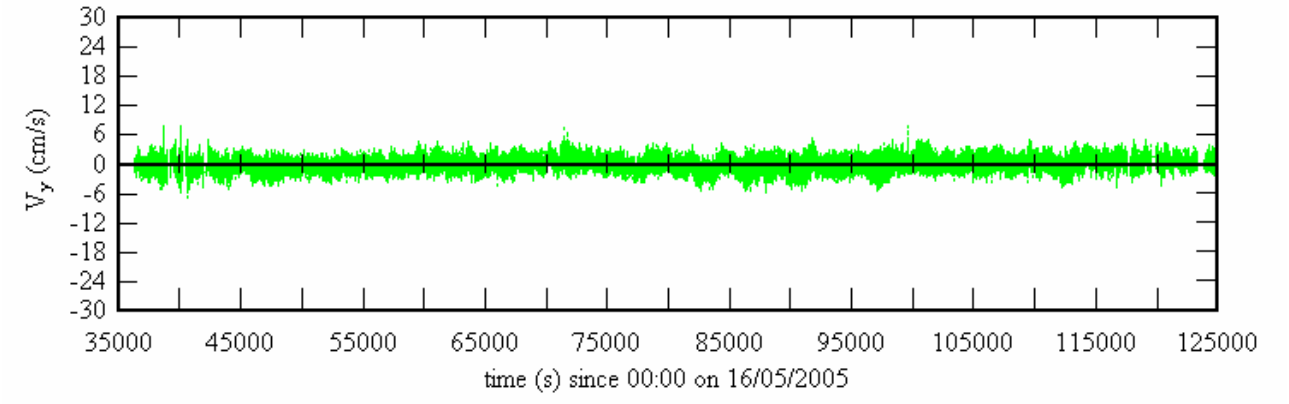

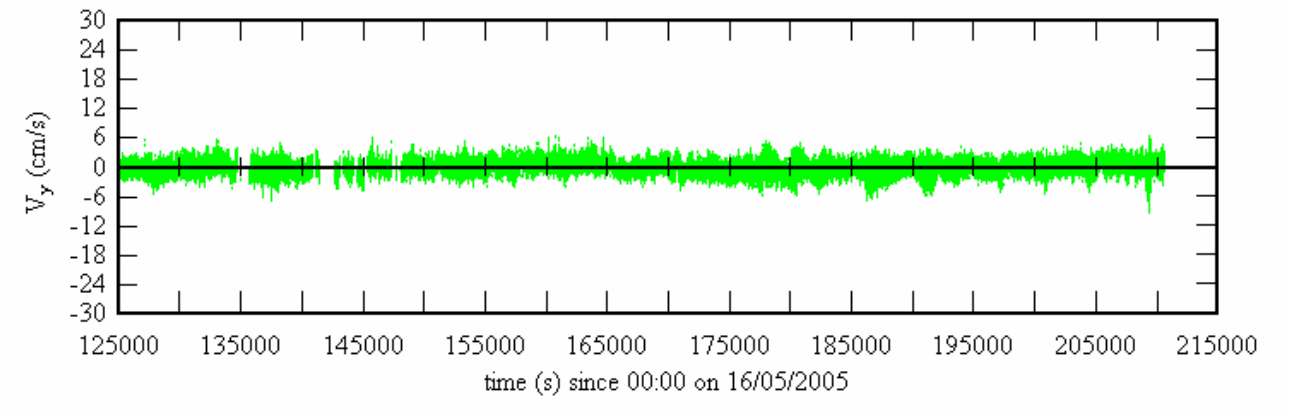

(C) Instantaneous vertical velocity V_z

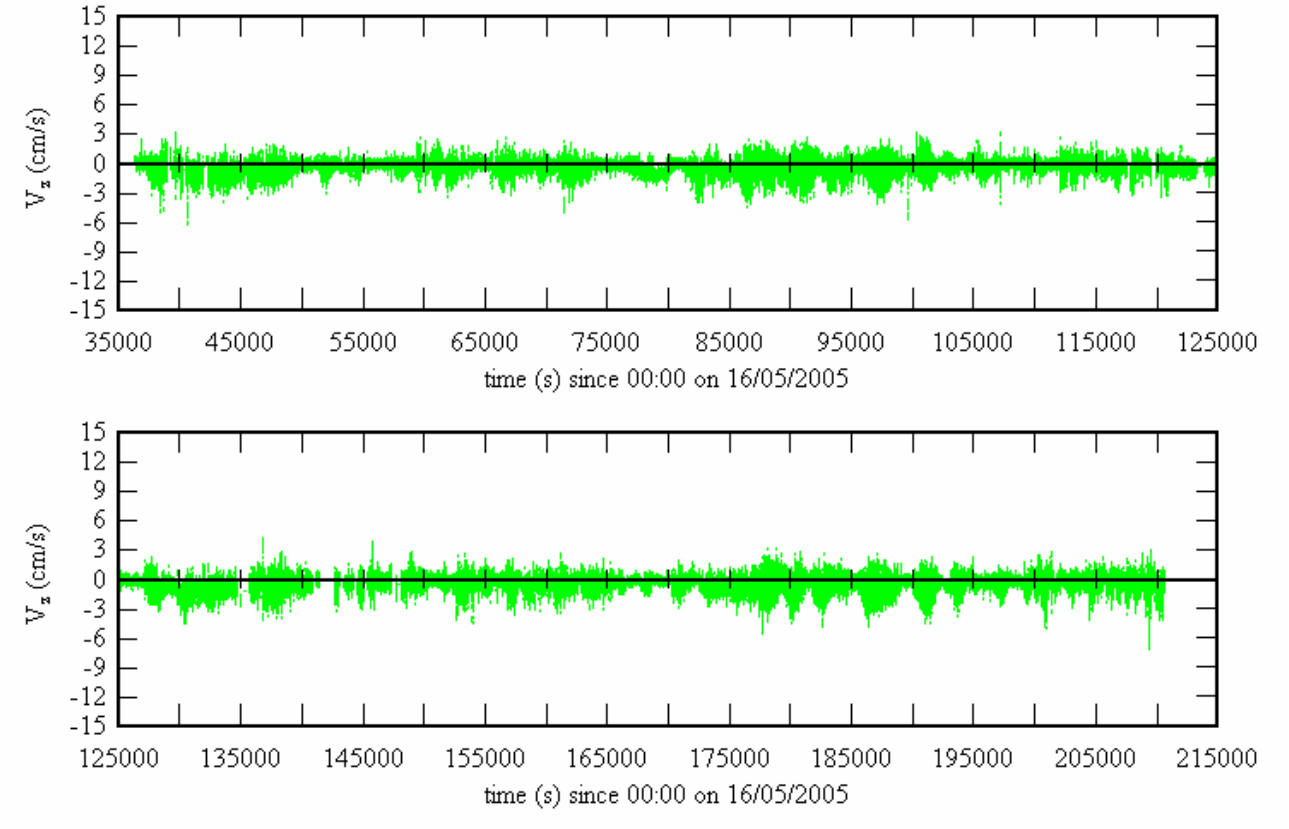

Fig. B-3 - Time-averaged velocity data collected at Site 2B Eprapah Creek (QLD) during field work E6 on 16-18 May 2005 - 3D ADV (10 MHz), scan rate: 25 Hz, Probe sensor: 0.4 m above bed, 10.7 m from left bank - Time average based upon 5000 data points (3.33 minutes) taken every 10 s along entire data set

(A) Time-averaged streamwise velocity $\overline{V_x}$

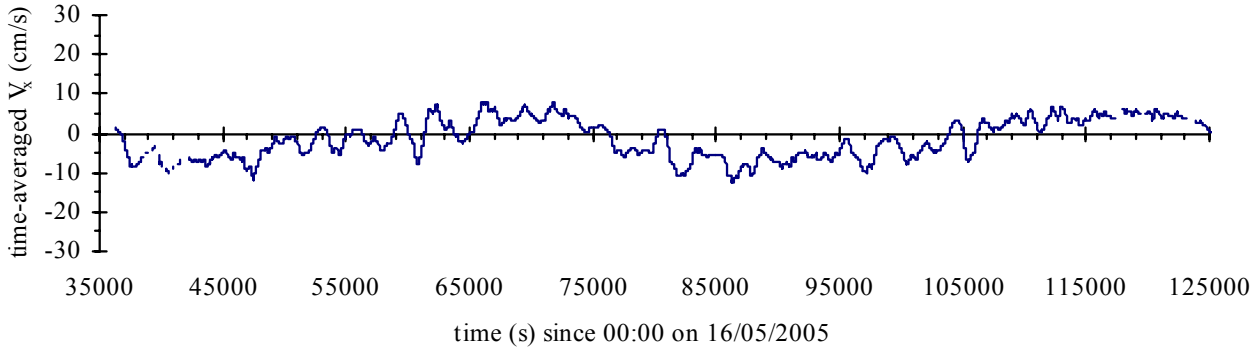

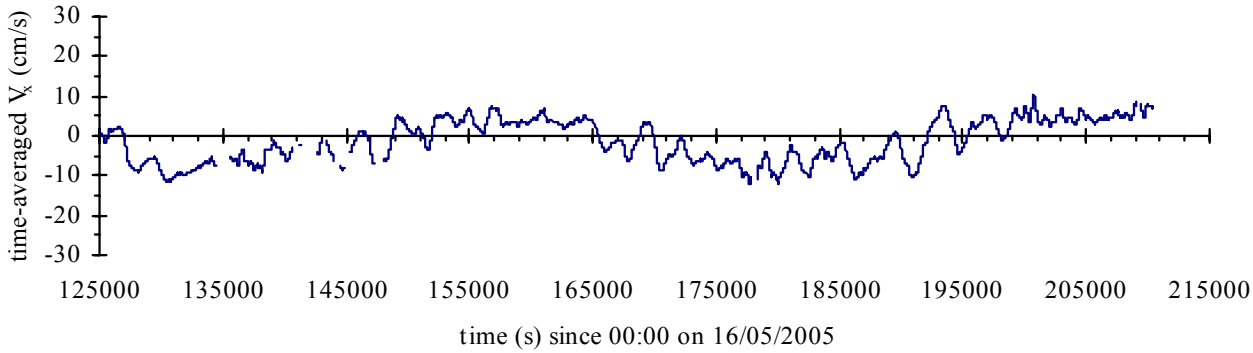

(B) Time-averaged transverse velocity $\overline{V_y}$

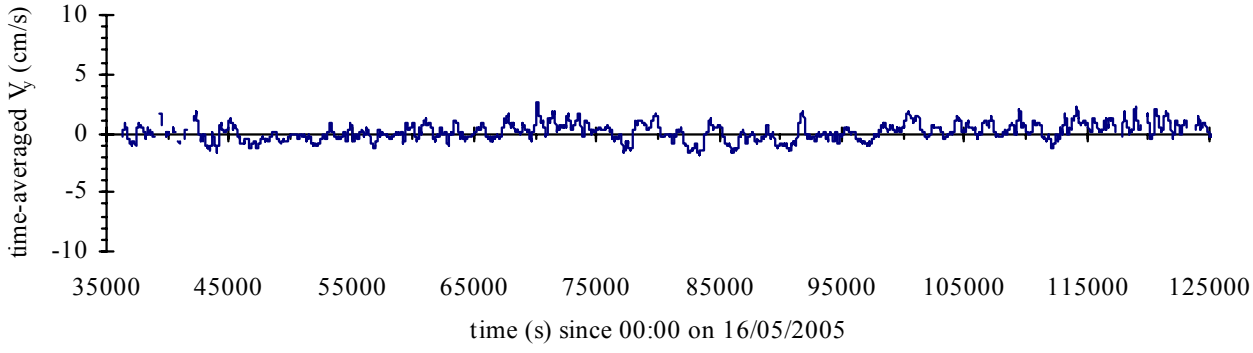

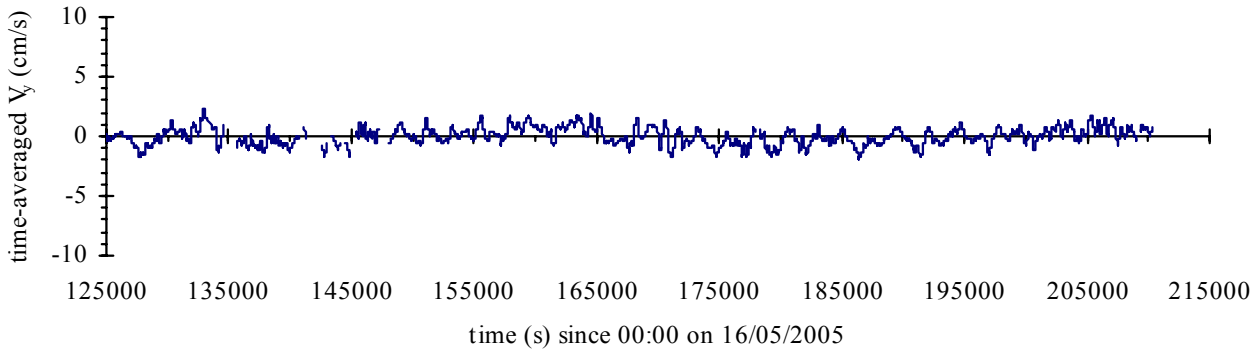

(C) Time-averaged vertical velocity $\overline{V_z}$

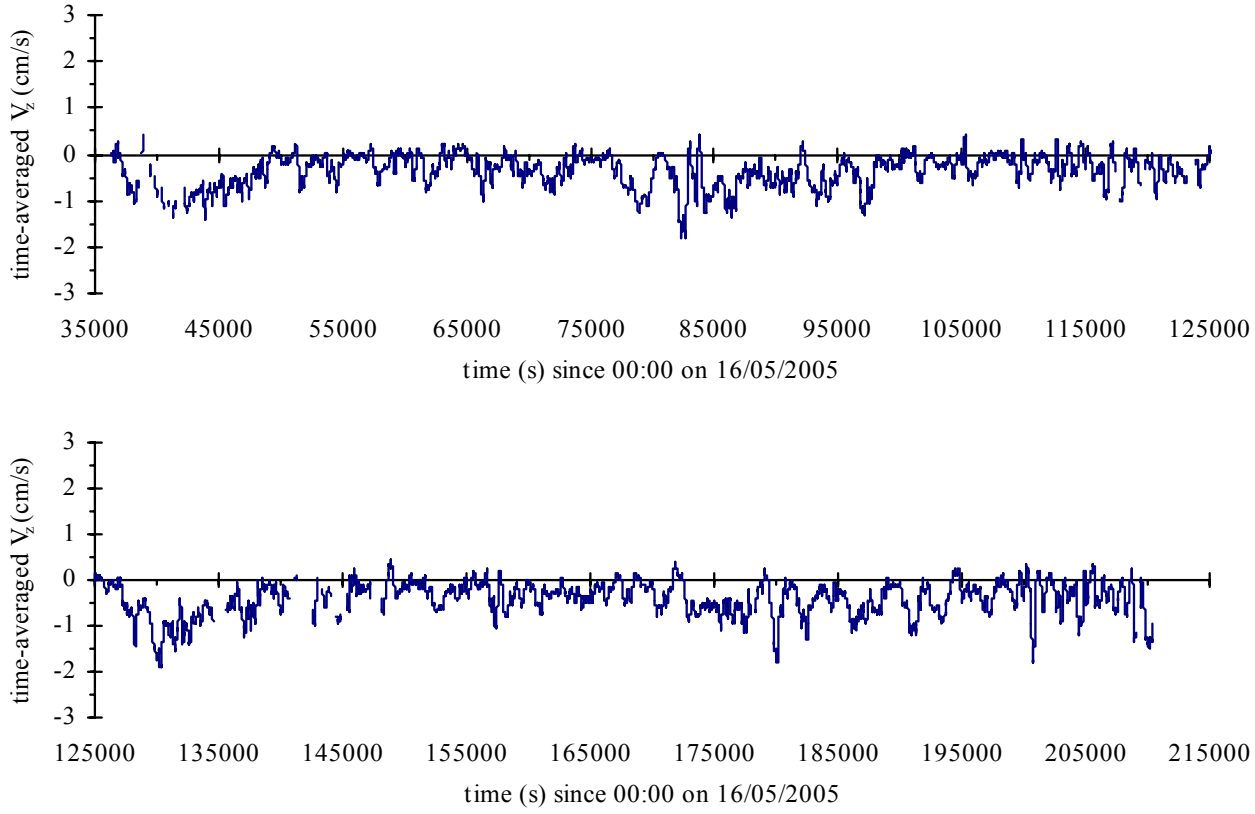

Fig. B-4 - Standard deviations of velocity data collected at Site 2B Eprapah Creek (QLD) during field work E6 on 16-18 May 2005 - 3D ADV (10 MHz), scan rate: 25 Hz, Probe sensor: 0.4 m above bed, 10.7 m from left bank - Standard deviations based upon 5000 data points (3.33 minutes) taken every 10 s along entire data set

(A) Standard deviations of streamwise velocity v_x'

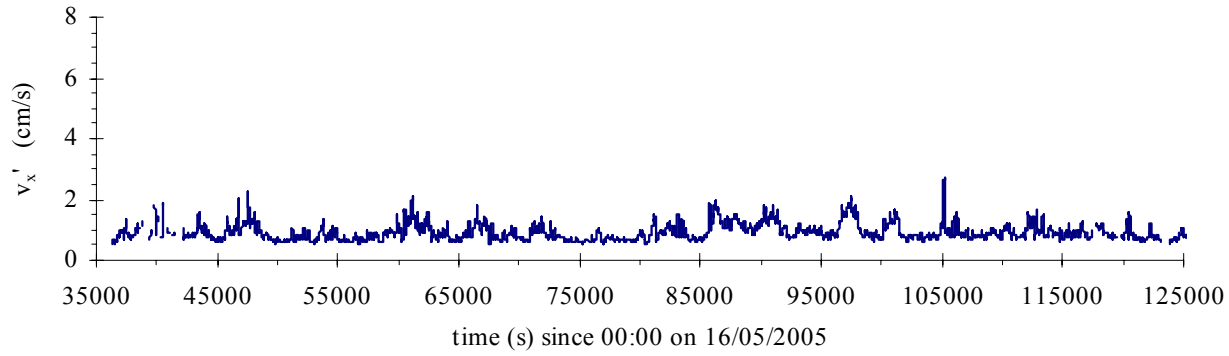

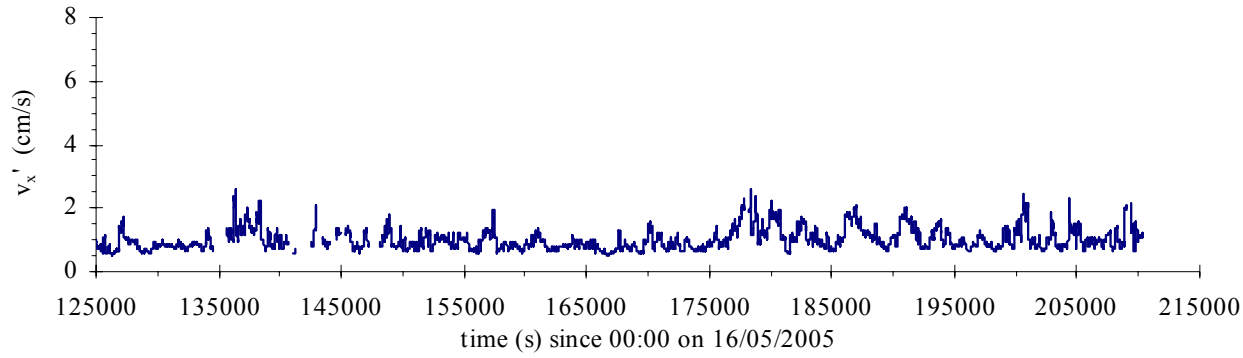

(B) Standard deviations of transverse velocity v_y'

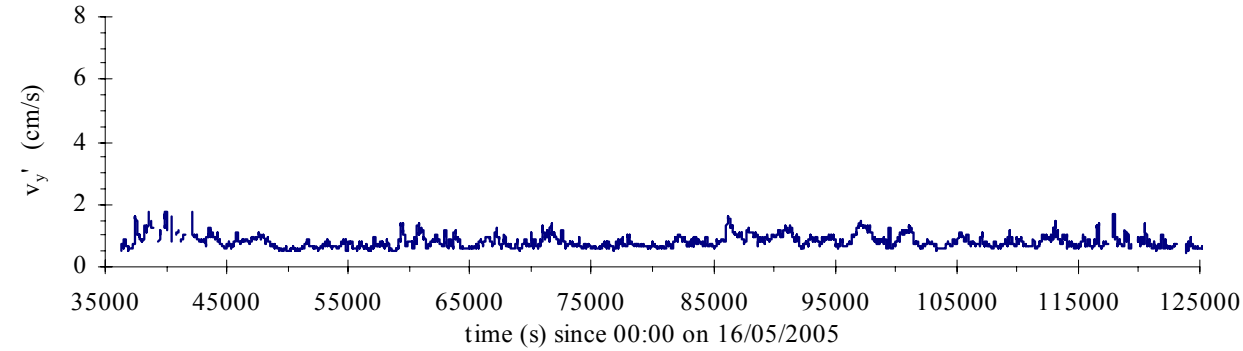

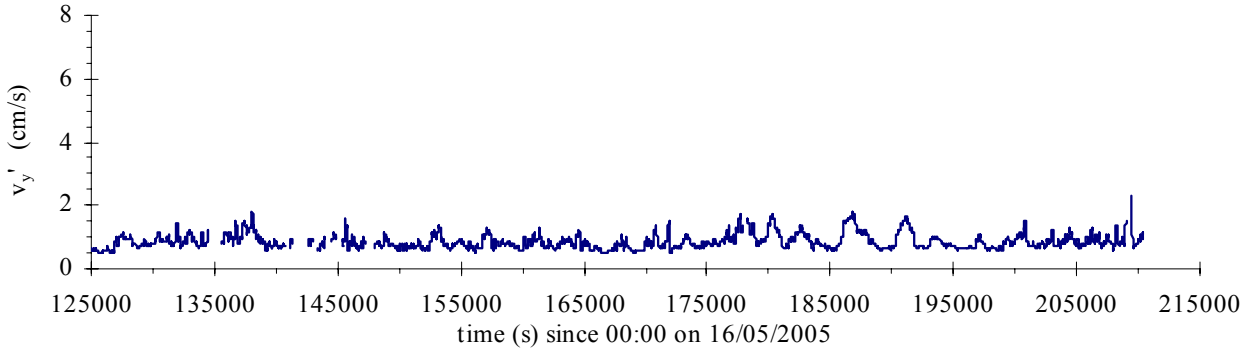

(C) Standard deviations of vertical velocity v_z'

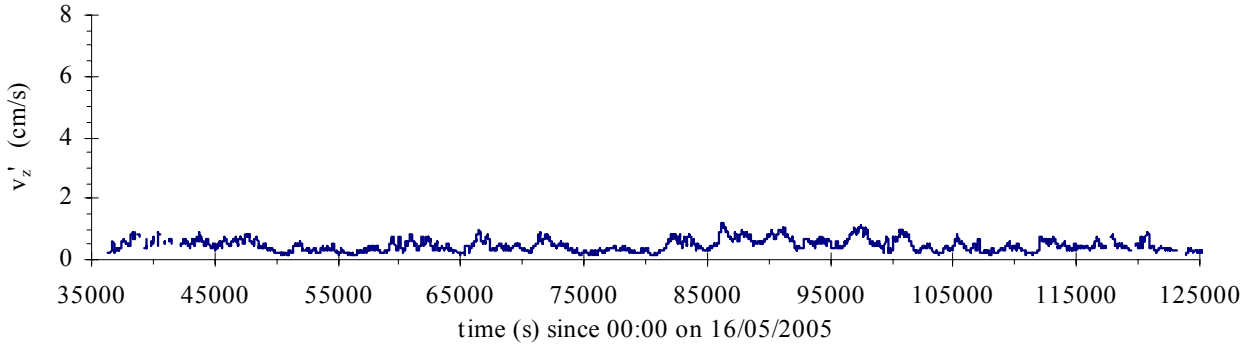

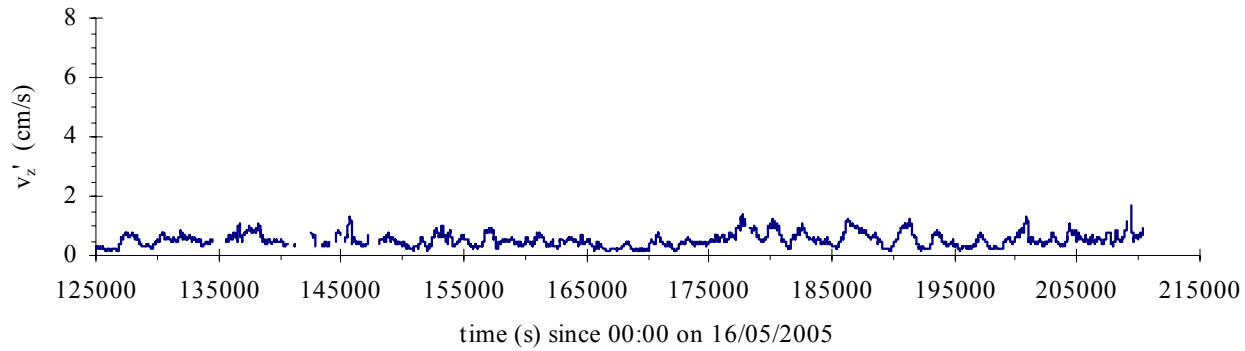

Fig. B-5 - Instantaneous tangential Reynolds stress data collected at Site 2B Eprapah Creek (QLD) during field work E6 on 16-18 May 2005 - 3D ADV (10 MHz), scan rate: 25 Hz, Probe sensor: 0.4 m above bed, 10.7 m from left bank - Instantaneous Reynolds stresses calculated every sample along entire data set (eg. $v_x = V_x - \overline{V_x}$) with $\overline{V_x}$ based upon 5000 data points (3.33 minutes)

(A) Instantaneous tangential Reynolds stress $\rho v_x v_y$

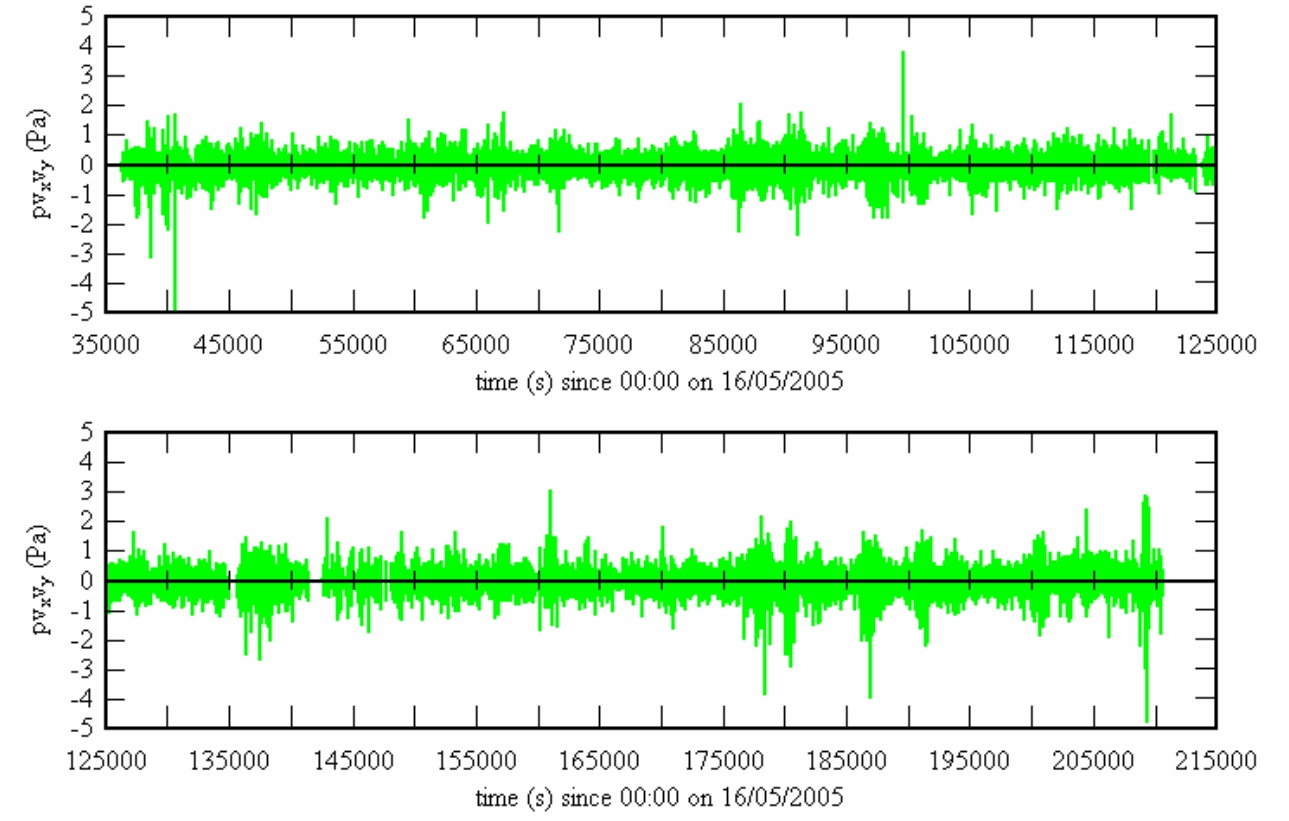

(B) Instantaneous tangential Reynolds stress $\rho v_x v_z$

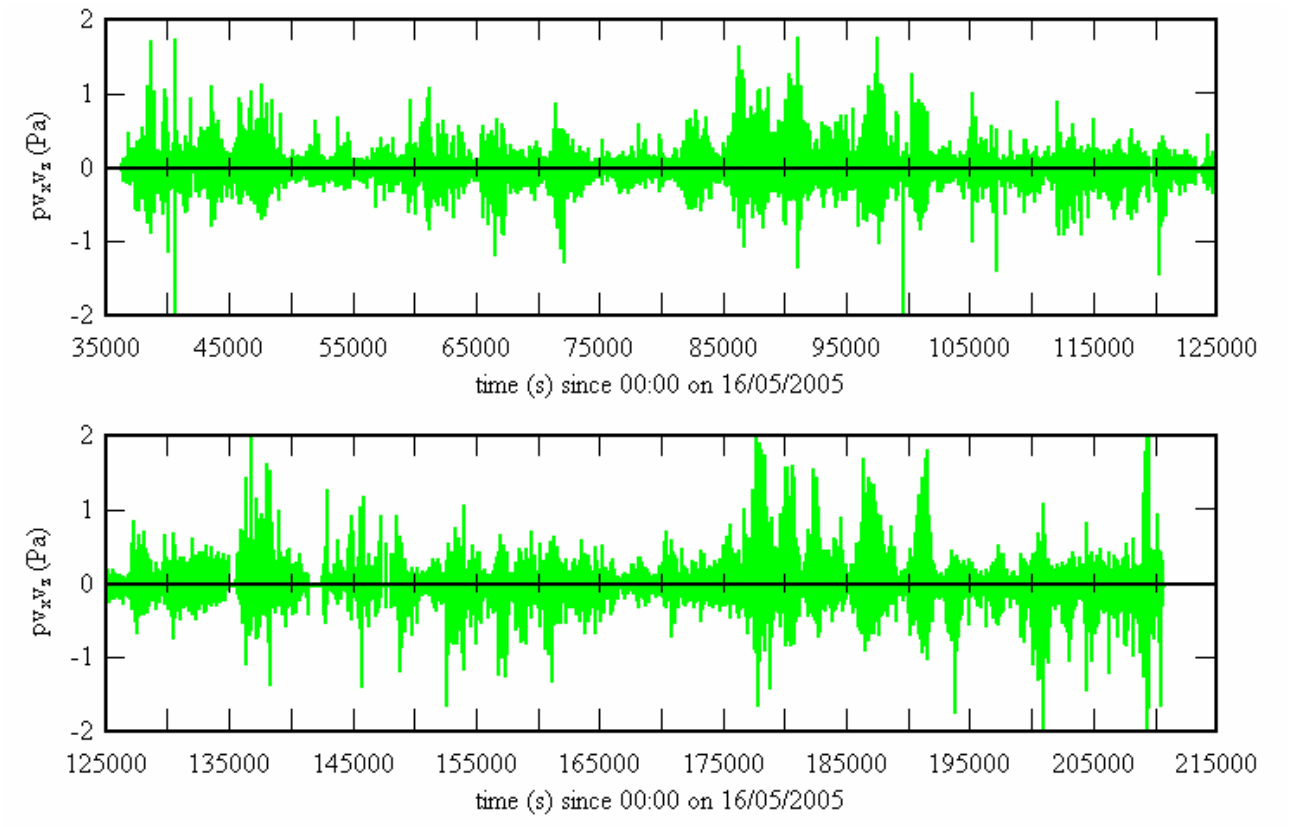

(C) Instantaneous tangential Reynolds stress $\rho v_y v_z$

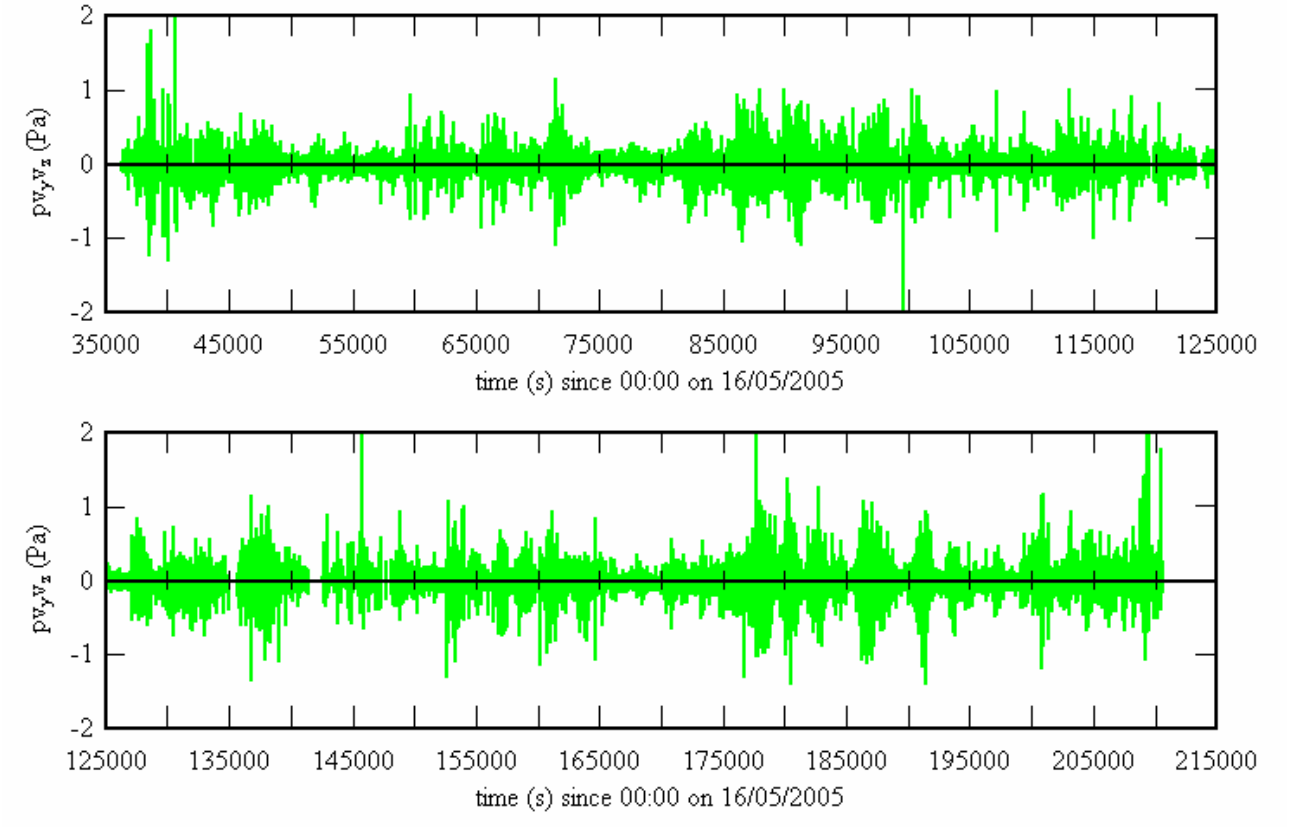

Fig. B-6 - Time-averaged tangential Reynolds stress data collected at Site 2B Eprapah Creek (QLD) during field work E6 on 16-18 May 2005 - The 3D ADV sampling volume was located 0.4 m above bed, 10.7 m from left bank reference position - Time-averaged Reynolds stress based upon 5000 data points (3.33 minutes) taken every 10 s along entire data set

(A) Time-averaged tangential Reynolds stress $\rho\overline{v_x v_y}$

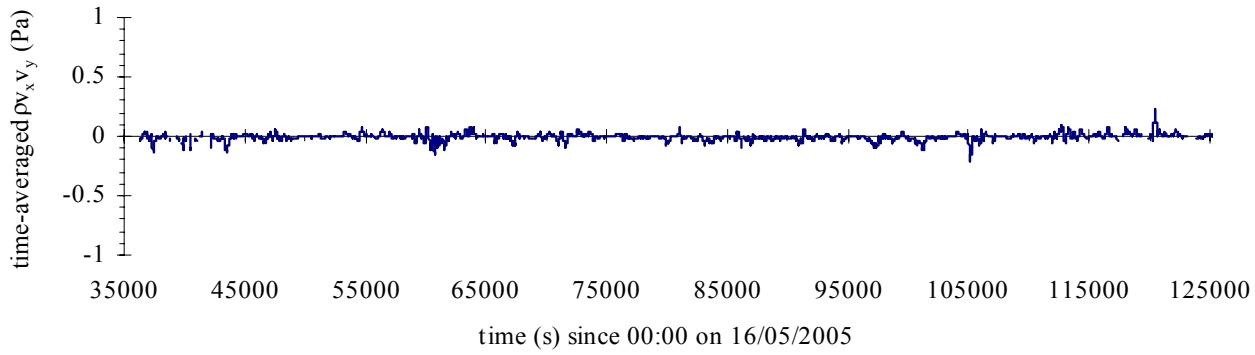

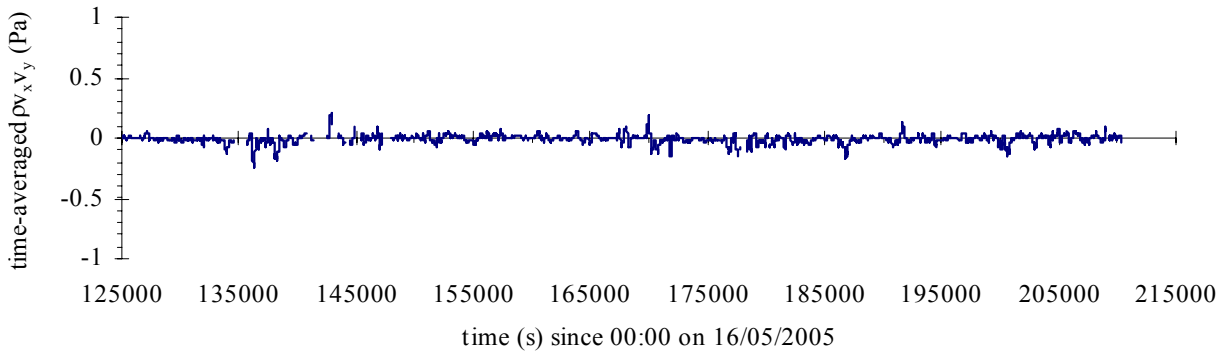

(B) Time-averaged tangential Reynolds stress $\rho\overline{v_x v_z}$

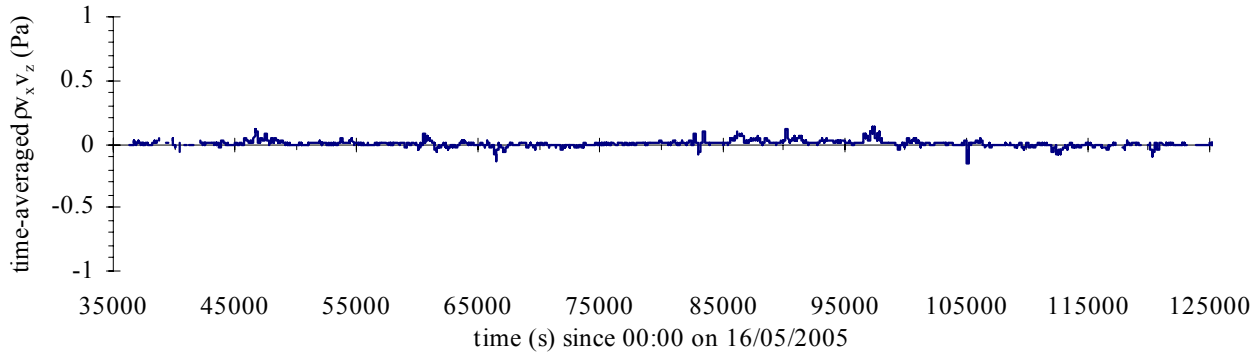

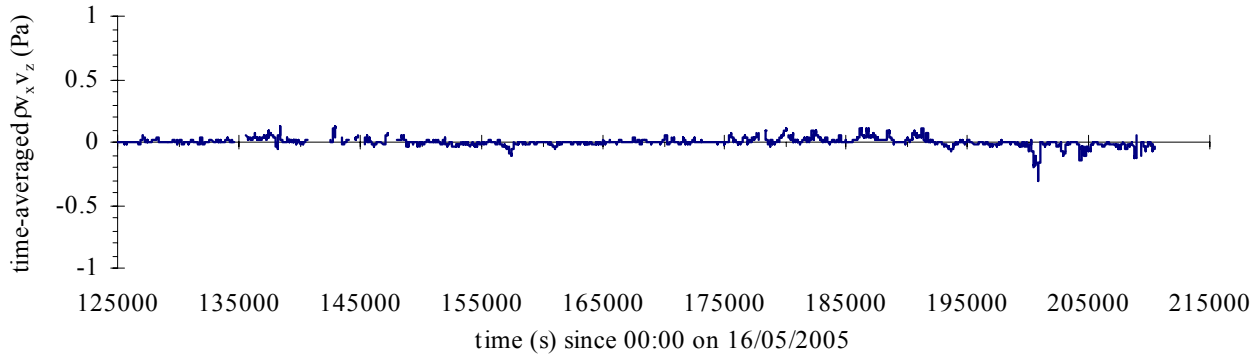

(C) Time-averaged tangential Reynolds stress $\rho\overline{v_y v_z}$

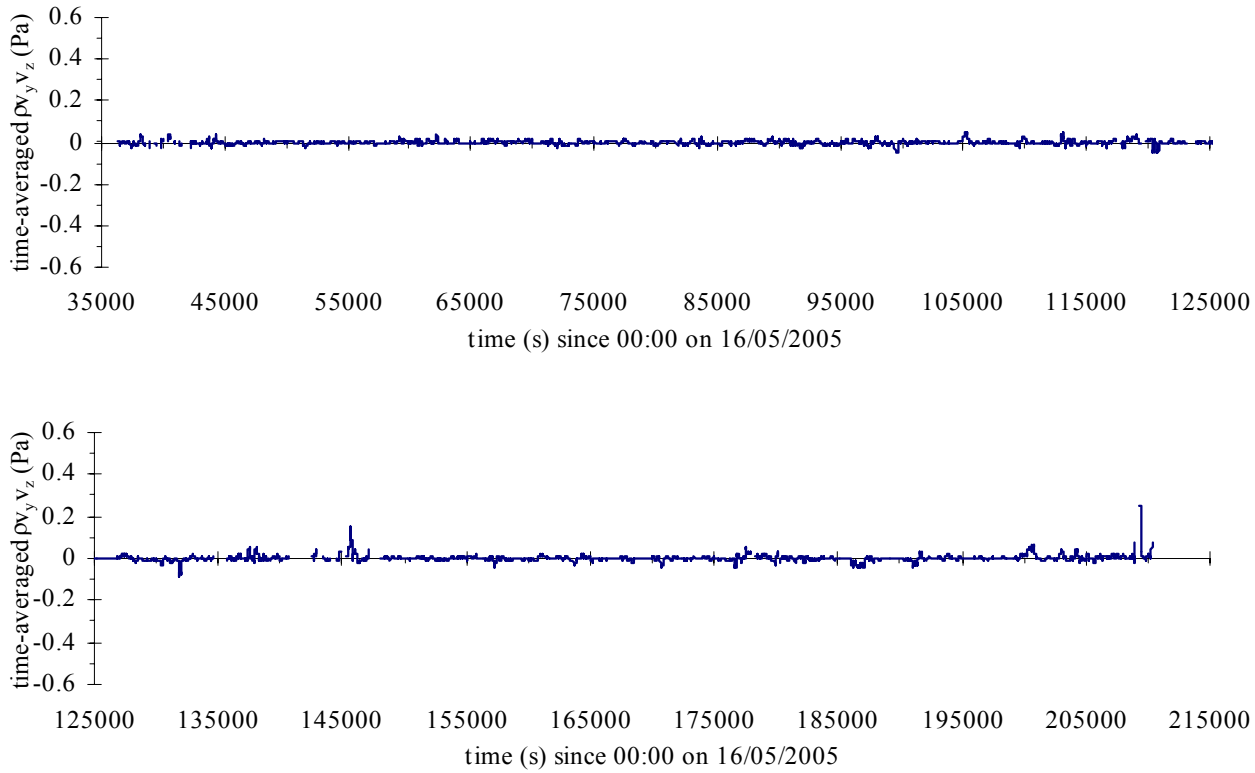

Fig. B-7 - Standard deviations of tangential Reynolds stress data collected at Site 2B Eprapah Creek (QLD) during field work E6 on 16-18 May 2005 - 3D ADV (10 MHz), scan rate: 25 Hz, Probe sensor: 0.4 m above bed, 10.7 m from left bank - Standard deviations of Reynolds stress based upon 5000 data points (3.33 minutes) taken every 10 s along entire data set

(A) Standard deviations of tangential Reynolds stress $\left(\rho v_x v_y\right)'$

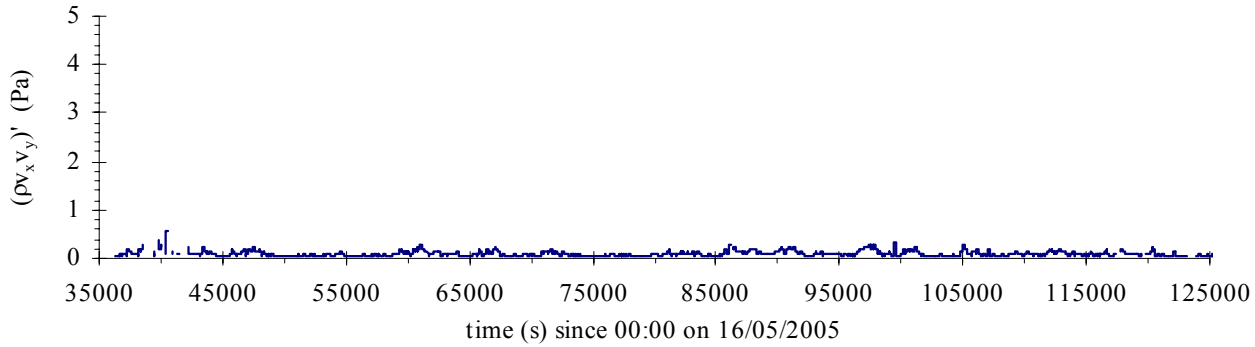

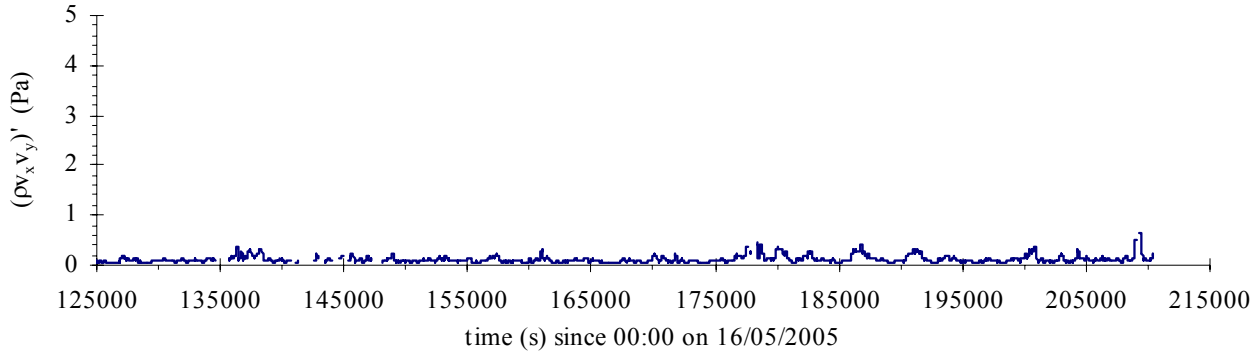

(B) Standard deviations of tangential Reynolds stress $\left(\rho v_x v_z\right)'$

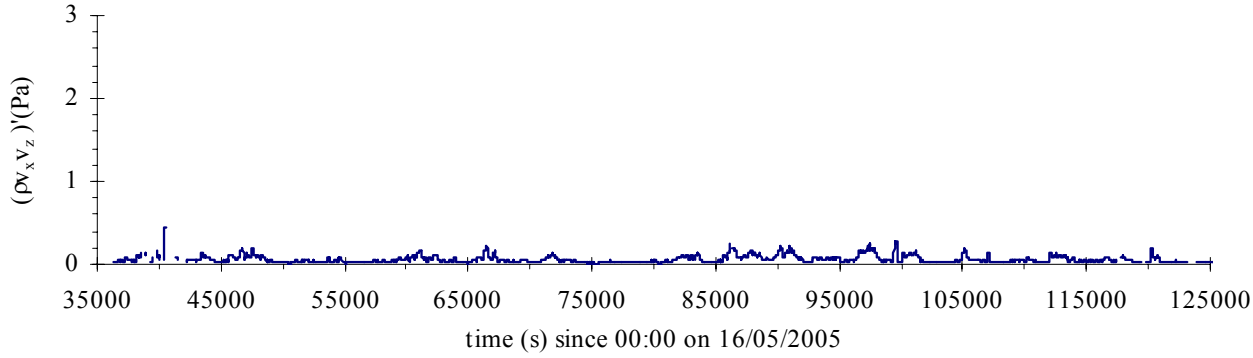

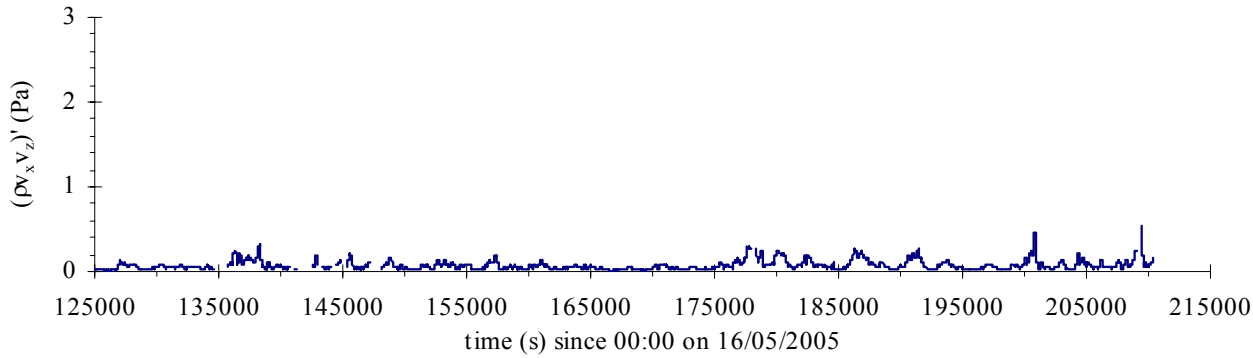

(C) Standard deviations of tangential Reynolds stress $\left(\rho v_y v_z\right)'$

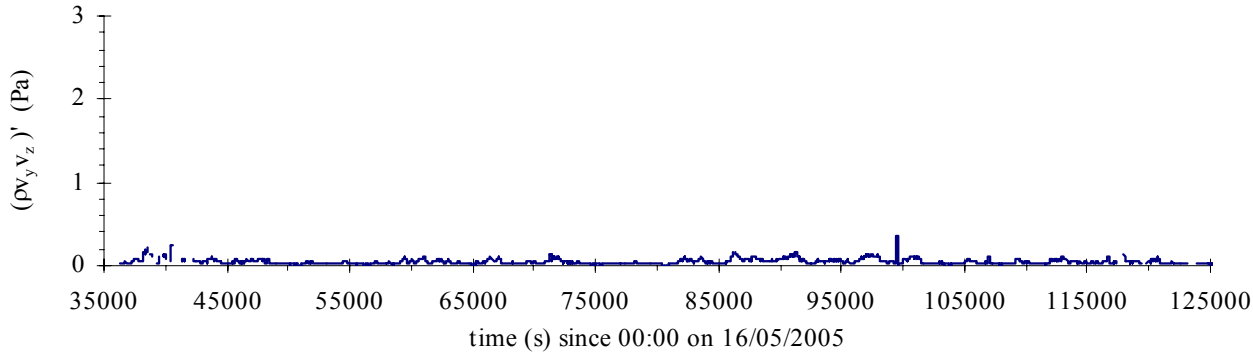

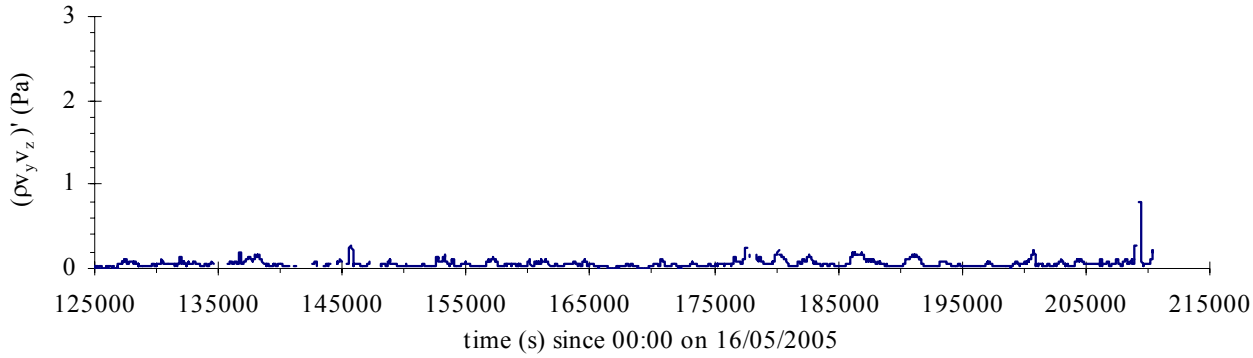

Fig. B-8 - Integral time scales T_E of velocity data collected at Site 2B Creek (QLD) during field work E6 on 16-18 May 2005 - 3D ADV (10 MHz), scan rate: 25 Hz, Probe sensor: 0.4 m above bed, 10.7 m from left bank - Integral time scales based upon average of 20 correlation curves (250 data points) collected from 5000 data points (3.33 minutes) taken every 10 s along entire data set
(A) Integral time scales of streamwise velocity T_{Ex}

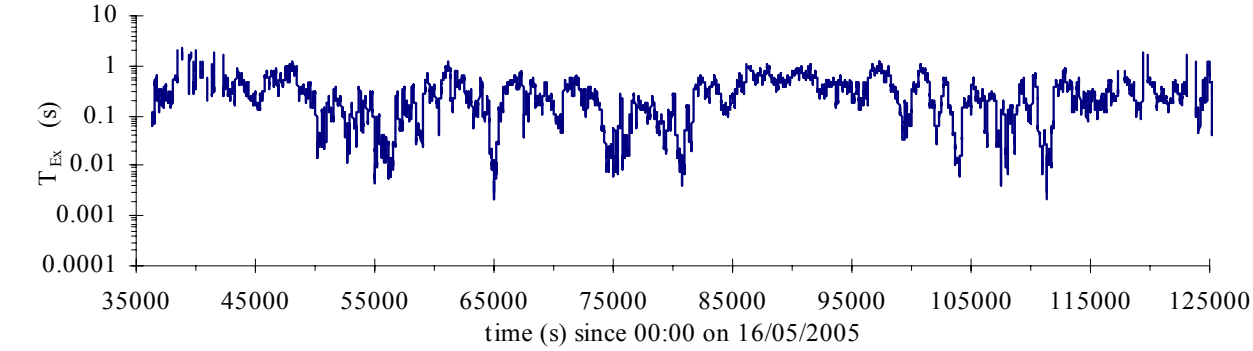

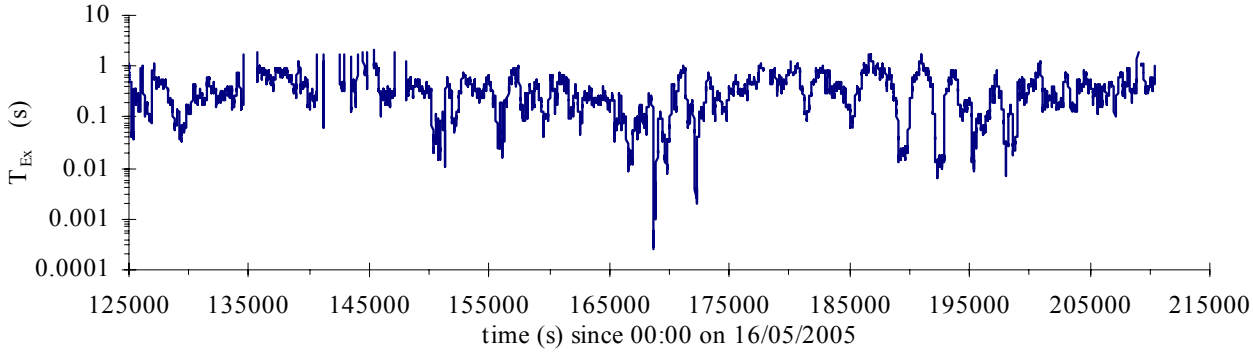

(B) Integral time scales of transverse velocity T_{Ey}

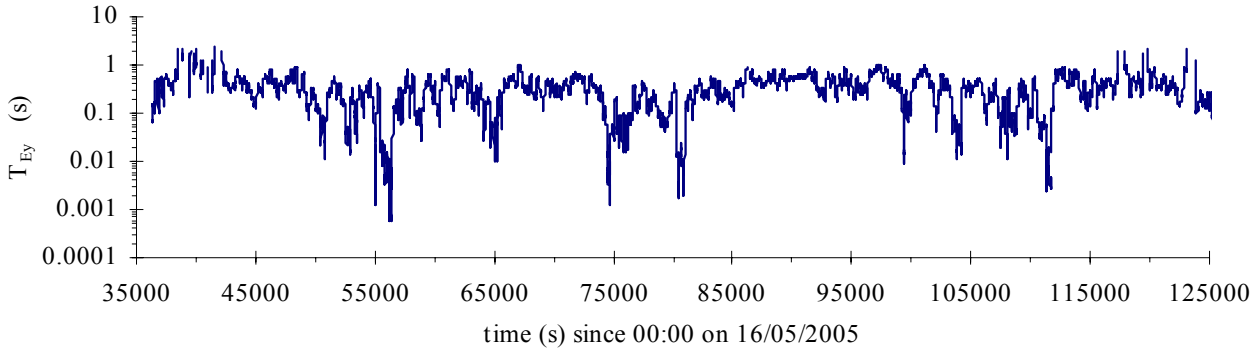

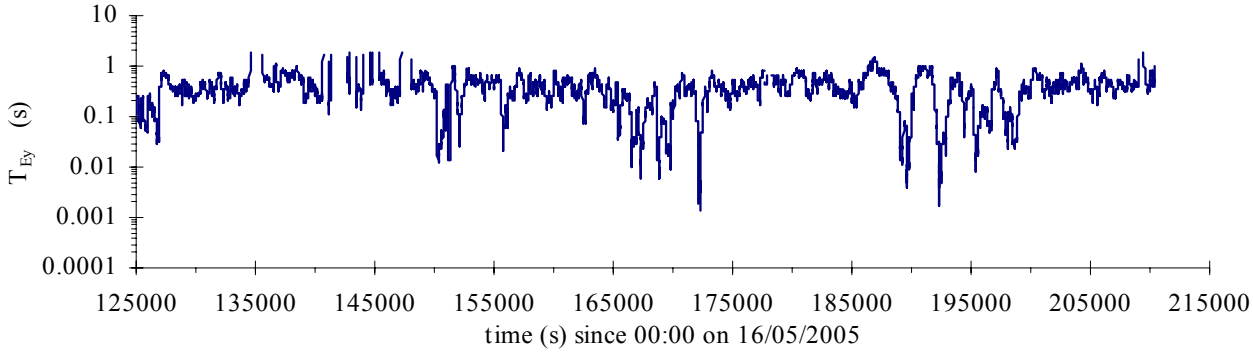

(C) Integral time scales of vertical velocity T_{Ez}

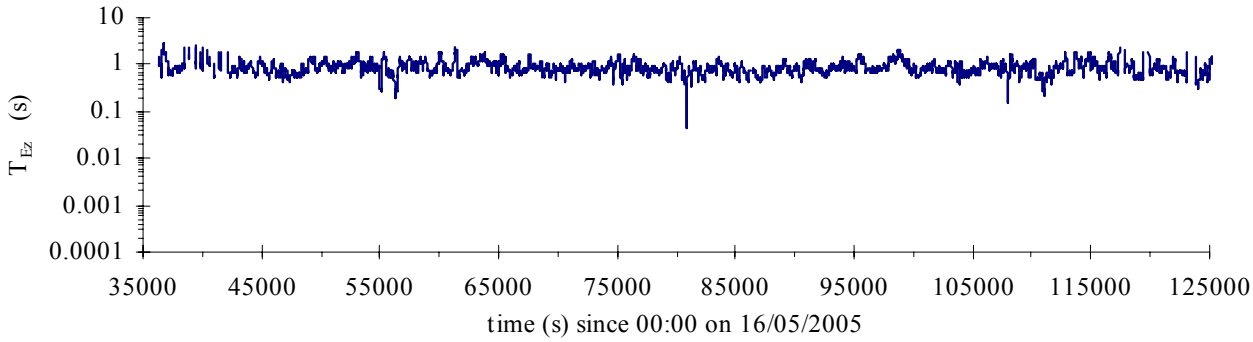

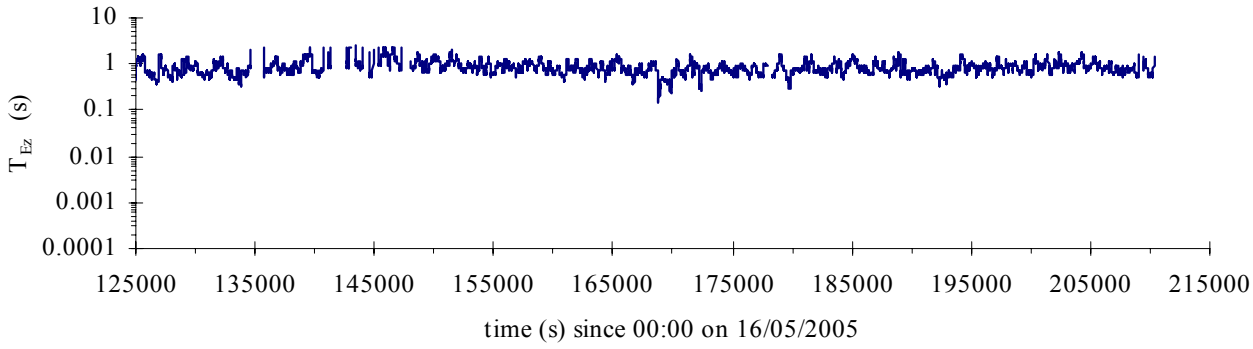

Fig. B-9 - Dissipation time scales τ_E of velocity data collected at Site 2B Eprapah Creek (QLD) during field work E6 on 16-18 May 2005 - 3D ADV (10 MHz), scan rate: 25 Hz, Probe sensor: 0.4 m above bed, 10.7 m from left bank - Dissipation time scales time-averaged over 5000 data points (3.33 minutes) taken every 10 s along entire data set

(A) Dissipation time scales of streamwise velocity τ_{Ex}

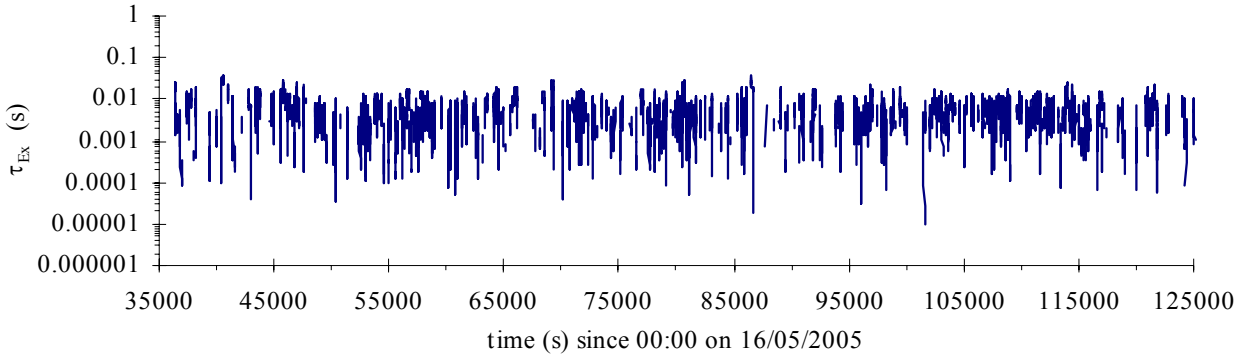

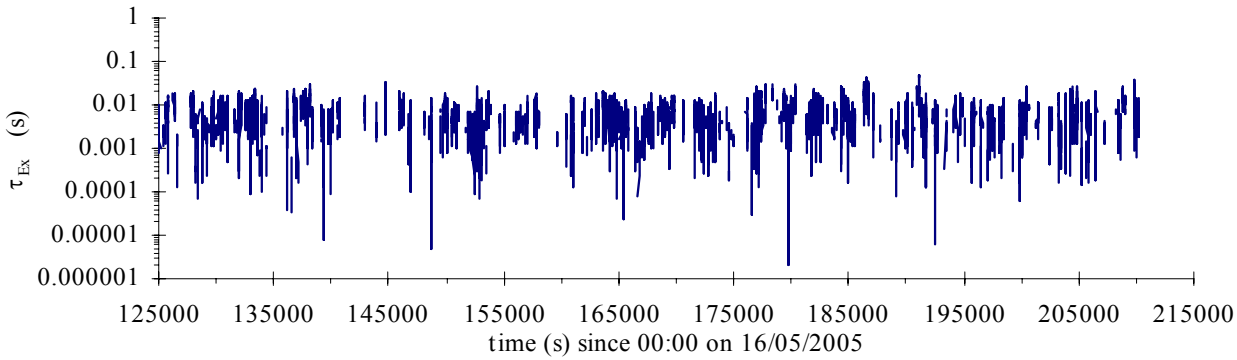

(B) Dissipation time scales of transverse velocity τ_{Ey}

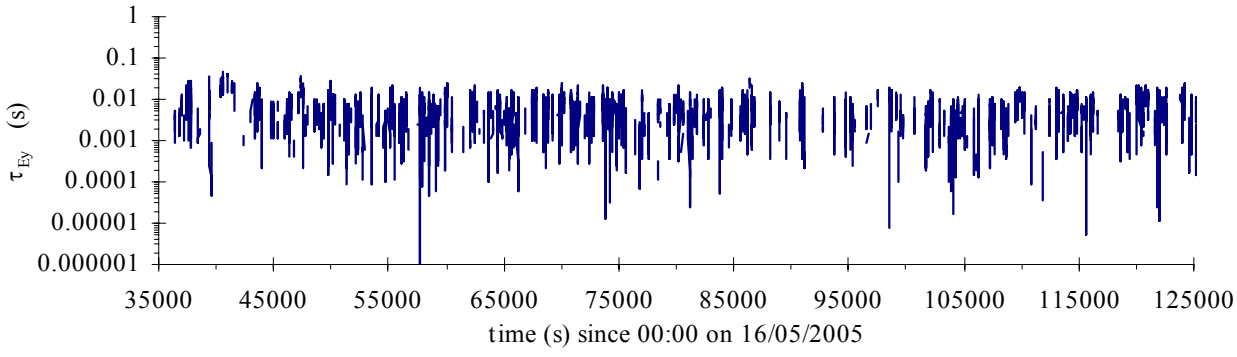

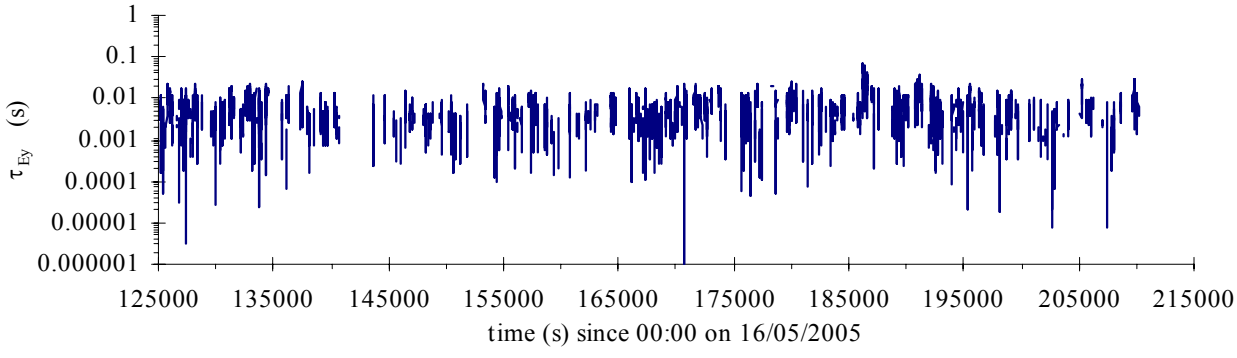

(C) Dissipation time scales of vertical velocity τ_{Ez}

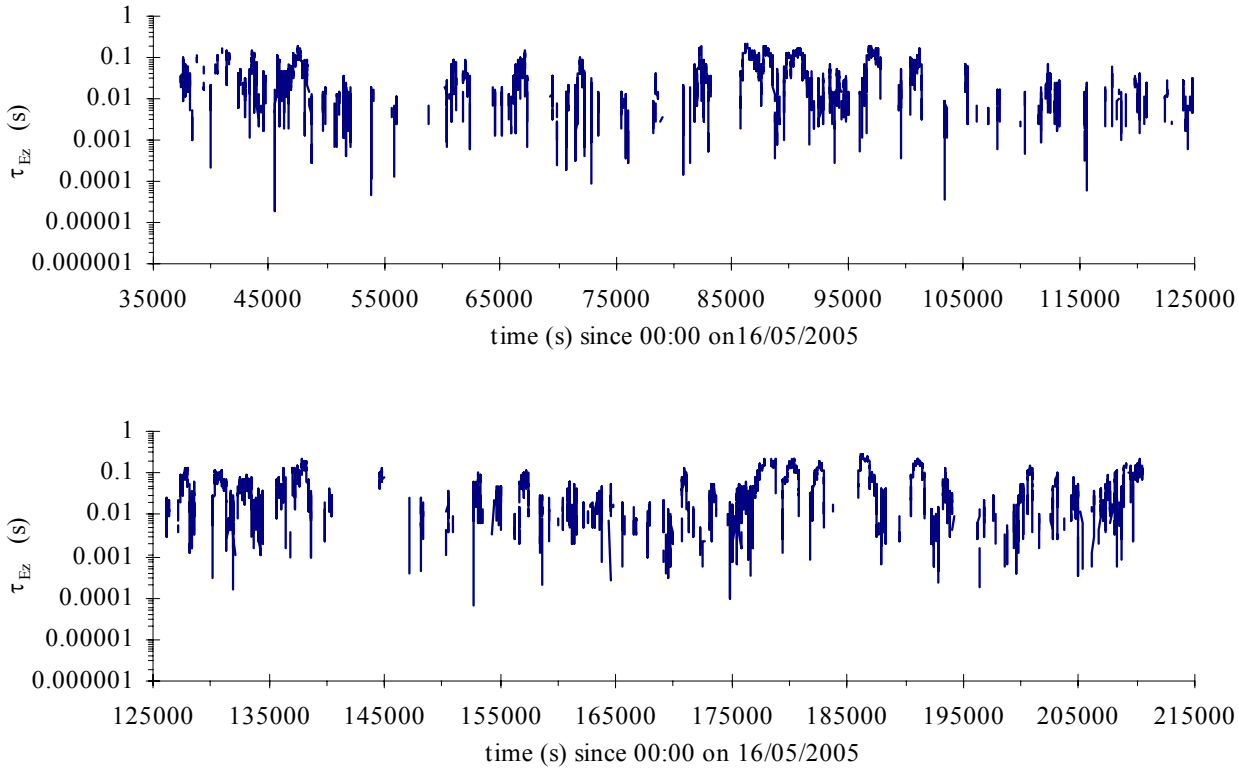

Fig. B-10 - Correlation coefficients of tangential Reynolds stress data collected at Site 2B Eprapah Creek (QLD) during field work E6 on 16-18 May 2005 - 3D ADV (10 MHz), scan rate: 25 Hz, Probe sensor: 0.4 m above bed, 10.7 m from left bank - Correlation coefficients of Reynolds stress based upon 5000 data points (3.33 minutes) taken every 10 s along entire data set

(A) Correlation coefficient of tangential Reynolds stress R_{vxvy}

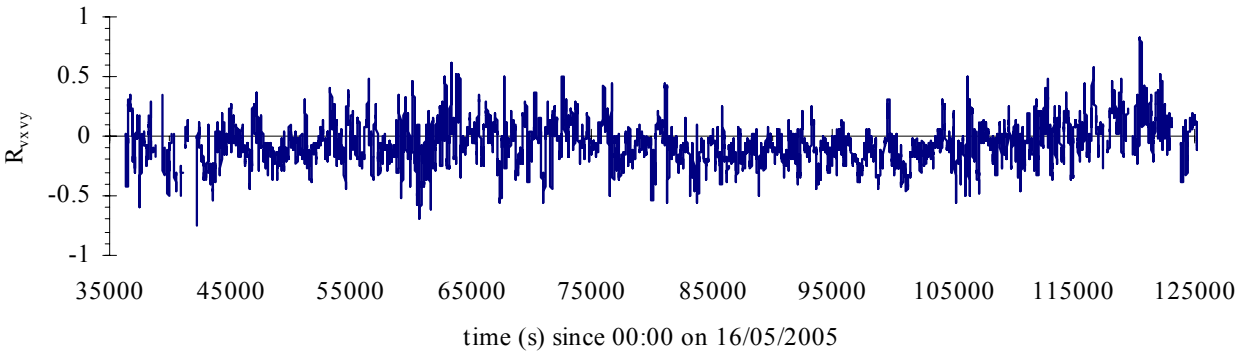

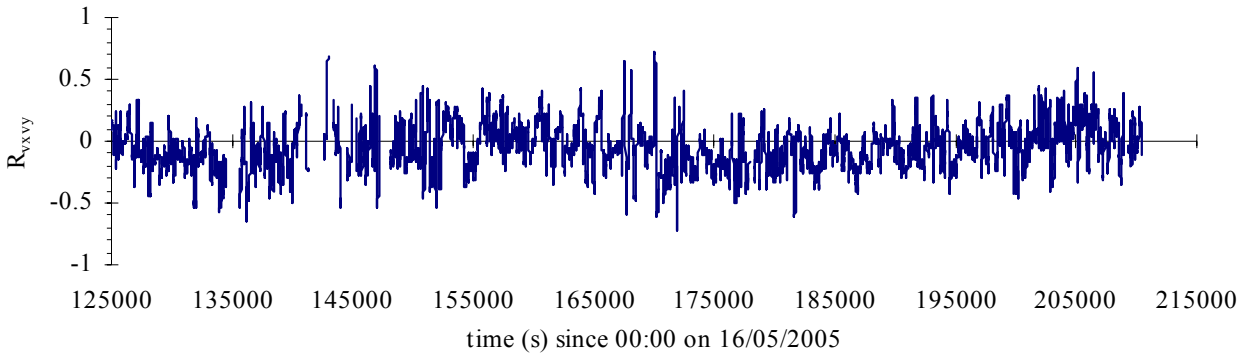

(B) Correlation coefficient of tangential Reynolds stress R_{vxvz}

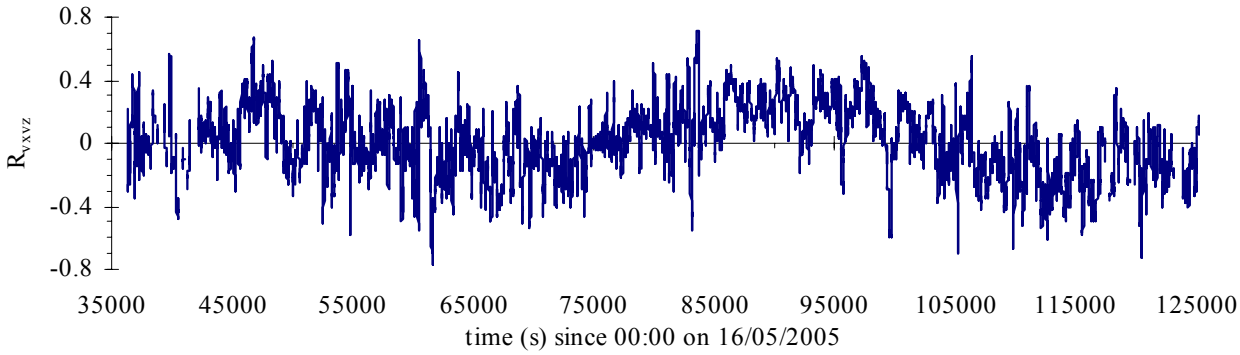

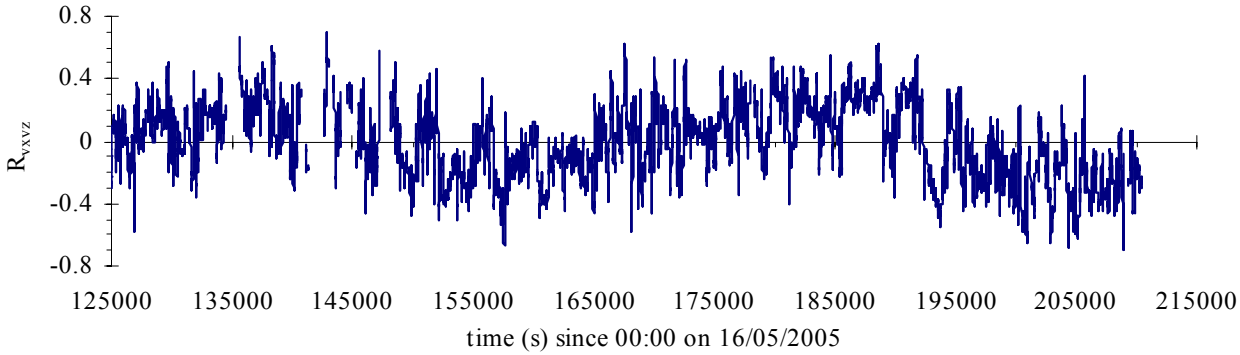

(C) Correlation coefficient of tangential Reynolds stress R_{vyvz}

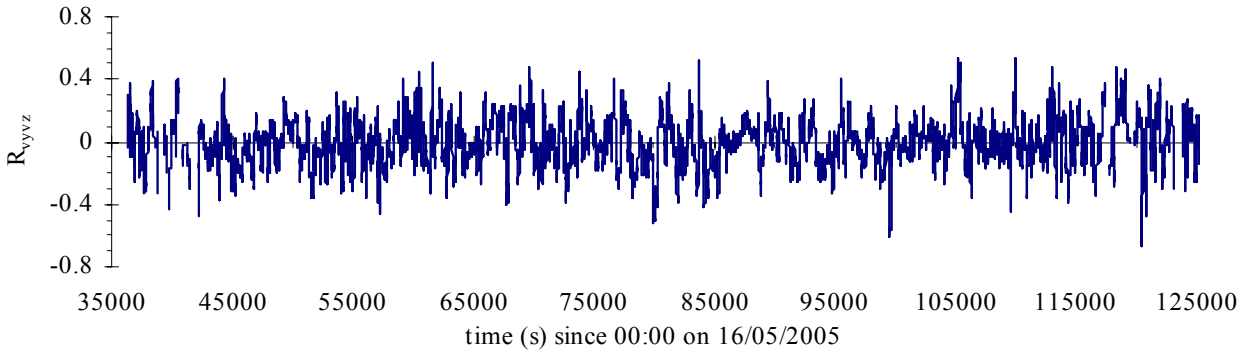

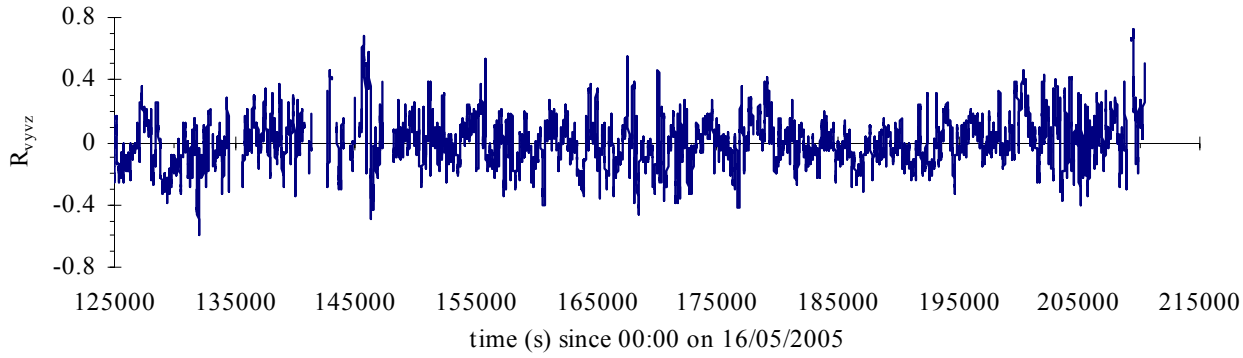

Fig. B-11 - Turbulence intensities data collected at Site 2B Eprapah Creek (QLD) during field work E6 on 16-18 May 2005 - 3D ADV (10 MHz), scan rate: 25 Hz, Probe sensor: 0.4 m above bed, 10.7 m from left bank - Turbulence intensities based upon 5000 data points (3.33 minutes) taken every 10 s along entire data set

(A) Horizontal turbulence intensity $v_y^{'}/v_x^{'}$

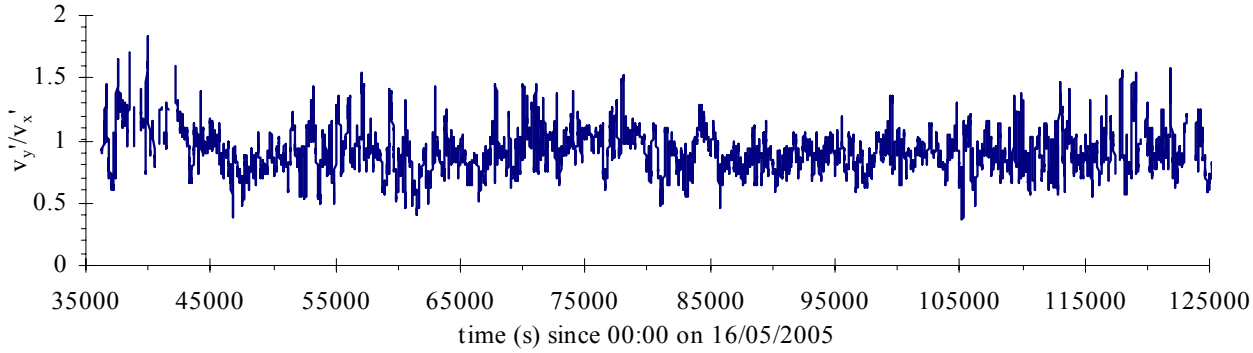

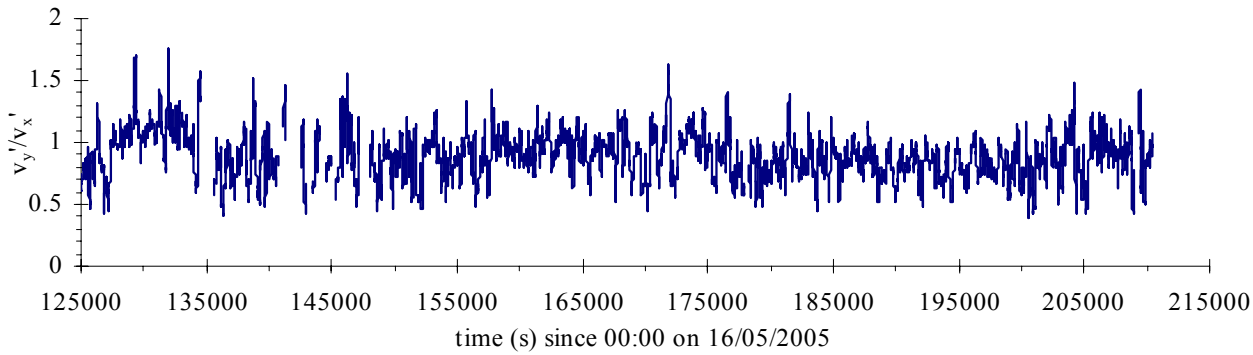

(B) Vertical turbulence intensity v_z'/v_x'

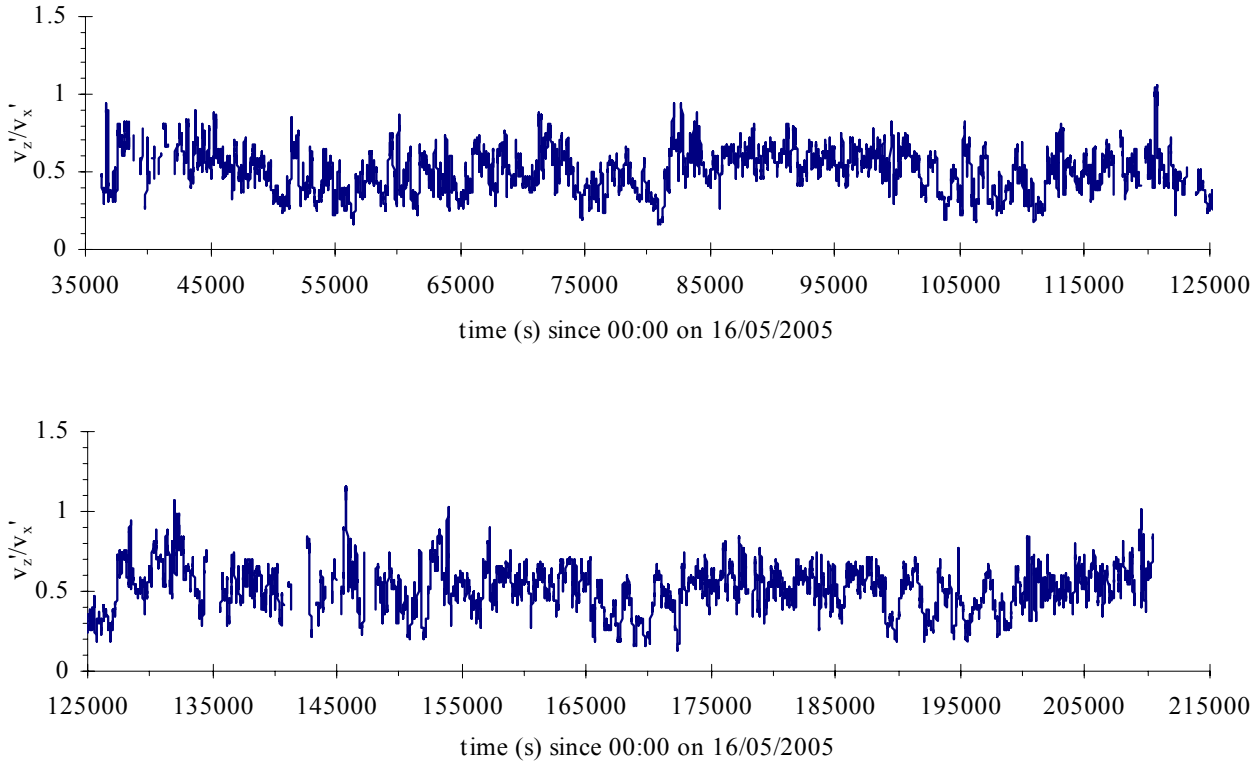

B.2.2 - Acoustic Doppler velocimetry, 2D microADV (16 MHz) located 0.2 m above the bed

Fig. B-12 - Instantaneous velocity data collected at site 2B Eprapah Creek (QLD) during field work E6 on 16-18 May 2005 - 2D microADV (16 MHz), scan rate: 25 Hz, Probe sensor: 0.2 m above bed, 10.7 m from left bank, Post-processed data

(A) Instantaneous streamwise velocity V_x

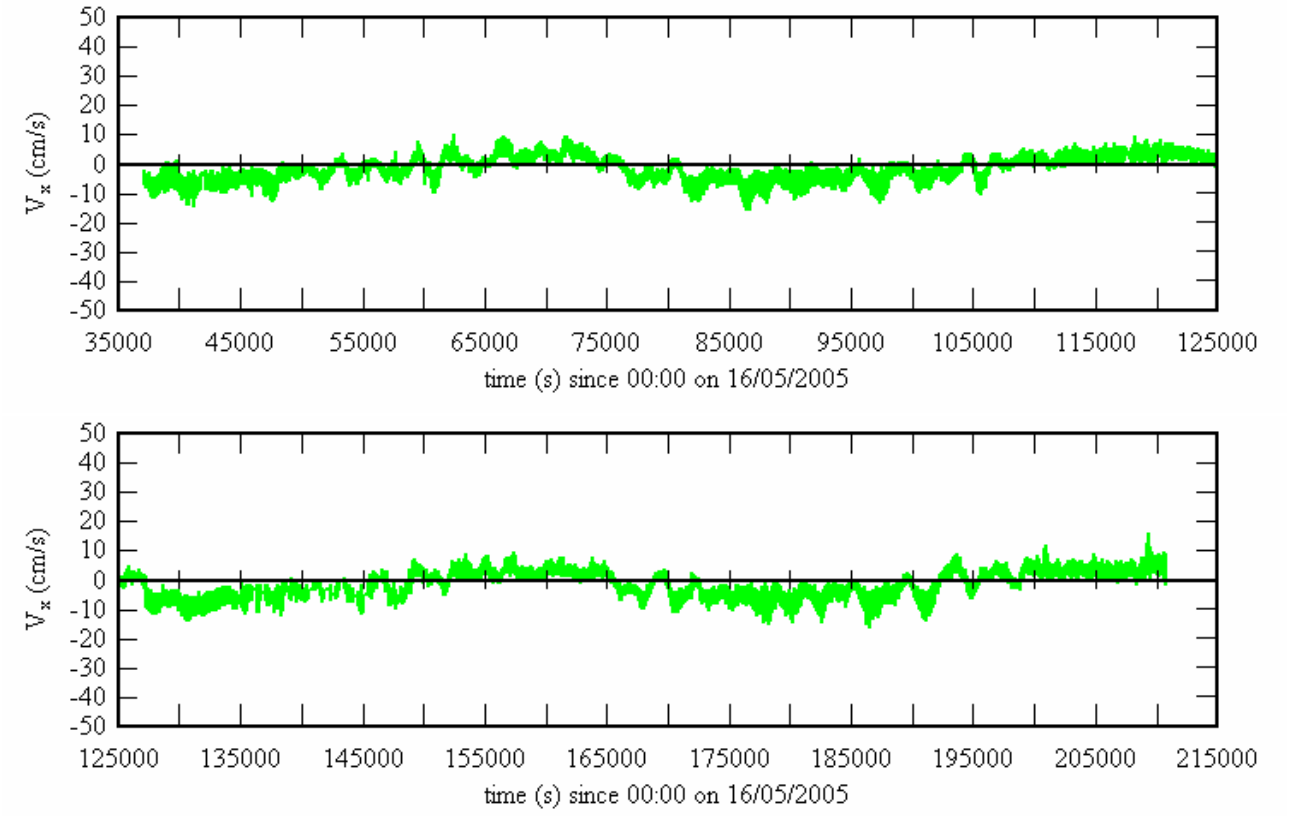

(B) Instantaneous transverse velocity V_y

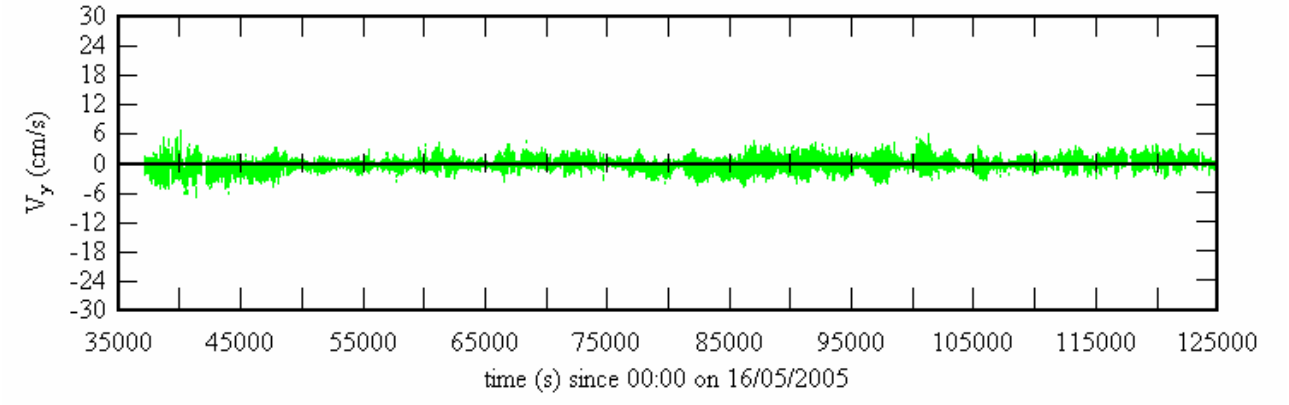

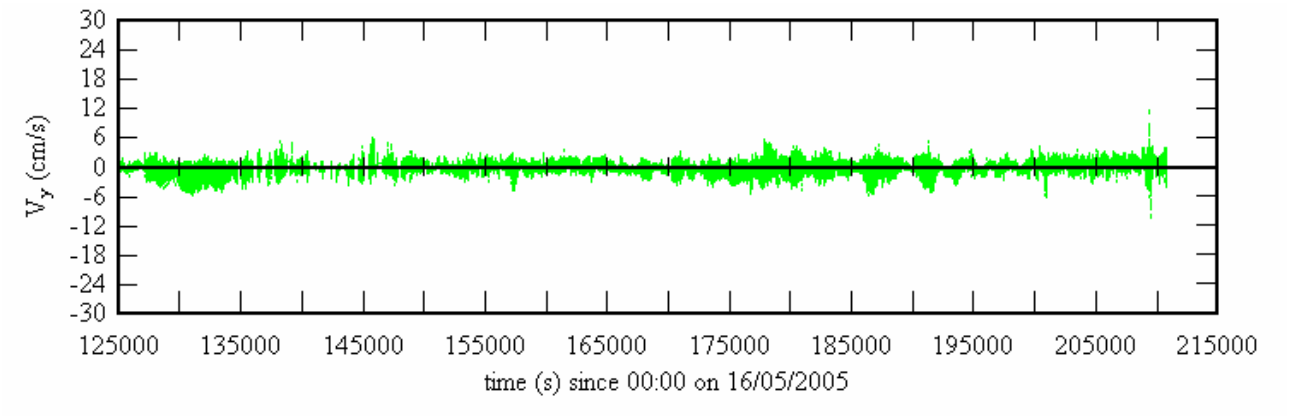

Fig. B-13 - Time-averaged velocity data collected at site 2B Eprapah Creek (QLD) during field work E6 on 16-18 May 2005 - 2D microADV (16 MHz), scan rate: 25 Hz, Probe sensor: 0.2 m above bed, 10.7 m from left bank - Time-average based upon 5000 data points (3.33 minutes) taken every 10 s along entire data set

(A) Time-averaged streamwise velocity $\overline{V_x}$

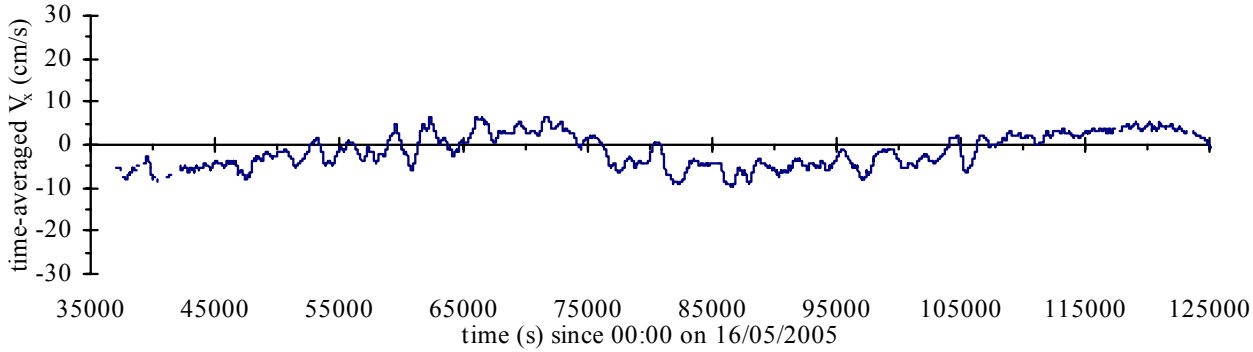

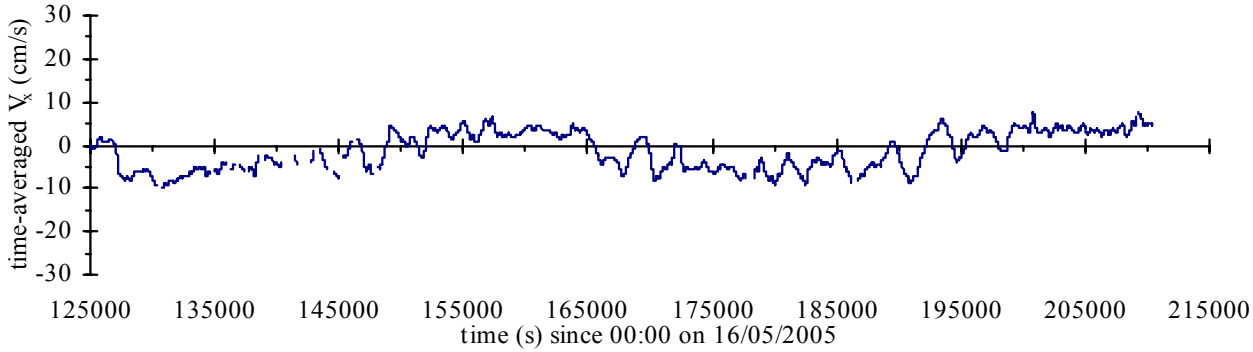

(B) Time-averaged transverse velocity $\overline{V_y}$

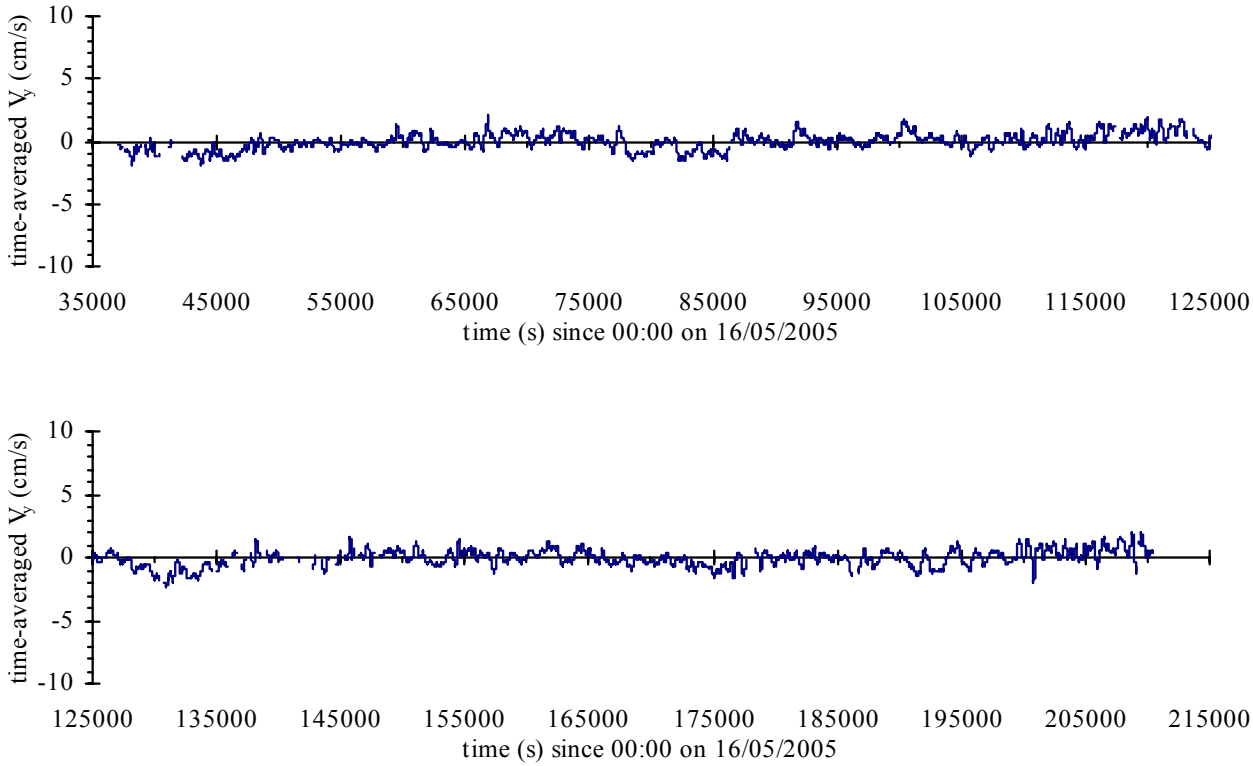

Fig. B-14 – Standard deviations of velocity data collected at site 2B Eprapah Creek (QLD) during field work E6 on 16-18 May 2005 - 2D microADV (16 MHz), scan rate: 25 Hz, Probe sensor: 0.2 m above bed, 10.7 m from left bank - Standard deviations based upon 5000 data points (3.33 minutes) taken every 10 s along entire data set

(A) Standard deviations of streamwise velocity v_x'

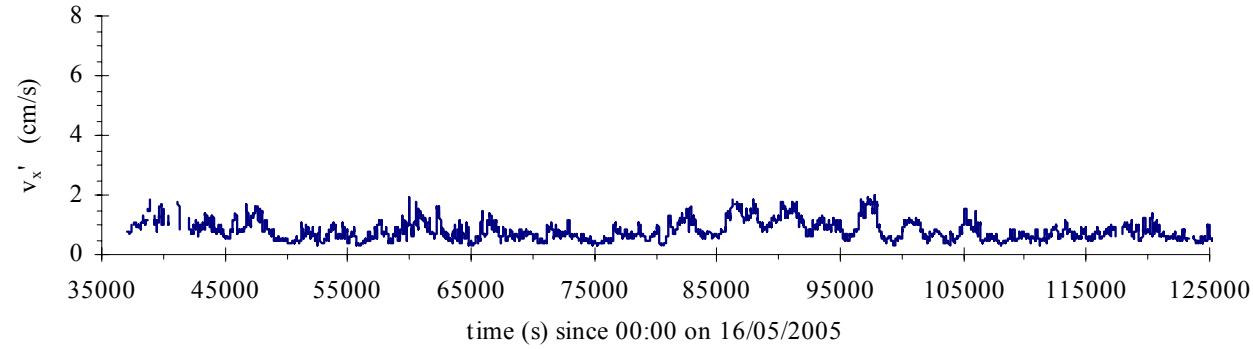

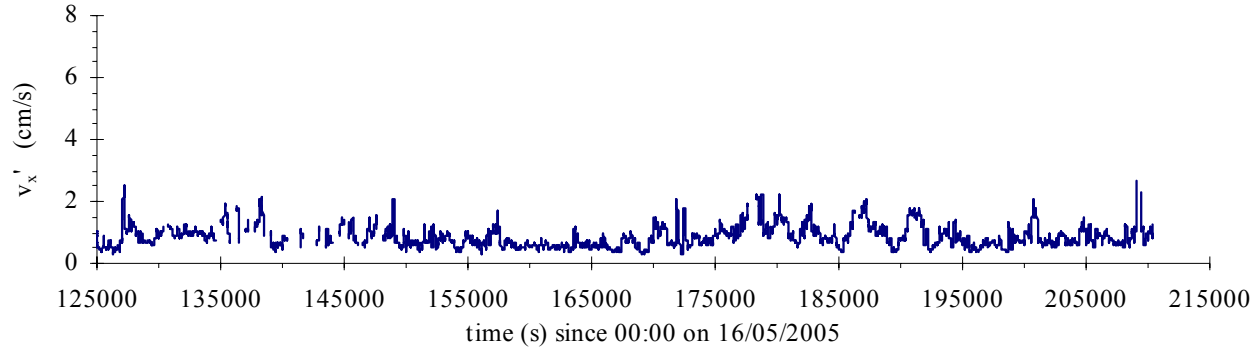

(B) Standard deviations of transverse velocity v_y'

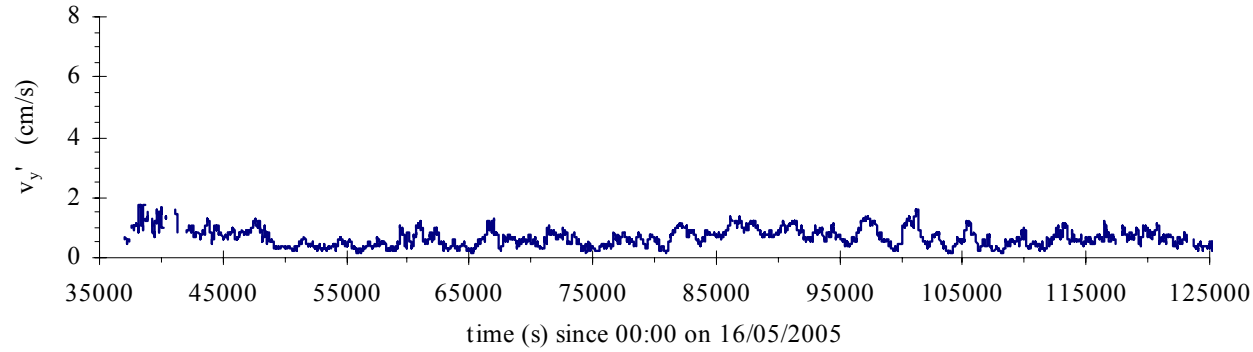

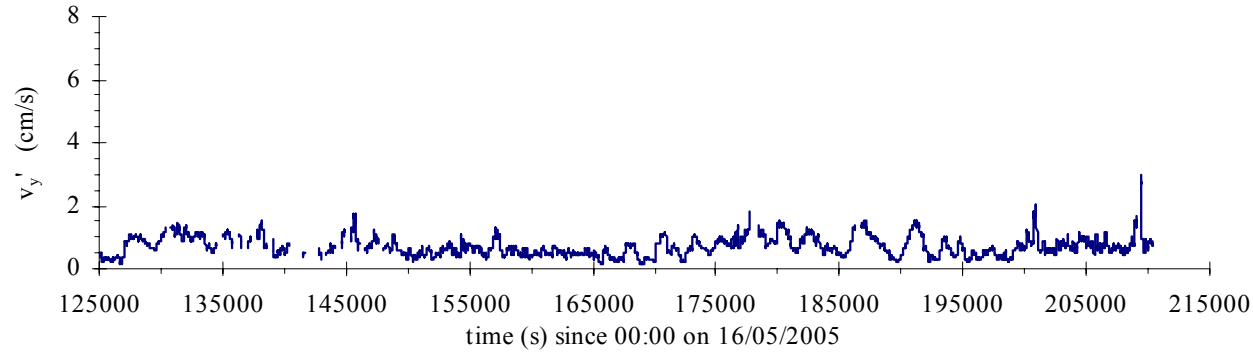

Fig. B-15 - Instantaneous tangential Reynolds stress data collected site 2B at Eprapah Creek (QLD) during field work E6 on 16-18 May 2005 - 2D microADV (16 MHz), scan rate: 25 Hz, Probe sensor: 0.2 m above bed, 10.7 m from left bank - Instantaneous Reynolds stresses calculated every sample along entire data set (eg. $v_x = V_x - \overline{V_x}$) with $\overline{V_x}$ based upon 5000 data points (3.33 minutes)

(A) Instantaneous tangential Reynolds stress $\rho v_x v_y$

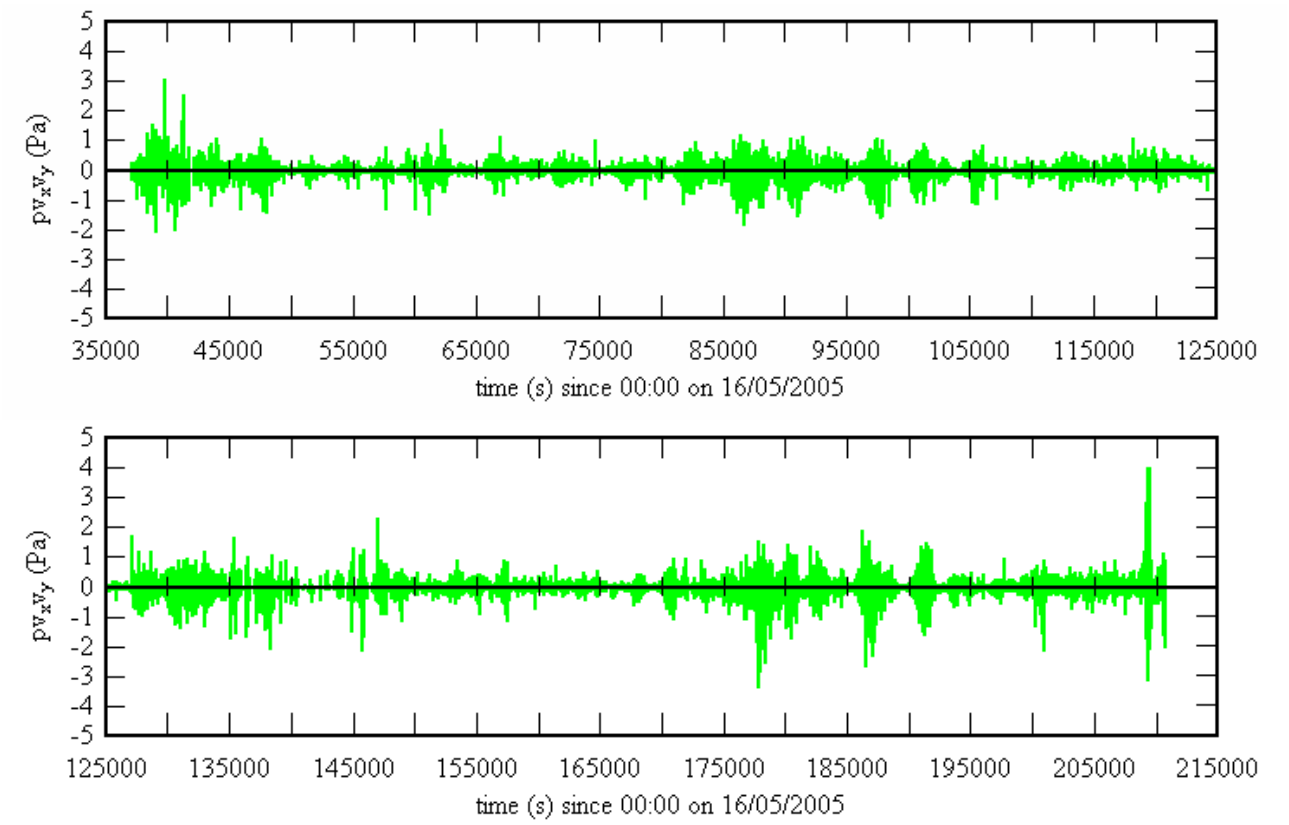

Fig. B-16 - Time-averaged tangential Reynolds stress data collected at site 2B Eprapah Creek (QLD) during field work E6 on 16-18 May 2005 - 2D microADV (16 MHz), scan rate: 25 Hz, Probe sensor: 0.2 m above bed, 10.7 m from left bank - Time-average based upon 5000 data points (3.33 minutes) taken every 10 s along entire data set

(A) Time-averaged tangential Reynolds stress $\rho \overline{v_x v_y}$

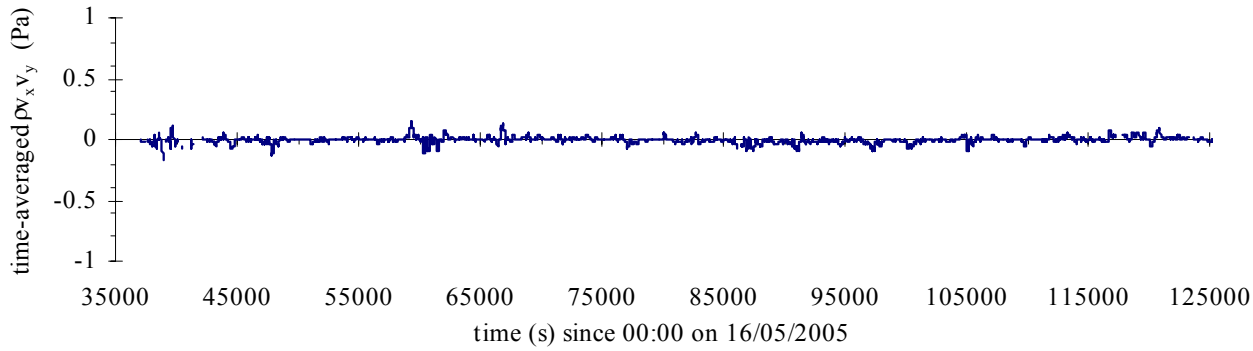

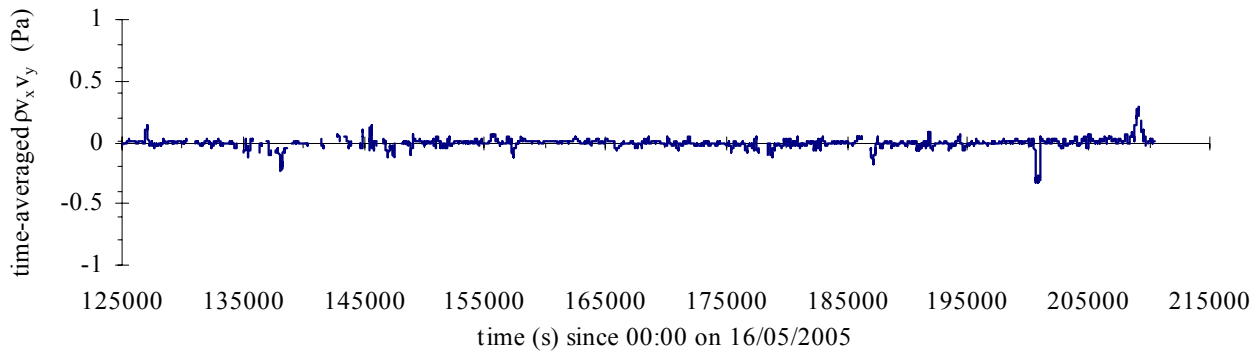

Fig. B-17 - Standard deviations of tangential Reynolds stress data collected at site 2B Eprapah Creek (QLD) during field work E6 on 16-18 May 2005 - 2D microADV (16 MHz), scan rate: 25 Hz, Probe sensor: 0.2 m above bed, 10.7 m from left bank - Standard deviations based upon 5000 data points (3.33 minutes) taken every 10 s along entire data set

(A) Standard deviations of tangential Reynolds stress $\left(\rho v_x v_y\right)'$

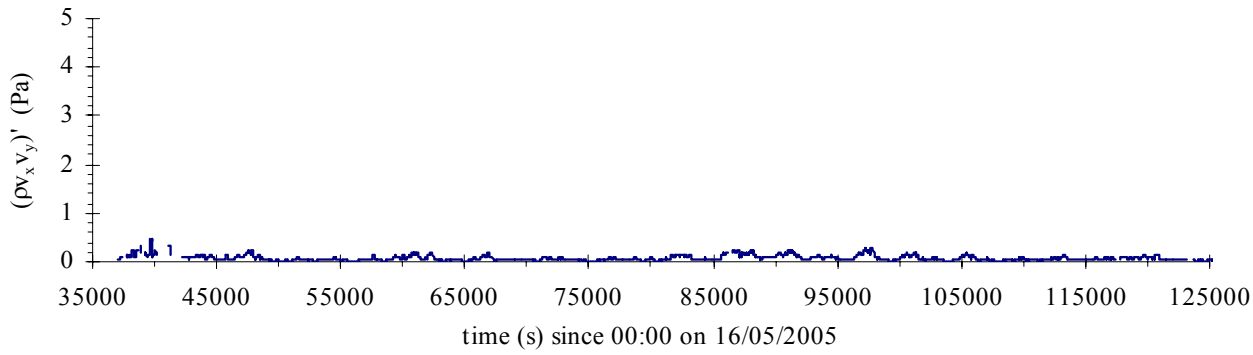

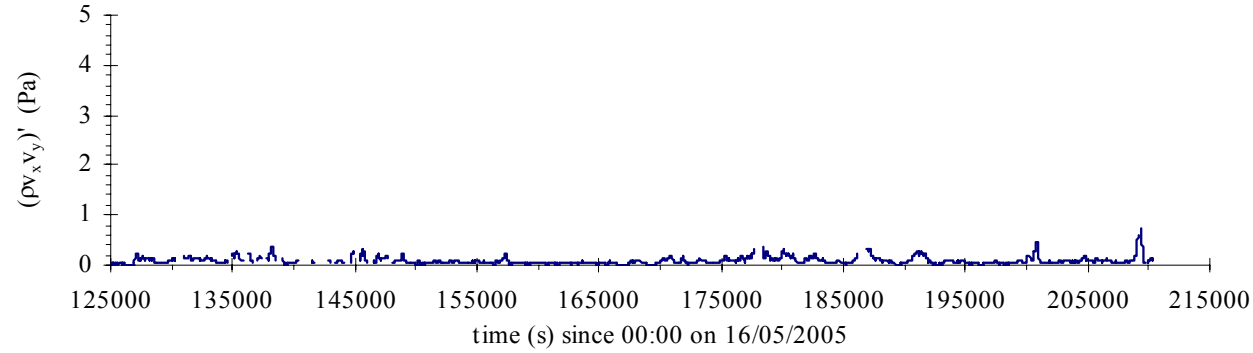

Fig. B-18 - Integral time scales T_E of velocity data collected at site 2B Eprapah Creek (QLD) during field work E6 on 16-18 May 2005 - 2D microADV (16 MHz), scan rate: 25 Hz, Probe sensor: 0.2 m above bed, 10.7 m from left bank - Integral time scales based upon average of 20 correlation curves (250 data points) collected from 5000 data points (3.33 minutes) taken every 10 s along entire data set

(A) Integral time scales of streamwise velocity T_{Ex}

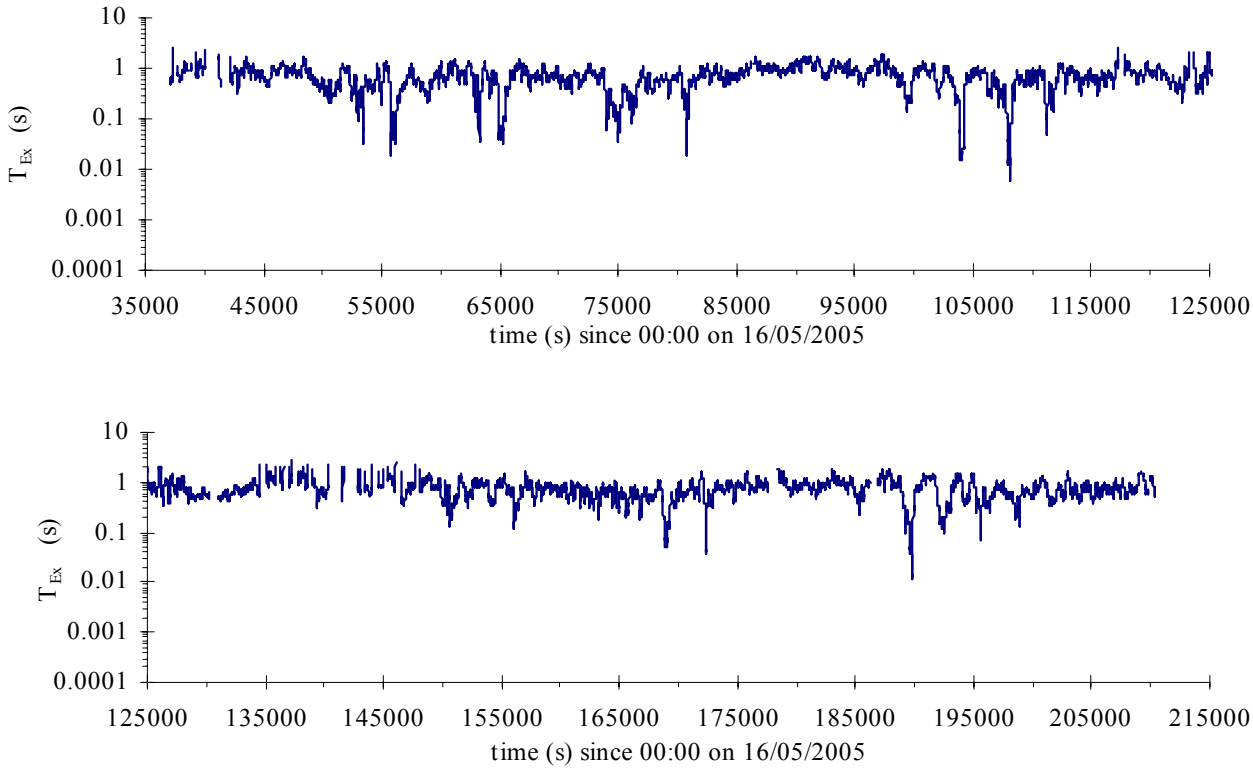

(B) Integral time scales of transverse velocity T_{Ey}

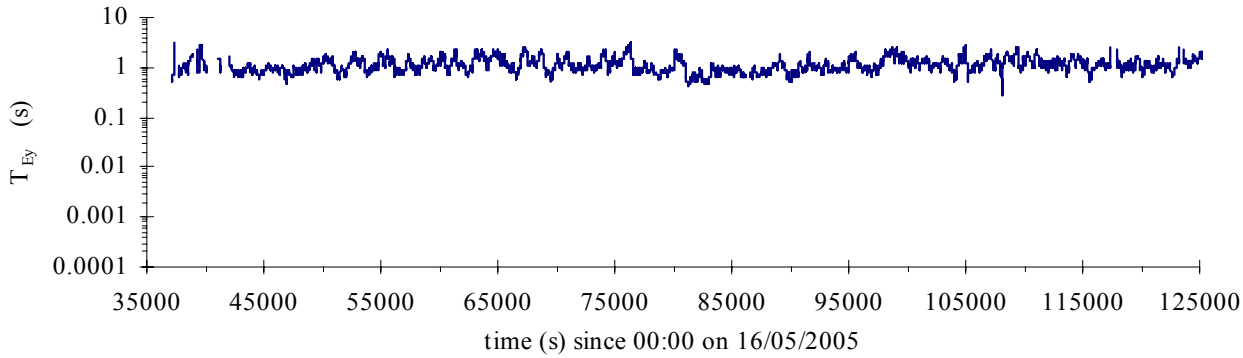

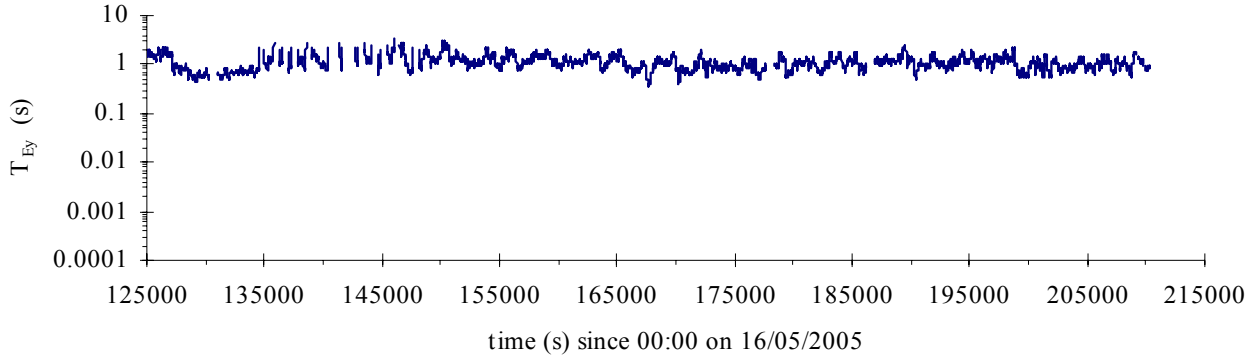

Fig. B-19 - Dissipation time scales τ_E of velocity data collected at site 2B Eprapah Creek (QLD) during field work E6 on 16-18 May 2005 - 2D microADV (16 MHz), scan rate: 25 Hz, Probe sensor: 0.2 m above bed, 10.7 m from left bank - Dissipation time scales time-average based upon 5000 data points (3.33 minutes) taken every 10 s along entire data set
(A) Dissipation time scales of streamwise velocity τ_{Ex}

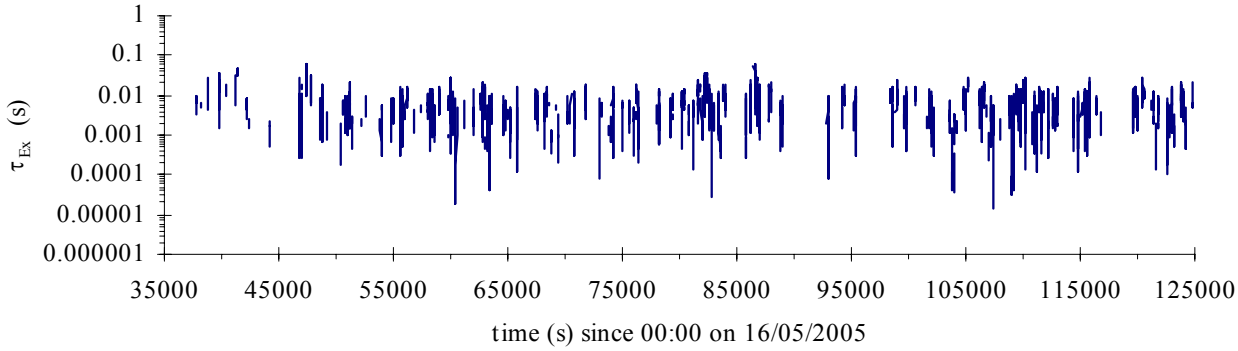

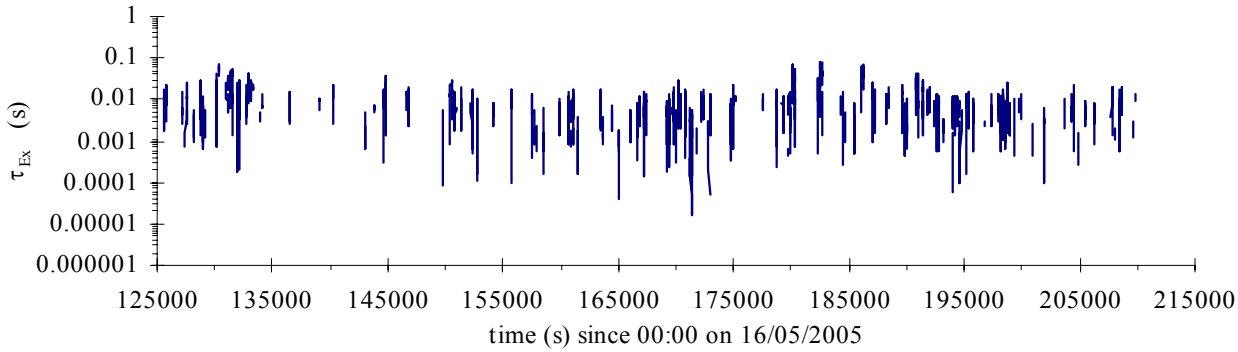

(B) Dissipation time scales of transverse velocity τ_{Ey}

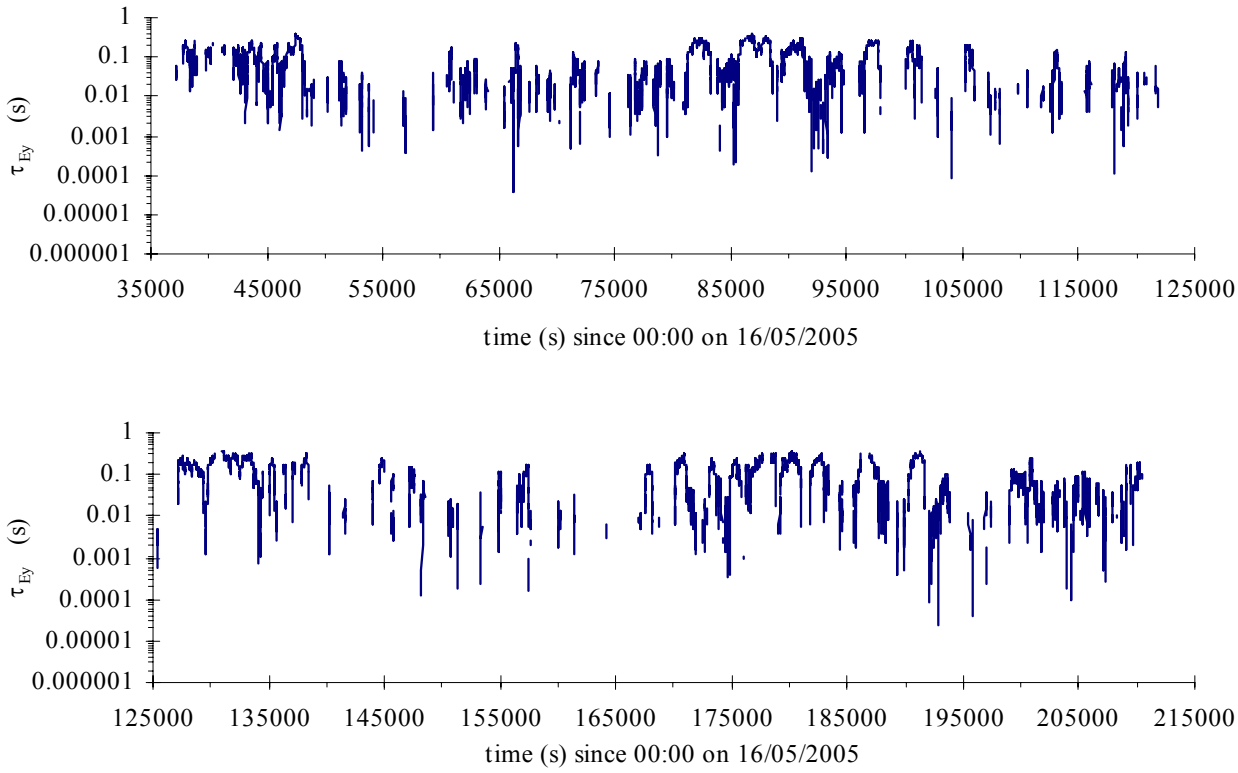

Fig. B-20 - Correlation coefficient of tangential Reynolds stress R_{vxvy} data collected at site 2B Eprapah Creek (QLD) during field work E6 on 16-18 May 2005 - 2D microADV (16 MHz), scan rate: 25 Hz, Probe sensor: 0.2 m above bed, 10.7 m from left bank - Correlation coefficients of Reynolds stress based upon 5000 data points (3.33 min.) taken every 10 s along entire data set

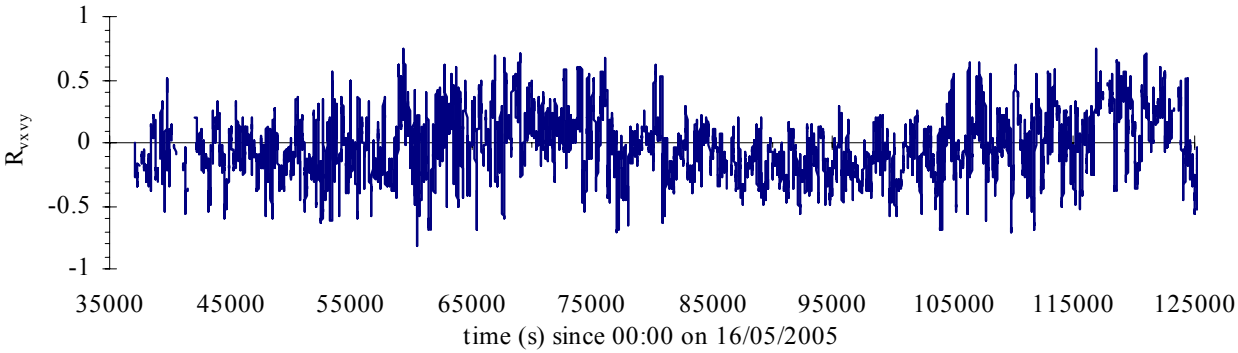

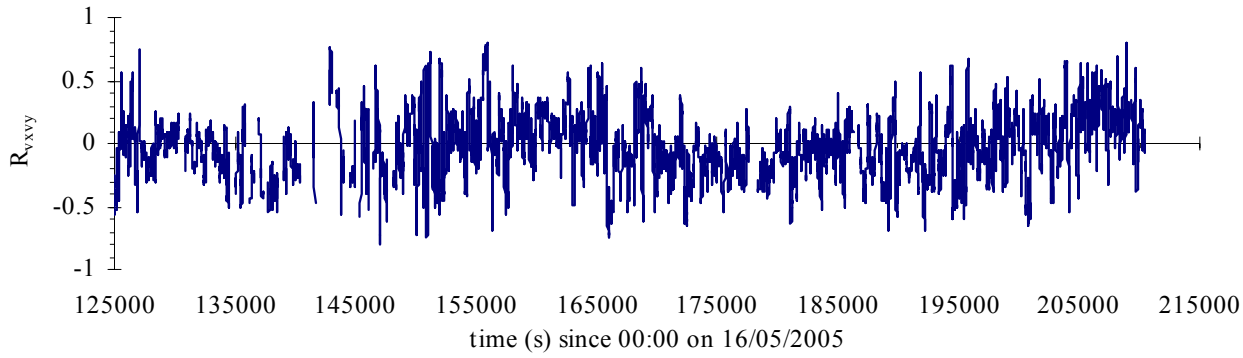

Fig. B-21 - Horizontal turbulence intensity v_y'/v_x' data collected at site 2B Eprapah Creek (QLD) during field work E6 on 16-18 May 2005 - 2D microADV (16 MHz), scan rate: 25 Hz, Probe sensor: 0.2 m above bed, 10.7 m from left bank - Turbulence intensities based upon 5000 data points (3.33 minutes) taken every 10 s along entire data set

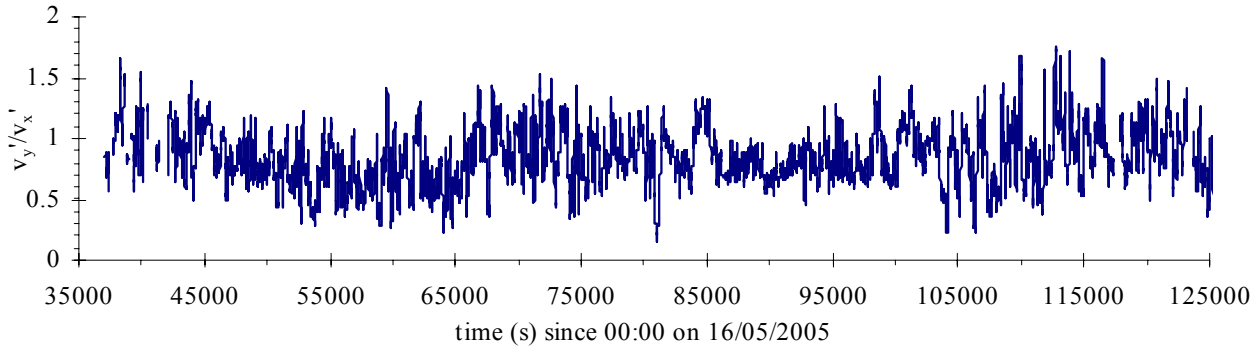

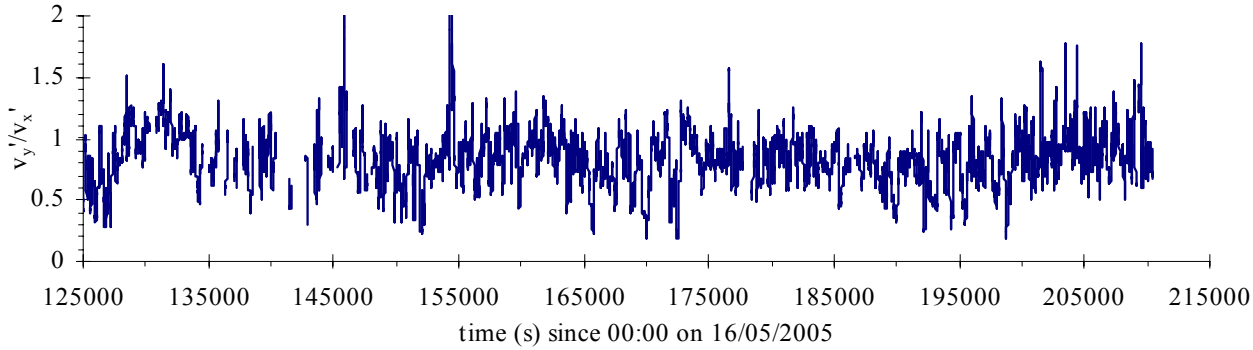

B.3 PHYSIO-CHEMISTRY DATA

Fig. B-22 - Instantaneous air temperature and water depth data collected at site 2B Eprapah Creek (QLD) during field work E6 on 16-18 May 2005 - Air temperature data collected every 15 min. and water depth data collected by YSI6600 probe every 12 s throughout field work E5
Legend: [——] water depth site 2B; [•] air temperature; [ ] period of darkness

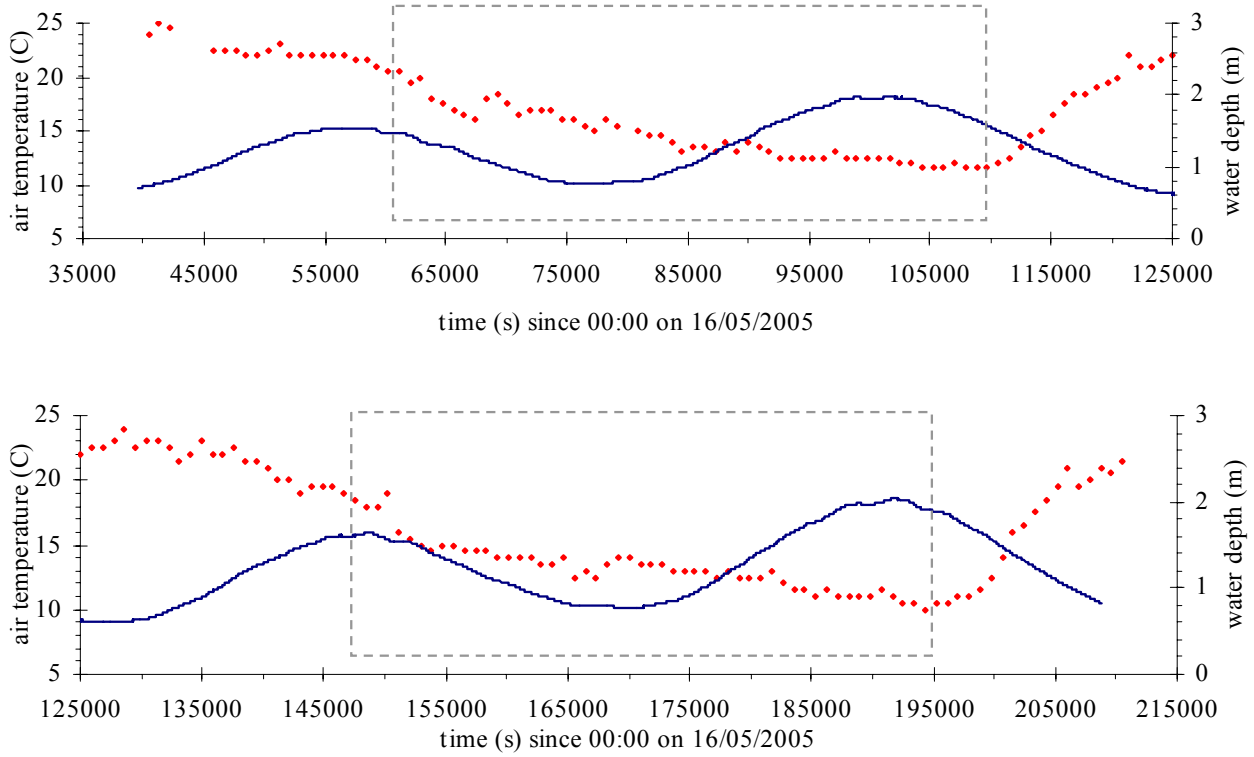

B.3.1 Physio-chemistry data from YSI6600 probe

Fig. B-23 - Instantaneous water temperature and conductivity data collected by YSI6600 at site 2B Eprapah Creek (QLD) during field work E6 on 16-18 May 2005 - Data sampled every 12 s at 0.4 m above bed, 10.4 m from left bank reference position
Legend: [——] water temperature; [——] conductivity.

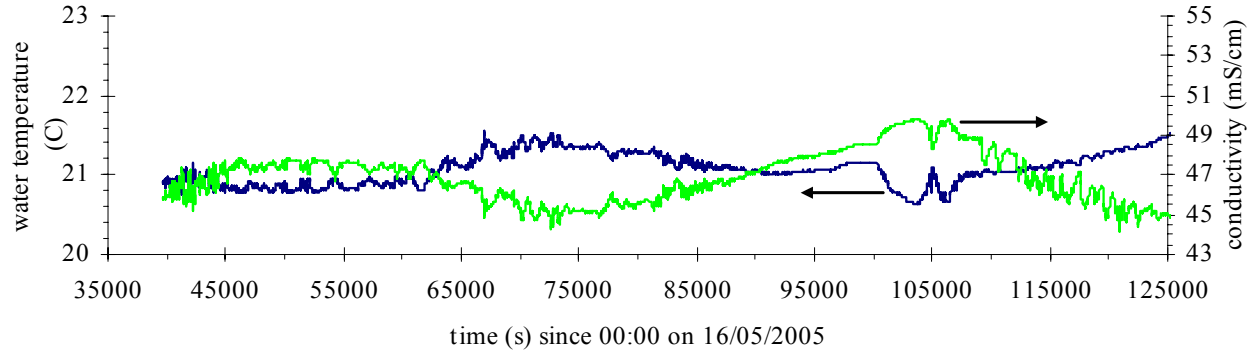

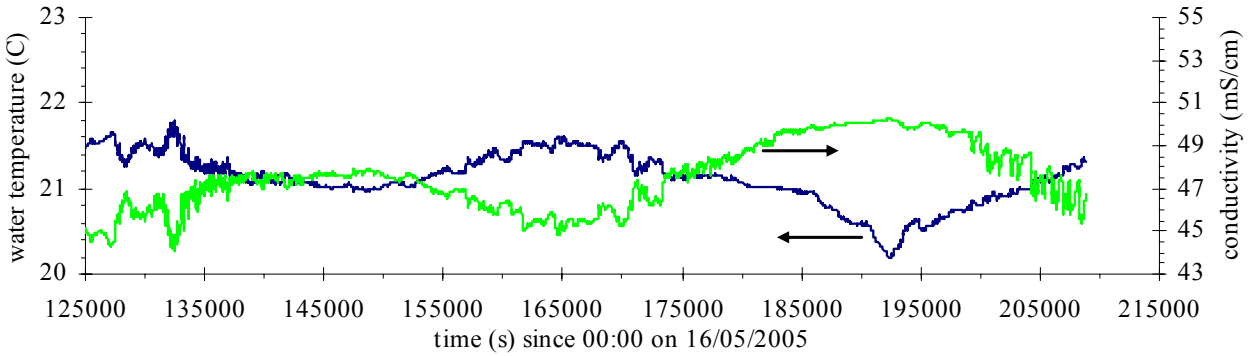

B.3.2 Physio-chemistry data from LTS9000 probes

Fig. B-24 – Instantaneous water temperature and conductivity data collected every 6 s by LTS9000 probes at site 2B Eprapah Creek (QLD) during field work E6 on 16-18 May 2005
Legend: [——] water temperature; [——] conductivity.
(A) Data collected by probe LTS-1 located 10.0 m from left bank, 0.29 m above bed

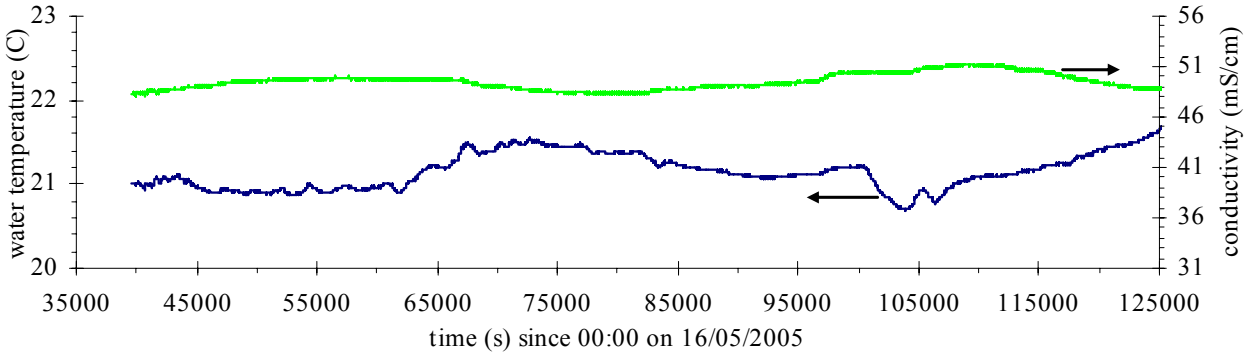

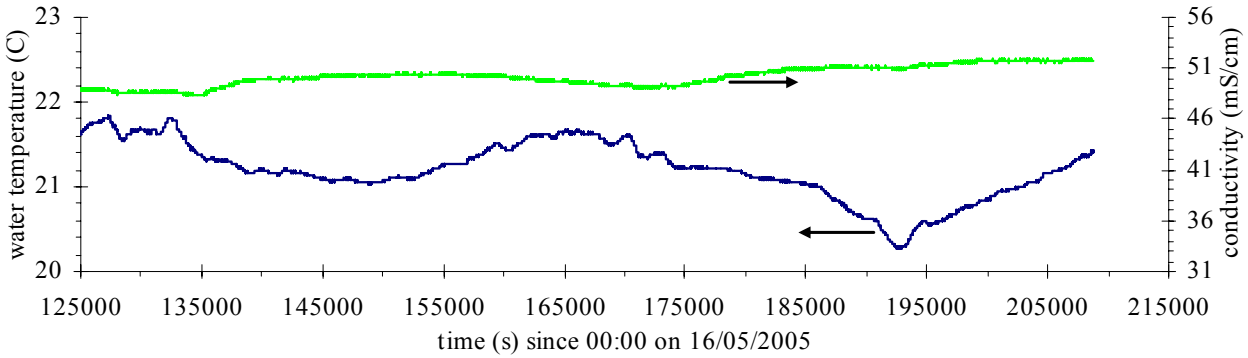

(B) Data collected by probe LTS-2 located 20.0 m from left bank, 0.41 m above bed

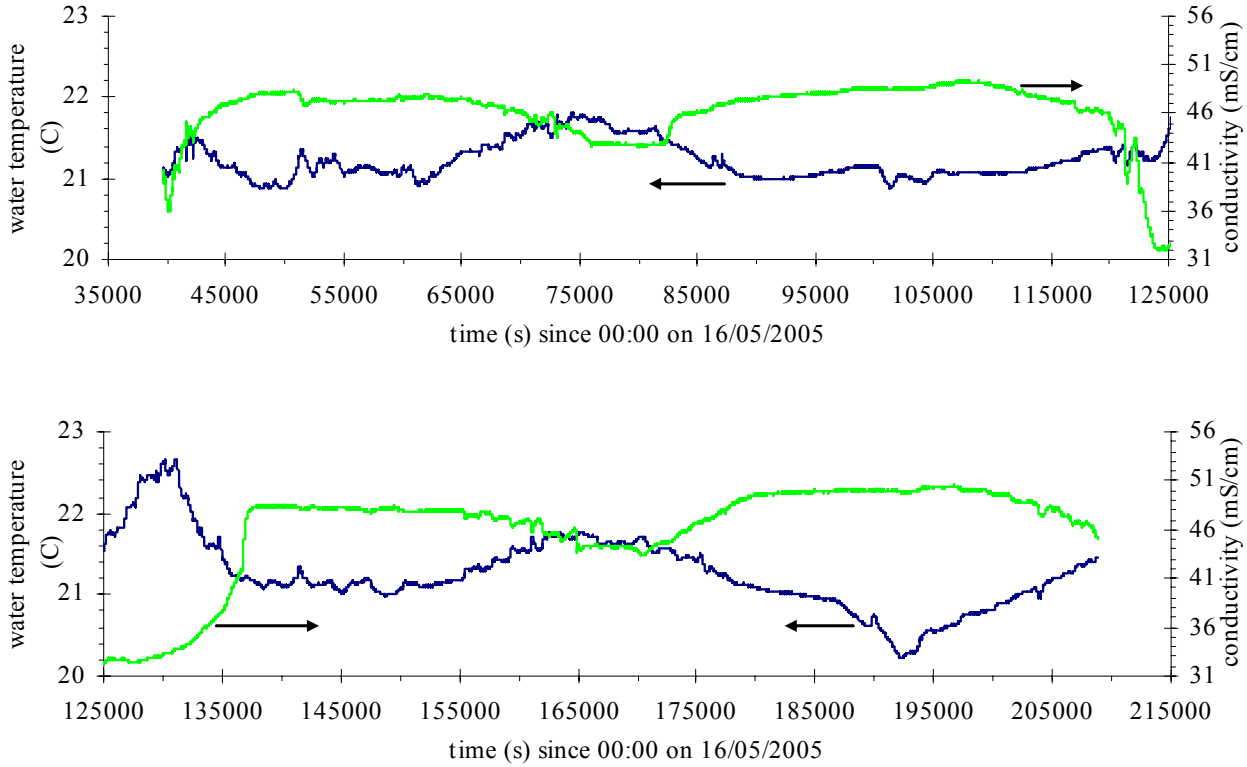

(C) Data collected by probe LTS-4 located 25.6 m from left bank, 0.15 m above bed

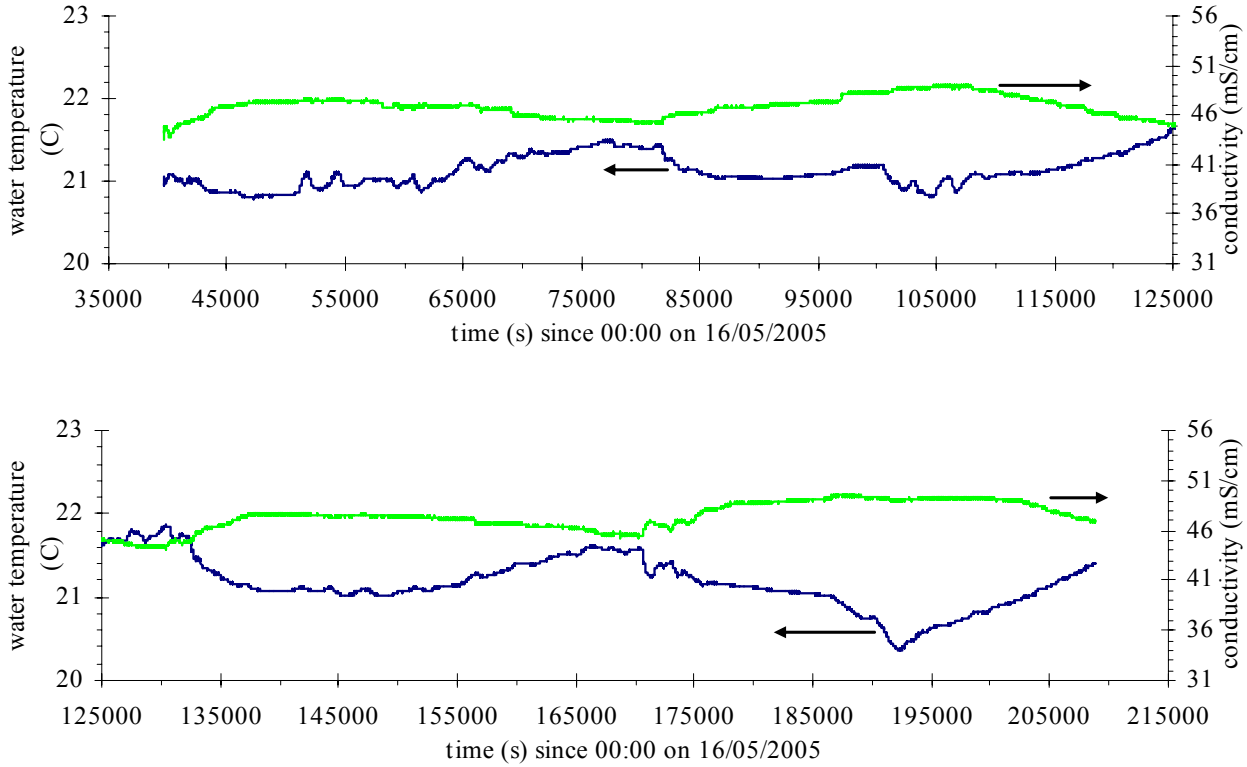

(D) Data collected by probe LTS-5 located 31.0 m from left bank, 0.38 m above bed

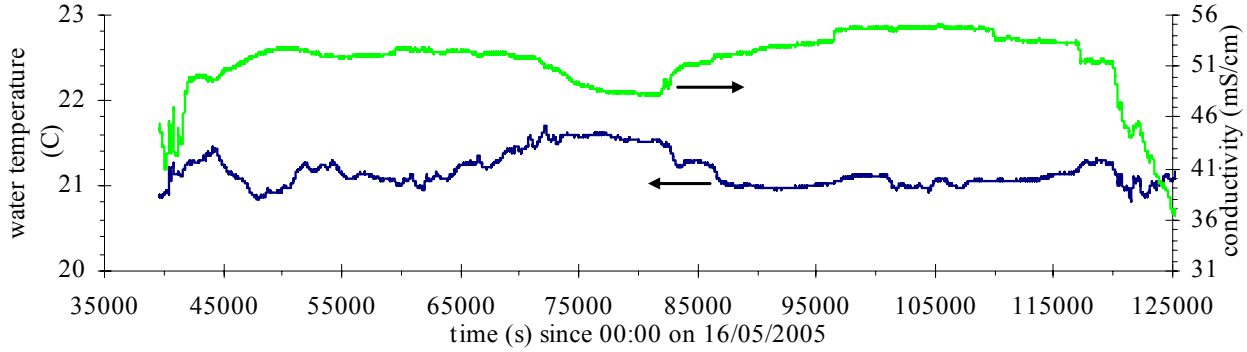

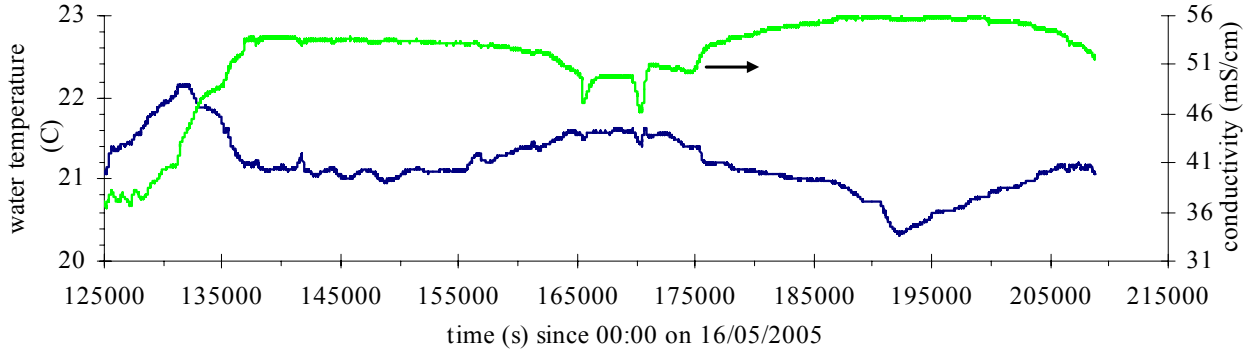

(E) Data collected by probe LTS-A located 25.6 m from left bank, 0.59 m above bed

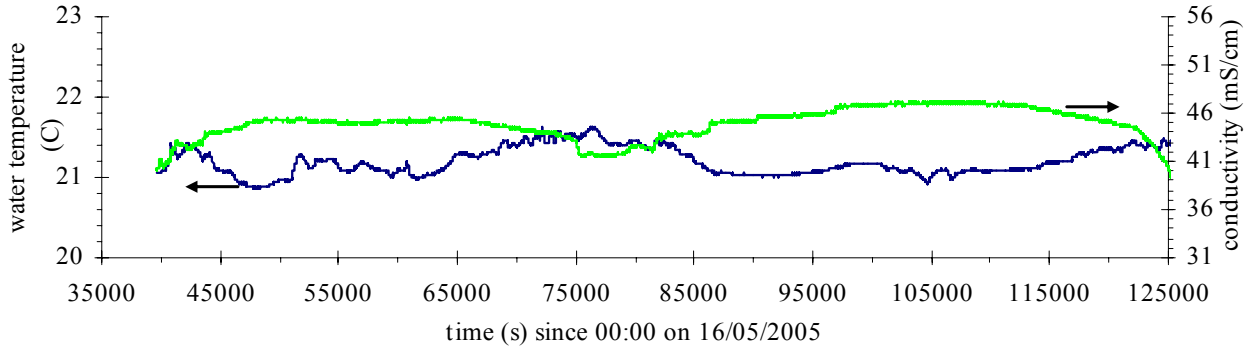

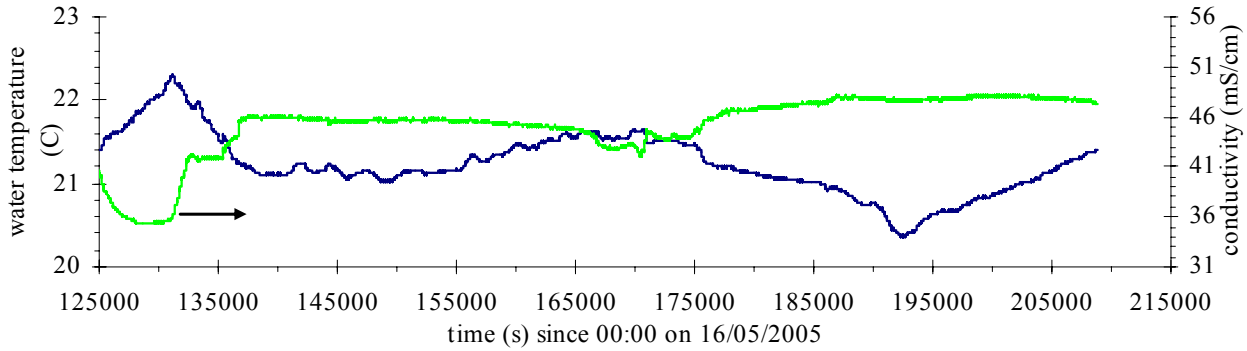

(F) Data collected by probe LTS-B located 14.0 m from left bank, 0.59 m above bed

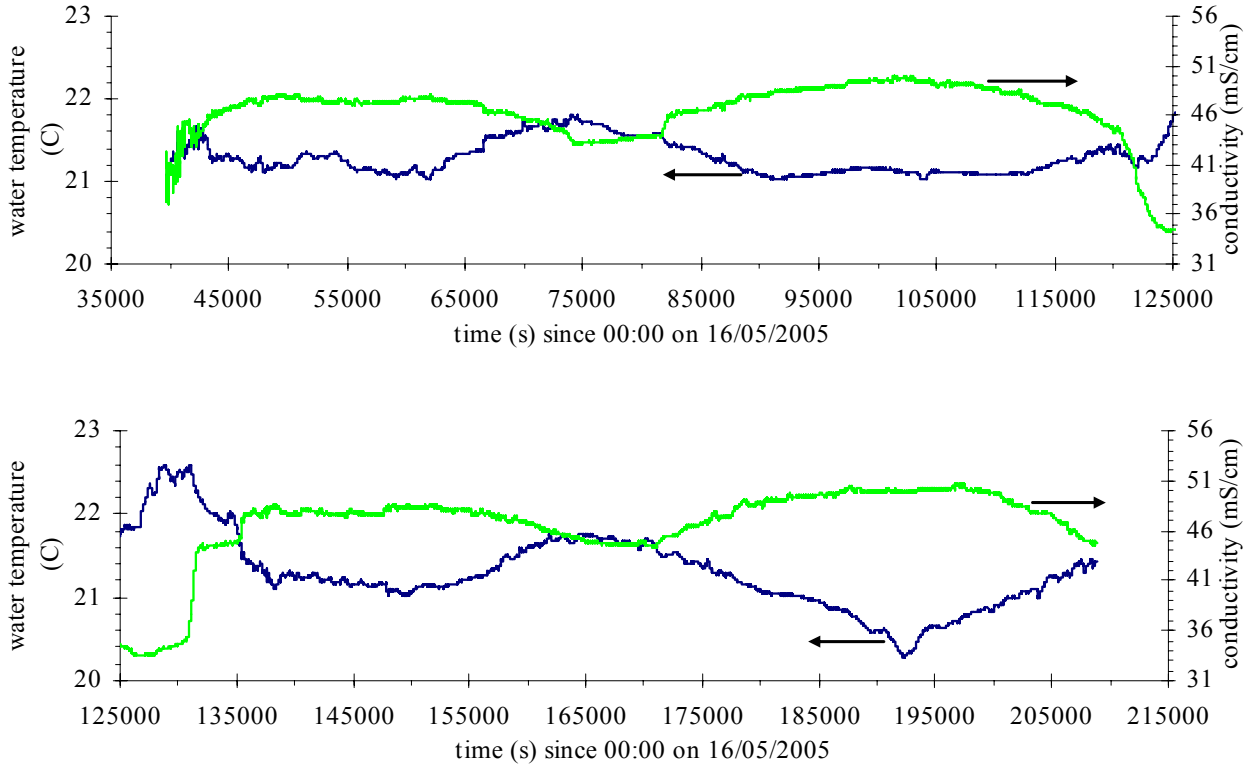

B.3.3 Physio-chemistry data from YSI6920 probe

Fig. B-25 - Vertical profiles of water temperature, conductivity, dissolved oxygen, turbidity and pH collected at Eprapah Creek (QLD) on 17 May 2005 - Data sampled with a YSI6920 probe lowered from a boat drifting mid-stream with the current during the mid ebb tide
(A) Water temperatures at the river mouth (AMTD 0 km), Site 1 (AMTD 0.6 km), Site 2 (AMTD 2 km), AMTD 2.7 km (treatment plant outfall) and Site 3 (AMTD 3.1 km)

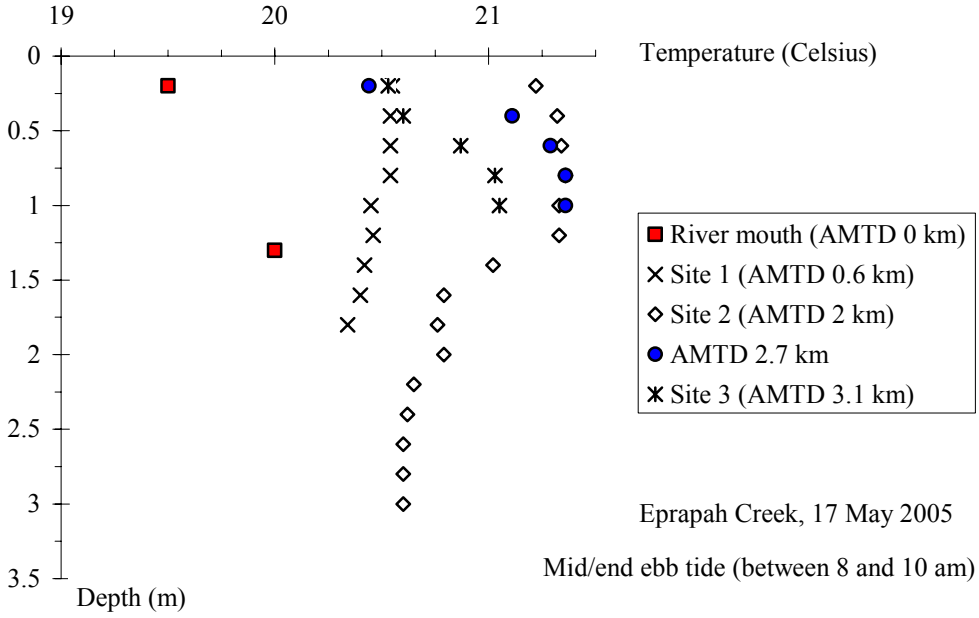

(B) Water conductivities at the river mouth (AMTD 0 km), Site 1 (AMTD 0.6 km), Site 2 (AMTD 2 km), AMTD 2.7 km (treatment plant outfall) and Site 3 (AMTD 3.1 km)

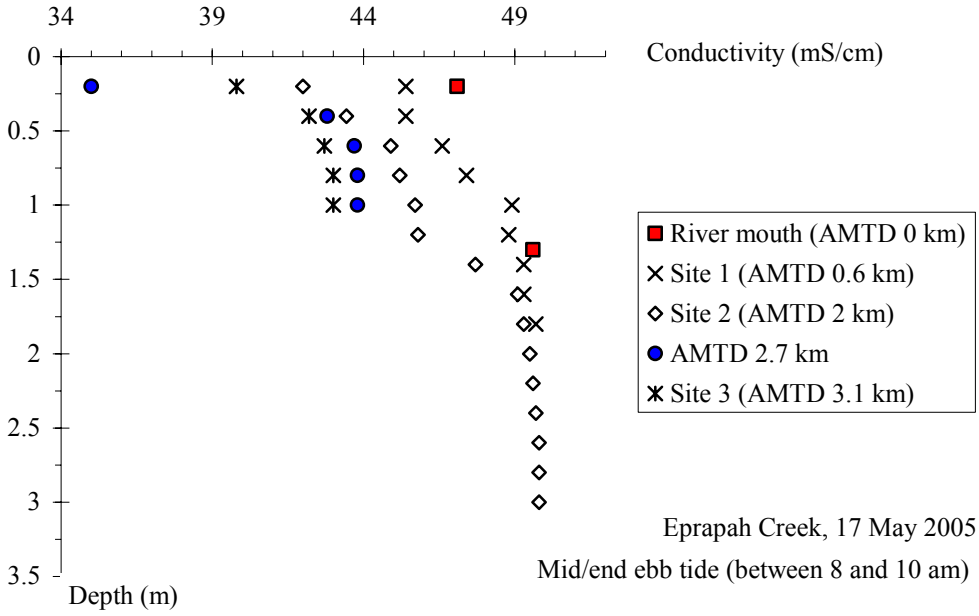

(C) Dissolved oxygen contents at the river mouth (AMTD 0 km), Site 1 (AMTD 0.6 km), Site 2 (AMTD 2 km), AMTD 2.7 km (treatment plant outfall) and Site 3 (AMTD 3.1 km)

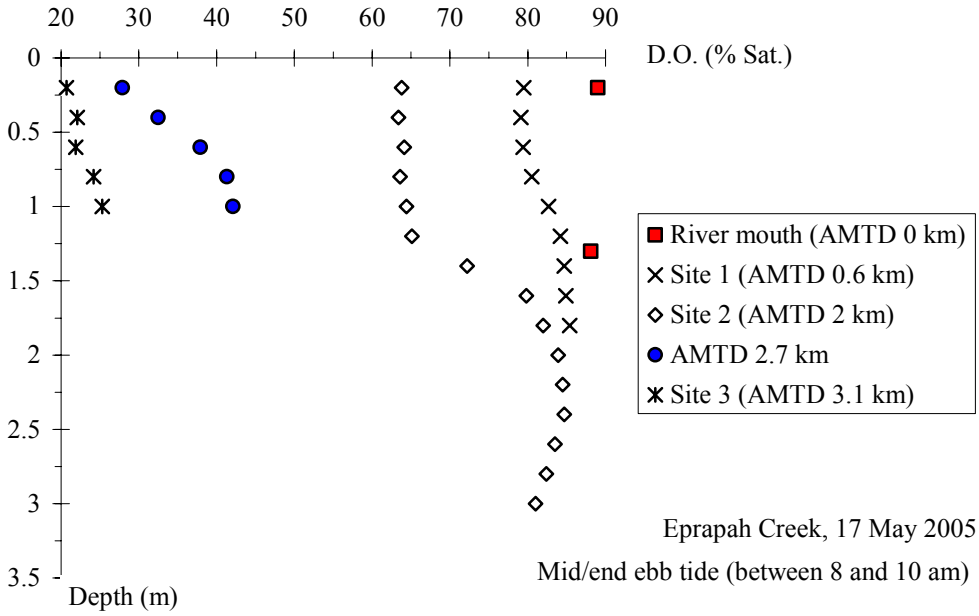

(D) Turbidities at the river mouth (AMTD 0 km), Site 1 (AMTD 0.6 km), Site 2 (AMTD 2 km), AMTD 2.7 km (treatment plant outfall) and Site 3 (AMTD 3.1 km)

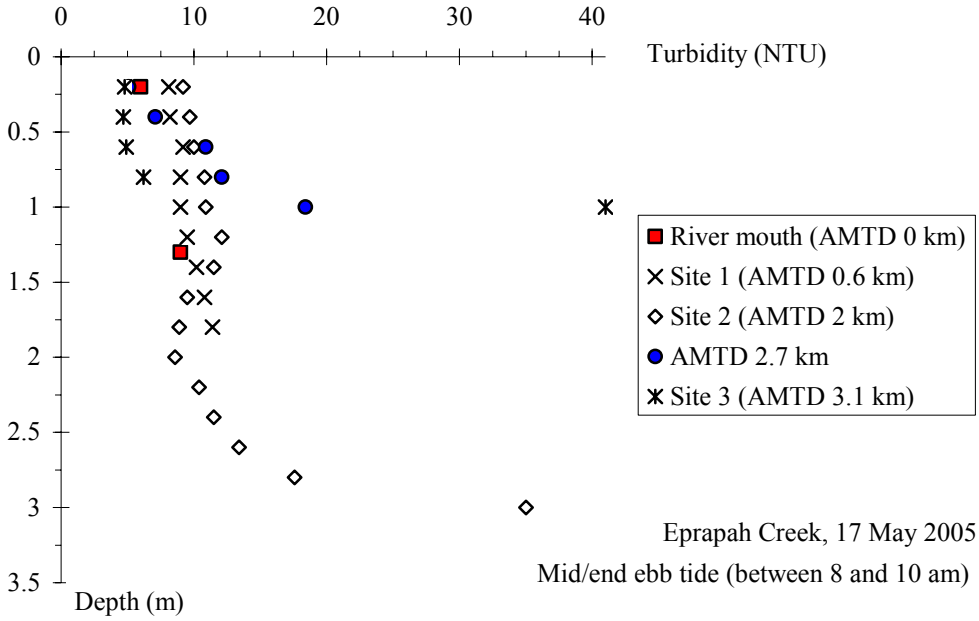

(E) pH levels at the river mouth (AMTD 0 km), Site 1 (AMTD 0.6 km), Site 2 (AMTD 2 km), AMTD 2.7 km (treatment plant outfall) and Site 3 (AMTD 3.1 km)

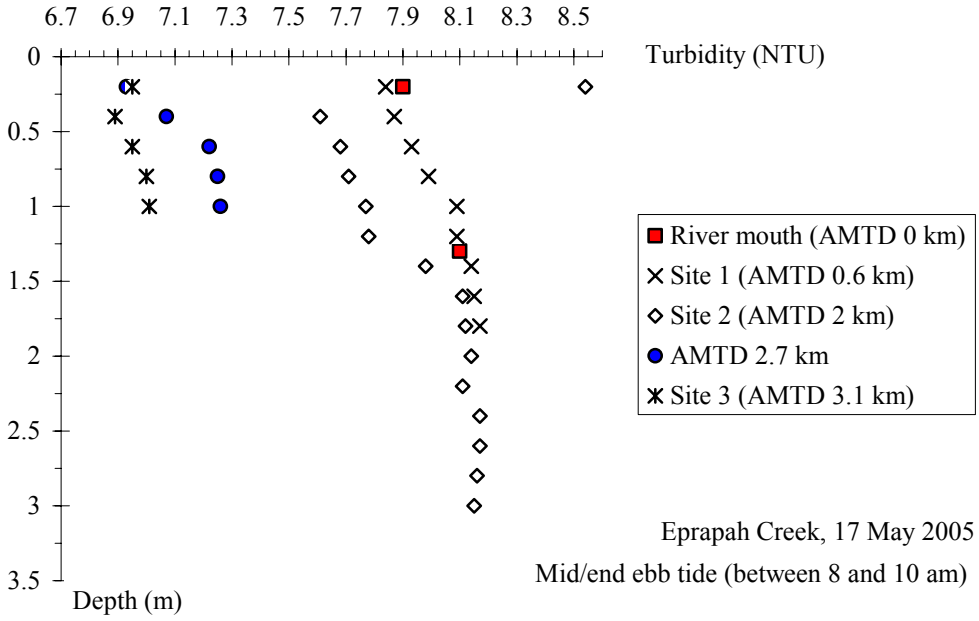

APPENDIX C - LIST OF FIELD WORK PARTICIPANTS

C.1 - FIELD STUDY E5 (8-9 MARCH 2005)

Hubert CHANSON, Project leader, The University of Queensland
Mark TREVETHAN, Ph.D. candidate, The University of Queensland
Clive BOOTH, Technical officer, The University of Queensland
Paul GUARD, Ph.D. candidate, The University of Queensland

Richard BROWN, Project leader, Queensland University of Technology
Ben LIM, Research officer, Queensland University of Technology
Dave McINTOSH, Technical officer, Queensland University of Technology
Peter TEOW, Student, Queensland University of Technology
S.W. Travis HO, Student, Queensland University of Technology

C.2 - FIELD STUDY E6 (16-18 MAY 2005)

Hubert CHANSON, Project leader, The University of Queensland
Mark TREVETHAN, Ph.D. candidate, The University of Queensland
Carlos GONZALEZ, Research associate, The University of Queensland
Masayuki TAKAHASHI, Visiting Research associate, Nihon University
Christian KOCH, Research associate, The University of Queensland
Clive BOOTH, Technical officer, The University of Queensland

Richard BROWN, Project leader, Queensland University of Technology
Ben LIM, Research officer, Queensland University of Technology
Dave McINTOSH, Technical officer, Queensland University of Technology
Jon JAMES, Technical officer, Queensland University of Technology
Peter TEOW, Student, Queensland University of Technology
S.W. Travis HO, Student, Queensland University of Technology
Swaroop CHAKRAVARTHI, Student, Queensland University of Technology

John FERRIS, Queensland Environmental Protection Agency

Koichi OKA, Honda (Japan)

Fig. C-1 - Photographs of the participants
(A) Photograph of the equipment retrieval on 18 May 2006 at low tide during the field study E6 (Photograph by M. TREVETHAN & M. TAKAHASHI) - From left to right : Peter TEOW, Hubert CHANSON, Masayuki TAKAHASHI, Christian KOCH, Richard BROWN, Carlos GONZALEZ (on boat), John JAMES, Clive BOOTH (behind boat in the water), Dave McINTOSH

(B) Photograph of team water sampling team on 17 May 2006 at 09:18 (mid ebb-tide) during the field study E6 (Photograph by H. CHANSON) - From left to right : John FERRIS, Masayuki TAKAHASHI, Carlos GONZALEZ

APPENDIX D – SUMMARY OF TURBULENCE CHARACTERISTICS AT EPRAPAH CREEK DURING THE FIELD WORKS E5 (8-9 MARCH 2005) AND E6 (16-18 MAY 2005)

D.1 PRESENTATION

This Appendix summarises the ranges of turbulence characteristics for the majority of samples during the field works E5 and E6. Each sample consisted of 5,000 data points and the samples were calculated every 10 s along the entire data sets for the field works E5 and E6. The tables below outline the sampling elevation and instrumentation (3D ADV or 2D microADV) along with the range of each turbulence property for the majority of samples for field works E5 and E6.

Notation

$Ku(V_x)$	kurtosis of streamwise velocity;
$Ku(V_y)$	kurtosis of transverse velocity;
$Ku(V_z)$	kurtosis of vertical velocity;
$Ku(\rho v_x v_y)$	kurtosis of tangential Reynolds stress $\rho v_x v_y$;
$Ku(\rho v_x v_z)$	kurtosis of tangential Reynolds stress $\rho v_x v_z$;
$Ku(\rho v_y v_z)$	kurtosis of tangential Reynolds stress $\rho v_y v_z$;
R_{vxvy}	correlation coefficient of tangential Reynolds stress $\rho v_x v_y$: $R_{vxvy} = \overline{v_x v_y} \big/ (v_x' v_y')$
R_{vxvz}	correlation coefficient of Reynolds stress $\rho v_x v_z$: $R_{vxvz} = \overline{v_x v_z} \big/ (v_x' v_z')$
R_{vyvz}	correlation coefficient of Reynolds stress $\rho v_y v_z$: $R_{vyvz} = \overline{v_y v_z} \big/ (v_y' v_z')$
$Sk(V_x)$	skewness of streamwise velocity;
$Sk(V_y)$	skewness of transverse velocity;
$Sk(V_z)$	skewness of vertical velocity;
$Sk(\rho v_x v_y)$	skewness of tangential Reynolds stress $\rho v_x v_y$;
$Sk(\rho v_x v_z)$	skewness of tangential Reynolds stress $\rho v_x v_z$;
$Sk(\rho v_y v_z)$	skewness of tangential Reynolds stress $\rho v_y v_z$;
T_{Ex}	Eulerian integral time scale of streamwise velocity (s);
T_{Ey}	Eulerian integral time scale of transverse velocity (s);
T_{Ez}	Eulerian integral time scale of vertical velocity (s);
$\overline{V_x}$	time-averaged streamwise velocity (m/s);
$\overline{V_y}$	time-averaged transverse velocity (m/s);
$\overline{V_z}$	time-averaged vertical velocity (m/s);
v_x'	standard deviation of streamwise velocity (m/s);
v_y'	standard deviation of transverse velocity (m/s);
v_z'	standard deviation of vertical velocity (m/s);
$v_y' \big/ v_x'$	horizontal turbulence intensity;
$v_z' \big/ v_x'$	vertical turbulence intensity;

$\rho\overline{v_x v_y}$ time-averaged tangential Reynolds stress (Pa);

$\rho\overline{v_x v_z}$ time-averaged tangential Reynolds stress (Pa);

$\rho\overline{v_y v_z}$ time-averaged tangential Reynolds stress (Pa);

$\left(\rho v_x v_y\right)'$ standard deviation of tangential Reynolds stress (Pa);

$\left(\rho v_x v_z\right)'$ standard deviation of tangential Reynolds stress (Pa);

$\left(\rho v_y v_z\right)'$ standard deviation of tangential Reynolds stress (Pa);

τ_{Ex} Eulerian dissipation time scale of streamwise velocity (s);

τ_{Ey} Eulerian dissipation time scale of transverse velocity (s);

τ_{Ez} Eulerian dissipation time scale of vertical velocity (s).

D.2 STATISTICAL SUMMARIES

Table D-1 - Statistical moments of velocity data ranges for the majority of samples during field works E5 and E6 - Data samples of 5,000 data points calculated every 10 s along entire data set for field works E5 and E6 - Majority of samples = approximately 90 % of all samples calculated

Field study	Sampling elevation above bed (m)	Instrumentation	Time-averaged velocity			Standard deviation		
			$\overline{V_x}$ (cm/s)	$\overline{V_y}$ (cm/s)	$\overline{V_z}$ (cm/s)	v_x' (cm/s)	v_y' (cm/s)	v_z' (cm/s)
E5	0.1	3D ADV (10 MHz)	-25 to 19	-8 to 3	-1.2 to 0.2	3 to 6	3 to 6	1 to 3
E6	0.4	3D ADV (10 MHz)	-10 to 6.5	-1.5 to 1.5	-1 to 0.1	0.6 to 1.8	0.6 to 1.3	0.2 to 0.9
	0.2	2D microADV (16 MHz)	-7.5 to 5.5	-1.2 to 1	----	0.5 to 1.5	0.4 to 1.2	----

Field study	Sampling elevation above bed (m)	Instrumentation	Skewness			Kurtosis		
			$Sk(V_x)$	$Sk(V_y)$	$Sk(V_z)$	$Ku(V_x)$	$Ku(V_y)$	$Ku(V_z)$
E5	0.1	3D ADV (10 MHz)	-0.16 to 0.17	-0.17 to 0.17	-0.2 to 0.2	0 to 1.3	0 to 2	-0.1 to 1.5
E6	0.4	3D ADV (10 MHz)	-0.3 to 0.5	-0.4 to 0.4	-0.6 to 0.6	-1 to 1	-0.5 to 1.5	-0.2 to 2
	0.2	2D microADV (16 MHz)	-0.4 to 0.6	-0.6 to 0.6	--	-1 to 1.5	-0.5 to 2	--

Note: -- data for that turbulence characteristic not measured.

Table D-2 - Statistical moments of tangential Reynolds stresses ranges for the majority of samples during field works E5 and E6 - Data samples of 5,000 data points calculated every 10 s along entire data set for field works E5 and E6 - Majority of samples = approximately 90 % of all samples calculated

Field study	Sampling elevation above bed (m)	Instrumentation	Time-averaged Reynolds stress			Standard deviation of Reynolds stress		
			$\rho\overline{v_x v_y}$ (Pa)	$\rho\overline{v_x v_z}$ (Pa)	$\rho\overline{v_y v_z}$ (Pa)	$(\rho v_x v_y)'$ (Pa)	$(\rho v_x v_z)'$ (Pa)	$(\rho v_y v_z)'$ (Pa)
E5	0.1	3D ADV (10 MHz)	-0.3 to 0.3	-0.2 to 0.5	-0.1 to 0.2	1 to 3	0.5 to 1.3	0.4 to 1.3
E6	0.4	3D ADV (10 MHz)	-0.07 to 0.04	-0.02 to 0.03	-0.02 to 0.015	0.05 to 0.25	0.02 to 0.16	0.02 to 0.1
	0.2	2D microADV (16 MHz)	-0.07 to 0.03	--	--	0.02 to 0.16	--	--

Field study	Sampling elevation above bed (m)	Instrumentation	Skewness of Reynolds stress			Kurtosis of Reynolds stress		
			Sk $(\rho v_x v_y)$	Sk $(\rho v_x v_z)$	Sk $(\rho v_y v_z)$	Ku $(\rho v_x v_y)$	Ku $(\rho v_x v_z)$	Ku $(\rho v_y v_z)$
E5	0.1	3D ADV (10 MHz)	-1.6 to 1.6	-2.4 to 1.8	-2.1 to 2	6 to 30	6 to 30	6 to 30
E6	0.4	3D ADV (10 MHz)	-2 to 2.3	-2 to 2.2	-1.9 to 2	3 to 21	3 to 21	4 to 24
	0.2	2D microADV (16 MHz)	-1.3 to 1.9	--	--	2 to 12	--	--

Note: -- data for turbulence characteristic not measured.

Table D-3 - Dissipation and integral time scales ranges for the majority of samples during field works E5 and E6 - Data samples of 5,000 data points calculated every 10 s along entire data set for field works E5 and E6 - Majority of samples = approximately 90 % of all samples calculated

Field study	Sampling elevation above bed (m)	Instrumentation	Dissipation time scales			Integral time scales		
			τ_{Ex} (s)	τ_{Ey} (s)	τ_{Ez} (s)	T_{Ex} (s)	T_{Ey} (s)	T_{Ez} (s)
E5	0.1	3D ADV (10 MHz)	0.0007 to 0.01	0.0007 to 0.01	0.001 to 0.05	0.02 to 0.4	0.03 to 0.4	0.1 to 0.5
E6	0.4	3D ADV (10 MHz)	0.0007 to 0.01	0.0007 to 0.01	0.003 to 0.09	0.06 to 1	0.07 to 1	0.6 to 2
	0.2	2D microADV (16 MHz)	0.0009 to 0.02	0.001 to 0.1	--	0.4 to 2	0.7 to 2	--

Note: -- data for turbulence characteristic not measured.

Table D-4 - Turbulence intensities and correlation coefficients of tangential Reynolds stress ranges for the majority of samples during field works E5 and E6 - Data samples of 5,000 data points calculated every 10 s along entire data set for field works E5 and E6 - Majority of samples = approximately 90 % of all samples calculated

Field study	Sampling elevation above bed (m)	Instrumentation	Correlation coefficient of Reynolds stress			Turbulence intensities	
			R_{vxvy}	R_{vxvz}	R_{vyvz}	v'_y/v'_x	v'_z/v'_x
E5	0.1	3D ADV (10 MHz)	-0.08 to 0.14	-0.3 to 0.3	-0.1 to 0.13	0.8 to 1.2	0.2 to 0.5
E6	0.4	3D ADV (10 MHz)	-0.3 to 0.3	-0.3 to 0.3	-0.15 to 0.2	0.7 to 1.2	0.4 to 0.7
	0.2	2D microADV (16 MHz)	-0.4 to 0.4	--	--	0.6 to 1.2	--

Note: -- data for turbulence characteristic not measured.

REFERENCES

ANZECC (2000). "Australian and New Zealand Guidelines for Fresh and Marine Water Quality." *Australian and New Zealand Environment and Conservation Council (ANZECC) and Agriculture and Resource Management Council of Australia and New Zealand (ARMCANZ)*, Paper No. 4, October 2000.

BOWDEN, K.F., and FERGUSON, S.R. (1980). "Variations with Height of the Turbulence in a Tidally-Induced Botom Boundary Layer." *Marine Turbulence*, J.C.J. NIHOUL, Ed., Elsevier, Amsterdam, The Netherlands, pp. 259-286.

BRADSHAW, P. (1971). "An Introduction to Turbulence and its Measurement." *Pergamon Press*, Oxford, UK, The Commonwealth and International Library of Science and Technology Engineering and Liberal Studies, Thermodynamics and Fluid Mechanics Division, 218 pages.

BROWN, R., FERRIS, J., WARBURTON, K., and CHANSON, H. (2004). "Hydrodynamic, Water Quality and Ecological Study of Eprapah Creek Estuarine Zone: a Multi-Disciplinary, Cross-Institutional Approach." *Proc. 8th National Conference on Hydraulics in Water Engineering*, IEAust., Gold Coast, Australia, H. CHANSON and J. MACINTOSH Ed., 8 pages (CD-ROM) (ISBN 085825 850 1).

CHANSON, H. (1999). "The Hydraulics of Open Channel Flows : An Introduction." *Edward Arnold*, London, UK, 512 pages (ISBN 0 340 74067 1).

CHANSON, H. (2003). "A Hydraulic, Environmental and Ecological Assessment of a Sub-tropical Stream in Eastern Australia: Eprapah Creek, Victoria Point QLD on 4 April 2003." *Report No. CH52/03*, Dept. of Civil Engineering, The University of Queensland, Brisbane, Australia, June, 189 pages (ISBN 1864997044).

CHANSON, H. (2004a). "Enhancing Students' Motivation in the Undergraduate Teaching of Hydraulic Engineering: the Role of Field Works" *Jl of Prof. Issues in Engrg Educ. and Practice*, ASCE, Vol. 130, No. 4, pp. 259-268 (ISSN 0733-9380).

CHANSON, H. (2004b). "Environmental Hydraulics of Open Channel Flows." *Elsevier Butterworth-Heinemann*, Oxford, UK, 483 pages (ISBN 0 7506 6165 8).

CHANSON, H., AOKI, S., and MARUYAMA, M. (2000). "Unsteady Two-Dimensional Orifice Flow: an Experimental Study." *Coastal/Ocean Engineering Report*, No. COE00-1, Dept. of Architecture and Civil Eng., Toyohashi University of Technology, Japan, 29 pages.

CHANSON, H., AOKI, S., and MARUYAMA, M. (2002). "Unsteady Two-Dimensional Orifice Flow: a Large-Size Experimental Investigation." *Jl of Hyd. Res.*, IAHR, Vol. 40, No. 1, pp. 63-71 (ISSN 0022-1686).

CHANSON, H. BROWN, R., and FERRIS, J. (2004). "Simultaneous Field Measurements of Turbulence and Water Quality in a Sub-Tropical Estuary in Australia." *Proc. 15th Australasian Fluid Mech. Conf.*, AFMC, Sydney, Australia, M. BEHNIA, W. LIN & G.D. McBAIN Ed., Paper AFMC00016, 4 pages (CD-ROM) (ISBN 1-864-87695-6).

CHANSON, H., BROWN, R., FERRIS, J., RAMSAY, I., and WARBURTON, K. (2005a). "Preliminary Measurements of Turbulence and Environmental Parameters in a Sub-Tropical Estuary of Eastern Australia." *Environmental Fluid Mechanics*, Vol. 5, No. 6, pp. 553-575 (ISSN 1567-7419).

CHANSON, H., TREVETHAN, M., and AOKI, S. (2005b). "Acoustic Doppler Velocimetry (ADV) in a Small Estuarine System. Field Experience and "Despiking"." *Proc. 31th Biennial IAHR Congress*, Seoul, Korea, B.H. JUN, S.I. LEE, I.W. SEO and G.W. CHOI Editors, Theme E2, Paper 0161, pp. 3954-3966 (ISBN 89 87898 24 5).

DIGBY, M.J., SAENGER, P., WHELAN, M.B., McCONCHIE, D., EYRE, B., HOLMES, N., BUCHER, D. (1999). "A Physical Classification of Australian Estuaries." *Report No. 9*, LWRRDC, National River Health Program, Urban sub-program, Occasional Paper, 16/99.

DYER, K. R. (1973). "Estuaries: A Physical Introduction." *John Wiley and Sons*, New York, USA.

DYER, K. R. (1997). "Estuaries: A Physical Introduction." *John Wiley and Sons*, New York, USA, 2nd edition.

FERRIS, J., CHANSON, H., and BROWN, R. (2004). "Mixing and Dispersion in Sub-Tropical Estuarine System: Field Works and Experience at Eprapah Creek (Australia)." *Proc. 9th Intl Symp. on River Sedimentation ISRS04*, Yichang, China, Oct. 18-21, Invited lecture, Tsinghua University Pres, Beijing, C. HU and Y. TAN Editors, Vol. 1, pp. 394-405 (ISBN 7 302 09684 8). (CD-ROM, 2004, Tsinghua University Press, 12 pages (ISBN 7 89494 565 X))

FRANSSON, J.H.M., MATSUBARA, M., and ALFREDSSON, P.H. (2005)." Transition Induced by Free-stream Turbulence." *Jl of Fluid Mech.*, Vol. 527, pp. 1-25.

FUGATE, D.C., and FRIEDRICHS, C.T. (2002). "Determining Concentration and Fall Velocity of Estuarine Particle Populations using ADV, OBS and LISST." *Continental Shelf Research*, Vol. 22, pp. 1867-1886.

GORING, D.G., and NIKORA, V.I. (2002). "Despiking Acoustic Doppler Velocimeter Data." *Jl of Hyd. Engrg.*, ASCE, Vol. 128, No. 1, pp. 117-126. Discussion: Vol. 129, No. 6, pp. 484-489.

HALLBACK, M., GROTH, J., and JOHANSSON, A.V. (1989). "A Reynolds Stress Closure for the Dissipation in Anisotropic Turbulent Flows." *Proc. 7th Symp. Turbulent Shear Flows*, Stanford University, USA, Vol. 2, Paper 17-2, pp. 17.2.1-17.2.6.

HINZE, J.O. (1975). "Turbulence." *McGraw-Hill Publ.*, 2nd Edition, New York, USA.

JONES, A.B., PRANGE, J., and DENNISON, W.C. (1999). "An Assessment of the Ecological Health of Eprapah Creek." *Report*, Marine Botany, Univ. of Queensland, Brisbane, Australia, 23 pages.

KAWANISI, K. (2004). "Structure of Turbulent Flow in a Shallow Tidal Estuary." *Jl of Hyd. Engrg.*, ASCE, Vol. 130, No. 4, pp. 360-370.

KAWANISI, K., and YOKOSI, S. (1994). "Mean and Turbulence Characteristics in a Tidal River." *Continental Shelf Research*, Vol. 17, No. 8, pp. 859-875.

KAWANISI, K., and YOKOSI, S. (1997). "Characteristics of Suspended Sediment and Turbulence in a Tidal Boundary Layer." *Estuarine, Coastal and Shelf Science*, Vol. 38, pp. 447-469.

KIRBY, R., and PARKER, W.R. (1982). "A Suspended Sediment Front in the Severn Estuary." *Nature*, Vol. 295, 4 Feb., pp. 396-399.

KOCH, C., and CHANSON, H. (2005). "An Experimental Study of Tidal Bores and Positive Surges: Hydrodynamics and Turbulence of the Bore Front." *Report No. CH56/05*, Dept. of Civil Engineering, The University of Queensland, Brisbane, Australia, July, 170 pages (ISBN 1864998245).

LEMMIN, U., and LHERMITTE, R. (1999). "ADV Measurements of Turbulence: can we Improve their Interpretation ? Discussion" *Jl of Hyd. Engrg.*, ASCE, Vol. 125, No. 6, pp. 987-988.

LEWIS, R. (1997). "Dispersion in Estuaries and Coastal Waters." *John Wiley & Sons*, New York, USA.

McLELLAND, S.J., and NICHOLAS, A.P. (2000). "A New Method for Evaluating Errors in High-Frequency ADV Measurements." *Hydrological Processes*, Vol. 14, pp. 351-366.

MARTIN, V., FISHER, T.S.R., MILLAR, R.G., and QUICK, M.C. (2002). "ADV Data Analysis for Turbulent Flows: Low Correlation Problem." *Proc. Conf. on Hydraulic Measurements and Experimental Methods*, ASCE-EWRI & IAHR, Estes Park, USA, 10 pages (CD-ROM).

NEZU, I., and NAKAGAWA, H. (1993). "Turbulence in Open-Channel Flows." *IAHR Monograph*, IAHR Fluid Mechanics Section, Balkema Publ., Rotterdam, The Netherlands, 281 pages.

NIKORA, V.I., and GORING, D.G. (1998). "ADV Measurements of Turbulence: can we Improve their Interpretation ?" *Jl of Hyd. Engrg.*, ASCE, Vol. 124, No. 6, pp. 630-634. Discusion: Vol. 125, No. 9, pp. 987-988.

NIKORA, V., and GORING, D. (2002). "Fluctuations of Suspended Sediment Concentration and Turbulent Sediment Fluxes in an Open-Channel Flow." *Jl of Hydr. Engrg.*, ASCE, Vol. 128, No. 2, pp. 214-224.

NIKORA, V., GORING, D., and ROSS, A. (2002). "The Structure and Dynamics of the Thin Near-Bed Layer in a Complex Marine Environment: A Case Study in Beatrix Bay, New Zealand." *Estuarine, Coastal and Shelf Sci.*, Vol. 54, pp. 915-926.

O'BRIEN, E., and FEARON, R. (2001). "South-East Queensland Monitoring Program. Redland Shire Waterways: Water Quality Study 1999." *Environmental Technical Report No. 43*, Queensland Environmental Protection Agency, 50 pages.

OSONPHASOP, C. (1983). "The Measurements of Turbulence in Tidal Currents." *Ph.D. thesis*, Dept of Mech. Eng., Monash Univ., Australia.

PIQUET, J. (1999). "Turbulent Flows. Models and Physics." *Springer*, Berlin, Germany, 761 pages.

PRANDTL, L. (1925). "Über die ausgebildete Turbulenz." ('On Fully Developed Turbulence.') *Z.A.M.M.*, Vol. 5, pp. 136-139 (in German).

PRESS, W. H., TEUKOLSKY, S. A., VETERLING, W. T. and FLANNERY, B. P. (1992). "Numerical Recipes in FORTRAN." *Cambridge University Press*, UK, 2nd edition, 2 volumes.

PRITCHARD, D. W. (1952). "Estuarine hydrography." in *Advances in Geophysics*, Vol. 1, pp. 243-280.

RALSTON, D.K., and STACEY, M.T. (2005). "Stratification and Turbulence in Subtidal Channels through Intertidal Mudflats." *Jl of Geophysical Research Oceans*, AGU, Vol. 110, Paper C08009, 16 pages.

SCHLICHTING, H. (1979). "Boundary Layer Theory." *McGraw-Hill*, New York, USA, 7th edition.

SCHLICHTING, H., and GERSTEN, K. (2000). "Boundary Layer Theory." *Springer Verlag*, Berlin, Germany, 8th edition., 707 pages.

SONTEK (2001). "Acoustic Doppler Velocimeter. Principles of Operations." *Sontek/YSI Technical Notes*, San Diego, USA, Sept., 14 pages.

STACEY, M.T., MONISMITH, S.G., and BURAU, J.R. (1999). "Observations of Turbulence in a Partially Stratified Estuary." *Jl Phys. Ocean.*, Vol. 29, Aug., pp. 1950-1970

THAIN, R.H., PRIESTLEY, A.D., and DAVIDSON, M.A. (2004). "The Formation of a Tidal Intrusion at the Mouth of a Macrotidal, Partially Mixed Estuary: a Field Study of the Dart Estuary, UK." *Estuarine, Coastal and Shelf Science*, Vol. 61, pp. 161-172.

VOULGARIS, G., and MEYERS, S.T. (2004). "Temporal Variability of Hydrodynamics, Sediment Concentration and Sediment Settling in a Tidal Creek." *Continental Shelf Research*, Vol. 24, pp. 1659-1683.

VOULGARIS, G., and TROWBRIDGE, J.H. (1998). "Evaluation of the Acoustic Doppler Velocimeter (ADV) for Turbulence Measurements." *Jl Atmosph. and Oceanic Tech.*, Vol. 15, pp. 272-289.

WAHL, T.L. (2003). "Despiking Acoustic Doppler Velocimeter Data. Discussion." *Jl of Hyd. Engrg.*, ASCE, Vol. 129, No. 6, pp. 484-487.

WEST, J.R., and ODUYEMI, K.O.K. (1989). "Turbulence Measurements of Suspended Solids Concentration in Estuaries." *Jl of Hyd. Engrg.*, ASCE, Vol. 115, No. 4, pp. 457-474.

WEST, J.R., and SHIONO, K. (1988). "Vertical Turbulent Mixing Processes on Ebb Tides in Partially Mixed Estuaries." *Estuarine, Coastal and Shelf Science*, Vol. 26, pp. 51-66.

XIE, Q. (1998). "Turbulent flows in non-uniform open channels : experimental measurements and numerical modelling." *Ph.D. thesis*, Dept. of Civil Eng., University Of Queensland, Australia, 339 pages.

INTERNET REFERENCES

A Hydraulic, Environmental and Ecological Assessment of a Sub-tropical Stream in Eastern Australia: Eprapah Creek, Victoria Point QLD on 4 April 2003	{http://www.uq.edu.au/~e2hchans/eprapa.html}
Queensland EPA water quality monitoring	{http://www.epa.qld.gov.au/environmental_management/water/water_quality_monitoring/}
Eprapah Creek Catchment Landcare Association Inc. (ECCLA)	{http://eprapah.scouting.net.au/index/projects/landcare.htm}

BIBLIOGRAPHIC REFERENCE OF THE REPORT CH58/06

The Hydraulic Model research report series CH is a refereed publication published by the Division of Civil Engineering at the University of Queensland, Brisbane, Australia.

The bibliographic reference of the present report is :

TREVETHAN, M., CHANSON, H., and BROWN, R.J. (2006). "Two Series of Detailed Turbulence Measurements in a Small Subtropical Estuarine System." *Report No. CH58/06*, Div. of Civil Engineering, The University of Queensland, Brisbane, Australia, March, 153 pages (ISBN 1864998520).

The Report CH58/06 is available, in the present form, as a PDF file on the Internet at EprintsUQ :

http://eprint.uq.edu.au/

It is listed in chronological order at :

http://eprint.uq.edu.au/view/person/Chanson,_Hubert.html

HYDRAULIC MODEL RESEARCH REPORT CH

The Hydraulic Model Report CH series is published by the Division of Civil Engineering at the University of Queensland. Orders of any of the Hydraulic Model Reports should be addressed to the Departmental Secretary.

Departmental Secretary, Division of Civil Engineering, The University of Queensland
Brisbane 4072, Australia - Tel.: (61 7) 3365 3619 - Fax : (61 7) 3365 4599
Url: http://www.eng.uq.edu.au/civil/ Email: hodciveng@uq.edu.au

Report CH	**Unit price**	Quantity	**Total price**
TREVETHAN, M., CHANSON, H., and BROWN, R.J. (2006). "Two Series of Detailed Turbulence Measurements in a Small SubTropical Estuarine System." *Report No. CH58/06*, Dept. of Civil Engineering, The University of Queensland, Brisbane, Australia, Mar. (ISBN 1864998520).	AUD$60.00		
KOCH, C., and CHANSON, H. (2005). "An Experimental Study of Tidal Bores and Positive Surges: Hydrodynamics and Turbulence of the Bore Front." *Report No. CH56/05*, Dept. of Civil Engineering, The University of Queensland, Brisbane, Australia, July (ISBN 1864998245).	AUD$60.00		
CHANSON, H. (2005). "Applications of the Saint-Venant Equations and Method of Characteristics to the Dam Break Wave Problem." *Report No. CH55/05*, Dept. of Civil Engineering, The University of Queensland, Brisbane, Australia, May (ISBN 1864997966).	AUD$60.00		
CHANSON, H., COUSSOT, P., JARNY, S., and TOQUER, L. (2004). "A Study of Dam Break Wave of Thixotropic Fluid: Bentonite Surges down an Inclined plane." *Report No. CH54/04*, Dept. of Civil Engineering, The University of Queensland, Brisbane, Australia, June, 90 pages (ISBN 1864997710).	AUD$60.00		
CHANSON, H. (2003). "A Hydraulic, Environmental and Ecological Assessment of a Sub-tropical Stream in Eastern Australia: Eprapah Creek, Victoria Point QLD on 4 April 2003." *Report No. CH52/03*, Dept. of Civil Engineering, The University of Queensland, Brisbane, Australia, June, 189 pages (ISBN 1864997044).	AUD$90.00		
CHANSON, H. (2003). "Sudden Flood Release down a Stepped Cascade. Unsteady Air-Water Flow Measurements. Applications to Wave Run-up, Flash Flood and Dam Break Wave." *Report CH51/03*, Dept of Civil Eng., Univ. of Queensland, Brisbane, Australia, 142 pages (ISBN 1864996552).	AUD$60.00		
CHANSON, H,. (2002). "An Experimental Study of Roman Dropshaft Operation : Hydraulics, Two-Phase Flow, Acoustics." *Report CH50/02*, Dept of Civil Eng., Univ. of Queensland, Brisbane, Australia, 99 pages (ISBN 1864996544).	AUD$60.00		
CHANSON, H., and BRATTBERG, T. (1997). "Experimental Investigations of Air Bubble Entrainment in Developing Shear Layers." *Report CH48/97*, Dept. of Civil Engineering, University of Queensland, Australia, Oct., 309 pages (ISBN 0 86776 748 0).	AUD$90.00		
CHANSON, H. (1996). "Some Hydraulic Aspects during Overflow above Inflatable Flexible Membrane Dam." *Report CH47/96*, Dept. of Civil Engineering, University of Queensland, Australia, May, 60 pages (ISBN 0 86776 644 1).	AUD$60.00		
CHANSON, H. (1995). "Flow Characteristics of Undular Hydraulic Jumps. Comparison with Near-Critical Flows." *Report CH45/95*, Dept. of Civil Engineering, University of Queensland, Australia, June, 202 pages (ISBN 0 86776 612 3).	AUD$60.00		

CHANSON, H. (1995). "Air Bubble Entrainment in Free-surface Turbulent Flows. Experimental Investigations." *Report CH46/95*, Dept. of Civil Engineering, University of Queensland, Australia, June, 368 pages (ISBN 0 86776 611 5).	AUD$80.00		
CHANSON, H. (1994). "Hydraulic Design of Stepped Channels and Spillways." *Report CH43/94*, Dept. of Civil Engineering, University of Queensland, Australia, Feb., 169 pages (ISBN 0 86776 560 7).	AUD$60.00		
POSTAGE & HANDLING (per report)	AUD$10.00		
GRAND TOTAL			

OTHER HYDRAULIC RESEARCH REPORTS

Reports/Theses	Unit price	Quantity	Total price
GONZALEZ, C.A. (2005). "An Experimental Study of Free-Surface Aeration on Embankment Stepped Chutes." *Ph.D. thesis*, Dept of Civil Engineering, The University of Queensland, Brisbane, Australia, 240 pages.	AUD$80.00		
TOOMBES, L. (2002). "Experimental Study of Air-Water Flow Properties on Low-Gradient Stepped Cascades." *Ph.D. thesis*, Dept of Civil Engineering, The University of Queensland, Brisbane, Australia.	AUD$120.00		
CHANSON, H. (1988). "A Study of Air Entrainment and Aeration Devices on a Spillway Model." *Ph.D. thesis*, University of Canterbury, New Zealand.	AUD$60.00		
POSTAGE & HANDLING (per report)	AUD$10.00		
GRAND TOTAL			

CIVIL ENGINEERING RESEARCH REPORT CE

The Civil Engineering Research Report CE series is published by the Division of Civil Engineering at the University of Queensland. Orders of any of the Civil Engineering Research Report CE should be addressed to the Departmental Secretary.

Departmental Secretary, Division of Civil Engineering, The University of Queensland
Brisbane 4072, Australia
Tel.: (61 7) 3365 3619 Fax : (61 7) 3365 4599
Url: http://www.eng.uq.edu.au/civil/ Email: hodciveng@uq.edu.au

Recent Research Report CE	Unit price	Quantity	Total price
GONZALEZ, C.A., TAKAHASHI, M., and CHANSON, H. (2005). "Effects of Step Roughness in Skimming Flows: an Experimental Study." *Research Report No. CE160*, Dept. of Civil Engineering, The University of Queensland, Brisbane, Australia, July (ISBN 1864998105).	AUD$10.00		
CHANSON, H., and TOOMBES, L. (2001). "Experimental Investigations of Air Entrainment in Transition and Skimming Flows down a Stepped Chute. Application to Embankment Overflow Stepped Spillways." *Research Report No. CE158*, Dept. of Civil Engineering, The University of Queensland, Brisbane, Australia, July, 74 pages (ISBN 1 864995297).	AUD$10.00		

HANDLING (per order)	AUD$10.00		
GRAND TOTAL			

Note: Prices include postages and processing.

PAYMENT INFORMATION

1- VISA Card

Name on the card :	
Visa card number :	
Expiry date :	
Amount :	AUD$ .....

2- Cheque/remittance payable to : THE UNIVERSITY OF QUEENSLAND and crossed "Not Negotiable".

N.B. For overseas buyers, cheque payable in Australian Dollars drawn on an office in Australia of a bank operating in Australia, payable to: THE UNIVERSITY OF QUEENSLAND and crossed "Not Negotiable".

Orders of any Research Report should be addressed to the Departmental Secretary.

Departmental Secretary, Division of Civil Engineering, The University of Queensland
Brisbane 4072, Australia - Tel.: (61 7) 3365 3619 - Fax : (61 7) 3365 4599
Url: http://www.eng.uq.edu.au/civil/ Email: hodciveng@uq.edu.au